

Mapping Iron Uptake by Spinach from Roots to leaves and Tracking Iron bioaccessibility of Spinach leaves and Isolated Chloroplasts.

Thesis submitted in fulfilment of the requirements for a degree of Master of Philosophy (MPhil) of both Food, Nutrition & Dietetics and Plant Sciences

University of Nottingham

3rd May 2024

Student ID Number: 20194859

Project Code: RL4519

I certify that I am the sole author of this thesis and no part of it has been published or submitted for publication. I certify to the best of my knowledge that this thesis does not infringe upon copyrighted material nor violate any proprietary rights and that any ideas, methods, quotations or any material from the work of other people included in this thesis are referenced accordingly to a recognisable convention.

I officially declare that this document is a true copy of my thesis as approved by my academic committee and the work has not been transferred to any other major institution without informed consent.

Signed by: Ardeshir Mohsen Farmanfarmaian (MPhil candidate)



Table of contents

Abstract	
Acknowledgements	
List of figures	
List of tables	
List of abbreviations and chemical compounds	
List of equations	

Chapter 1: Introduction

1.1 General introduction to iron and its importance.....	
1.2 Iron uptake and distribution in humans.....	
1.2.1 Summary of iron release and uptake in human digestive system.....	
1.3 Current global state of iron deficiency.....	
1.4 General benefits of iron for plant nutrition.....	
1.5 Strategy I and Strategy II plant responses/adaptations to iron deficiency.....	
1.5.1 Strategy I – reduction-based strategy.....	
1.5.2 Strategy II – chelation-based strategy.....	
1.6 Plant responses and adaptations to iron toxicity.....	
1.6.1 Fate of absorbed iron inside plants.....	
1.7 Chloroplasts and iron transport processes.....	
1.7.1 Introduction to chloroplasts.....	
1.7.2 General benefits of iron for chloroplasts.....	
1.7.3 Iron uptake mechanisms in chloroplasts.....	
1.8 Nutritional significance of green leafy vegetables (GLVs).....	
1.8.1 GLVs in general – iron contents in the most consumed.....	
1.8.2 Spinach health benefits.....	
1.9 Aims and objectives.....	

Chapter 2: The method of growing spinach hydroponically

2.1 Introduction to hydroponics.....	
2.2 Preparation of Hoagland nutrient solution containing NaFe-EDTA.....	
2.2.1 Preparation of standard Hoagland nutrient solution – Fe only.....	
2.2.2 Preparation of Hoagland nutrient solution with NaFe-EDTA with enriched ⁵⁷ Fe stable isotope.....	
2.2.2.1 Preparation of the individual stock solution.....	
2.2.2.2 Integration of final stock solution into Hoagland nutrient solution.....	
2.3 Growth room facilities – an overview.....	
2.4 Spinach seed sowing and harvesting in perlite.....	
2.5 Post-harvest handling and measurement.....	
2.6 Chloroplast extraction and storage.....	
2.7 Analysis of spinach plant iron concentration.....	
2.7.1 Mineral acid digestion of plant material and dilutions.....	
2.7.2 Microwave digestion of plant material.....	
2.7.3 Nitric reflux digestion of organic samples.....	
2.7.4 Injecting digestion samples into ICP-MS.....	
2.8 Preliminary experiment – measurement of photosynthetic pigments in commercial spinach lipid extracts.....	

Chapter 3: Growing spinach plants under controlled conditions to measure systemic Fe uptake

3.1 Introduction.....	
3.2 Results and Discussion.....	
3.2.1 Scoping a range of spinach-growing methods and locations on Sutton Bonington Campus.....	

- 3.2.2 Effect of selected growth conditions on perlite spinach leaf surface areas (SAs).....
- 3.2.2.1 Spinach grown in the glasshouse facilities.....
 - 3.2.2.1.1 Surface areas (SAs) of spinach leaves grown on compost in the glasshouse.....
 - 3.2.2.1.2 Surface areas (SAs) of spinach leaves grown on rockwool hydroponics in the glasshouse.....
- 3.2.2.2 Spinach grown in the growth room facilities.....
 - 3.2.2.2.1 Surface areas (SAs) of spinach leaves grown on compost in the growth room.....
 - 3.2.2.2.1 Surface areas (SAs) of spinach leaves grown on rockwool in the growth room.....
- 3.3 Effect of growth conditions on the yields of spinach leaves.....
- 3.4 Finalising the growth conditions of spinach plants for this project.....
- 3.5 Post-harvest treatment of spinach plants.....
 - 3.5.1 Effect of NaFe-EDTA concentrations on the yield of spinach roots and leaves.....
 - 3.5.1.1 Dosing trials with different Fe concentrations in Hoagland nutrient solution.....
 - 3.5.1.2 Dosing trials of spinach plants within the toxicity range.....
 - 3.5.1.3 Observations for spinach plants in the deficiency range.....
- 3.6 Iron distribution in spinach roots and leaves.....
- 3.7 Iron isotope enrichment trials.....

3.6.1 Preparation of Hoagland solution containing ^{57}Fe

3.8 Conclusions.....

Chapter 4: Mathematical modelling of spinach plant Fe uptake kinetics.....

4.1.1 Introduction to modelling and ordinary differential equations (ODEs).....

4.1.1.1 ODE for growth matrix.....

4.1.1.2 ODE for roots.....

4.1.1.3 ODE for stem + leaf.....

4.1.1.4 Initial conditions of Fe in each domain.....

4.2 Materials and methods

4.2.1 Growing spinach after dosing with different external NaFe-EDTA concentrations in Hoagland solution.....

4.2.2 Measuring Fe contents in leaves and roots.....

4.3 Results and Discussion

4.3.1 Initial DWs per plant part.....

4.3.2 Fe concentrations in spinach root and leaf material.....

4.3.3 Fe contents in spinach root and leaf material.....

4.3.4 Residual Fe contents in the spinach growth matrix.....

4.3.5 Percentage of plant Fe in spinach leaf and root material.....

4.4 The impact of iron dosing on the content of other minerals in spinach leaf and root material.....

4.4.1 Magnesium.....

4.4.2 Zinc.....

4.4.3 Copper.....

4.4.4 Potassium.....

4.5 The Bayesian approach for estimating unknown parameters from the data.....

4.5.1 Introduction to Bayesian statistics and Markov Chain Monte Carlo (MCMC) method.....

4.5.2 Explaining the likelihood function.....

- 4.5.3 Prior distributions of unknown parameters.....
- 4.5.4 The Gamma distribution.....
- 4.5.5 The uniform distribution.....
- 4.5.6 Markov Chain Monte Carlo (MCMC) algorithm.....
- 4.5.7 Using Python software for mathematical modelling.....
- 4.5.8 ODE modelling simulation outputs.....
- 4.6 Discussion and evaluation.....
- 4.7 Conclusions.....

- Chapter 5: Tracing iron distribution in spinach leaves and the bioaccessibility of different iron forms in the WLM and CRF.....**
- 5.1 Introduction to bioaccessibility, bioavailability and bioactivity from plant-based food sources.....
- 5.2 Materials and methods.....
 - 5.2.1 CRF preparation from commercial spinach leaves – juicing procedure.....
 - 5.2.1.1 Leaf pre-treatment and preparation.....
 - 5.2.1.2 Heat treatment.....
 - 5.2.1.3 CRF isolation.....
 - 5.2.1.4 Pre-digestion sample preparation.....
 - 5.2.2 Static in vitro digestion procedure.....
 - 5.2.2.1 Pre-digestion preparation.....
 - 5.2.2.2 In vitro digestion.....
 - 5.2.2.3 Dialysability procedure.....
 - 5.2.2.4 Post-digestion fractionation.....
 - 5.2.3 Mineral analysis.....
 - 5.2.3.1 Sample preparation with microwave acid digestion.....
 - 5.2.3.2 Injecting digestion samples into ICP-MS.....
 - 5.2.4 Final calculations – dialysability and solubility.....
 - 5.2.5 Statistical analysis.....

5.3 Results and discussion.....	
5.3.1 The distribution of Fe after fractionating spinach leaves with an extrusion juicer.....	
5.3.2 The distribution of chloroplast marker-pigments after fractionating spinach leaves with an extrusion juicer.....	
5.3.3 Key pigments distribution between CRF and juice from fresh and HT leaves.....	
5.3.4 Observations during CRF isolation and in-vitro digestion.....	
5.3.5 Protocol optimisation.....	
5.3.5.1 The impact on ⁵⁷ Fe dialysability from the addition of oil, ascorbic acid and gastric pH alterations.....	
5.3.5.2 Iron bioaccessibility of different spinach leaf treatments.....	
5.3.5.3 Iron bioaccessibility using CRF materials labelled with ⁵⁷ Fe.....	
5.4 Limitations and further study suggestions.....	
5.5 Conclusions.....	
6.0 Grand discussion.....	
6.1 Introduction.....	
6.2 Methodology.....	
6.3 Mathematical modelling.....	
6.4 Bioaccessibility and in-vitro digestion.....	
7.0 Grand conclusions	
8.0 References.....	
9.0 Appendices.....	
Appendix 1.....	
Appendix 2.....	
Appendix 3.....	
Appendix 4.....	
Appendix 5.....	

Abstract

Iron (Fe) is one of the most essential micronutrient minerals for human health such that it forms part of enzymes synthesising amino acids, hormones, neurotransmitters and collagen. It is also utilised for production of respiratory pigments including haemoglobin and myoglobin. Fe-deficiency is one of the most prevalent global micronutrient deficiencies and affects one-third of the global population, with anaemia being the key symptom.

This project aimed to map the flow of Fe from the growth matrix to the human digestive system via chloroplasts of spinach plants. A novel Hoagland nutrient solution containing all essential nutrients was produced in the laboratory and supplied to the spinach plants. Plants were grown in hydroponic system on perlite, under controlled conditions in a growing room. Once at maturity, they were harvested for experiments including in-vitro digestion and bioaccessibility of spinach chloroplast rich fractions (CRFs).

In subsequent experiments, spinach plants were dosed with seven distinct external Na Fe-EDTA solution concentrations; 10, 25, 50, 75, 100, 150 and 200 μM of Fe. This process proved the variability of growth indicators including Fe contents per plant part, and DWs during the observed growth periods. A typical method used to model the dynamically changing quantities is the application of Ordinary Differential Equations (ODEs). The modelling work showed that Fe toxicity limits and C_{max} (maximum rate of uptake) were never reached within this concentration range. Moreover, the maximum yields and Fe contents for both root and stem material were reached after dosing with 50, 75 up to 100 μM Fe in feed solution. However, at higher dosing concentrations of

Fe (150 and 200 μM Fe), internal concentrations of Fe, in both leaves and roots were higher but the yield represented by dry weight of leaves was lower. This indicates that the toxicity limits might have been reached based on the morphological observation at 150 and 200 μM Fe in solution, and the roots experienced Fe stress. Finally, the Markov Chain Monte Carlo (MCMC), is the most effective way in determining the posterior distribution, which in turn compares the actual data to any given model.

The digestion work showed that the bioaccessibility of Fe from powdered leaf material was higher than the CRF as a percentage of initial iron content. However, as an absolute amount, the bioaccessible iron from CRF, either heated or fresh, was significantly higher than that in leaves. This finding was further supported by the use of CRF materials which has been labelled with ^{57}Fe . The bioaccessibility of ^{57}Fe using the same in-vitro digestion model followed by dialysability method showed no significant differences in the bioaccessibility of ^{57}Fe and total Fe in both FCRF and HTCRF. However, the absolute amount of bioaccessible ^{57}Fe and total Fe was significantly higher in FCRF than HTCRF. Overall, this work proved the possibility of using a hydroponic system to maximise the iron content inside spinach leaves up to 300 mg/kg of dry weight. With the help of ascorbic acid addition, about 4.5% of this Fe can be bioaccessible for human consumption once consumed as fresh leaves. Heat treatment does reduce this bioaccessibility to 3.6%. Isolating the chloroplasts rich fraction can provide an iron dense material (up to 4 times higher than the leaves materials) which can give 1.6% of its Fe content as bioaccessible iron in case of soil grown spinach and about 6% of this Fe using hydroponically grown spinach.

Acknowledgements

I would like to first express my immense gratitude to Prof. David Gray, Prof. Liz Bailey, Prof. Dov Stekel from the University of Nottingham for their valuable supervision and continuous support during my journey of completing this MPhil degree. Without your guidance and constant support, this thesis would not have been successful. I would like to thank you all for encouraging my research and preparing me for my future career path. Furthermore, I also would like to thank Dr. Anastasia Kadochnikova for providing us with extra assistance with the mathematical modelling component and undertaking additional mathematical modelling for us.

I also would like to thank Dr. Randa Darwish, Dr. Mohamed A. Gedi, and the technical staff in the UoN Food Sciences Department including Dr. Khatija Nawaz-Hussain and Darrell Cobon, for all the additional support during my laboratory work stage. Owing to my diagnosis of Asperger's Syndrome, I would like to offer my foremost gratitude to Randa Darwish and Mohamed A. Gedi for forming my support bubble during the Coronavirus (COVID-19) pandemic.

I would like to say a special thanks to Dr. Saul Vasquez-Reina and Lolita Wilson for their assistance with sample digestion and Inductively Coupled Plasma-Mass Spectroscopy (ICP-MS) analysis, and to Richard Argent for offering us the licence to use the laboratory facilities in a safe and secure manner, especially at the height of COVID-19. I would also like to say a special thanks to Sue Flint and Mark Meacham for offering us the growth room facilities and enough perlite material for the spinach plants to grow.

I also want to say a special thanks to PhD student, Mohammadamin Aliyari for being a great friend and brother to me, during my final year, and making my stay in Nottingham more enjoyable. Finally, I also greatly acknowledge my family for funding my degree together with my friends and support team including Jenifer Shahin, Juan Gonzalez, John Saba and Shawn McGill with providing me with all the necessary support psychologically and mentally during my candidature, especially during my most sensitive phases.

List of tables

Chapter 1: Introduction

Tables 1.1A—C: Concentrations (per 100 g FW) of macro and micronutrients of various raw green leafy vegetables (GLVs) A) macronutrients, B) minerals and C) vitamins. * represents 100 g per unit dry weight (DW).....

Chapter 2: General materials and methods

Table 2.1: Modified Hoagland nutrient solution macro and micronutrient details (for Total Fe) for 2L.....

Table 2.2: Optimal growth parameters for hydroponic spinach germination.....
.....

Chapter 3: Growing spinach plants under controlled conditions to measure systemic Fe and ⁵⁷Fe uptake.

Chapter 4: Mathematical modelling of spinach plant Fe uptake kinetics

Tables 4.1A—D: Sample statistics of the estimated values from Equations 5B—C, for all dosing concentrations.....

Tables 4.2A—C: Sample statistics of the estimated values from Equations 14A—B, for all dosing concentrations.....

Tables 4.3A—B: Sample statistics of the estimated values from Equation 15A—B, for all dosing concentrations.....

Tables 4.4A—B: Sample statistics of the estimated values from Equation 16A—B, for all dosing concentrations.....

Table 4.5: Sample statistics of r_{MR} values inferred from subsets of dosing concentrations of 10—75 and 100—200 μM Na Fe-EDTA in solution.....

Table 4.6: Sample statistics of r_{RL} values inferred from subsets of dosing concentrations of 10—75 and 100—200 μM Na Fe-EDTA in solution.....

Chapter 5: Tracing iron distribution in spinach leaves and the bioaccessibility of iron in Whole Leaf Material (WLM) vs Chloroplast Rich Fraction (CRF)

Table 5.1: Percentage mass distribution and ^{57}Fe distribution from 1kg raw perlite spinach leaves (on a DW basis); both fresh and HT, between the main leaf fractions; juice, fibre and foam.....

Table 5.2: Mass (g/DW) and percentage mass (% DW) of fresh and HT CRF recovered from juice fraction, total ^{57}Fe from juice to CRF and total ^{57}Fe in recovered CRF (mg/kg DW) and percentage ^{57}Fe recovered from 1kg of fresh leaves.....

List of figures

Chapter 1: Introduction

Figure 1.1: How iron (Fe) enters the human body.....

Figure 1.2: Schematic diagram on human dietary iron (Fe) intestinal epithelial uptake and transportation.....

Figure 1.3: Schematic representation of Strategy I plants' (non-graminaceous) Fe uptake from the soil environment.....

Figure 1.4: Schematic representation of Strategy II plants' (graminaceous) Fe uptake from the soil environment.....

Figure 1.5: Schematic overview of the iron (Fe) pathway, translocation and storage mechanisms from the roots to leaves – different valence forms also acknowledged...

Figure 1.6: Labelled cross-sectional diagram of the chloroplast organelle.....

Figure 1.7: Photosynthetic light-dependent reactions in chloroplast thylakoids, involving Photosystem I and II.....

Figure 1.8: Overview of Arabidopsis and Strategy I plant chloroplast ion transporters/channels and their mechanisms.....

Chapter 2: General materials and methods

Figure 2.1: Growth room perlite spinach setup.....

Figure 2.2 Rinsing spinach root and leaf material in 600 mL beakers followed by blotting them dry on tissues.....

Figure 2.3: Flowchart of Tesco spinach leaf fractionation procedure.....

Figures 2.4A—B: Two distinct mineral acid digestion methods; 2.4A) microwave oven and B) nitric reflux digestion.....

Chapter 3: Growing spinach plants under controlled conditions to measure systemic total Fe and ⁵⁷Fe uptake

Figure 3.1: The Nutrient Film Technique (NFT).....

Figures 3.2A—F: Visual representations, after scoping various growth matrices and locations for spinach growth, across the SB campus.....

Figure 3.3: Leaf SAs (in cm²/pot) of *Trombone F1* spinach grown on compost in a glasshouse, from Days 19—36 of growth.....

Figure 3.4: Leaf SAs (in cm²/cube) of *Trombone F1* spinach grown on rockwool in a glasshouse, from Days 19—36 of growth.....

Figure 3.5: Leaf SAs (in cm²/pot) of *Trombone F1* spinach grown on compost in the growth room, from Days 15—35 of growth.....

Figure 3.6: Leaf SAs (in cm²/cube) of spinach grown on rockwool, in the growth room, from Days 29—55 of growth.....

Figures 3.7A—B: 3.7A) FWs and B) DWs of cultivated *Trombone F1* spinach leaves in different growth environments; varying locations and matrices.....

Figures 3.8A—D: Stagnated process of *Trombone F1* spinach seed germination and growth in the growth room, using perlite and Hoagland nutrient solution.....

Figures 3.9A—B: FW and B) DWs per plant of perlite-sown *Trombone F1* spinach, grown in the growth room, after dosing with 3.10A) 5, B) 25, C) 50, D) 100, E) 150 and F) 200 μM Na Fe-EDTA in Hoagland nutrient solution.....

Figures 3.10A—F: Comparisons of leaf morphologies of perlite-sown *Trombone F1* spinach, grown in the growth room, after dosing with 3.10A) 5, B) 25, C) 50, D) 100, E) 150 and F) 200 μM Na Fe-EDTA in Hoagland nutrient solution.....

Figure 3.11: Plant morphology of perlite-sown *Trombone F1* spinach grown in the growth room facilities, after dosing with 400 μM Na Fe-EDTA, in Hoagland nutrient solution.....

Figure 3.12: Root and leaf concentrations of Fe for *Trombone F1* spinach plants grown in the growth room, after dosing with six external concentrations of Na Fe- EDTA in Hoagland nutrient solution.....

Figure 3.13: True ⁵⁷Fe/total Fe ratios for CRF, roots, WLM and tomato leaf CRM for

Chapter 4: Mathematical modelling of spinach plant Fe uptake kinetics

Figure 4.1: Visual representation of plant parts of perlite spinach grown in the growth room.....

Figures 4.2—4.3: Average DW values of perlite spinach 4.2) root and 4.3) leaf material, per plant, after dosing with 10, 25, 50, 75, 100, 150 and 200 μM Na Fe- EDTA in solution.....

Figures 4.4A—B: Spinach 4.4A) leaf and B) root Fe concentrations, after dosing with 10, 25, 50, 75, 100, 150 and 200 μM Na Fe-EDTA in solution.....

Figure 4.4C—D: Linear regression analysis for slope values for spinach leaf and root Fe concentrations, after dosing with 10, 25, 50, 75, 100, 150 and 200 μM NaFe-EDTA in solution. R^2 and p-values shown.....

Figure 4.5A—B: Average Fe contents of spinach 4.5A) root and B) leaf material (in mg Fe/plant part), in one plant, on the last 21 days of growth (starting from Day 0) after dosing with 10, 25, 50, 75, 100, 150 and 200 μM Na Fe-EDTA in solution.....

Figure 4.5C—D: Linear regression analysis for slope values for spinach leaf and root Fe contents, after dosing with 10, 25, 50, 75, 100, 150 and 200 μM NaFe-EDTA in solution. R^2 and p-values shown.....

Figure 4.6: Residual Fe contents in the perlite spinach growth matrix (in mg Fe/compartment), on the last 21 days of growth (starting from Day 0) after dosing with 10, 25, 50, 75, 100, 150 and 200 μM Na Fe-EDTA in solution.....

Figures 4.7A—B: Percentage of total plant Fe in spinach 4.7A) leaf and B) root material, on the last 21 days of growth (starting from Day 0) after dosing with 10, 25, 50, 75, 100, 150 and 200 μM Na Fe-EDTA in solution.....

Figures 4.8A—B: Average Mg contents of spinach 4.8A) root and B) leaf material (in mg Mg/plant part), on the last 21 days of growth (starting from Day 0) after dosing with 10, 25, 50, 75, 100, 150 and 200 μM Na Fe-EDTA in solution.....

Figures 4.9A—B: Average Zn contents of spinach 4.9A) root and B) leaf material (in mg Mg/plant part), on the last 21 days of growth (starting from Day 0) after dosing with 10, 25, 50, 75, 100, 150 and 200 μM Na Fe-EDTA in solution.....

Figures 4.10A—B: Average Cu contents of spinach 4.10A) root and B) leaf material (in mg Cu/plant part), on the last 21 days of growth (starting from Day 0) after dosing with 10, 25, 50, 75, 100, 150 and 200 μM Na Fe-EDTA in solution.....

Figures 4.11A—B: Average K contents of spinach 27A) root and B) leaf material (in mg K/plant part), on the last 21 days of growth (starting from Day 0) after dosing with 10, 25, 50, 75, 100, 150 and 200 μM Na Fe-EDTA in solution.....

Figure 4.12A: Assumed prior distributions of the unknown parameters, θ , of the ODEs in Equations 7A – C.....

Figure 4.12B: Assumed prior distributions on the modelling error variance, σ^2 , and the initial Fe contents from each domain, $x(\mathbf{0})$, based on Equation 7D.....

Figure 4.13: Sample representation of the Anaconda Python Spyder simulation software with model code notation inputted and model run in the Output console.....

Figure 4.14: Cubic B-spline interpolation function of perlite spinach root DWs and growth matrix Fe contents, after dosing with all seven Na Fe-EDTA concentrations.....

Figure 4.15: Contour plot of posterior distributions of Equations 5B—C after dosing with 100 μM Na Fe-EDTA in solution – variable decay rate.....

Figure 4.16: Cubic B-spline function of root (left column) and leaf (right column) growth rates, after dosing with all seven Na Fe-EDTA concentrations.....

Figures 4.17A—B: Modelling output corresponding to the 500 samples and the posterior mean from Equations 13A—B, after dosing with 4.17A)10 and B)100 μM Na Fe-EDTA in solution.....

Figure 4.18: Contour plot of posterior distributions of Equations 14A—B after dosing with 100 μM Na Fe-EDTA in solution – minimal Fe content in the growth matrix.....

Figures 4.19A—B: Modelling output corresponding to the 500 samples and the posterior mean from Equations 14A—B, after dosing with 4.19A)10 and B)100 μM Na Fe-EDTA in solution.....

Figure 4.20: Contour plot of the posterior distributions of Equations 15A—B after dosing with 100 μM Na Fe-EDTA in solution – no inhibition of Fe uptake.....

Figures 4.21A—B: Modelling output corresponding to the 500 samples and MCMC posterior mean, from Equations 15A—B, after dosing with 4.21A)10 and B) 100 μ M Na Fe-EDTA in solution.....

Figures 4.22A—B: Modelling output represented by Equation 15, fitted to the data after dosing with 10—75 μ M Na Fe-EDTA in solution.....

Figures 4.23A—B: Modelling output represented by Equation 15, fitted to the data after dosing with 100—200 μ M Na Fe-EDTA in solution.....

Chapter 5: Tracing iron distribution in spinach leaves and the bioaccessibility of iron in Whole Leaf Material (WLM) vs Chloroplast Rich Material (CRM)

Figure 5.1: Flowchart of CRF preparation via juicing for heat-treated (HT) and fresh CRF, and untreated samples from WLM.....

Figure 5.2: Overview of the four key stages, timings and volumes used during *in vitro* digestion.....

Figure 5.3: Fe concentrations of chloroplast-marker pigments (mg/g DW) of five fractionated components of Tesco spinach leaves.....

Figure 5.4: Concentrations of chloroplast-marker pigments (mg/g DW) of five fractionated components of Tesco spinach leaves.....

Figure 5.5: Flowchart illustrating the process and distribution of Fe in three main spinach leaf fractions collected.....

Figure 5.6: Images of the colour differences between fresh (F) and heat-treated (HT) samples left to right.....

Figure 5.7: Enzyme-only digestate showing coagulation of proteins when adding HCl to adjust the pH.....

Figure 5.8: Light micrographs of spinach material before and after *in vitro* digestion.....

Figure 5.9: Flowchart illustrating the process and distribution of ⁵⁷Fe in the three main fractions collected.....

Figures 5.10A—D: Mean 5A) Mg Fe in 0.5g samples, B) dialysability (%), C) dialysable (%) and D) soluble (%) Fe of fresh chloroplast rich fraction (FCRF), heat-treated chloroplast rich fraction (HCRF), incubated chloroplast rich fraction (ICRF), fresh whole leaf material (FWL) and heat-treated whole leaf material (HTWLM).....

List of equations

Equation 1: Balanced chemical equation for photosynthesis.....

Equation 2: Moisture content.....

Equation 3: Standard error of the mean (SEM).....

Equations 4A – D: Chlorophyll-a, chlorophyll-b, total chlorophyll and carotenoid concentrations.....

Equation 5: Percentage localisation of pigments.....

Equations 6A – C: BCFs in roots, stems, leaves and CRF.....

Equations 7A – B: TFs from 7A) roots to leaves and B) leaves to CRF.....

Equation 8: Example calculation on determining the weight of Na Fe-EDTA for 75 μ M Fe.....

Equation 9: Calculation of total plant DWs and FWs (in g).....

Equations 10A – D: ODEs for growth matrix, roots, stems and WLM.....

Equation 11: Calculation of final Fe content (in μ g Fe/plant) in plant tissues given Fe concentrations and DW.....

Equation 12: Indirect calculation of final Fe concentrations in perlite growth matrix.....

Equation 13: General Bayesian theorem.....

Equation 14: Calculation of the Bayesian posterior distribution.....

Equation 15: Multivariate distributions.....

List of abbreviations and chemical compounds

- **ABA** – Abscisic Acid
- **ANOVA** – Analysis of Variance
- **ATP** – Adenosine Triphosphate
- **BCF** – Bioconcentration Factor
- **CRF** – Chloroplast Rich Fraction
- **DW** – Dry Weight
- **EDTA** – Ethylene Diamine Tetraacetic Acid
- **FW** – Fresh Weight
- **ICP-MS** – Inductively Coupled Plasma-Mass Spectrometry
- **IVD** – In-Vitro Digestion
- **MCMC** – Markov Chain Monte Carlo
- **MES** – 2-(N-morpholino) ethane sulphonic acid
- **ODE (s)** – Ordinary Differential Equation (s)
- **PDE (s)** – Partial Differential Equation (s)
- **PIC1** – Permease in Chloroplast 1
- **PSI** – Photosystem 1
- **PSII** – Photosystem 2
- **RGE** – Rabbit Gastric Extract
- **RO** – Reverse Osmotic
- **RCF** – Relative Centrifugal Force
- **RDV** – Recommended Daily Value
- **RPM** – Revolutions Per Minute
- **SA** – Surface Area
- **SSF** – Simulated Salivary Fluid
- **SGF** – Simulated Gastric Fluid
- **SIF** – Simulated Intestinal Fluid
- **TAME** – p-toluene-sulphonyl-L-arginine methyl ester
- **TEM** – Transmission Electron Microscopy
- **TF** – Transfer Factor
- **WLM** – Whole Leaf Material
- **WHO** – World Health Organisation
- **UoN** – University of Nottingham

1.0 Introduction

1.1 General introduction to iron and its importance

Humans require at least 22 elements for their growth, well-being, and development (White & Broadley, 2009). Iron is the 26th element on the Periodic Table with an atomic mass of roughly 55.85 (Dasa & Abera, 2018).

Iron has an essential biological role in a wide range of metabolic processes and is thus a vital component for all living organisms (Abbaspour *et al.*, 2014 Roschztardt *et al.*, 2013). It is an example of a micronutrient, because compared to macronutrients like carbohydrates, protein, and fat, it is needed in smaller amounts, and is generally less than 0.005% of total body mass. In excess, micronutrients have negative effects on human health (Brown and Ford, 2008).

Iron is an important constituent of macromolecules involved in the synthesis of nucleotides, chlorophyll and enzymes. It is also a crucial element in some vital biological processes such as respiration and photosynthesis, where it participates in electron transfer through reversible redox reactions, alternating between ferrous (II) Fe^{2+} and ferric (III) Fe^{3+} (Roschztardt *et al.*, 2013). The Italian scientist, Antonio Menghini (1704—1759) was the first to ascertain that blood Fe is concentrated in red corpuscles. Although this discovery predated that of haemoglobin, it is more logical to first determine what makes blood red, before understanding the composition of this blood material. This discovery was communicated to the Academy of Sciences of the Bologna Institute in 1746, which led to samples of blood from mammals, birds, fish and humans being examined for iron content (Sheftel *et al.*, 2012).

Nearly 2 billion people suffer from deficiencies of essential trace elements or micronutrients (Şimşek & Çelik, 2021). The mineral elements most commonly lacking in human diets are iron, zinc, copper, magnesium, iodine, and selenium (White & Broadley, 2009). The WHO considers anaemia to be one of the top 10 global health priorities which affects around 25% of global population, with half of that figure resulting from Fe deficiency anaemia (IDA) (McLean *et al.*, 2009). According to the WHO, this issue is most acute in children, pregnant and childbearing women with an estimation of 42% of children less than 5 years old and 40% of pregnant women worldwide suffering from Fe deficiency anaemia (McLean *et al.*, 2009).

There are two main Fe forms in nature and present in the human diet; haem and non-haem. Both forms have a major influence on uptake and fate in the body. Non-haem Fe is the major form of Fe found in plant-based food, accounting for 80—90% of Fe in standard diets (Carpenter & Mahoney, 1992); (Hallberg, 1981). However, 9% of the total leaf Fe, exists as haem Fe. Non-haem Fe proteins contain about 19% of total Fe and are found in the ferredoxin, thylakoids and mitochondrial complexes. Chlorophyll-a and b are an indirect measure of ferredoxin activity in chloroplast thylakoids. For example, in Fe-stressed citrus leaves, the lower ferredoxin content resulted in lower chlorophyll content (Miller *et al.*, 1995). Haem Fe representing the remaining 10—20% is largely derived from haemoglobin and myoglobin from animal sources. Haem Fe is more efficiently absorbed than non-haem Fe. Although there is adequate uptake of Fe from animal sources, most of the global population depends upon diets of plant origin. Because of the vital role of Fe in many biological functions, many eukaryotic organisms including humans have developed mechanisms of adapting to Fe deficiency. Many of the adaptive mechanisms to Fe deficiency found in lower prokaryotic organisms have

similar counterparts in higher eukaryotic organisms, including plants and humans (Anderson *et al.*, 2005).

1.2 Iron uptake and distribution in humans.

In the human body, Fe is primarily found bound to proteins such as haemoglobin, myoglobin, or to non-haem compounds such as transferrin, and ferritin. Of this bodily Fe, almost 65% is in the haemoglobin present in red blood cells, and 25% exists as mobilisable ferritin. The remaining 15% is present in other components such as myoglobin in muscle tissue, and in a variety of enzymes involved in oxidative metabolism and other cellular functions (Trumbo *et al.*, 2001).

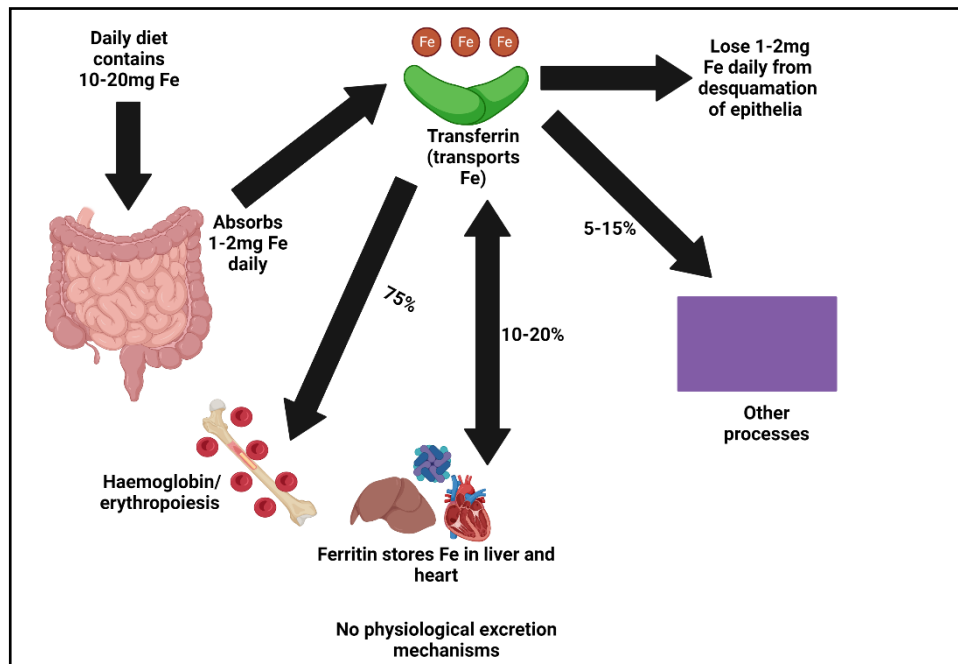


Figure 1.1: Schematic diagram of Fe transfer in the human body – adapted from Abbaspour *et al.* (2014).

Fe is conserved in the body by being recycled as illustrated in Figure 1.1. It is first absorbed by the intestinal enterocytes and reticuloendothelial macrophages and then into the plasma. Once captured by a transferrin transporter, Fe finally gets delivered to tissues. The binding of Fe-laden transferrin to the cell-surface Transferrin Receptor 1 (TFR1) results in endocytosis and uptake of the metal cargo. Internalised Fe is transported to the mitochondria of intestinal tissues for the synthesis of haem or Fe-sulphur clusters, which are fundamental parts of several metalloproteins, and excess Fe is stored and detoxified in cytosolic ferritin. Once Fe is absorbed, there are no physiological mechanisms for excretion of excess Fe from the body, except by blood loss, often through pregnancy and menstruation (Abbaspour *et al.*, 2014). Finally, 1—2 mg of Fe gets lost per day from the skins and enteric desquamation and minor blood losses (Abbaspour *et al.*, 2014).

Following Fe-deficiency, a feedback mechanism exists that enhances Fe absorption. In contrast, people with Fe surplus control Fe absorption via hepcidin transporters. It is now generally accepted that Fe absorption is controlled by ferroportin which sometimes allows transport of Fe from the mucosal cell into the plasma. Dietary haem can also be transported across the apical membrane by a yet unknown mechanism and subsequently gets metabolised in the enterocytes by Haem Oxygenase 1 (HO-1) to liberate Fe²⁺. This process is more efficient than the absorption of inorganic Fe and is independent of duodenal pH. It is thus not influenced by inhibitors such as phytate and polyphenols. Consequently, red meats high in haemoglobin are excellent nutritional sources of Fe (Abbaspour *et al.*, 2014). Haem Fe is always readily bioavailable for target tissues and gets absorbed as an intact metalloporphyrin ring which is less influenced by luminal ligands which render the non-haem Fe less bioavailable. This has been a key contributor to global Fe anaemia.

1.2.1 Summary of iron release and uptake in the human digestive system

For Fe to be bioavailable, it must first become bioaccessible. Several parameters including the food matrix, Fe valence forms such as ferric (Fe^{3+}) versus ferrous (Fe^{2+}), pH, and Fe uptake promoting or inhibiting complexes, all have a major influence on Fe bioaccessibility. Detailed discussions on these factors are provided in Chapter 5.

In the gastric phase, limited uptake of certain minerals like Cu^{2+} occurs, with the bulk of elemental uptake, Fe^{2+} included, occurring in the upper portion of the small intestine, known as the duodenum (Gulec *et al.*, 2014). As the bolus passes from the stomach, the fasting pH is lowered from neutral 7.0 to around 5.5, thus favouring elemental solubility. However, following a bicarbonate release by the pancreas, a gradual rise of pH back to 7.0 at the terminal ileum section occurs.

In the intestinal phase, haem Fe gets transported across the apical membrane of duodenal enterocytes via haem carrier protein 1 (HCP1) transporters and gets complexed in porphyrin rings before being released in the intestinal body in Fe labile form. Porphyrin rings are a group of organic compounds which bind most metals. The four nitrogen sections act as teeth, grabbing and bonding Fe^{2+} in the centre. With respect to non-haem Fe, ferric Fe^{3+} gets reduced to ferrous Fe^{2+} by duodenal cytochrome-b (DCYTB) (Dasa and Abera, 2018; Gulec *et al.*, 2014; Li and Lan, 2017; Miert *et al.*, 2010). Reduced Fe^{2+} then gets absorbed into the duodenum, via divalent metal transporter 1 (DMT1) as the main intracellular storage haem protein. Intestinal non-haem Fe can get transported to other organs as well (Anderson *et al.*, 2005; Conrad and Umbreit, 2000). For example, excess Fe^{2+} is readily transported into the liver via hephaestin (HEPH) in the basolateral membrane. Haem-Fe gets transported

into the bloodstream via an oxidation reaction back to Fe³⁺ in ferroprotein 1 (FPR1) (Milman, 2020).

Compared to haem Fe, which is easily absorbable in the intestinal phase, bioaccessibility and bioavailability of non-haem Fe is more variable and is governed by promoters and inhibiting antinutrients of Fe uptake in the human diet. The fraction of Fe absorbed from the amount of plant-based food ingested is typically low but may range from 5% to 35% depending on circumstances and type of Fe (McDowell, 1992). Promoters include meat factors such as haemoglobin, β -carotene (provitamin A), ascorbic acid (Vitamin C), lactic acid, citric acid, certain organic and amino acids, and cysteine-rich polypeptides. For example, ascorbates and citrates form chelates to help solubilise haem Fe in the duodenum (Abbaspour *et al.*, 2014; White and Broadley, 2009). These also stimulate the absorption of essential mineral elements by the human alimentary canal. Iron fortification has also proven to be most effective when added with Vitamin C to cereal flours and dairy products (Brown and Ford, 2008).

Inhibitors include phytate/phytic acid, polyphenols, calcium and oxalate/oxalic acid (Figure 1.2) (Amagloh, 2017; Dasa and Abera, 2018; Li and Lan, 2017). In addition, transgenic approaches may be used to reduce the concentrations of antinutrients and increase the concentrations of promoter substances in the growth environment. This can either involve genetic manipulation or the application of mineral fertilisers to address the issue of malnutrition. For example, Fe-efficient varieties of soybean have been developed, which can tolerate Fe-deficient soils, which would otherwise not favour high yields (Hochmuth, 2011). Care must be taken to ensure that these approaches do not alter the appearance, taste, texture, cooking quality or other material properties of foods (White and Broadley, 2009).

1.3 Current global state of iron deficiency

Iron deficiency is believed to be directly related to adverse functional consequences with economic implications (Bermejo and García-López, 2009). For example, it has an impact on children’s psychomotor development as well as their cognitive abilities. Iron deficiency can be a result of either excessive loss of iron or decreased absorption (Bermejo and García-López, 2009). It can also result in brittle nails, fatigue and lowered immunity (Brown and Ford, 2008).

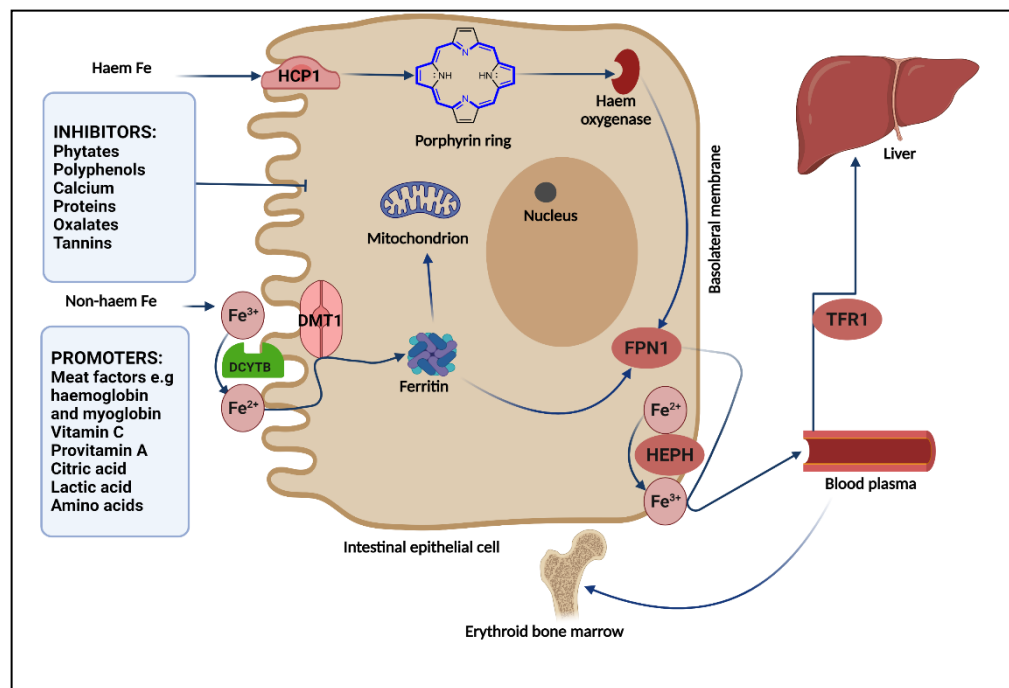


Figure 1.2: Schematic diagram on human dietary iron (Fe) intestinal uptake and transportation; HCP1: Haem Carrier Protein 1; DMT1: Divalent Metal Transporter 1; DCYTB: Duodenal Cytochrome B; HEPH: Hepaphaestin; FPN1: Ferroportin 1; TFR1: Transferrin 1 – Adapted from Gulec *et al.* (2016)

The WHO threshold for diagnosis of iron deficiency in adults is ferritin levels lower than 15 ng/mL, and levels lower than 12 ng/mL for children younger than the age of 5 (<30 ng/mL where inflammation is coexistent (WHO/UNICEF/UNU, 2001). Usually iron deficiency is characterised by 3 successive steps; iron store depletion, iron-deficient erythropoiesis, and eventually, iron-deficiency anaemia (IDA) (Stoltzfus, 2001).

Some primary causes of iron deficiency include deficient iron intake, digestive disorders, gastric ulcers, reduced iron absorption, intestinal parasites, and inflammatory bowel disease (Bermejo and García-López, 2009). Anaemia is also associated with menstrual blood loss combined with mortality for both the mother and the baby, increasing rates of miscarriages and prematurity (Li and Lan, 2017).

The most common symptoms include bodily fatigue and lethargy, shortness of breath, heart palpitations, stunted growth, impaired immunity, and functional impairment. Around 50% of anaemia can be attributed to Fe deficiency conditions (Rodríguez-Ramiro *et al.*, 2019).

1.4 General benefits of Fe for plant nutrition

Fe is a vital micronutrient for plants. The ability of plants to absorb and store Fe in their edible tissues has a direct effect on human nutrition (Morrissey and Guerinot, 2009). Fe- deficiency hinders their normal growth and causes morphological symptoms. The main symptoms of all Fe-deficient plants are diminished respiratory abilities of plants, and interveinal chlorosis. This interveinal chlorosis often occurs in the youngest leaves, resulting in impaired photosynthesis rates necessary for optimum growth and development (Borowski, 2013; Wang *et al.*, 2022). This is also associated with Fe dependency for chlorophyll synthesis and other pigment protein complexes (Roschztardt *et al.*, 2013). Furthermore, Fe chlorosis is most common in arid and semi-arid regions. It can also be alleviated by foliar applications of FeSO₄ solution, to chlorotic tobacco leaves, which gradually result in further greening (Miller *et al.* 2015).

Wang *et al.*, (2022) reported the contents of nutrients ranging from ascorbic acid (Vitamin C), soluble protein and soluble sugar in leaves and stalks being significantly

reduced under Fe deficiency stress, however, the contents of cellulose and nitrate were increased. These promoters also impact the reduction of ferric Fe^{3+} to ferrous Fe^{2+} via the enzyme, Fe^{2+} reductase.

All plant species have evolved physiological, morphological and genetic mechanisms to regulate Fe uptake and homeostasis in order to supply amounts enough for optimal growth while preventing excess accumulation (Li and Lan, 2017). Chemically, organisms have developed specific mechanisms for Fe acquisition from the Fe-oxides (III): (1) protonation, (2) chelation and (3) reduction. Excess free Fe is harmful to living cells due to possible reactions with O_2 , producing harmful free Fe oxide radicals or Reactive Oxygen Species (ROS). This reaction is known as the Fenton reaction (*Abbaspour et al.*, 2014). Plants generally absorb Fe from the rhizosphere. Once Fe enters the plant roots, the apoplast plays the main role in storage after absorption (*Roschztardt et al.*, 2013). However, it plays very little role in supplying Fe at the onset of shoot deficiency (Hochmuth, 2011). However, some plants absorb Fe through their leaves after foliar spraying. For example, foliar spraying $250 \mu\text{g mL}^{-1}$ of ferrous sulphate (FeSO_4) is known to rapidly increase the chlorophyll-a and chlorophyll-b contents in tobacco leaves (*Miller et al.*, 1995).

In soil, Fe availability to plant roots is very low and strongly influenced by soil pH, redox potential, and organic matter (OM) content (Hochmuth, 2011). In aerobic or alkaline soil, Fe is predominantly oxidised and in the form of ferric oxides which are insoluble. Therefore, most plant Fe deficiency occurs in high pH soils, especially above pH 7.2 (Borowski, 2013). Since 30% of global soils are too alkaline or calcareous for optimal Fe uptake by roots, there has been thorough investigation on how plants cope with and respond to Fe deficiencies in these soils (*Wang et al.*, 2022; White and Broadley, 2009). Once soil pH is acidic, ferric oxides get reduced to free up the Fe^{3+} which then

become more soluble and thus bioavailable for root uptake. An increase of just one pH unit after 4 can provide a 99% decrease in Fe availability for plants (Krohling *et al.*, 2016). However, Hochmuth (2011) reported acidic soils sometimes leading to Fe deficiency, following antagonistic reactions of Mn.

Plant root systems operate similarly to tree branch systems. Therefore, when roots grow, they form sub-branches including primary and lateral, which are of smaller radii, and grow further to generate more sub-branches (Roose *et al.*, 2001).

Morphological changes in the roots as well as up-regulation of gene expression in the root regions involved in Fe uptake enables plants to cope with low Fe. Root layers can also detect responses to Fe deficiency. These results indicate that plants can detect the deficiency of soluble Fe and respond to it in the vasculature. Based on these epidermal changes, two strategies of Fe uptake by the roots have been identified in plants. First, the reduction-based strategy where Strategy I (non-graminaceous) plants reduce Fe^{3+} via a membrane-bound reductase and thus render it accessible for uptake by a Fe^{2+} transporter (Borowski, 2013). Second, Strategy II (graminaceous) is a chelation-based strategy seen in grasses, involving the secretion of phytosiderophores (PS), which readily bind Fe^{3+} into Fe-PS complexes which are then transported into the roots. Moreover, in soil culture there is a symbiosis interaction between some bacteria and fungi in the soil with plant roots to enhance the absorption of some nutrients and micronutrients. For example, the symbiosis of Arbuscular mycorrhizal fungi (AMF) facilitates iron absorption by enhancing the expression of phytosiderophores in plants root, which is an iron chelate (Rajapitamahuni *et al.*, 2023).

Sections 1.5.1 and 1.5.2 will expand on these two strategies in greater depth.

1.5 Strategy I and Strategy II plant responses/adaptations to iron deficiency

1.5.1 Strategy I – reduction-based strategy

Strategy I is a broad adaptation mechanism used by all higher plants except graminaceous grasses, which use Strategy II (see Figure 1.3). Model plants that have been used in research to investigate Strategy I include the common dicotyledonous plants, including *Arabidopsis thaliana*, *Lycopersicon esculentum* (tomato) and *Pisum sativum* (pea) (Hell and Stephan, 2003).

The mechanism and elements of this strategy have been well characterised in non-graminaceous species in response to Fe deficiency such as most herbaceous plants; Green Leafy Vegetables (GLVs), sunflowers, hops, strawberries, and oil crops. Figure 1.3 below illustrates the reduction strategy steps as characterised in *Arabidopsis*. The process starts within the roots once subject to Fe deficiency stress, through upregulation of expression of ATP synthase in root epidermis. These enzymes release protons into the rhizosphere which then lower the soil pH and hence make Fe more soluble/readily available.

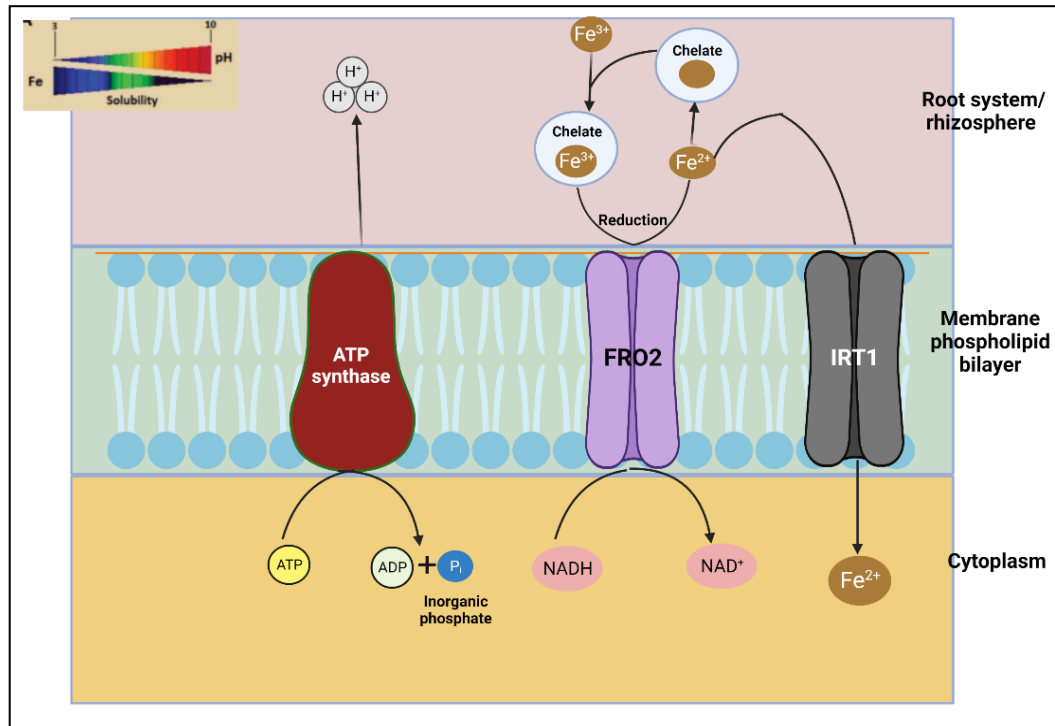


Figure 1.3: Schematic representation of Strategy I plants' (non-graminaceous) Fe uptake from the soil environment. Adapted from Krohling *et al.* (2016)

With the help of ferric chelate reductase FRO2, Fe^{3+} is then reduced to Fe^{2+} . The NADPH-dependent ferric chelate reductase, FRO2, donates an electron, to become NADH^+ across four haem groups, to Fe^{3+} in the rhizosphere to generate Fe^{2+} (Jain *et al.*, 2014; White and Broadley, 2009). However, different plants within this Strategy I category, show different responses to Fe deficiency stress. For example, cucumber and tomato plants engage in enlargement of their root tips and root hairs, which in turn excretes an abundance of H^+ , which then significantly enhance Fe^{3+} reduction to Fe^{2+} (Wang *et al.*, 2022).

In fact, the transgenic overexpression of ferric chelate reductases (reconstructed yeast ferric reductase) in roots of rice, tobacco and soybean has been successful in increasing tolerance to Fe-limiting conditions. Oki *et al.*, (2004) and Wang *et al.*, (2022) reported ethylene also playing a major role in the adaptive response to Fe

deficiency stress, in rice. However, further elucidation is required on its response to Fe deficiency in leafy vegetables including Chinese cabbage (Cai *et al.*, 2017).

Fe²⁺ is transported by the divalent metal transporter, IRT1 into root epidermis and once absorbed in the root epidermal cells, Fe gets translocated to the shoots through a vascular system.

1.5.2 Strategy II – chelation-based strategy

Strategy II graminaceous plants include all the major cereals, including wheat, maize, rice, barley, and oats that absorb the Fe²⁺ in the form of metal chelates (White and Broadley, 2009). These plants rely on soluble phytosiderophores (PS) with a high affinity for Fe³⁺ to obtain iron from the rhizosphere. The process starts with the synthesis of soluble metal chelator phytosiderophores (PS), with a high affinity for Fe³⁺ to obtain iron from the rhizosphere. They are derived from the mugineic acid (MA) family from L-methionine. They are composed of amino acids not found in proteins, representatives of the family of MA that include 2'-desoximugineic acid (DMA), 3-3-epihydroximugineic acid (epiHMA), and 3-epihydroxy-2'-deoxymugineic acid (epiHDMA), which all form stable compounds with Fe³⁺. PS molecules are released from Transporter of Mugenic Acid (TOM1), then PS chelates Fe³⁺, and this complex then gets transported to plant root material by Yellow Stripe 1 (YSL1) (see Figure 1.4). Yellow Stripe (YSL) transporters are also known to load and unload Fe²⁺ nicotianamine (Fe²⁺-NA) complexes into the phloem, for redistribution across the plant (White and Broadley, 2009).

The PS are released from the root epidermis via anionic channels or vesicles to the rhizosphere. The resulting Fe³⁺-PS complexes are readily transported into the root

epidermis via a high-affinity uptake system. The chelation strategy is less sensitive to pH than the reduction strategy, and there is a strong correlation between the number of PS released and resistance to Fe-limiting calcareous soils. There is also enough evidence that some graminaceous plants including rice contain the genes necessary for both Strategy I and II Fe acquisition simultaneously. However, there are quantitative differences in their number and qualitative differences in their structure and activity (White and Broadley, 2009). For example, rice is Strategy II, however it contains a Strategy I-like system where uptake of Fe^{2+} by IRT1 occurs. However, the reduction step via FROs has not yet been detected (Krohling *et al.*, 2016). Rice plants also produce Fe^{3+} -PS complexes, however at lower amounts compared with other graminaceous plants (Thomine and Lanquar, 2011).

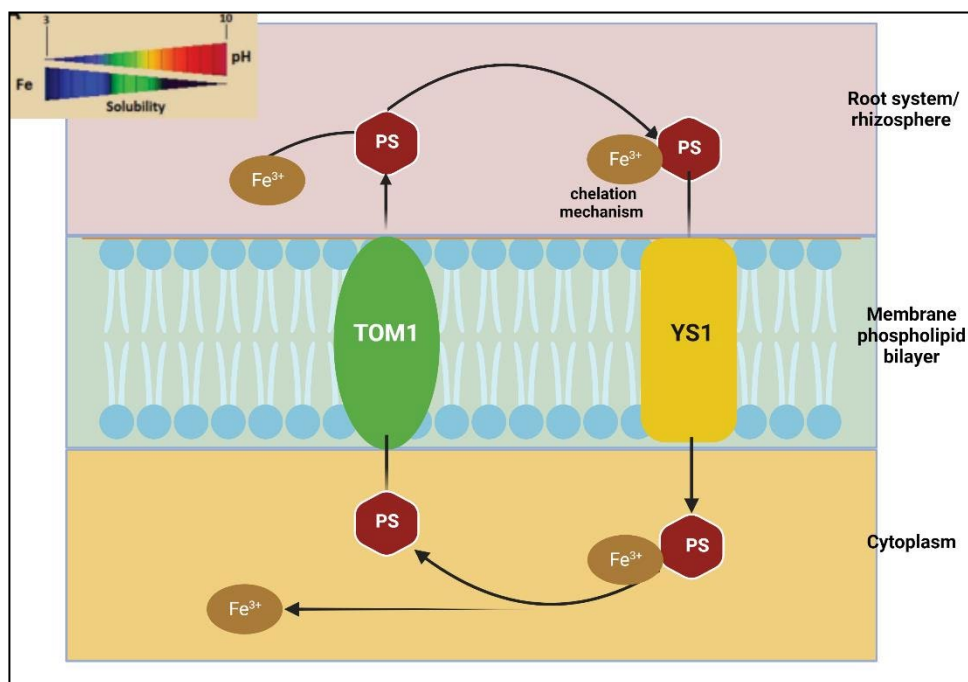


Figure 1.4: Schematic representation of Strategy II plants' (graminaceous) Fe uptake from the soil environment. Adapted from Krohling *et al.* (2016)

1.6 Plant responses and adaptations to iron toxicity

Damage by plant Fe toxicity in plant roots generally occurs, due to excessive accumulation. Fe precipitation reactions occur, forming a crust on the root surface. This Fe precipitation adsorbs these other elements strongly and prevents their uptake impermeable such as phosphorus (P), potassium (K) and zinc (Zn) (Liu *et al.*, 1998).

Morrissey and Guerinot, (2009) reported the importance of buffering mechanisms for Fe accumulation in *Arabidopsis* following poor root growth when toxic Fe concentrations were reached. Some generic examples of toxicity symptoms include leaf bronzing, necrosis, and dark roots (Li *et al.*, 2016). Cationic imbalance also promotes nutritional imbalances and loss of crop yields and quality in the long term (Li and Lan, 2017). Fe staining procedures have proven that in most Wild Type (WT) plants optimal Fe concentrations result in higher localisation in chloroplast vasculature (xylem and phloem) and excess concentrations generate high localisations in the mesophyll cells. Whether or not ferritins exist in these mesophyll cells requires further investigation (Roschztardt *et al.*, 2013).

1.6.1 Fate of absorbed iron inside plants

In both Strategy I (non-graminaceous) and Strategy II (graminaceous) plants, ferric Fe^{3+} gets transformed to the ferrous Fe^{2+} state (Lee *et al.*, 2016). This occurs in the root symplastic pathway connected to epidermal cells, eventually reaching the mesophyll layer (Malhotra *et al.*, 2020). Following this, the rest of the Fe regulatory pathway involves its translocation to organs such as leaves, seeds, xylem, phloem and target organelles, especially chloroplasts and mitochondria (see Figure 1.5). For example, within the xylem, Fe gets transported as Fe^{3+} citrate and it is loaded by Ferric Reductase Defective (FRD3) (White and Broadley, 2009).

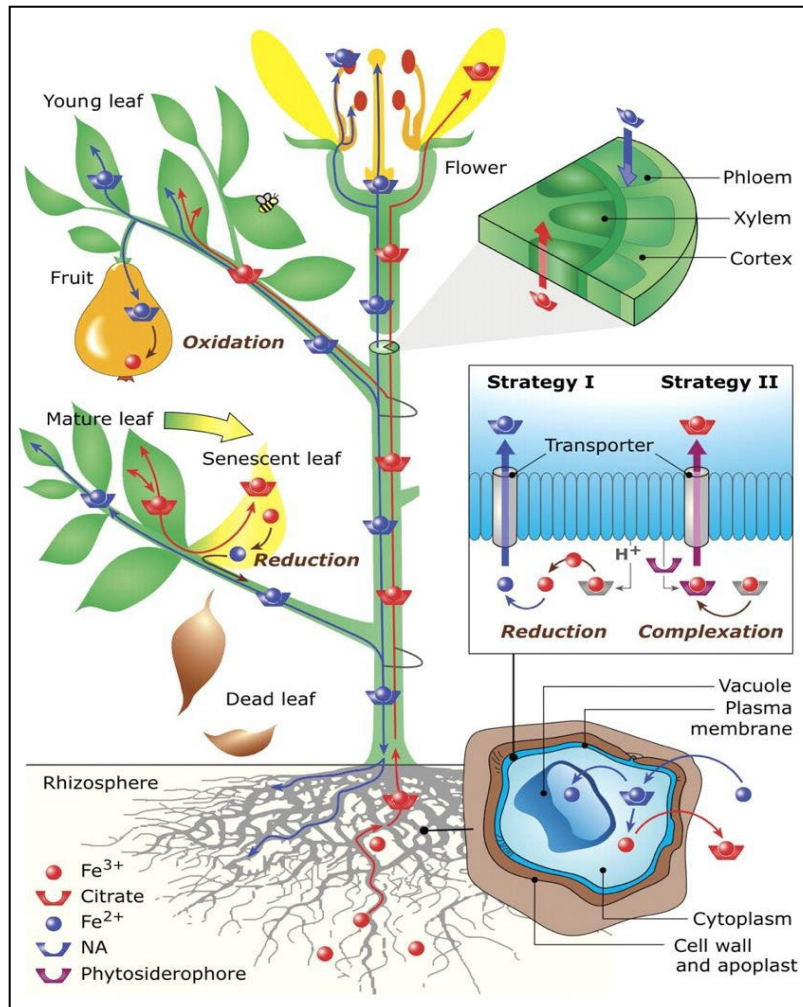


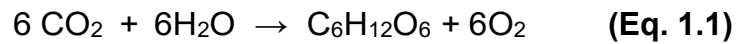
Figure 1.5: Schematic overview of the iron (Fe) pathway, translocation and storage mechanisms from roots to leaves – different Fe valence forms at different stages. Adapted from Connorton *et al.* (2017)

1.7 Chloroplasts and iron transport processes

1.7.1 Introduction to chloroplasts

Chloroplasts are among a group of organelles in the plastids umbrella category, and are differentiated from other plastids, due to being induced by light or other photochemical signals. They are 4–6 μm in diameter, and their main role is photosynthesis; a biochemical process where sunlight energy gets converted to chemical energy, for plants to produce their own food (Maréchal, 2018; Gedi *et al.*,

2019). Their reactants, carbon dioxide (CO₂) and water (H₂O) get converted to their products, glucose (C₆H₁₂O₆) and oxygen (O₂) as seen in the balanced chemical Equation 1.1. Chloroplasts are green coloured because of the green pigment, chlorophyll which plays a crucial role in absorption of sunlight (Damon *et al.*, 2007; Rebeiz *et al.*, 2010).



Chemical energy produced during photosynthesis is used for the biosynthesis of lipids, plant hormones, amino acids, fatty acids, minerals, and polyatomic ions, for examples, nitrates (NO₃⁻) and sulphates (SO₄⁻²) (Maréchal, 2018). Chloroplasts consist of a double membrane envelope where the entry and exit of essential substances is controlled, and where the primary photosynthetic apparatus is located (see Figure 1.6). The thylakoid membranes are formed from stacks known as grana which are linked by the central lamellae structures in the stroma. They are the prime characterisation of mature chloroplasts. The space between the thylakoid membranes is known as the lumen (Maréchal, 2018).

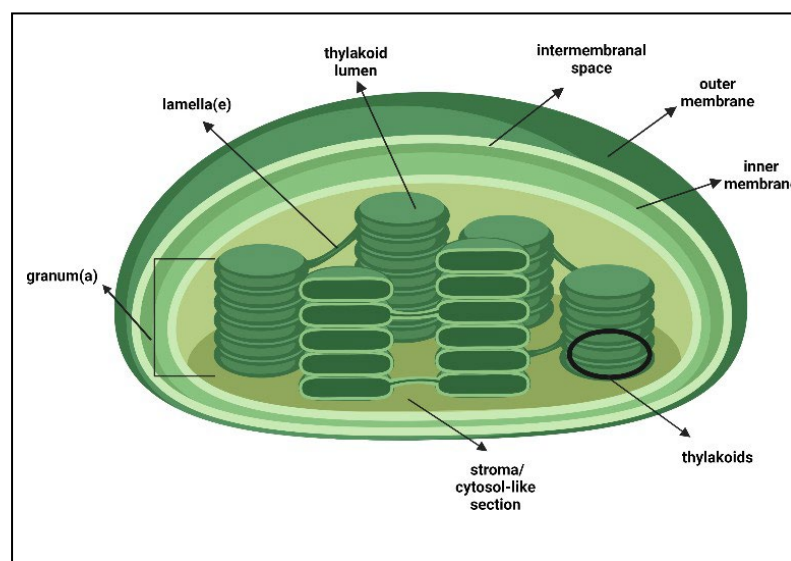


Figure 1.6: Labelled cross-sectional diagram of the chloroplast organelle. Adapted from Damon *et al.* (2007)

The conversion of light to chemical energy is brought about in the thylakoid membranes in Photosystem I (PSI) and Photosystem II (PSII). Light energy is absorbed in PSII by chlorophyll-a (chl-a) and chlorophyll-b (chl-b) and these absorbed photons eventually get converted from H₂O to oxygen (O₂) via photolysis. During the reaction, O₂ is lost and the reducing H⁺ ions are involved in replenishing NADPH. Photosystem I (PSI) receive excited electrons from the thylakoid membrane complexes in PSII, such as cytochrome b₆f to eventually form an electrochemical gradient where NADP⁺ gets converted into NADPH (Damon *et al.*, 2007) (see Figure 1.7). The ATP and NADPH produced in the thylakoid membranes finally get relayed into the stroma, which is a colourless liquid, that supports the structure of the cell, and is the site of all light-independent reactions. These light-independent reactions form the Calvin-Benson cycle, where CO₂ gets converted to carbohydrates, most importantly C₆H₁₂O₆ (in the form of glucose phosphate) enzymatically, primarily with RuBisCo (Rebeiz *et al.*, 2010).

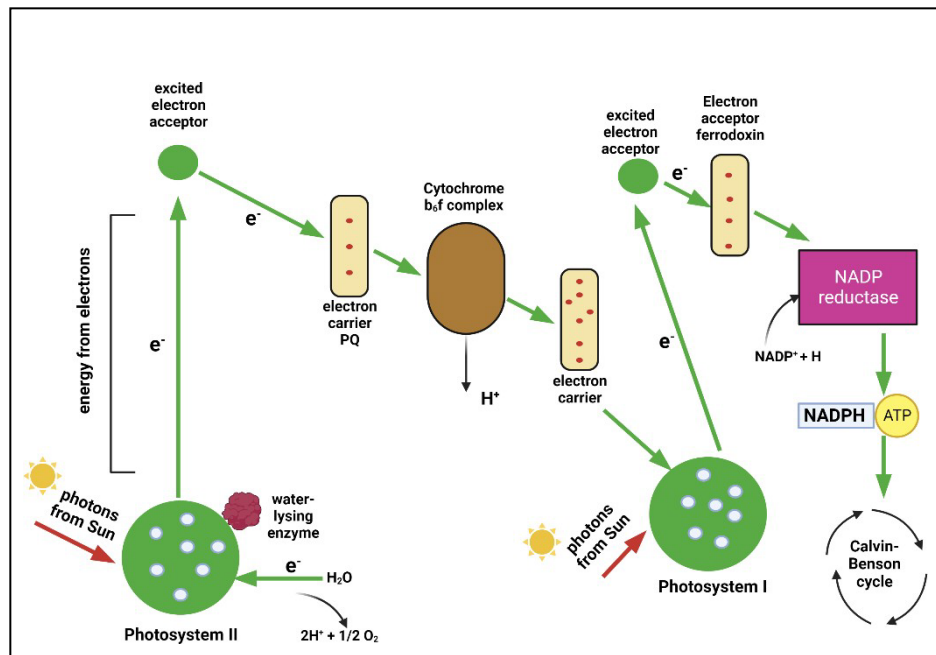


Figure 1.7: Photosynthetic light-dependent reactions in chloroplast thylakoids, involving Photosystem I and II. Adapted from Damon *et al.* (2007)

1.7.2 General benefits of iron for chloroplasts

There is strong evidence that 80—90% of Fe in the entire leaf material is confined in the chloroplast fraction, with thylakoid membranes themselves containing about 60% of the entire leaf Fe content (Gong *et al.*, 2015; Lysenko *et al.*, 2020; Solti *et al.*, 2012). The remainder of the Fe is often found distributed in the cytoplasm, and other organelles, containing haem and Fe-sulphur proteins (Miller *et al.*, 1995). However, the exact mechanisms involved in chloroplast Fe uptake, and how they function for the biosynthesis and maintenance of chlorophyll, are still not fully clear, and require further investigation (Divol *et al.*, 2013; Miller *et al.*, 1995).

In chloroplasts, high concentrations of redox active trace metal ionic concentrations of Fe, Cu and Mn are required for ATP synthesis and the electrochemical gradients in the thylakoid membranes (López-Millán *et al.*, 2016). Iron is also a major player in the photosynthetic apparatus of the electron transport chain including PSI, PSII, ferredoxins and the cytochrome b_6f complex (Finazzi *et al.*, 2015).

Although ferritins are not a major Fe store in chloroplasts, they play an important role in Fe homeostasis and prevention of oxidative stress (Salgado *et al.*, 2010). Ferritins form 40% of protein carriers of the entire thylakoid membranes in leaves. In the stroma, Fe is caged in ferritins (Thomine and Lanquar, 2011).

1.7.3 Iron uptake mechanisms in chloroplast.

Chloroplasts possess a double-membrane envelope with thylakoids as their intermembrane structures. The outer membrane is permeable to almost all ionic forms, however, the thylakoids and inner membranes contain specialised ion transporters to

maintain efficient ion homeostasis, photosynthetic and other biological functions. Some ions are transported passively and some actively. Active transport always involves ATP synthesis (Finazzi *et al.*, 2015) (see Figure 1.8).

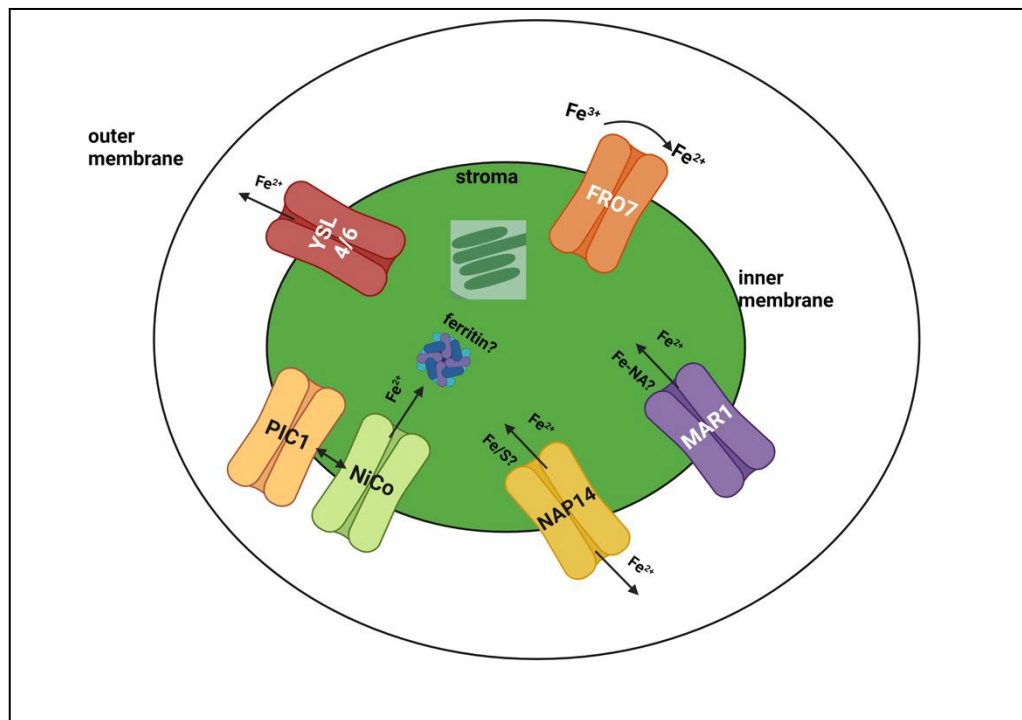


Figure 1.8: Overview of Arabidopsis and Strategy I plant chloroplast ion transporters/channels and their mechanisms. Adapted from Finazzi *et al.* (2015).

Iron enters the chloroplasts in the divalent Fe^{2+} form and recent studies have identified unique iron transporters responsible for import into the chloroplast (Solti *et al.*, 2012). The source iron which enters the chloroplast to form the iron containing protein for photosynthesis is the iron storage protein, ferritin, which is also named phytoferritin in plants. Ferritin is a protein with conservative spherical structure occur in plants and animals containing an apoferritin shell and iron atoms core. Ferritin forms during the early development of plants leaves just after the germination and play a dual role as iron receptor and doner (Dawidziak, 2015). Moreover, Ferritin contains a conservative ferroxidase center which can convert/ oxidise iron from Fe^{+2} to Fe^{+3} (Zhao, 2010).

Divalent Fe gets translocated from the cytoplasm, into the inner membrane via transporters, most commonly Permease in Chloroplast 1 (PIC1) (White and Broadley, 2009). It plays a role in general uptake, metabolic and homeostatic mechanisms within both the chloroplast and the entire plant (López-Millán *et al.*, 2016; Morrissey and Guerinot, 2009).

Multiple Antibiotic Resistance 1 (MAR1) (see Figure 1.8) is known to sequester chelated Fe complexes into chloroplasts (Finazzi *et al.*, 2015). It is also known to contribute to Fe²⁺ homeostasis in Arabidopsis (Divol *et al.*, 2013; Malhotra *et al.*, 2020; Solti *et al.*, 2012). Yellow Stripe 4 (YSL4) and YSL6 also maintain Fe²⁺ homeostasis in the chloroplasts by preventing excessive accumulation to toxic levels (Roschttardt *et al.*, 2013). Multiple Antibiotic Resistance NAP1 and NAP14 are often involved in ferredoxin (Fe-S) cluster synthesis and are also part of major homeostatic pathways (Finazzi *et al.*, 2015; Malhotra *et al.*, 2020). López-Millán *et al.*, (2016) reported FRO7 being necessary for efficient photosynthesis in Fe deficient conditions, however, their exact complex mechanisms and localisations still require further inquiry.

1.8 Nutritional significance of green leafy vegetables (GLVs)

1.8.1 GLVs in general – iron contents

By 2050, global human population is predicted to reach as high as 9.7 billion (https://knowledge4policy.ec.europa.eu/foresight/global-population-growing_en).

Eight million children in south-east Asia and sub-Saharan Africa currently die before the age of five as a result of famine and malnutrition (Hess *et al.*, 2002; Uusiku *et al.*, 2010). This will put extra pressure on finite food resources and further exacerbate deficiencies in essential nutrients for human health, especially in developing countries.

Currently, more than three billion people worldwide are prone to macro and micronutrient famine which explains the need for effective biofortification approaches (Waters and Sankaran, 2011). This can also be done through possible improvements of nutrient contents in staple foods, through genetic modification (Brown and Ford, 2008). However, strategies aimed to enhance dietary diversification, mineral supplementation and biofortification have not always proven successful (White and Broadley, 2009). Molecular genetic approaches have also been considered, where the physiological basis of a plant's response to Fe deficiency is also considered, including increased PS production (Hochmuth, 2011).

General shrinkage of food supply and micronutrients in scarce amounts, primarily, minerals from fresh fruits and green leafy vegetables (GLVs), will exacerbate chronic diseases such as cancer, heart disease, Type II diabetes and obesity, especially in poorer countries and low-income households (Gedi *et al.*, 2017; Maunder and Meaker, 2007). Producing GLVs which satisfy optimal nutritional levels still pose a major challenge for third-world countries (Alvino and Barbieri, 2015).

Edible GLVs are relatively cheap and rich in nutrients such as proteins, vitamins, minerals and phenolic compounds, and are commonly used in raw salad, purees and cooked dishes (Gupta *et al.*, 1989; Natesh *et al.*, 2017; Das, 2019; Reinhardt *et al.*, 2007). Epidemiological studies have proven that consumption of GLVs reduces the risk of chronic diseases, including cancer and cardiovascular diseases (Odhav *et al.*, 2007).

Roberts and Moreau, (2016) and Gedi *et al.*, (2017) reported spinach promoting substantial health benefits because of its diverse macronutrient, vitamin and mineral composition. These characteristics contribute in the long-term to their anti-cancer, anti-inflammatory and anti-obesity properties.

The nutritional value of GLVs is governed by storage, processing methods, cooking

methods, shelf-life, variety, leaf maturity, cultivation, and preservation methods. For example, autumn-sown spinach contains higher levels of N, K, Ca, Mg and Zn compared with winter-sown spinach (Natesh *et al.*, 2017; Roberts and Moreau, 2016).

1.8.2 Spinach health benefits

Spinach is a dark GLV and the most well-known cultivar is *Spinacia oleracea* (*S. oleracea*), also known as garden spinach (Alvino and Barbieri, 2015). It has a diverse nutritional composition in terms of minerals, vitamins, phytochemicals, and exceptionally high antioxidant capacity (Machado *et al.*, 2018). Therefore, it is important to improve the nutritional quality of spinach without yield reduction, in hydroponic cultures (Jin *et al.*, 2013). It can also be grown in high amounts, even on a global scale in most temperate countries including the UK, USA, China, Japan, Turkey, France, Italy and Portugal (Eid *et al.*, 2018; Machado *et al.*, 2018). Bhattacharjee *et al.*, (1998) reported it being composed of moisture (92.1%), protein (2.0%), carbohydrate (2.6%), lipids (0.7%) and minerals (1.7%).

Phytochemicals such as polyphenols and carotenoids are present in GLVs. Epidemiological studies reveal that these phytochemicals are linked to a reduction in cancer risk, heart diseases, obesity, inflammatory and neurological diseases (Alvino and Barbieri, 2015). Therefore, the concentration of these phytochemicals, highly influenced by cooking and cultivation techniques, increases functional and nutritional value of GLVs (Machado *et al.*, 2018).

Tables 1 A—C summarise the nutritional compositions per 100g dry weight (DW) serving of daily recommended nutrient intake (RNI) in the whole leaf materials (WLMs) of various GLVs.

Tables 1.1A—C: Concentrations (per 100g FW) of macro and micronutrients of various raw green leafy vegetables (GLVs) 1.1A) macronutrients, B) Vitamins and C) Minerals. * Represents 100g per unit dry weight (DW).

GLV	A) Macronutrient				
	Protein (g)	Fat (g)	CHO (g)	Fibre (g)	Energy (kJ/Cal)
Aragula	2.6 ^a	0.66 ^a	3.7 ^a	1.6 ^a	25 ^a
Broccoli	2.8 ^a	0.37 ^a	6.6 ^a	2.6 ^a	34 ^a
Chicory	1.7 ^a	0.30 ^a	4.7 ^a	4 ^a	23 ^a
Coriander	2.1 ^a	0.52 ^a	3.6 ^a	2.8 ^a	23 ^a
Lettuce	1.4 ^a	0.15 ^a	2.8 ^a	1.3 ^a	15 ^a
Swiss Chard	1.8 ^a	0.20 ^a	3.7 ^a	1.3 ^a	19 ^a
Watercress	2.3 ^a	0.10 ^a	1.2 ^a	1.6 ^a	11 ^a
Cabbage	0.9 ^e	0.02 ^e	7.2 ^e	3 ^e	-
Amaranth	2.5 ^a 6.00 ^d	0.33 ^a 0.50 ^d	4.0 ^a 6.1 ^d	2.8 ^d	53 ^d
Spinach	2.9 ^a 2.1 ^c	0.40 ^a †1.20 ^c	3.6 ^a 1.6 ^c	2.2 ^a	23 ^a
Kale	4.3 ^a 7.3 ^c	0.93 ^a †3.4 ^c	8.8 ^a 6.4 ^c	3.6 ^a	49 ^a

Species	B) Vitamins							
	β -Car (mg)	Thiamin (Vit B ₁) (mg)	Riboflavin (Vit B ₂) (mg)	Vit-B ₆ (mg)	Folate (Vit B ₉) (mg)	Vit-C (mg)	α -Toc (mg)	Vit-K (mg)
Aragula	1.42 ^a	0.04 ^a	0.09 ^a	0.07 ^a	0.1 ^a	15 ^a	0.43 ^a	0.11 ^a
Broccoli	0.36 ^a	0.07 ^a	0.12 ^a	0.18 ^a	0.06 ^a	89 ^a	0.78 ^a	0.10 ^a
Chicory	3.43 ^a	0.06 ^a	0.1 ^a	0.11 ^a	0.11 ^a	24 ^a	2.26 ^a	0.28 ^a
Coriander	3.93 ^a	0.06 ^a	0.16 ^a	0.15 ^a	0.06 ^a	27 ^a	2.5 ^a	0.31 ^a
Lettuce	4.44 ^a	0.07 ^a	0.08 ^a	0.09 ^a	0.04 ^a	9 ^a	0.22 ^a	0.13 ^a
Swiss Chard	3.65 ^a	0.04 ^a	0.09 ^a	0.1 ^a	0.01 ^a	30 ^a	1.89 ^a	0.83 ^a
Watercress	1.91 ^a	0.09 ^a	0.12 ^a	0.13 ^a	0.09 ^a	43 ^a	1.00 ^a	0.25 ^a
Cabbage	0.004 ^f	-	-	-	-	30 ^f	-	-
Amaranth	1.80 ^a 6.20 ^f	0.03 ^a	0.16 ^a	0.19 ^a	0.09 ^a	43 ^a 70 ^{b*} 126 ^f	-	1.14 ^a
Spinach	5.63 ^a 4.56 ^c 4.03 ^f	0.08 ^a 0.9 ^g	0.19 ^a 1.8 ^g	0.2 ^a 1.8 ^g	0.19 ^a	43 ^a 70 ^{b*} 126 ^f 256 ^g	2.03 ^a 0.62 ^c	0.48 ^a
Kale	5.93 ^a 15.40 ^c	0.11 ^a 0.9 ^g	0.13 ^a 1.8 ^g	0.2 ^a 0.9 ^g	0.14 ^a	120 ^a 1014 ^g	1.54 ^a 1.80 ^c 9.3 ^g	0.70 ^a

Species	C) Mineral							
	Ca (mg)	Fe (mg)	Mg (mg)	P (mg)	K (mg)	Na (mg)	Zn (mg)	Cu (mg)
Aragula	160 ^a	1.46 ^a	47 ^a	52 ^a	369 ^a	20 ^a	0.47 ^a	0.08 ^a
Broccoli	47 ^a	0.73 ^a	21 ^a	66 ^a	316 ^a	33 ^a	0.41 ^a	0.05 ^a
Chicory	100 ^a	0.90 ^a	30 ^a	47 ^a	420 ^a	45 ^a	0.42 ^a	0.30 ^a
Coriander	67 ^a	1.77 ^a	26 ^a	48 ^a	521 ^a	46 ^a	0.50 ^a	0.23 ^a
Lettuce	36 ^a	0.86 ^a	13 ^a	29 ^a	194 ^a	28 ^a	0.18 ^a	0.03 ^a
Swiss Chard	51 ^a	1.8 ^a	81 ^a	46 ^a	379 ^a	213 ^a	0.36 ^a	0.18 ^a
Watercress	120 ^a	0.20 ^a	21 ^a	60 ^a	330 ^a	41 ^a	0.11 ^a	0.08 ^b
Cabbage	20 ^e 31 ^f	0.75 ^e 0.30 ^f	23 ^e 13 ^f	32 ^f	53 ^e 173 ^f	10 ^e 29 ^f	0.31 ^e 0.15 ^f	0.05 ^e
Amaranth	215 ^a 401 ^d 306 ^f	2.32 ^a 3.57 ^d 6.00 ^f	55 ^a 223 ^d 182 ^f	50 ^a 102 ^d 64 ^f	611 ^a 768 ^f	20 ^a 73 ^d 4 ^f	0.90 ^a 3.06 ^d 0.63 ^f	0.16 ^a 0.34 ^d
Spinach	99 ^{af} 141 ^c 1036 ^g 70 ^h	2.71 ^a 0.96 ^c 0.3 ^f 8.3 ^g 35 ^h	79 ^a 23 ^c 13 ^f 265 ^g 70 ^h	49 ^{af} 52 ^c 519 ^g 740 ^h	558 ^a 776 ^c 276 ^g 991170 ^h	79 ^{af} 39 ^c 827 ^g 3818 ^h	0.53 ^{af} 0.89 ^c Zn ^g 4.250 ^h	0.13 ^a 0.10 ^c 0.83 ^h
Kale	150 ^a 520 ^c 846 ^g 1970 ⁱ	1.47 ^a 2.44 ^c 8.3 ^g 7.26 ⁱ	47 ^a 74 ^c 265 ^g 240 ⁱ	92 ^a 151 ^c 519 ^g 9573 ⁱ	491 ^a 833 ^c 276 ^g 991350 ⁱ	38 ^a 2 ^c 827 ^g 9170 ⁱ	0.56 ^a 0.48 ^c 3.29 ^g 3.94 ⁱ	1.50 ^a 0.10 ^c 0.51 ⁱ

Alvino and Barbieri (2016)^a, Yadav *et al.* (2013)^b, Gedi *et al.* (2017)^c, Odhav *et al.* (2007)^d, Ashfaq *et al.* (2018)^e, Steyn *et al.* (2001)^f, Natesh *et al.* (2017)^g, Gupta and Wagle (1988)^h, Satheesh and Fantaⁱ (2020)

Deficiencies in Fe are regarded as the most prevalent nutritional problems globally (Raes *et al.*, 2014). The World Health Organisation (WHO) reported one-third of global population suffering from Fe deficiencies, with it being most widespread in less-developed countries. It is currently estimated for 40—45% of school-age children being anaemic (Connorton *et al.*, 2017; Rodriguez-Ramiro *et al.*, 2019). Pregnant women experiencing anaemia are also more susceptible to delays in embryonic development, premature births and at worse, maternal and perinatal mortality (Orechet *et al.*, 2005). It is also known to reduce children's learning abilities (Abbaspour *et al.*,

2014). The worldwide prevalence of diet-related diseases has been on the rise over the past few decades (Brodkorb *et al.*, 2019). Deficiencies can also be caused by overprocessing of food, for transport and storage, and the use of chemical treatments including pesticides and herbicides during food production (Brown and Ford, 2008).

Anaemia currently affects more than two billion people worldwide with Africa currently having the highest number of affected individuals, as high as 68% in 2005 (Gulec *et al.*, 2014; Uusiku *et al.*, 2010). Approximately 50% of this anaemia occurs as a result of Fe deficiency and is believed to impact mostly children with impaired cognitive development and pregnant women with poor pregnancy outcomes (Bryszewska, 2019; Etcheverry *et al.*, 2012; Raes *et al.*, 2014; Zielińska-Dawidziak, 2015).

The novelty of this project is that no other studies have utilised ^{57}Fe to investigate human bioaccessibility of chloroplastic spinach Fe. Furthermore, the project also aims to mathematically model the transfer of Fe in growth-room perlite-sown spinach root and leaf material.

1.9 Aims and objectives.

This project aims to:

- 1) Optimise a hydroponic method to grow spinach at the University of Nottingham (UoN) Sutton Bonington Campus. This included formulation of an optimal nutrient solution.
- 2) Establish the optimum concentration of iron in the growth medium to promote healthy growth and to allow ^{57}Fe to be dosed into the nutrient mix and taken up into the plant.
- 3) Fractionate both commercial and perlite-sown spinach leaves to identify the fraction/component with the highest localisation of Fe and ^{57}Fe .

- 4) Establish the use of ^{57}Fe stable isotope to discriminate the iron in the food sample (spinach CRF) from the iron in the reagents (enzymes, simulated digestive juices).
- 5) Formulate mathematical models, in the form of ordinary differential equations (ODEs), to simulate the kinetics of Fe uptake into the plant, from the growth matrix to the root and finally, the stem + leaf material. Generate model outputs and analyse the degree of fit.
- 6) Investigate the bioaccessibility of ^{57}Fe biomarker, in a cell-free chloroplast-rich fraction (CRF) in the human digestive system, using a static in vitro digestion method for perlite-sown spinach leaves.

Chapter 2: General Materials and Methods

2.1 Introduction to hydroponics for growth and cultivation of spinach plants

Hydroponics is defined as the method of cultivating plants without the need for soil, often in liquid nutrient solution. It promotes a more controlled environment than soil systems (Jones Jr, 2016). Globally, hydroponic production methods allow for reliable production of spinach and other GLVs (Brechner and De Villiers, 2013).

Some other advantages of hydroponic systems include high quality yields and economic advantage together with reduced labour costs, evaporative loss, and ecological impact. They also serve as good root supply systems because they directly provide plant roots with nutrient water without extra effort. Plants have also been proven to accumulate higher levels of nutrients and antibiotics in hydroponic culture than in the soil (Tang *et al.*, 2021). Şimşek and Çelik, (2021) also reported hydroponic systems being the best way to achieve optimal concentrations of all essential nutrients, to get a desirable level of plant growth.

Some disadvantages include high aeration demands, the need for qualified personnel and the risk of fungal and nematode invasions (Jones-Jr, 2016 Oztekin *et al.*, 2018; Silvana, 2005). Floating hydroponic systems run the risk of premature bolting and Pythium fungal invasions during spinach production (Reinhardt, 2007).

Hydroponic systems can be subdivided into two main categories: medium and mediumless. Examples of mediumless systems include standing aerated nutrient solution, nutrient film technique (NFT) and medium hydroponic systems include aeroponics, ebb-and-flow, pot drip, rockwool slabs and perlite (Di Marzio *et al.*, 2005; Jones Jr, 2016; Öztekin *et al.*, 2018). For example, NFT involves running a constant

film of nutrient water across the roots on a sloped pipe, moving against gravity. The nutrient water must be mixed well in order to ensure uniform nutrient distribution for the root oxygenation (Reinhardt *et al.*, 2007). Ebb-and-flow involves raising and lowering water around the plant roots. The flooding process must ensure an equilibrium between oxygen and water, and the top 60% of root mass must be aerated (Mainly and Reinders, 1996).

In both forms of systems, the circulation of the nutrient solution involves either active or passive flow and any unwanted nutrients are recirculated back into the system (Jones Jr, 2016). Finally, pH is the most important factor for hydroponic production because it impacts electrical conductivity (EC) levels of the roots and enzymatic activities (Mainly and Reinders, 1996).

2.2 Preparation of standard Hoagland nutrient solution

A standard modified Hoagland nutrient solution was formulated using Table 2.1 as a guide. A NaFe-ethylene diamine tetracetic acid (EDTA) chelate was necessary to prevent damaging oxidation reactions at high pHs.

To maintain an optimal germination pH of approximately 5.8, \cong 0.78g of 2-(N-morpholino) ethanesulphonic acid (MES) hydrate anhydrous buffer powder (VWR® Life Sciences/Sigma Aldrich®) was dissolved and combined with \cong 0.8 – 1mL (80000 –1000 μ L) of 2M sodium hydroxide (NaOH) (therefore 20 g and \cong 0.025 mL (Kumwimba *et al.*, 2013; Lee *et al.*, 2016). Gilson pipettes were used to transfer measured amounts of each nutrient into the final Hoagland nutrient solution.

The pH was measured with a standard pH probe (Mettler Toledo FE20/EL20 benchtop) (see Appendix 3) fitted with a combined glass electrode. A two-point calibration was performed with buffer solutions of pH 4.006 and 6.865 (Puffer-Buffer Trace).

The final volume of the Hoagland nutrient solution was exactly 2 L. Extra Milli-Q water (Suez) (outlet quality of 18.2M Ω , flow rate of 1.30 L min⁻¹, temperature of 21°C) was utilised for any extra watering.

Table 2.1: Modified Hoagland nutrient solution macro and micronutrient info – for 2L

Compound	Molecular weight	Concentration of stock solution	Volume of stock solution of final solution	Element	Final concentration of the element
	g/mol	g/L	mL/L		μ M
Macronutrients					
KNO ₃	101.10	101.10	12.0	N	16
Ca (NO ₃) ₂ * 4H ₂ O	236.16	236.16	8.0	K	6.0
NH ₄ H ₂ PO ₄	115.08	115.08	4.0	Ca	4.0
MgSO ₄ * 7H ₂ O	246.48	246.49	2.0	P	2.0
				S	1.0
				Mg	1.0
Micronutrients					
KCl	74.55	1.864	4.0	Cl	50
H ₃ BO ₃	61.83	0.773	4.0	B	25
MnSO ₄ * H ₂ O	169.01	0.169	4.0	Mn	2.0
ZnSO ₄ * 7H ₂ O	287.54	0.288	4.0	Zn	2.0
CuSO ₄ * 5H ₂ O	249.68	0.062	4.0	Cu	0.5
H ₂ MoO ₄ (85% MoO ₃)	161.97	0.040	4.0	Mo	0.5
NaFe-EDTA (Fe ²⁺ form)	468.20	30.0	1.0	Fe	50

2.3 Preparing ^{57}Fe enriched Hoagland nutrient solution with NaFe-EDTA

2.3.1 Preparation of the individual stock solution

The Fe stock contained 894 mg/L and 1.2 M HCl which was equal to 0.0157 M or 15.7 mM. Preparation of 10 mL of Fe chelate at exactly 1 mM (meaning the 10 mL contained 10 μmol) occurred as follows. The chelation mix was a 1:3 $\text{Fe}^{57}:\text{NaOH}$ stock solution with the concentration of this solution being identical to the naturally abundant Fe which was 50 μM in Hoagland nutrient solution. To achieve 50 μM , 1.86 g of NaFe-EDTA was dissolved in 1L Milli-Q water, so each 200 mL contained 1 mM and 2 mL contained 10 μM . Then, 5 mM of NaOH (0.2 g in 1 L) was prepared for 600 mL to contain 3 mM and 6 mL to contain 30 μL . Following this, 2 mL of the prepared ^{57}Fe was added to 6 mL of NaOH, which in turn, adjusted the pH to 11.25.

Individual NaFe-EDTA stock solution (0.636 mL) was spiked with ^{57}Fe to give 10 μM +0.0318mL, to account for the extra 5% for chelation of enough Fe, which totalled up to 0.6678 mL. The pH then dropped to 1.69 which was why the pH needed to be readjusted with 10M NaOH and not exceed 10 mL in total.

The final mixture had to be shaken thoroughly and was covered with aluminium foil to prevent damaging photodecomposition reactions. It was then stored in total darkness for 24 hours, in the cupboard, at room temperature. The solution was filtered the next day with a 0.45 μM polyvinylidene fluoride (PVDF) syringe filter membrane (Whatman), to eliminate the formation of possible iron hydroxides (Orera *et al.*, 2010). It was finally diluted to a specified volume of deionised Milli-Q water as well (Oliveira *et al.*, 2014; Rodriguez-Castrillón *et al.*, 2008).

2.3.2 Integration of final stock solution into Hoagland solution

To prepare the final Hoagland solution, 10 μ M enriched ^{57}Fe stable isotope was added with the rest of macro and micronutrients seen in Table 2. The total Fe concentration of the final solution had to be completed to 50 μ M using 0.4 mL of the NaFe-EDTA stock solution (100 μ M). As for the NaFe-EDTA, the Hoagland solution had to be maintained at pH 5.8, using \cong 0.78 g of MES anhydrous buffer powder combined with exactly 1mL of 2M NaOH.

Finally, to prepare Hoagland solution with 3 μ M of ^{57}Fe , only 3 mL of the 10 mL in stock solution needed to be added. The total iron concentration in the final Hoagland solution was 50 μ M using both the NaFe EDTA stock solution (100 μ M) and the enriched ^{57}Fe isotope solution. To prepare Hoagland solution with 10 μ M and 3 μ M of ^{57}Fe , only 10 mL or 3 mL of the ^{57}Fe -EDTA solution, was needed.

2.4 Germination and growth of hydroponic spinach

2.4.1 Growth room facilities

All spinach plants were sown in the growth room facilities at UoN Sutton Bonington Campus. They were exposed to a temperature range of 18 – 23°C, relative humidity of 60 – 100% and a light intensity of 80 – 200 $\mu\text{mol m}^{-2} \text{s}^{-1}$ under fluorescent lighting, for a 16:8 hour light/dark photoperiod (Liu *et al.*, 1998; Lee *et al.*, 2016; Reinhardt, 2007). Table 2.2 summarises the optimal growth parameters for spinach germination (Brechner and Villiers, 2013).

Table 2.2: Overview of the general optimal growth parameters for spinach germination: Adapted from Brechner and Villiers (2013).

Factor	Optimum range
Light intensity	17 - 22 mol/m ² /d both natural & artificial
Air temperature	18 – 24°C
Water temperature	22 – 26°C
Relative humidity	≈ 60 – 80%
pH	5 – 6.7
Light:dark photoperiod	16:8 hours
Optimum sowing period	March – May, July – October
Optimum harvesting period	May – June, August – December

2.4.2 Sowing and harvesting in perlite.

Compared to organic hydroponic substrates such as peat or rockwool, perlite is pH neutral, more sterile and has a reliable aeration and oxygen retention capacity. Therefore, there was no need for prevention of pests or diseases, especially during anaerobic conditions (Storey, 2016).

All spinach seeds (King's Seeds Trombone F1 SPI019) were initially sterilised by soaking in 10% hydrogen peroxide (H₂O₂) for 10 minutes, followed by 3 rounds of cleaning in distilled reverse osmotic (RO) water (Kumwimba *et al.*, 2013; Zhu *et al.*, 2003)

A total of 6 drip trays, each containing 4 half-seed trays each with 6 individual compartments, were used for sowing the spinach seeds in the growth room facilities.

3 – 4 seeds were sowed per compartment initially. All trays were covered with propagator lids during germination (see Figure 2.1).

Within each harvesting round, spinach seeds were left to germinate and de-etiolate while feeding with 30 mL of Hoagland solution containing total Fe, every 2 – 3 days. In some experiments, after 3 weeks of growth, 30 mL of a Hoagland solution spiked with ^{57}Fe was added repeatedly, until harvest. A sieve was used to ensure that the Hoagland solution was evenly distributed to each compartment and that the seeds were not exposed or buried too deep. Once more than one seedling finished germinating in one compartment, only one seedling was left behind to inhibit intraspecific competition for nutrients. All spinach plants were harvested roughly after 4 weeks (1 month) from sowing.

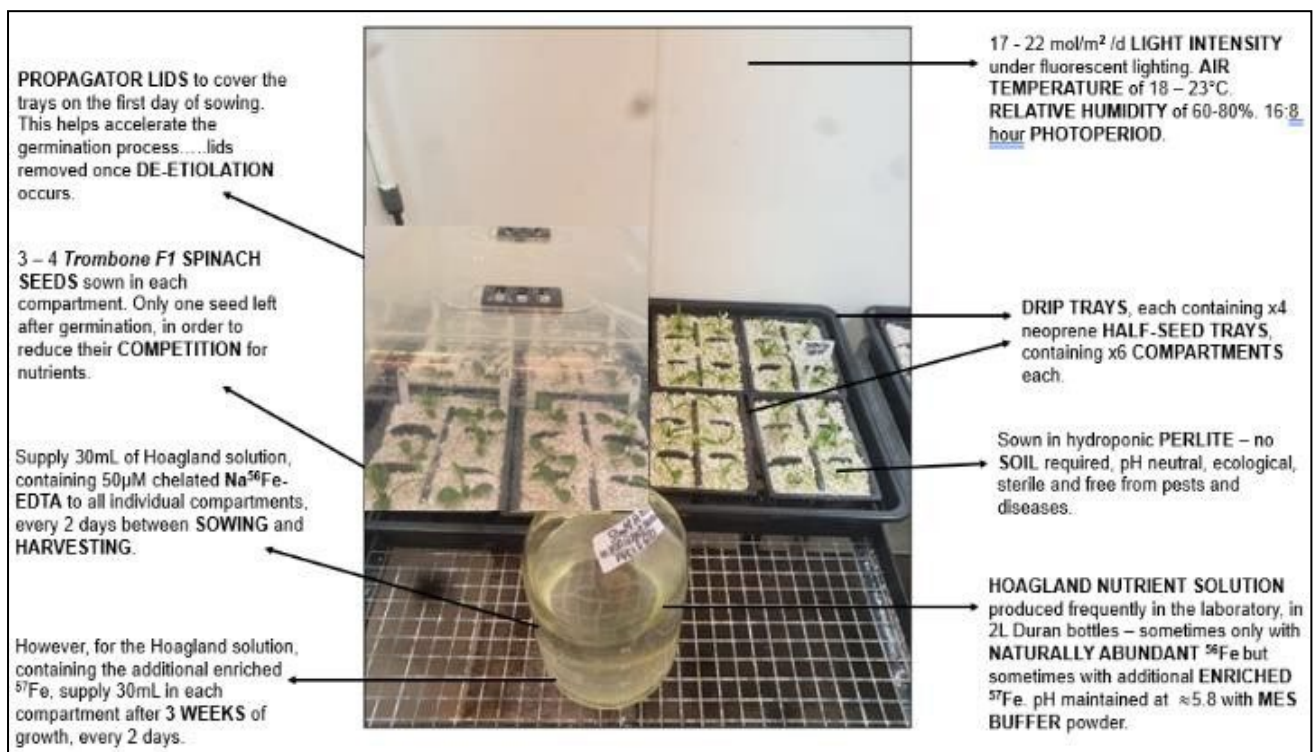


Figure 2.1: Visual summary of important aspects of growth room perlite spinach leaf setup

2.4.3 Post-harvest treatment of spinach plants

The plants were harvested using a scalpel to harvest the leaves and separate them from roots material. They were then immediately stored in plastic container with lid on to avoid moisture loss, and were then either washed directly, or stored at 4°C, in dark bags. The washing process involved washing twice in tap water, followed by three times rinsing in Milli-Q water. The rinsing process involved soaking with gentle stirring for a minute in each of three beakers containing Milli-Q water, followed by blotting dry with tissues (Kumwimba *et al.*, 2013). FWs were measured after washing and drying, by blotting them on tissue to remove excess water. They were then oven-dried for 72 hours at 105°C, followed by measurement of dry weight of each plant part (Memmert UN 110, Sanyo Convection Oven or Fiestream). Oven dried samples were then used for subsequent mineral analysis. However, for lipophilic compounds analysis, the washed leaves were frozen at -80°C, followed by freeze-drying for a week and grinding, using the pestle and mortar.



Figure 2.2: Rinsing spinach root and stem + leaf material in 600mL beakers followed by blotting them dry on tissues.

For further reference, moisture contents of all root and stem + leaf biomass were also measured. They were reweighed 24 hours after being placed in the vacuum oven, at 105°C. The moisture contents were calculated gravimetrically based on Equation 2, where FW refers to the fresh weight and DW refers to the dry weight.

$$\text{Moisture content (\%)} = \left(\frac{\text{FW (g)} - \text{DW (g)}}{\text{FW (g)}} \right) \times 100 \quad (\text{Eq. 2})$$

2.5 Spinach Fe uptake using ^{57}Fe as a tracer.

2.5.1 Juicing, centrifuging, freeze-drying and fractionation processes

A 'juicing and centrifugation' process to liberate essential nutrients from cell-confined units and to concentrate the chloroplast rich fractions (CRFs) has been recently developed at the UoN Food Nutrition and Dietetics Department. This work is geared towards establishing a cocktail of bioaccessible nutrients in liberated chloroplasts, using a physical process rather than a chemical process with the need of solvents (Gedi et al., 2017).

Fresh raw spinach WLM material was purchased on the morning of sample preparation. A modern juicer (Angelia 7500) was initially used to separate the spinach WLM into juice and fibre. The juice was filtered with a 75 micrometre (μm) sieve and the filtrate was centrifuged (4°C , 20 minutes, RPM 10000) (Beckman J2-21M/E Centrifuge) in Falcon centrifuge tubes to separate the pelleted CRF from the supernatant (see Figure 2.3). At least two centrifugation runs were completed to ensure maximum yield of CRFs with as much supernatant discarded.

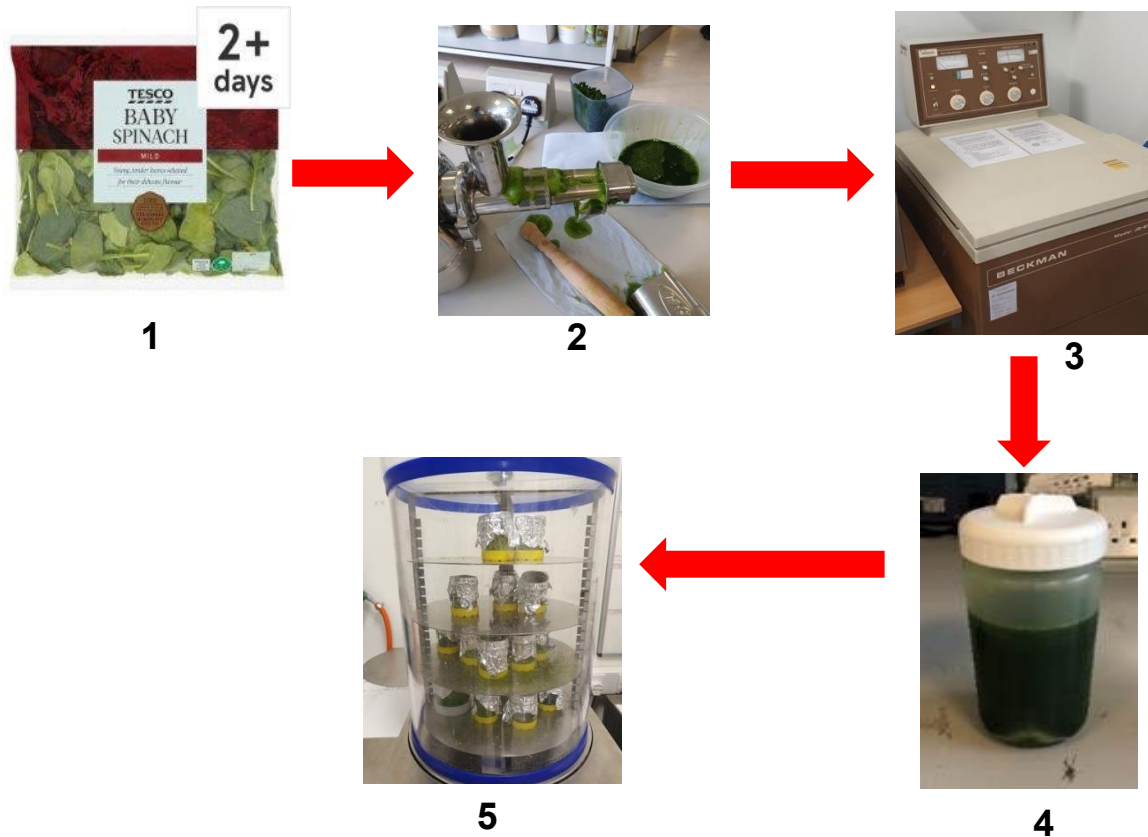
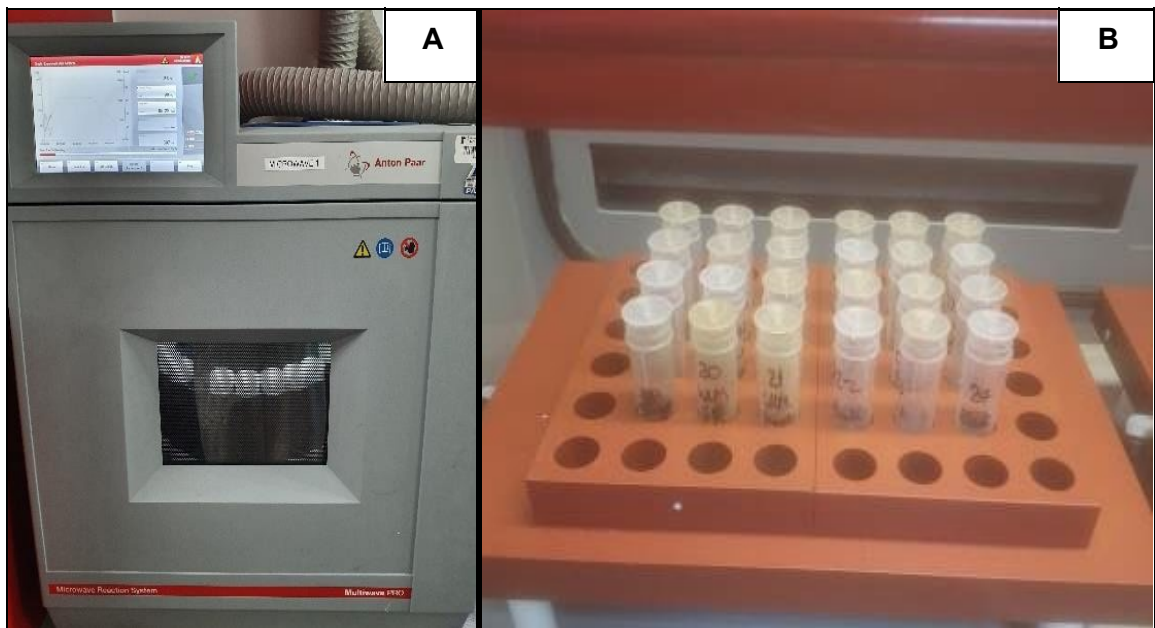


Figure 2.3: Flowchart of spinach leaf fractionation procedure; 1) parent leaf material, 2) juicing, 3) centrifugation of juice, 4) isolation of CRF pellets from supernatant and 5) freeze-drying final CRF pellets

All CRF material was stored overnight at -80°C , prior to freeze-drying (Edwards Freeze Dryer, Super Modulyo). Freeze-drying for a week at -60°C transformed the samples to powdered form for subsequent analyses. During this process, all containers containing the samples were covered with aluminium foil with pierced holes to allow for aeration. Samples were then homogenised to fine powdered form using a pestle and mortar before storage in plastic containers at room temperature prior to analysis (see Figure 2.3). Five fractionated components of the spinach leaves were then analysed for mineral and photosynthetic pigment contents: WLM, fibre, supernatant, juice and CRFs (Rachma *et al.*, 2010).

2.5.2 Mineral acid digestion and ICP-MS facilities

The concentrations of both total Fe and ^{57}Fe in spinach root and stem + leaf material were measured using ICP-MS (Thermo-Fisher Scientific iCapQ) after acid digestion. Two different methods of acid digestion were used a) microwave assisted for organic plant material (see Figure 2.4 A) and b) concentrated primary grade nitric acid reflux digestion for growth substrates and liquid samples.



Figures 2.4 A – B: Two distinct mineral acid digestion methods; 14A) microwave (Anton Paar™) and B) concentrated nitric acid reflux digestion.

2.5.3 Microwave digestion of plant material

Microwave digestion is feasible with all organic material such as leaves, roots and soils. Approximately 0.2 g of powdered WLM, root, and CRF samples were weighed with an analytical balance (Sartorius 1773MP) for digestion. Two replicates of tomato leaf samples, used as Certified Reference Material (NIST CRM 1573a), were used to establish recoveries (Bryzeweska, 2019).

Samples were weighed in 50 mL microwave high-pressure Teflon vessels (Anton Paar™ 227935). Subsequently, 6 mL of nitric acid (HNO₃) (>68% Primar Plus™ trace reagent grade) was added to the vessels in a fume hood, with a multi-volume adjustable pipette (Finnpipette™ Thermo Scientific) before digestion on the hot plate.

Microwave digestion (Anton Paar™ Multiwave Pro) was completed over a 40-minute time frame, using variable heating and power programming. During the digestion run, both temperature (max 200°C) and power varied at different stages (see Appendices 4 and 5), and were impacted by the number and arrangements of polypropylene digestion tubes. Following this, digestion samples were transferred from the 6 mL HNO₃ mix from the polypropylene digestion vessels, into 30 mL Universal tubes (60.9922.241 Sarstedt Tube Universal). The Teflon digestion vessels were then rinsed with Milli-Q water, added to the acid digest, before being topped up to 20 mL. Finally, a 1 mL aliquot of each sample from was diluted, up to 10 mL with Milli-Q water for mineral analysis.

2.5.4 Nitric reflux digestion of organic samples

Fe concentrations for the growth matrix; both perlite and Hoagland nutrient solution, were analysed with the nitric reflux digestion method. The digestion heating blocks are made from graphite, inert to all acids, and minimising contamination.

Just like with the microwave digestion, 0.2 g of all samples were weighed into PFA digestion vessels and placed in the heating blocks under the fume hood. Then, 8 mL of nitric acid (HNO₃) (>68% Primar Plus™) and 2 mL of hydrogen peroxide (H₂O₂) (30% Primar Plus™) were added.

After 2 hours of heating at 95°C, a final dilution volume to 50 mL was completed through transferring the sample and 40 mL of Milli-Q H₂O, in four separate washing

rounds to another vessel. Finally, 1 mL of each sample from the digestion vessels and 9 mL Milli-Q H₂O were transferred to ICP-MS tubes for elemental analysis.

2.5.5 Injecting the digested samples into the ICP-MS

Multi-element analysis of diluted solutions was undertaken using inductively coupled plasma mass spectrometry (ICP-MS) (Thermo-Fisher Scientific iCAP-Q; Thermo Fisher Scientific, Bremen, Germany), after appropriate calibration. Interferences due to the formation polyatomic ions (especially Ar and Ca-based polyatomics) at masses that coincide with Fe isotopes, make isotope ratio determination difficult (Oliveira *et al.*, 2014; Rodríguez-Castrillón *et al.*, 2008). To minimise this, the instrument was run in collision-cell mode with kinetic energy discrimination (CCT-KED) to eliminate polyatomic interferences (Oliveira *et al.*, 2014; Orera *et al.*, 2010; Rodríguez-Castrillón *et al.*, 2008).

Samples were introduced from an autosampler (Cetac ASX-520) incorporating an ASXpress™ rapid uptake module through a PFA nebuliser. Internal standards were introduced to the sample stream on a separate line via the ASXpress unit and included Sc (20 µg L⁻¹), Rh (10 µg L⁻¹), Ge (10 µg L⁻¹) and Ir (5 µg L⁻¹) in a 2% trace analysis grade HNO₃ (Fisher Scientific, UK). External multi-element calibration standards (Claritas-PPT grade CLMS-2 from SPEX Certiprep Inc., Metuchen, NJ, USA) included As, Cd, Cu, Fe, Mn, Pb, Se and Zn, in the range 0 – 100 µg L⁻¹ (0, 20, 40, 100 µg L⁻¹). A bespoke external multi-element calibration solution (PlasmaCAL, SCP Science, France) was used to calibrate major elements Ca, Mg, Na, and K in the range 0-30mg L⁻¹. Phosphorus calibration utilised an in-house KH₂PO₄ solution standard (10mg L⁻¹ P). Sample processing was undertaken using Qtegra™ software (Thermo-Fisher

Scientific) utilising external cross-calibration between pulse-counting and analogue detector modes when required.

2.6 Measurement of photosynthetic pigments in spinach lipid extracts

2.6.1 Extracting lipids from spinach leaf fractions

The following photosynthetic pigments were measured for the five fractionated components (see Section 3.1.1); chlorophyll-a (chl-a), chlorophyll-b (chl-b), total chlorophyll (total-chl; chl-a + chl-b) and carotenoids, and were analysed using a spectrophotometer (CARY 50 Probe-UV visible). All samples were homogenised with pestle and mortar and 0.1g of dried lipid extract was weighed into 15mL Falcon tubes, followed by continuous vortexing for 2 minutes. Samples had to be cold soaked overnight, at 4°C, to inhibit hydrolytic conversion of chlorophyll into chlorophyllide (Hu et al., 2013). All extracts were then flush dried under inert nitrogen (N₂), to hinder damaging photo-oxidation reactions (Pasquet *et al.*, 2011). Extracts were then dissolved in 10mL High Precision Liquid Chromatography (HPLC)-grade ≥99.9% acetone (Sigma-Aldrich, UK) and further diluted by a factor of 1:1000.

2.6.2 Measuring photosynthetic pigments in lipid extracts.

Small aliquots of each sample were inserted into glass cuvette tubes and were exposed to the following wavelengths while utilising the spectrophotometer; 661.6 nanometres (nm) for chl-a, 644.8 nm for chl-b and 470 nm for carotenoids. The blank cuvette tubes contained pure acetone with no samples and if the original samples were

too concentrated by observation or to fall under the absorption range, then they were diluted further with 1 – 2mL of pure acetone.

The following equations by Lichtenthaler and Buschmann (2001) (Equations 4A—D) were applied in the final calculations of the concentrations of the pigments (in $\mu\text{g/mL}$):

$$\text{Chl-a} = (11.24 \times A_{661.6}) - (2.04 \times A_{644.8}) \quad (\text{Eq. 4A})$$

$$\text{Chl-b} = (20.13 \times A_{644.8}) - (4.19 \times A_{661.6}) \quad (\text{Eq. 4B})$$

$$\text{Carotenoids} = ((1000 \times A_{470}) - (1.90C_a) - (63.14C_b)) / 214 \quad (\text{Eq. 4C})$$

$$\text{Total-chl} = \text{Chl-a} + \text{Chl-b} \quad (\text{Eq. 4D})$$

where A represents absorbance, C_a for chl-a concentration and C_b for chl-b concentration. A one-way ANOVA and Tukey test was used to compare them once again (McKillup, 2012).

Chapter 3: Growing spinach plants under controlled conditions to measure systemic Fe uptake.

3.1 Introduction

Iron is one of the most essential elements for plant growth and development. Iron deficiency in plants can be caused by any distress with iron uptake, transport and/or storage. It is known to cause many metabolic disorders and morphological abnormalities, such as changes in chloroplast structure and colour, resulting in reduced photosynthetic rates and reduced chlorophyll synthesis. This is also accompanied by abnormalities of chloroplast morphology and diminished respiratory abilities of the plant (Riaz and Guerinot, 2021). These changes eventually lead to adverse impacts on plant yield, quality, and morphology.

Iron is the most abundant element in both the inner and outer layers of the Earth, by mass. However, iron deficiency affects almost 40% of plants grown in soil, due to reduced solubility, as one-third of global soils are calcareous alkaline (Wang *et al.*, 2022). This is when the soil is high in calcium carbonate (CaCO_3), which fixes ferrous iron into ferric oxide, immediately causing the iron to become unavailable for root absorption.

This has eventually led to higher dependency for iron-containing chemical fertilisers, to help achieve the required amount of available iron. However, they are known to have their environmental consequences.

To increase the amount of iron in food chains generally, growers are seeking to increase the level of iron in the edible components of plants, through a process known as biofortification. This process involves increasing the concentrations and

bioavailability of iron in different plants. This can be done below from the roots, or directly to the plant leaves from above, using leaf foliar applications. Although foliar fortification of iron is a quick remedy for iron deficiency, its application needs to be repeated through the growing season, and it also has its technical problems (White and Broadley, 2009).

In hydroponic systems, this problem has been addressed by producing the readily soluble ferrous form of iron, Fe^{2+} , in the feed solution. Hydroponic systems allow growers to achieve both a balanced, and available supply of all essential nutrients, and thus higher quality, and good yields of vegetable production. Additionally, in situations where the control of nutrients fed to plant is required and the intact roots need to be collected, the use of hydroponic growth systems are more advantageous (Nguyen, 2016). In this study, a hydroponic system was used to fortify spinach with total Fe, by increasing the dosing concentrations of chelated Na Fe-EDTA, to the original hydroponic Hoagland nutrient solution, containing all the essential plant nutrients, at the correct pHs.

It is not yet known, which form of iron fertiliser is the most effective in increasing the amount of Fe taken up by spinach and what is the optimal concentration of this iron in the nutrient feed, which results in maximum fortification of iron in the edible part of spinach. This concentration is also expected to impact the uptake of other nutrients by spinach. This chapter represents the initial stage of this project which aimed to:

- 1) Select an effective method to grow spinach plants throughout the year at Sutton Bonington Campus under conditions where feed, and specifically the amount of iron fed to the plants, can be controlled.

- 2) Establish the optimum feed concentration (dose) of iron to promote plant growth and to avoid toxicity.
- 3) Monitor the uptake of iron into roots and leaves.
- 4) Prepare an ^{57}Fe chelate that can be added to the plant feed to trace Fe uptake by the plant.

3.2 Results and Discussion

3.2.1 Scoping a range of spinach growth methods and locations on Sutton Bonington Campus

Various growth systems and locations were explored for most of 2019, the first year of this project, to gain the field experience of growing spinach. Sutton Bonington Campus offers a vast range of plant growth facilities, including open fields, heated glasshouses, and fully controlled growth room environments, known as the Phytotron. These facilities allow researchers to use a wide range of growth systems, including both soil and hydroponic growth techniques.

A soil growth system was used as a control; however, it was not suitable for the purpose of this project. This is because it was difficult to control the amount of iron in the soil in which the plants were supplied with, which was one of the main priorities of the project. Work started with collaboration with the technicians from the SB Glasshouse and Growth Trials team. They explained and demonstrated all the available hydroponic growth systems and techniques available on campus, and how to manipulate them. Firstly, the Nutrient Film Technique (NFT), was explored, as shown in Figure 3.1.

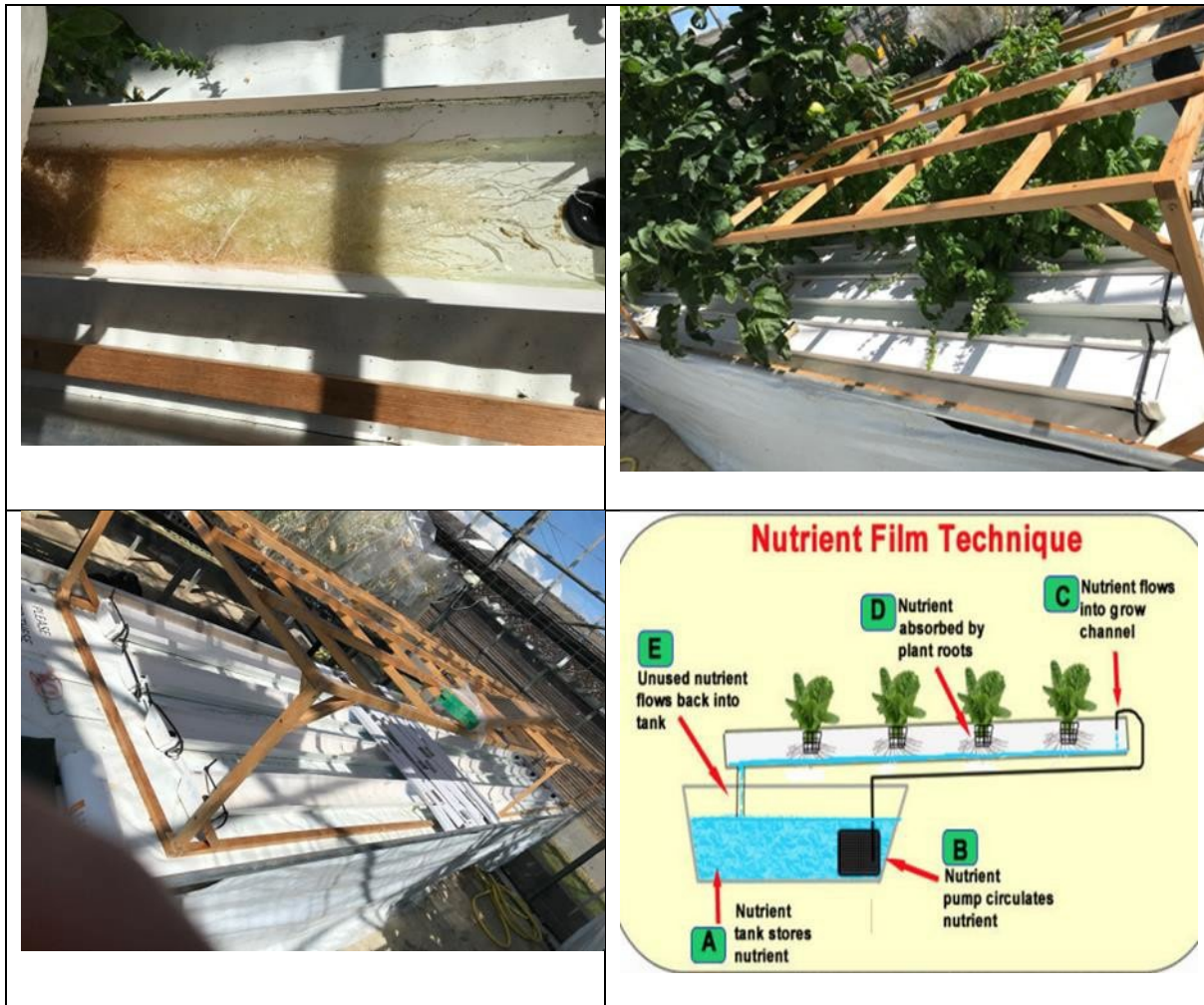


Figure 3.1: The Nutrient Film Technique (NFT) hydroponic procedure, explained.

While observing the NFT system running by another research team, it was excluded for this project. This is because it needs running nutrient solution in larger amounts, which also hinders the viability of controlling the amount of Fe in the nutrient feed solution, as well as the application of enriched ^{57}Fe isotope. This could be achieved

by using a closed, contained hydroponic system, easily supporting the roots within a known size of a growth compartment, such as rockwool cubes, perlite granules or sand filled in growth trays or pots. For hydroponic systems, sand was also initially tested, however, it was immediately abandoned, because it resulted in a poor germination ratio (see Equation 3.1).

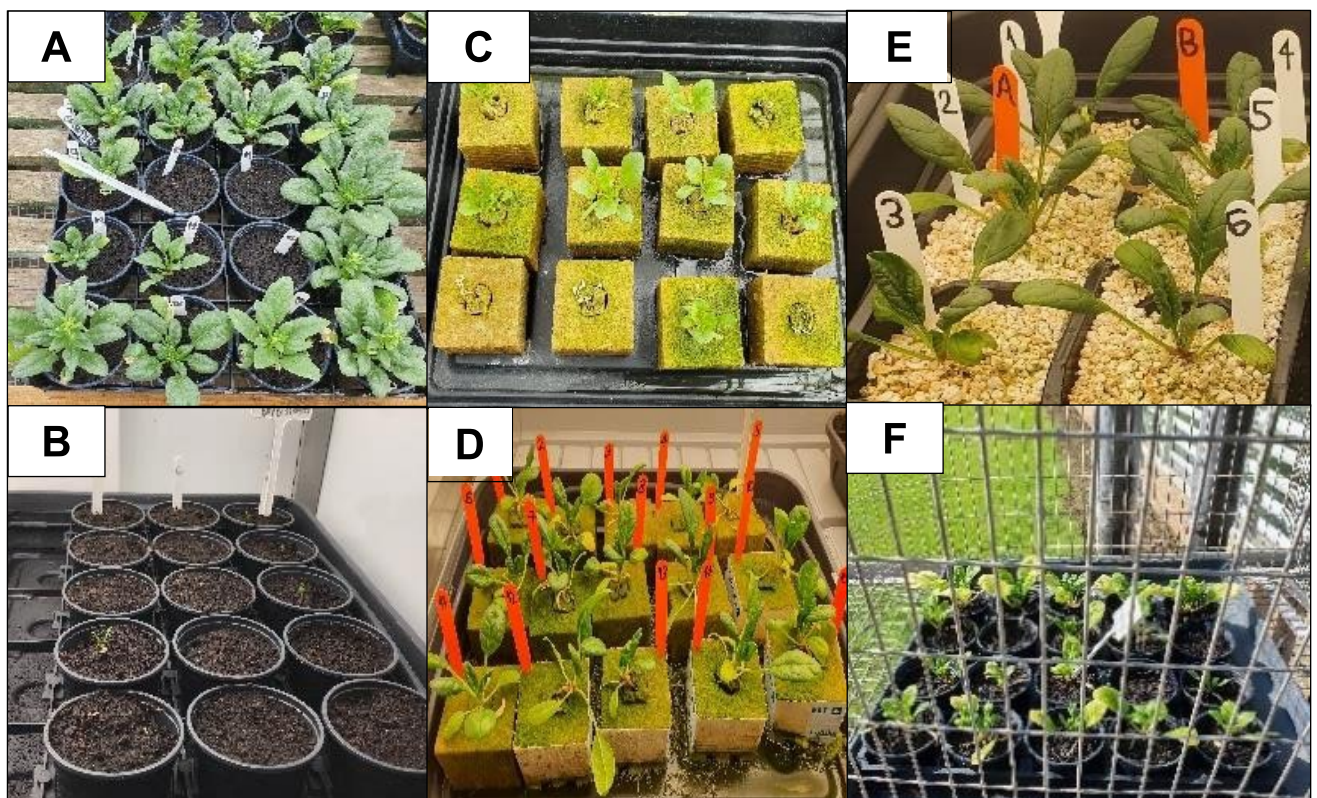
$$\text{Germination ratio} = \frac{\% \text{ of germinated seeds}}{\text{Initial number of sown seeds}} \quad (\text{Eq 3.1})$$

From May—August 2019, spinach plants were initially sown on hydroponic rockwool cubes (Cultilene®), a fibre, made from volcanic, basaltic rock. Its primary chemical composition is aluminium and silicon oxides (Bussell and Mckennie, 2004). Growing spinach in rockwool also resulted in poor germination and a fluctuating rate of growth. After further investigation, it was noticed that after soaking one rockwool cube in water, its pH rose rapidly to an alkaline 8-8.5, after dissolution. This prevented the seeds from germinating efficiently. Because of this, the pH of this water was adjusted after submergence of the rockwool cubes. However, the process was not practical because of difficulties with separation of the root and wool sections of the rockwool cubes. This is something which was needed to enable separation of the intact root system.

A general-use nutrient feed supplied in the glasshouses was initially used to water and feed the plants grown on hydroponic rockwool. The facility can be heated but not cooled, and the light period can be extended with extra artificial lighting during reduced daylight hours in winter, but not reduced during the long daylight hours of summer. Therefore, plants grown during the period from May—September 2019, in the glasshouse, were subject to fluctuations in light intensity and temperature. The hottest periods of the summer resulted in excessively high temperatures inside the

glasshouse (as high as 55°C), causing overheating and premature bolting, badly affecting the quality and yield of the spinach leaves (see Figures 3.2C and D). Open-air compost (OAC) was also tested; however, it was immediately abandoned, because it resulted in stunted spinach leaf development (see Figure 3.2F). In conclusion, compost produced the highest yields and leaf sizes, which were similar in size to those found commercially, however their growth patterns were not always consistent.

A soil system using compost (Levington Advance® Sphagnum Moss Peat) was also applied as a control to monitor healthy spinach plant growth in the glasshouse facilities (see Figure 3.2B).



Figures 3.2A—F: Visual representations, after scoping various growth matrices and locations for spinach growth, across the SB campus; 3.2A) glasshouse compost, B) growth room compost, C) glasshouse rockwool, D) growth room rockwool, E) growth room perlite and F) open-air compost (OAC).

3.2.2 Effect of growth conditions on spinach leaf surface area (SA)

To develop an appreciation of the growth kinetics of spinach plants grown both on compost and hydroponically, plants were grown on compost (control system), or rockwool (hydroponic system), in both the glasshouse and growth room facilities. Leaf surface areas (SAs) per one plant were measured as a primary quantitative indicator of healthy growth. During the second stage, when growth on perlite was finalised and applied for the rest of this study, two essential yield parameters were measured as a more reliable estimate of plant growth; fresh weight (FW) and dry weight (DW) of the spinach leaves per plant, which is technically the only edible part of the plant.

3.2.2.1 Spinach grown on compost and on rockwool in the glasshouse facilities

3.2.2.1.1 Surface area (SA) of spinach leaves grown in compost in the glasshouse

Spinach leaf surface areas (SAs) per one plant were measured using ImageJ software (Version 1.53). Figure 3.3 shows that for when grown in compost in the glasshouse the seeds could be sown directly without the need for transplanting. When more than one seed germinated, thinning was applied to retain only one in each pot. This was done to prevent intraspecific competition for nutrients within the same compartment.

Day 12 represents the day where germination was complete, and when the first true leaves emerged from the shoots. In compost, the behaviour of the leaf SAs was as follows; From Days 12—20, there was approximately a linear increase in SA by 7 cm², followed by no further increase until the end of the growth period.

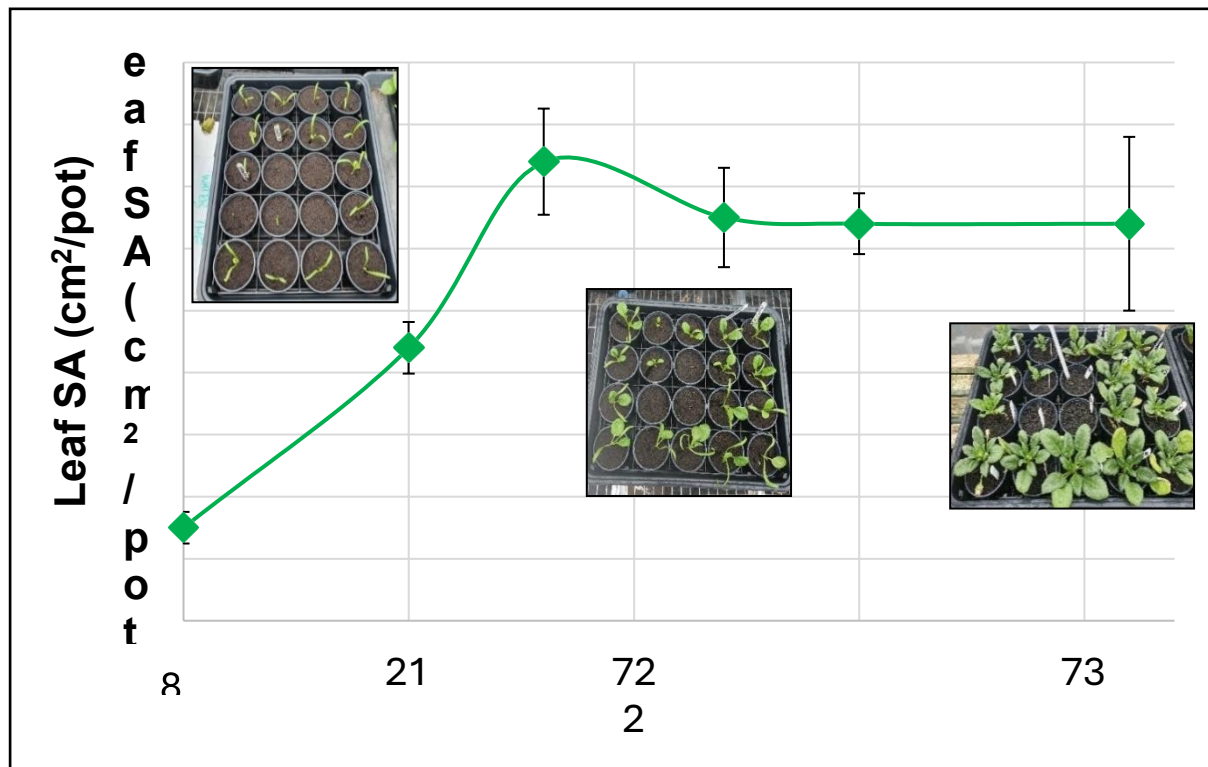


Figure 3.3: Leaf SAs (in cm²/pot) of Trombone F1 spinach grown on compost in the glasshouse, from Days 19—36 of growth. See the visuals of the leaves within each stage of growth. Performed in June 2019.

3.2.2.1.2 Surface areas (SAs) of spinach leaves grown on rockwool hydroponics in the glasshouse

When using rockwool, seeds were initially sown in small cubes for the germination period, before being transplanted into larger cubes, to continue their growth.

Thinning was also applied in this case, to keep only one plant in each cube. On Day 19, the germination phase was completed and the first true leaves de-etiolated. Plant growth was indicated by the average SAs of the fully mature leaves per one plant, during the growth period between Days 19—35. Figure 3.4 refers to the rockwool cubes, where there was an increase from approximately 2 cm²/cube to 8 cm²/cube, between Days 20—36.

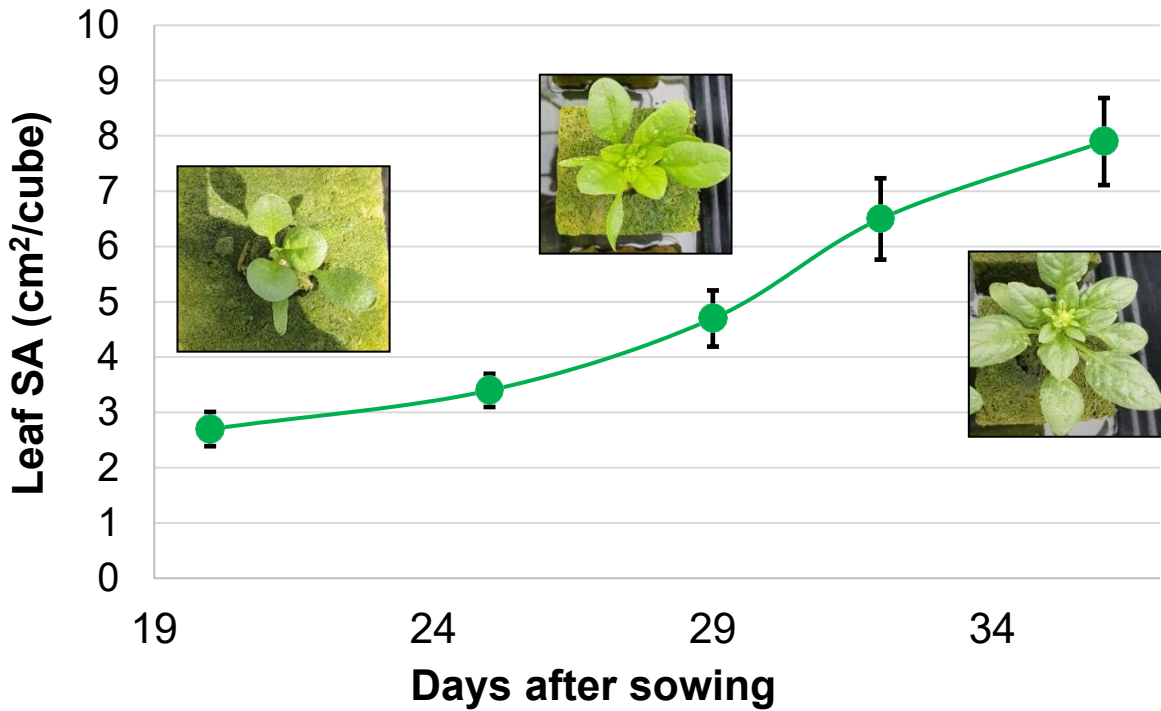


Figure 3.4: Leaf SAs (in cm²/cube) of Trombone F1 spinach grown on rockwool cubes, inside the glasshouse, from Days 19—36 of growth. See the visuals of the leaves within each stage of growth. Performed in June 2019.

3.2.2.2 Spinach grown in the growth room facilities.

By September 2019, the second stage of work started, and a new growth location was made available, which was a fully controlled growth room on campus. Spinach plants were sown on both compost and hydroponic rockwool. The growth conditions can be seen in Table 2.2, Section 3.3. Plants were exposed to a temperature range of 18—23°C, relative humidity of 60—100% and a light intensity of 80—200 $\mu\text{mol m}^{-2} \text{s}^{-1}$, under fluorescent lighting, for a 16:8 hour, light:dark photoperiod.

3.2.2.1 Surface area (SA) of spinach leaves grown on compost in the growth room

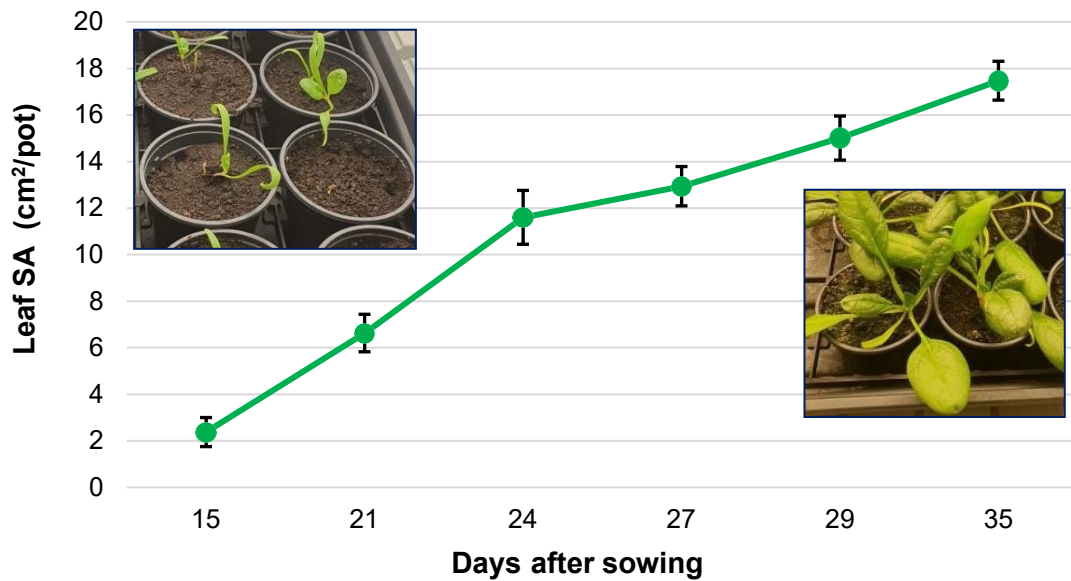


Figure 3.5: Leaf SAs (in cm²/pot), of Trombone F1 spinach grown on compost in the growth room, from Days 15—35, of growth. See the visuals of the leaves within each stage of growth. Performed in October 2019.

Based on Figure 3.5, there was a steady increase in spinach leaf SA, from approximately 2 to 25 cm²/pot, from Days 15—35 of their growth. They also grew to a size like that found for commercially grown spinach, such as the ones sold in Tesco.

3.2.2.2.2 Surface areas (SAs) of spinach leaves grown on rockwool in the growth room

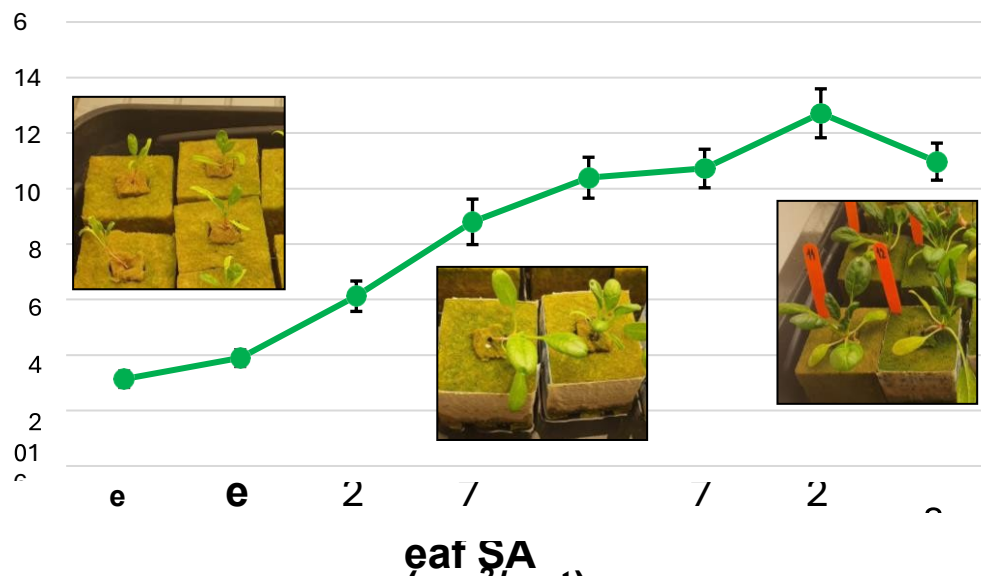


Figure 3.6: Leaf SAs (in cm²/pot), of Trombone F1 spinach grown on rockwool cubes in the growth room, from Days 29—55, of growth. See the visuals of the leaves within each stage of growth. Performed in October 2019.

Spinach took longer to germinate on the rockwool in the growth room, than in the glasshouse facilities (see Figure 3.6). Also, most of the spinach leaves senesced, by the time of harvesting. This occurred halfway through their proliferation. This also explains the reduction in leaf SAs between Days 51—55.

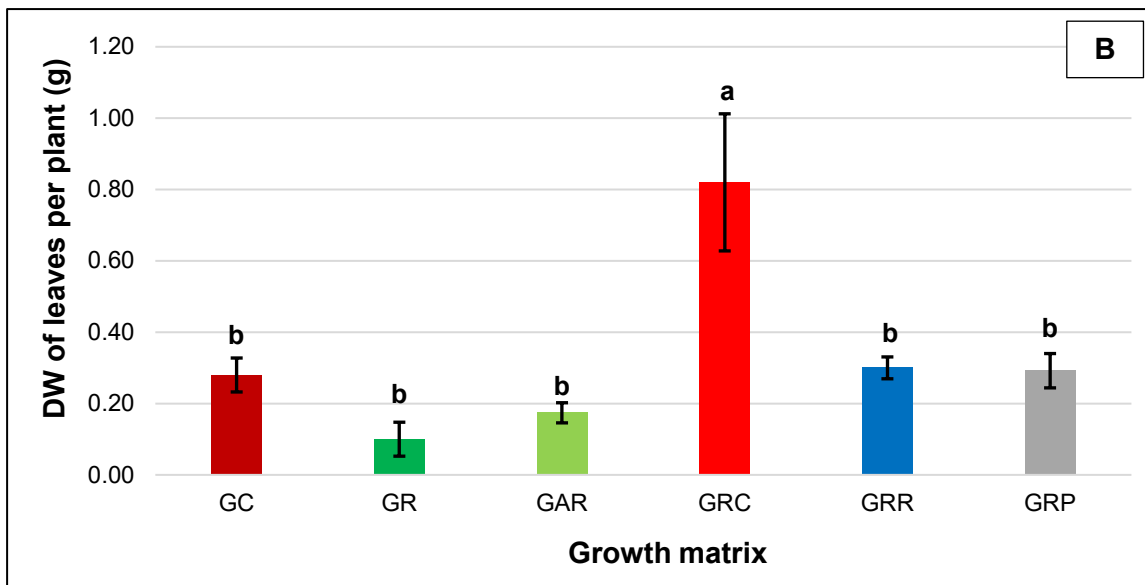
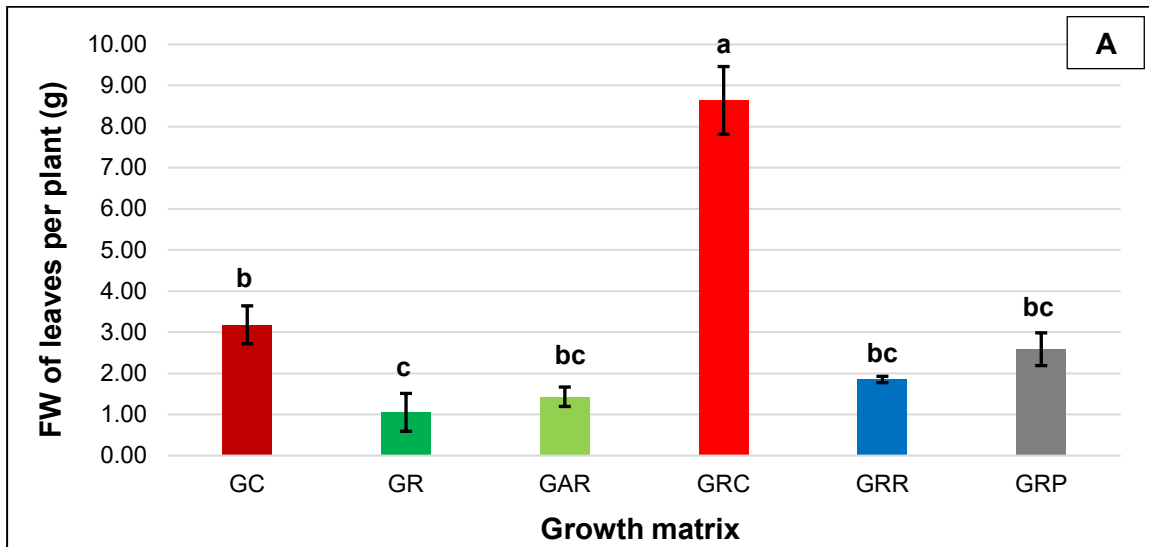
Watering and feeding regimes were also examined during the same period of May – September 2019, and in the end, it was decided to produce our own Hoagland nutrient solution (see Table 2.2) (Soberg *et al.*, 2016). External environmental factors including light intensity, temperature and humidity were not measured throughout the entire experiment, which in turn, made it difficult to carry out a more detailed study of the impact of different growth conditions. The only variables which were changed, were the growth matrices and locations. Thus, the data obtained in these scoping trials were mostly qualitative, as opposed to quantitative, hence non-numerical

observations on plant growth, were used to decide the final most optimal growth method.

At this subsequent stage, perlite was introduced as a hydroponic growth medium, which is a granular amorphous volcanic aluminosilicate, which is natural, sterile, inert and pH neutral. Perlite granules were filled up in potting trays with 6 compartments each, measuring 9 cm² in area (see Figure 3.2E) and were watered with Hoagland nutrient solution, starting from Day 0, of sowing the seeds with 50 mL per compartment on Monday, Wednesday, and Friday, until harvesting, usually within 6 weeks of sowing.

3.3 Effect of growth conditions on the yield of spinach leaves

Growth conditions were selected based on which regime produced the most consistent spinach growth and yield patterns, as well as good germination rates. The two locations tested were the 1) glasshouse and 2) growth room facilities. The two growth systems tested were 1) the soil system, using standard peat compost matrix, and 2) the hydroponic system using rockwool cubes and perlite. At this stage of work, yield was measured to give us insight into the amount of leaves biomass we can get of each growth method/system and to direct us more toward the best method forward in this study.



Figures 3.7A—B: 3.7A) FWs and B) DWs of the leaves per one plant of cultivated spinach Trombone F1 in different growth matrices; varying locations and matrices; glasshouse compost (GC), glasshouse rockwool (GR), glasshouse adjusted rockwool (GAR), growth room compost (GRC), growth room rockwool (GRR), growth room perlite (GRP). Error bars represent SEM and the presence of different letters a and b denote a significant difference between samples at $p < 0.05$ using Tukey post-hoc test.

Figure 3.7A shows the highest FW of 8.5 g/leaf was achieved for GRC, and it was significantly different to all the other growth matrices. Glasshouse rockwool (GR) spinach had the lowest FW of 1 g/leaf and was most likely a result of inconsistencies of environmental parameters, including light intensity, and temperature, given the climatic fluctuations. It was also only significantly different with GC.

Student ID: 20194859

It also occurred because of alkaline dissolution of the rockwool as well. All rockwool samples generally had lower leaf FWs compared to compost and perlite samples, however their differences were not always significant. There are only significant differences between GR and GC.

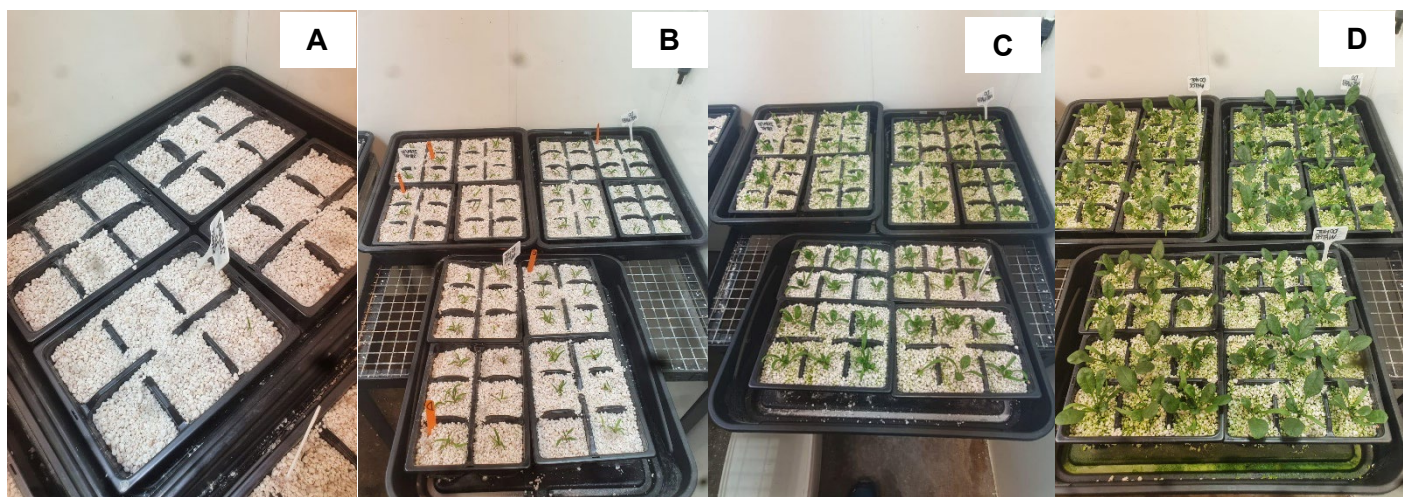
Figure 3.7B also shows the highest DW of roughly 0.80 g/leaf was also recorded for GRC, and it was significantly different to the other growth methods.

3.4 Finalising the growth conditions of spinach plants for this project

This work has given us an insight of the best practical location and logistics of the work, added to the experience in determining healthy plant growth. The location was finalised to be in the growth room for the remaining duration of the project.

Although there were no significant differences between DWs of perlite and rockwool, the perlite resulted in more consistent growth, in terms of germination rate and growth parameters. There was also no need for transplanting, as the seeds were sown directly in the perlite, and hence, achieved very good germination rates. Additionally, there were problems with alkaline dissolution in the rockwool, for in both the glasshouse and growth room facilities (see Figures 3.7A—B).

Figures 3.8A—D, on the next page, show the stagnated process of germination and growth of spinach in the growth room, on perlite, fed with Hoagland nutrient solution.



Figures 3.8A—D: Stagnated process of Trombone F1 spinach seed germination and growth in the growth room, using perlite and Hoagland nutrient solution, representing 3.8A) sowing, B) germination/de-etiolation, C) growth and D) harvesting periods.

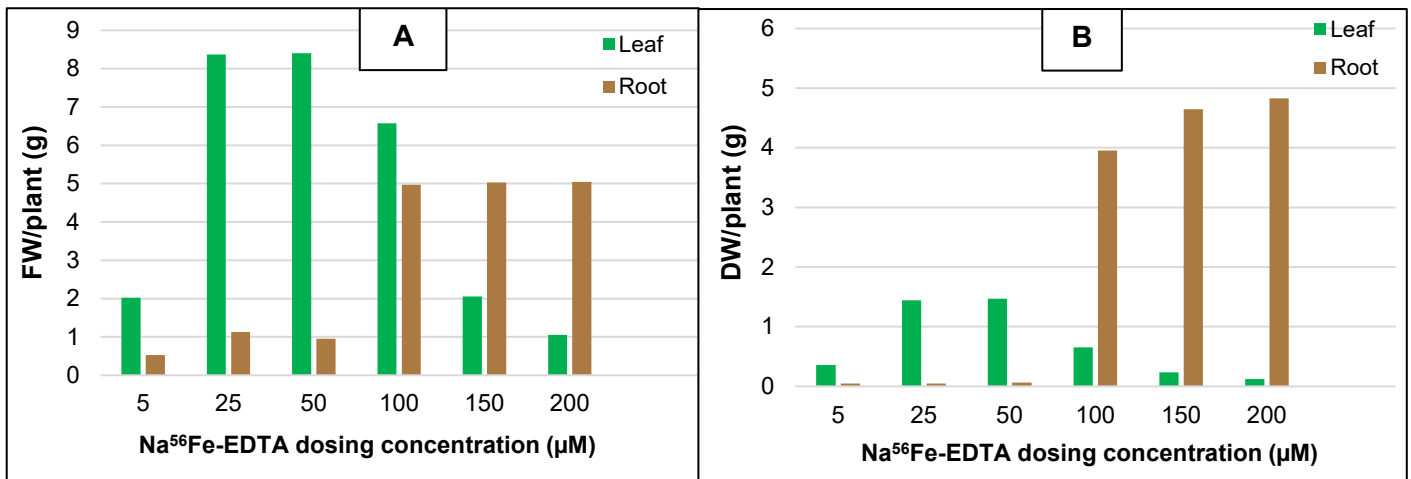
Overall, perlite resulted in the highest consistency of spinach growth, a good germination rate, and the practicality in separation of intact and clean root material.

3.6.1 Effect of Fe dosing on spinach growth and yield

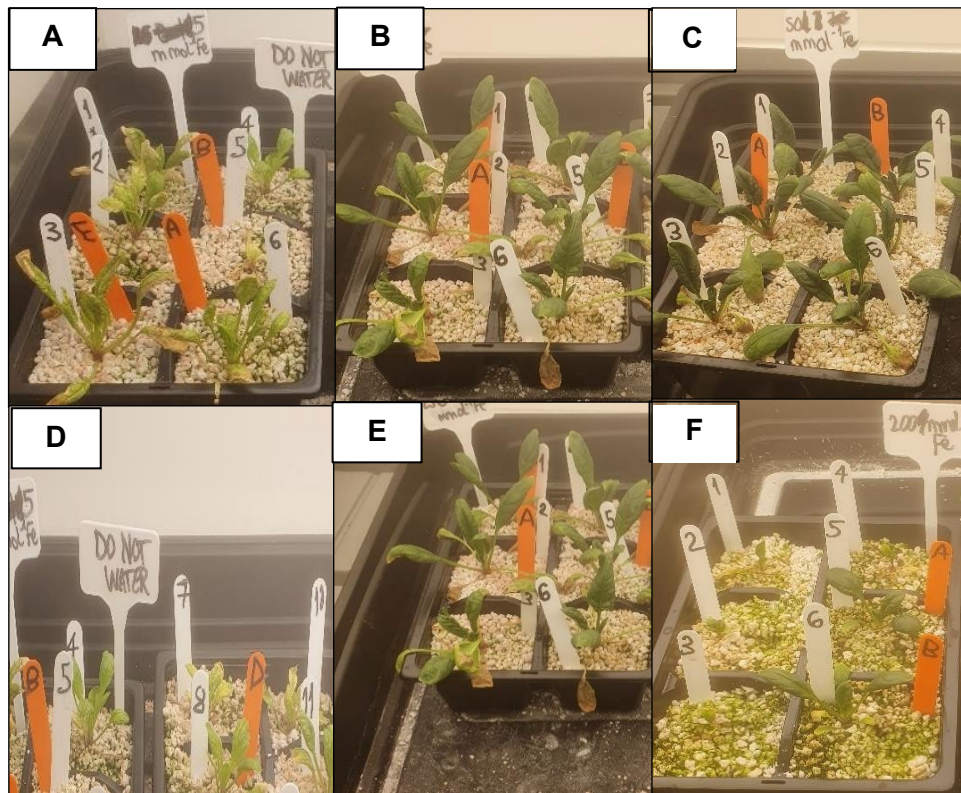
3.6.1.1 Dosing trials with different NaFe-EDTA concentrations in Hoagland nutrient solution

After the initial period of setting up the growth environment, trials of exploring the optimal Fe concentration in the feed solution, which is Hoagland nutrient solution, combined with the effect of the gradient increase of iron in the feed solution, on plant growth. This was represented by root and leaf morphology, FWs and DWs. Firstly, 6 distinct dosing concentrations of Na Fe-EDTA in Hoagland nutrient solution were fed to the plants, from Day 0, the day of sowing. They were 5, 25, 50, 100, 150 and 200 μM of Fe.

A preliminary experiment was performed to compare the FW and DWs/plant of spinach leaf and root material of spinach, grown in the growth room, after the per mentioned Fe dosing process. These are clearly outlined in Figures 3.9A—B below.



Figures 3.9A—B: A) FWs and B) DWs per plant grown on perlite in the growth room, after dosing with 5, 25, 50, 100, 150 and 200 µM Na Fe-EDTA in Hoagland nutrient solution.



Figures 3.10A—F: Comparisons of leaf morphologies of Trombone F1 spinach, grown on perlite, in the growth room, after dosing with 3.10A) 5, B) 25, C) 50, D) 100, E) 150 and F) 200 µM Na Fe-EDTA in Hoagland nutrient solution.

The highest FW weight/plant of spinach leaves of roughly 8.5 g was reached after dosing with both 25 and 50 µM Na Fe-EDTA in solution (see Figure 3.9A). Leaf FWs

were exactly 2 g/plant after dosing with 5 μM , suggesting it falling within the plausible deficiency range. This also parallels with Mori (1999).

After dosing with 200 μM Na Fe-EDTA, the average leaf FW was only 1 g, accompanied with limited growth, small leaves size and suggesting this concentration being within the toxicity range. Figures 3.10 A—F visually prove that the optimal spinach dosing concentrations ranged between 25—100 μM NaFe-EDTA. After dosing with 150—200 μM , leaf sizes and yields decreased most rapidly, also explaining the similar patterns between DWs and FWs from Figure 3.9 A—B.

The root DWs were noticeably (but not significantly) lower between 5—50 μM , in comparison to 100—200 μM Na Fe-EDTA, with a difference as large as approximately 5 g between 5 and 200 μM . The leaf DWs peaked at approximately 1.4 g, after dosing with 25 and 50 μM Na Fe-EDTA and linearly decreased between 100—200 μM (see Figure 3.9B). The same was true for the FWs, however the DWs were of lower values. These results agree with Oztekin *et al.* (2018), with spinach root amounts increasing, after increasing nutrient solution dosing concentrations. For instance, for the first harvesting round, for the half dose Fe (2.5 mg/L), the root FW was 0.51 g compared with 0.62 g for the full dose (5 mg/L). For the second harvesting round, for the half dose, the leaf FW was 2.89 g compared to 3.05 g for the full dose. However, the differences were not significant, and this data was only preliminary and requires further investigation.

3.6.1.2 Dosing trials of spinach plants within the toxicity range of iron

Based on Figure 3.11, because the toxicity range was reached after dosing with solution concentrations higher than 200 μM Na Fe-EDTA, it was finally decided to stick

to a range of 5—200 μM Na Fe-EDTA, in solution. The morphological indications of toxicity included the senescence, drying and burning of all the spinach leaves.



Figure 3.11: Plant morphology of Trombone F1 spinach grown on perlite, in the growth room, after dosing with 400 μM Na Fe-EDTA in Hoagland nutrient solution.

Extra trials were run using 4 gradient concentrations of Fe in the toxicity range; 250, 300, 350 and 400 μM , to test the morphological indications of toxicity. This was clearly seen, because of the senescence and drying of the leaves (see Figure 3.11). Spinach was sown in perlite, in the growth room, and dosed with six distinct Na Fe-EDTA concentrations in Hoagland nutrient solution; 5, 25, 50, 100, 150 and 200 μM (see Figure 3.12) were analysed by ICP-MS, (see Section 2.8). Owing to a lack of samples for all the dosing concentrations, further statistical analysis, including the generation of error bars was not possible.

For root material, there was a gradual increase of Fe concentrations from approximately 220 to 500 mg/DW after increasing the dosing concentrations of Na Fe-EDTA within the selected optimal range.

For the leaf material, Fe concentrations remained between 30 and 100 mg/kg DW, after dosing with all solution concentrations, with a peak of 90 mg/kg DW being reached, after dosing with 150 μM . Öztekin *et al.*, (2018) reported slightly different spinach leaf Fe^{2+} concentrations after increasing the nutrient doses of Fe, Mn, Zn, Cu and Mo. In this study, they report that at the full doses of Fe, in the feeding solution (89 μM) the corresponding Fe concentration in the leaves was 80.45 mg/kg which has decreased to 76.45 mg/kg for the half dose of Fe in the feeding solution.

3.6 Iron stable isotope enrichment trials

Very few studies have investigated the pathways of other Fe isotopes in spinach plant leaves and their chloroplasts and novelty will be added to the research, through addition of enriched ^{57}Fe , which is a stable isotope. An enriched stable isotope of iron (^{57}Fe) was provided as free iron in HCl solution, which required chelation with EDTA, before being added to the final amended Hoagland solution. The chelating process is provided in Appendix 2.

3.6.1 Observation on spinach response to ^{57}Fe does in the feed solution

Spinach was grown for 21 days and watered every Monday, Wednesday, and Friday, using 50 μM Hoagland solution, followed by three consecutive watering days (Days 21, 24 and 27), with Hoagland solution containing, an additional 10 μM ^{57}Fe . Plants were harvested, rinsed, and CRF material was extracted for the big leaves, small leaves, and the mixed leaf sizes. All plant parts and CRF material were then dried and digested for ICP-MS analysis, and data for the ^{57}Fe /total Fe mass ratios are shown in Figure 3.13.

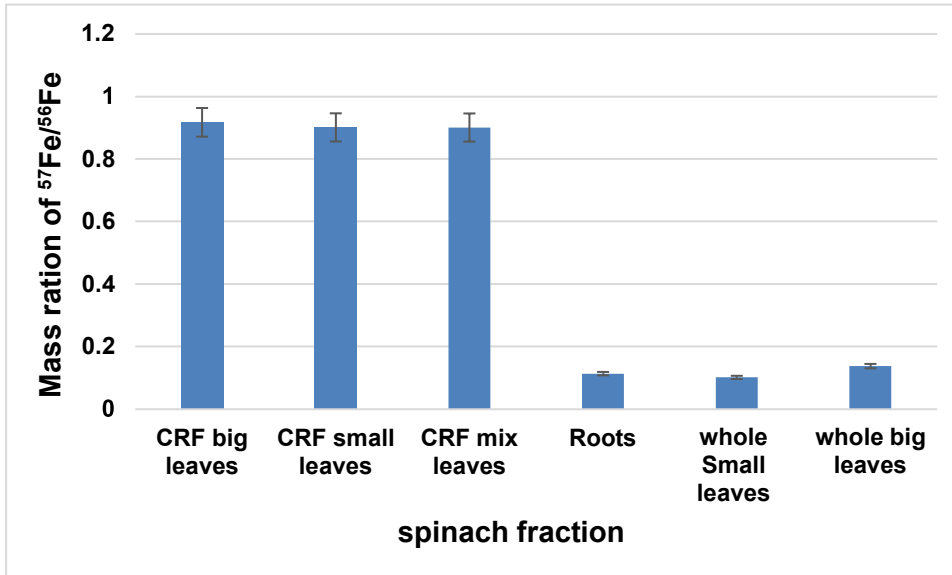


Figure 3.13 ^{57}Fe /total Fe mass ratios for CRF, roots, WLM and CRM for Trombone F1 spinach plants grown in the growth room and spiked with ^{57}Fe in their feed solution.

The amount of ^{57}Fe which has been distributed between different fractions of spinach as response to feeding them with Hoagland solution spiked with ^{57}Fe is plotted in Figure 3.13 the graph shows that the largest amount of ^{57}Fe goes to the chloroplast which is consistent with the observation of total iron content in each part.

3.7 Conclusions

- To obtain a consistent yield and quality of spinach plants throughout the year, glasshouse and outdoor growing are not recommended. A growth room at 19 – 24°C, relative humidity between 50 – 70%, and light intensity of 17—22 mol/m²/d provided optimal growing conditions.
- The yield of spinach leaves grown on compost in a growth room was 6 times higher, than for plants grown on perlite or rockwool. However, compost could not be used to carry out a mineral uptake study, because it was not easy to control the amount of iron originating from the soil/compost.
- Rockwool and perlite offered inert platforms to grow spinach hydroponically and allow a controlled addition of liquid feed.

- Perlite outperformed rockwool as a platform for growing spinach plants hydroponically in terms of germination rate, yield, constancy of plant quality and the practicality of plants harvesting and roots separation.
- Spinach plants grown on perlite in a growth room provided an effective way to measure the rate of iron uptake into roots and leaves. They also yielded enough leaf material to recover Chloroplast Rich Fraction (CRF), for the bioaccessibility trials.
- ^{57}Fe chelates were prepared by chelating the acidic ^{57}Fe solution with EDTA before adding to the Hoagland feed to provide an effective means to load plants with a stable isotope of iron.
- ^{57}Fe enrichment was achieved through watering mature spinach plants (grown for 21 days), a further 3 consecutive times with Hoagland nutrient solution containing $3\ \mu\text{M}$ ^{57}Fe .

Chapter 4: Mathematical modelling of spinach plant Fe uptake kinetics

4.1 Introduction to modelling and ordinary differential equations (ODEs)

A model is defined as a formal representation of a system or phenomenon in the real-world context. They help predict changes in systems by modelling reality and explaining both their inputs and outputs, furthermore, by providing explanations and predictions. They exist in different forms including physical models such as a globe or aquarium, software programmes such as for climate predictions and mathematical equations (Rutherford, 2009). The main emphasis of this project will be on mathematical equations.

Models have their strengths and weaknesses. The strengths are models allowing scientists to predict and simplify complex systems, results easily being shown to other scientists and the public, and inputs easily being changed and closely examined before waiting for real-world events to occur. Some weaknesses include oversimplification, resulting in reduced accuracy, subjectivity, and different models sometimes show different effects based on the same data (Rutherford, 2009).

The key steps in mathematical modelling are identifying all variables and parameters, determining model structures that would describe all phenomena of interest, and finally solving them (Harcet *et al.*, 2012). When building any model, the core parts to consider are 1) entities/components, 2) interactions/reactions, 3) what forms the interactions can take, 4) writing down the equations term by term and 5) analysis and simulation.

The biological phenomenon analysed by the means of mathematical modelling was the Fe uptake by root and leaf material of growth room perlite-sown spinach plants.

These spinach plants were dosed with seven distinct external NaFe-EDTA solution concentrations; 10, 25, 50, 75, 100, 150 and 200 μM . This process shows the variability of growth indicators including Fe contents per plant part, and DWs during the observed growth periods. A typical method used to model the dynamically changing quantities is the application of Ordinary Differential Equations (ODEs). In mathematical calculus, ODEs consider time to flow continuously and consider concentrations of different entities including particles, molecules, and populations of all living organisms. The key concept is time, t , and rates of change of entities are measured through time, including velocities of particles and concentrations of molecules. ODEs originate whenever a universal mathematical law is expressed by the means of one independent variable and their relationship with their derivatives. The derivative is defined as the rate in which one quantity changes with respect to one another (Harcet *et al.*, 2013).

ODEs are written with respect to the state variable x and one or more of its derivatives. In the ODE, the derivatives are notated in the form of $\frac{dx}{dt}$ (Tenenbaum and Pollard, 1985) and quantitatively defined by the right-hand-side function of the state $f(x)$. The term 'ordinary' is used in contrast with 'partial' differential equations (PDEs) in the fact that they are used with respect to more than one independent variable. These ODEs were implemented through coding on MCMC package on Anaconda Python Spyder Software (see Figure 4.13).

Equations 4.1A—C on the following page are the three preliminary ODEs formulated for this experiment. Equation 4.1D shows a list of all measurable parameters.

4.1.1.1 ODE for growth matrix

$$\frac{dx_M}{dt} = -r_{MR} \frac{dw(t)}{x_M + K_M} X_M \quad (\text{Eq. 4.1A})$$

Here, we model the Fe contents in the perlite growth matrix.

where:

- x_M is the time-varying Fe content in the growth matrix (Roose *et al.*, 2001).
- $dw(t)$ is the time-varying dry weights of the plant parts over the number of days (Kumwimba *et al.*, 2013).
- K_M is the Michaelis-Menten (MM) constant corresponding to the Fe content in the growth matrix, required for half-maximal uptake (Mankin and Fynn, 1996; Roose *et al.*, 2001; Verma *et al.*, 2007).
- r_{MR} is the rate of Fe uptake from the growth matrix to roots. This parameter represents the maximum amount of Fe that plant roots can absorb at their present physiological state e.g root surface area.
- $\frac{dw(t)}{x_M + K_M}$ is the scaling factor of the rate of Fe uptake from the growth matrix. This changes proportionally to the root DWs.

4.1.1.2 ODE for roots

$$\frac{dx_R}{dt} = r_{MR} \frac{dw(t)}{x_M + K_M} X_M - r_{RL} X_R - r_D X_R \quad (\text{Eq. 4.1B})$$

Here, we model the transfer of Fe, from the growth matrix to the roots.

where:

- x_R is the time-varying Fe content in the roots.
- r_{RL} is the rate of Fe uptake from the roots to leaf material.
- r_D is the rate of depletion of Fe from the plant.

4.1.1.3 ODE for leaf

$$\frac{dx_L}{dt} = r_{RL} X_R - r_D X_L \quad (\text{Eq. 4.1C})$$

Here, we model the transfer of Fe, from the roots to the leaf material.

where:

- x_L is the time-varying Fe content in the leaf material.

4.1.1.4 Initial conditions of Fe content in each domain

$$x(0): \quad 1) x_{M_{t=0}} = x_M(0), \quad 2) x_{R_{t=0}} = x_R(0), \quad 3) x_{L_{t=0}} = x_L(0) \quad (\text{Eq. 4.1D})$$

4.1D)

where:

- $x(0)$ represents the initial conditions of Fe content in each domain, with the corresponding time of $t = 0$ (Salgado *et al.*, 2010).
- $x_M(0)$ is the initial Fe content in the growth matrix.
- $x_R(0)$ is the initial Fe content in the roots.
- $x_L(0)$ is the initial Fe content in the leaves.

In Equations 4.1A—C, x_M , x_R and x_L were measurable, which will constitute the final data, Y . However, K_M , r_{MR} , r_{RL} and r_D are unknown, which will constitute part of the final model, θ . These unknown model parameters can be estimated by fitting Equations 4.1A—C to the experimental data.

4.2 Materials and methods

4.2.1 Growing spinach after dosing with different external NaFe-EDTA concentrations in Hoagland solution

Spinach plants were grown in perlite and supplied with Fe as in Section 2.5, for the purpose of mathematically modelling their uptake by root and leaf material.

Within each trial, during the first three weeks (21 days) of growth, spinach plants were fed with the Hoagland solution, dosing with the optimal concentration of 50 μM NaFe-EDTA (Jin *et al.*, 2013). After this period, there were 10 separate watering points, which spanned another 21 days including gaps of two days during weekends. They were dosed with Hoagland solution (30 mL per watering point) with different external

concentrations of NaFe-EDTA; 10, 25, 50, 75, 100, 150 and 200 μM . The other stock solution concentrations for the Hoagland solution, were kept constant throughout (Jin *et al.*, 2013) (see Table 2).

A concentration of 10 μM was in the potential deficiency range, whereas 150—200 μM were in the potential toxicity range. After 21 days of each treatment, the plants were harvested randomly for the final 10 watering time points, after exposure to all dosing concentrations (Jin *et al.*, 2013). For each time point, random samples of plant root and leaf material were separated and then rinsed, applying the same method as Section 2.3.3, and a sieve separated the excess perlite bound to the root. After rinsing, all plant material was again blotted on tissues to fully dry for 20 minutes. At this point onwards, fresh weights (FWs) were measured for each plant part, by placing them in pre-weighed aluminum trays followed by weighing the total weights, to finally calculate FW material. The materials were then oven-dried at a 105°C, for 48 hours followed by taking the weight and calculating the dry weights (DWs). This was calculated through deducting the initial weights of the aluminum trays. FWs and DWs were measured for both root and leaf materials and the total FW and DW materials (see Equation 4.2) were also calculated, as a direct indicator of their growth (see Figures 4.2A—B).

Finally, all plant material was then stored in airtight plastic containers for subsequent measurement of internal Fe concentrations. The same acid digestion and ICP-MS experiments from Section 2.6 were performed.

$$\text{Total Fe (g/DW or FW)} = \text{Fe}_{\text{stem+leaf}} + \text{Fe}_{\text{root}} \quad \text{(Eq. 4.2)}$$

4.2.2 Measuring Fe contents in leaves and roots

For the final modelling analysis, the final Fe contents (in $\mu\text{g}/\text{plant}$) of root and leaf material, were calculated through incorporation of both DW values and final Fe concentrations (see Equation 4.3) (Şimşek and Çelik, 2021).

$$\text{Fe content } (\mu\text{g} / \text{plant}) = \frac{\text{Total weight plant part DW (g)} \times \text{Fe concentration } (\mu\text{g}/\text{kg})}{1000} \quad (\text{Eq. 4.3})$$

From Equation 4.4, the internal Fe contents of the entire perlite growth matrix were also indirectly calculated, with direct measurement from the beginning:

$$\Sigma\text{Fe}_{\text{perlite growth matrix}} = \Sigma\text{Fe}_{\text{supplied on day}} - (\Sigma\text{Fe}_{\text{root}} + \Sigma\text{Fe}_{\text{stem+leaf}}) \quad (\text{Eq. 4.4})$$

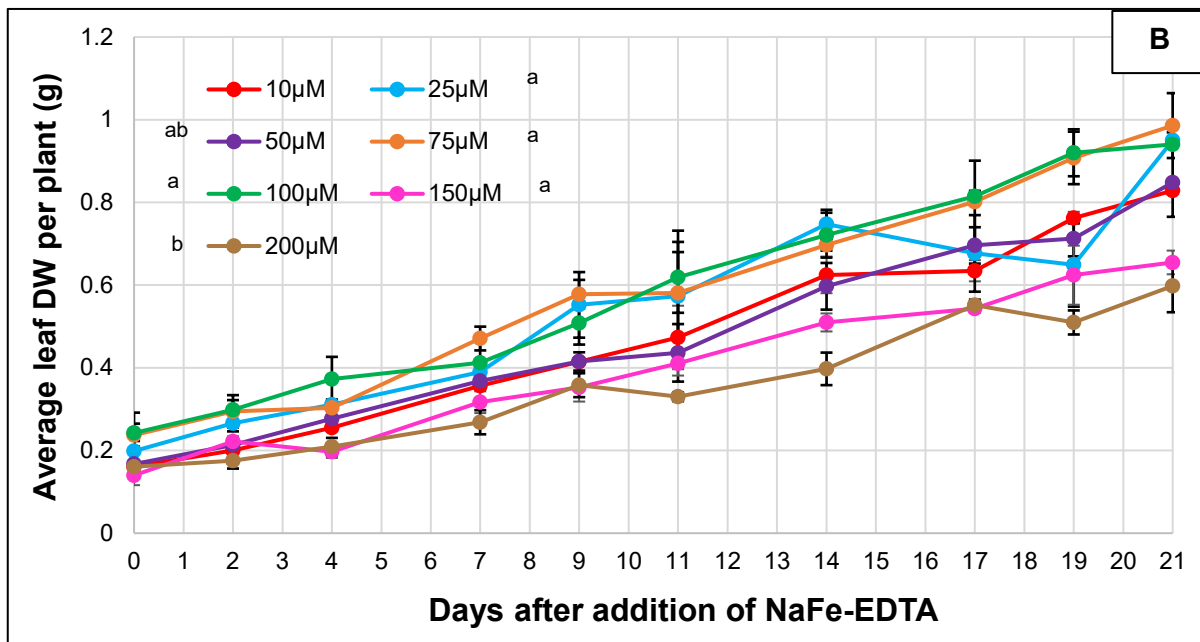
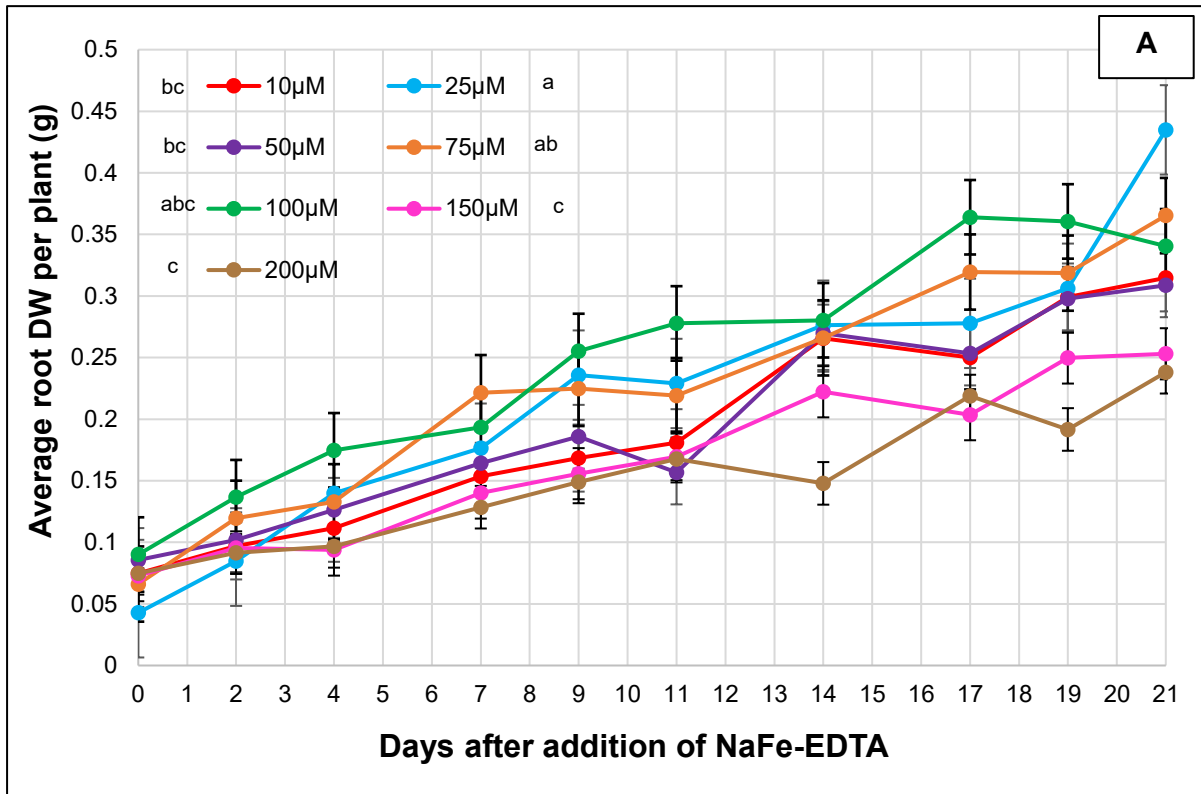
4.3 Results and Discussion

Figure 4.1 clearly illustrates the different plant parts of the perlite-sown spinach, for this project.



Figure 4.1: Visual representation of plant parts of perlite spinach grown in the growth room

4.3.1 Initial DWs per plant part



Figures 4.2—4.3: Average DWs per plant, of 4.2) root and 4.3) leaf material after dosing with 10, 25, 50, 75, 100, 150 and 200 μM NaFe-EDTA in solution. There were 10 time points in total. Error bars represent SEM and the letters are derived from ANOVA post-hoc Tukey testing ($p < 0.05$) on Minitab 21 software.

Figure 4.2 shows the peak average root DW per plant of 0.44 g, being reached on Day 21, after dosing with 25 μM NaFe-EDTA in solution. Conversely, the lowest average root DW of 0.05 g was reached on Day 0, after dosing with the same concentration in solution. Overall, the average root DWs per plant were the highest, after dosing with 100 μM NaFe-EDTA, and lowest after dosing with 200 μM NaFe-EDTA. This was because of the potential toxicity range being reached. There were also significant differences in average leaf DW per plants after dosing between 25 and 50 μM NaFe-EDTA in solution.

Figure 4.3 shows the peak average leaf DW per plant, of 1 g, being reached on Day 21, after dosing with 75 μM NaFe-EDTA in solution. All dosing concentrations had their peak average DWs on Day 21. The lowest average leaf DW per plant of approximately 0.18 g was reached on Day 0, after dosing with 150 μM NaFe-EDTA in solution.

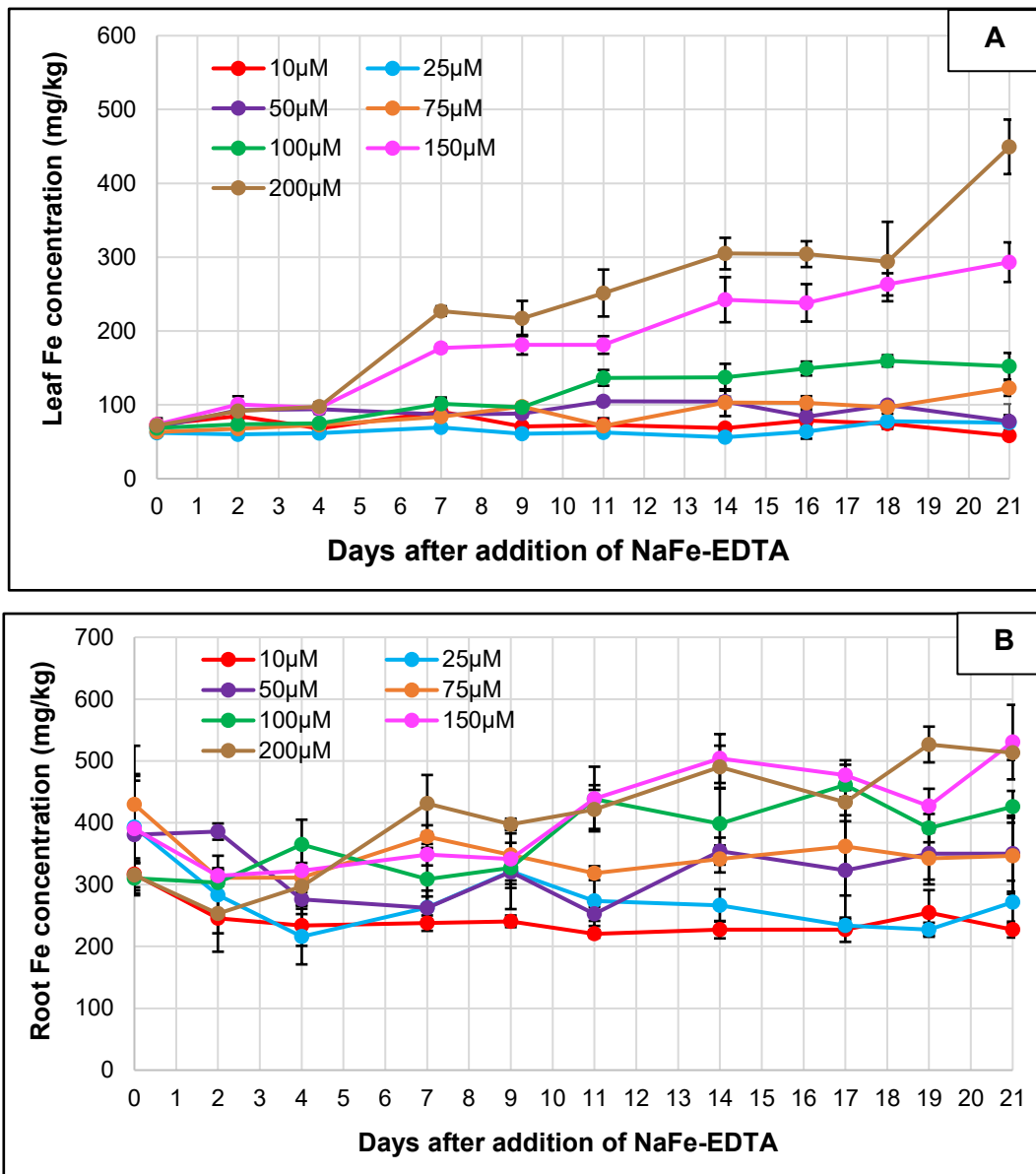
Compared to the root material, average leaf DWs per plant, all showed similar linear increases for all dosing concentrations, with some variations after dosing with 200 μM NaFe-EDTA. Şimşek and Çelik, (2021) reported spinach leaf material having the highest DW of 20.14 g, after dosing with 120 μM Fe-EDTA in solution, followed by a decrease at the highest dosing concentration of 150 μM Fe-EDTA in solution. It was believed that the toxicity range was reached after dosing with 150 μM Fe-EDTA in solution and beyond. There were also significant differences in average leaf DWs per plant, between dosing with 75, 25 and 100, and 150 and 200 μM NaFe-EDTA in solution.

Jin *et al.*, (2013) reported that dosing spinach with lower Fe concentrations, such as 1 μM NaFe-EDTA, helps to obtain a mild deficiency status in plants. This will not only increase biomass production, however, it will also improve their qualities, by

decreasing NO₃⁻ concentration, which accumulates more in soilless systems following higher reliability of NO₃⁻ fertilisers. Furthermore, Fe deficiency is expected to facilitate spinach plants to obtain higher levels of N, P and K.

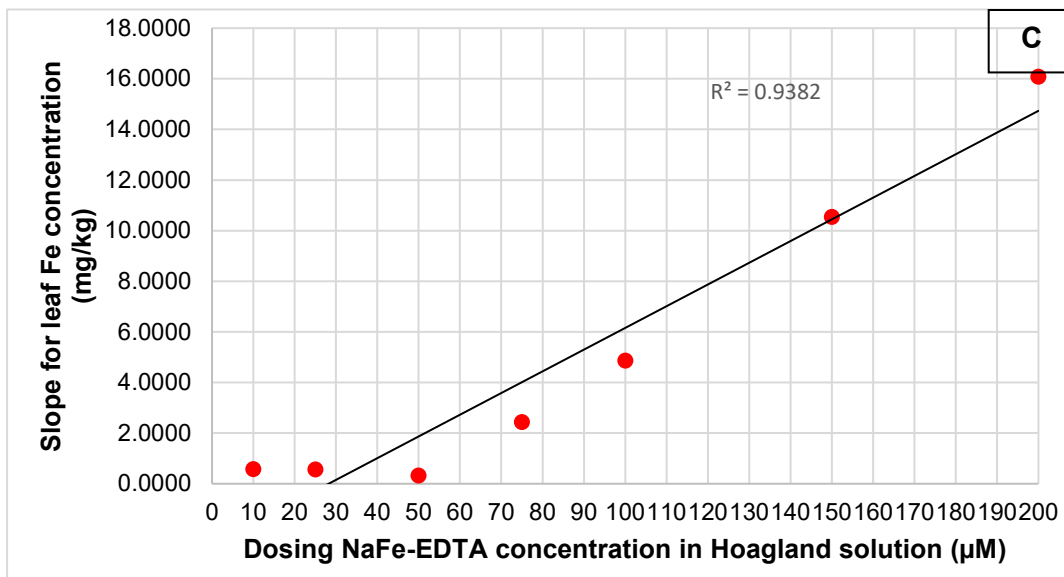
4.3.2 Fe concentrations in spinach leaf and root material

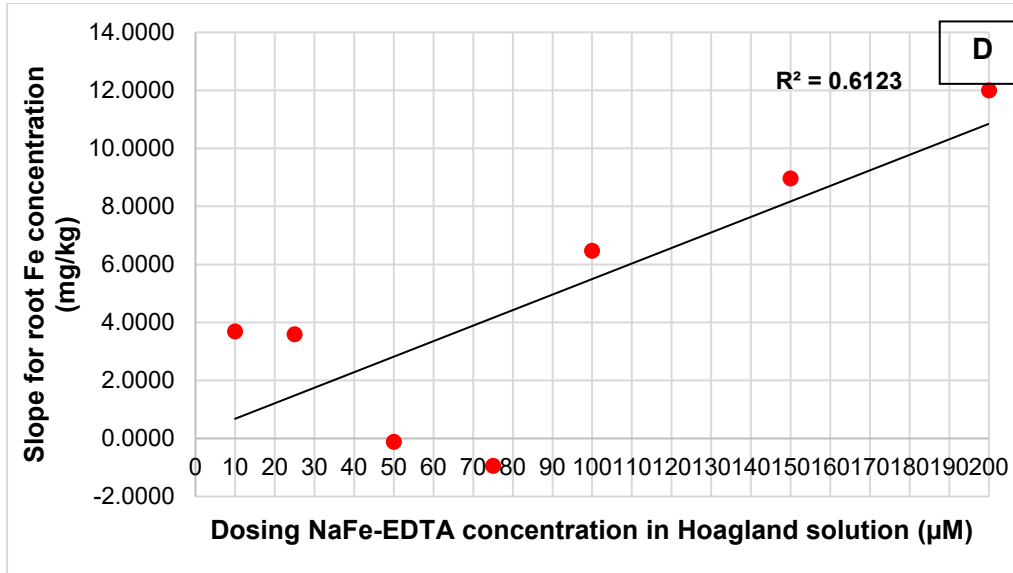
Figure 4.4A clearly shows that Fe concentrations for leaf material were by far the highest, after dosing with 200µM Fe-EDTA in solution, compared to the lowest after dosing with 25µM Fe-EDTA.



Figures 4.4A—B: Spinach 4.4A) leaf and B) root Fe concentrations, after dosing with 10, 25, 50, 75, 100, 150 and 200 μM NaFe-EDTA in solution. There were 10 time points in total. Error bars represent SEM.

Figure 4.4B also shows the highest Fe concentrations of root material, after dosing with 200 μM Fe-EDTA in solution, compared to the lowest after dosing with 10 μM Fe-EDTA. However, the overall lowest Fe concentration for root material, was recorded after dosing with 25 μM Fe-EDTA in solution, on Day 4.





Figures 4.4C—D: Linear regression analysis for slope values for spinach leaf and root Fe concentrations, after dosing with 10, 25, 50, 75, 100, 150 and 200 µM NaFe-EDTA in solution. R^2 and p-values shown.

Figure 4.4 C shows a strong and significant relationship between dosing concentrations of NaFe-EDTA in solution and slope values for spinach leaf Fe concentrations. This is because the p-value is far below 0.05 and R^2 is closer to 1. This shows that the rate of Fe concentrations in mg/kg leaf/day, is strongly linearly dependent on Fe dosing concentrations (in µM) in Hoagland nutrient solution. This suggests that the saturation point was not reached.

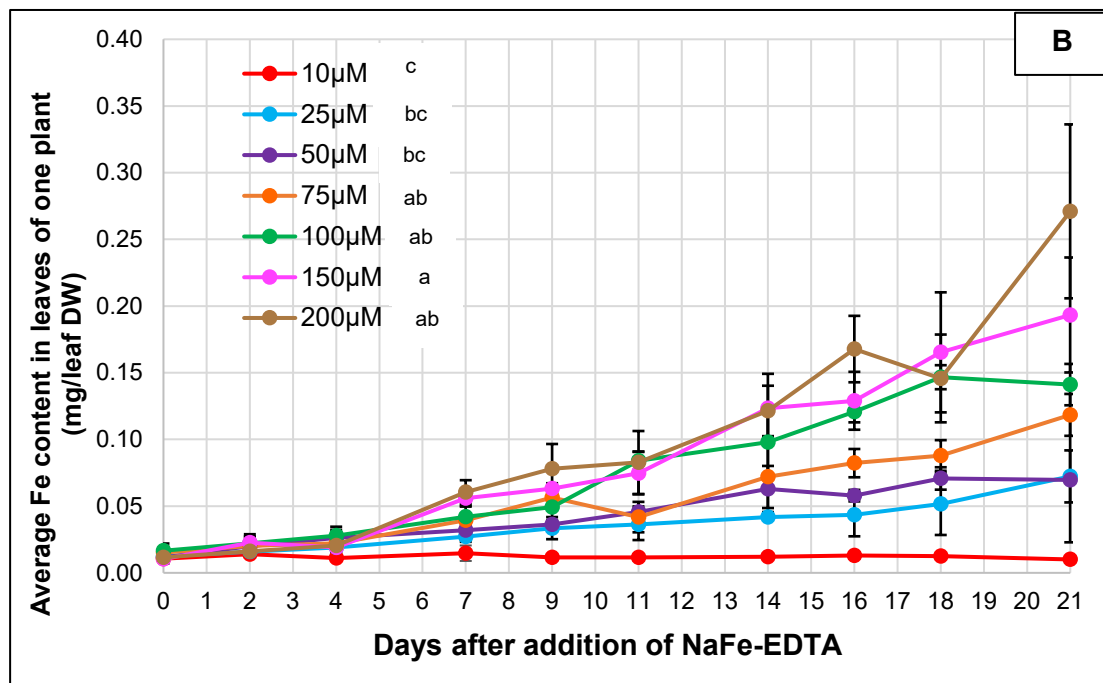
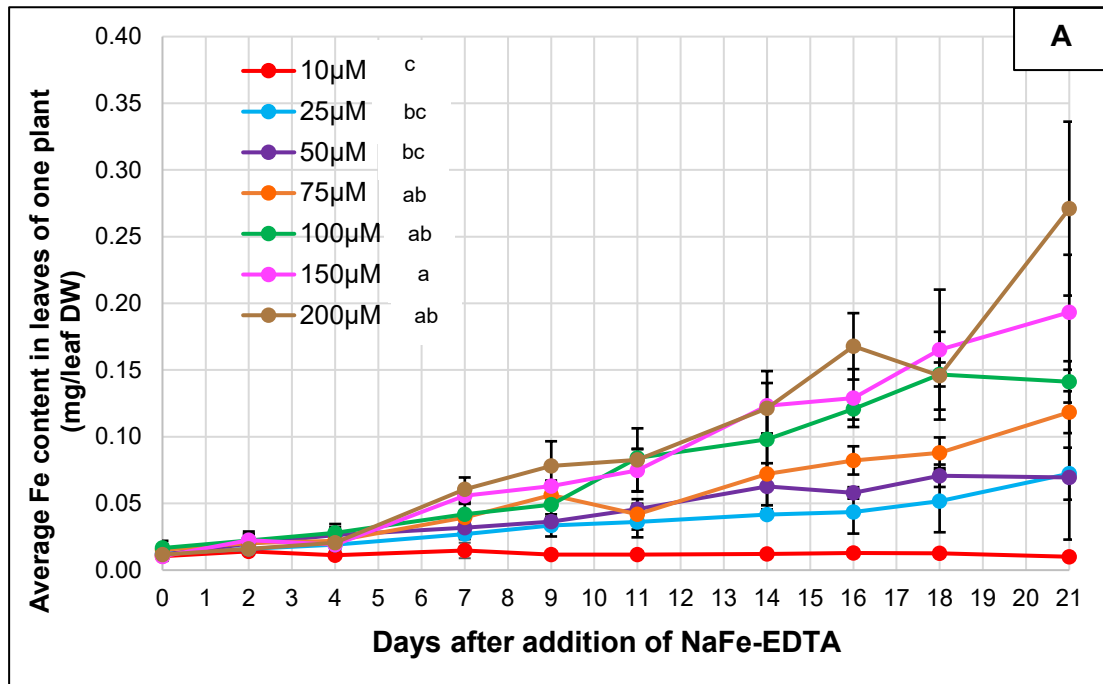
However, Figure 4.4D shows a weaker and non-significant relationship between dosing concentrations of NaFe-EDTA in solution and slope values for spinach root Fe concentrations, because of the p-value being above 0.05 and R^2 being only 0.6123. This means that the saturation point of Fe concentration in the roots has been reached.

4.3.3 Fe contents in spinach root and leaf material

Figures 4.5A—B show that the internal Fe contents were always higher in root material compared to leaf material. A more recent study by Eid *et al.*, (2018) mentioned all

heavy metals, except for Zn, being localised in the roots of spinach plants, with a minority being transferred to the leaves. This indicates that the roots serve as a barrier to translocation, being the first target organ to touch the trace element ions.

Figure 4.5A shows the lowest average Fe contents in the leaves of one spinach plant, after dosing with 10 μM NaFe-EDTA, where it remained consistent at 0.01 and 0.03mg Fe/leaf throughout. It was the highest after dosing with 200 μM NaFe-EDTA, in which the peak of 0.27mg Fe/leaf was recorded on Day 21. However, there was an exception on Day 18, where the average Fe contents of the leaves of one spinach plant, were higher after dosing with 150 μM NaFe-EDTA, at approximately 0.17 mg Fe/leaf. For all NaFe-EDTA dosing concentrations, average Fe contents of the leaves of spinach remained constant at approximately 0.01 mg Fe/leaf until about Day 5. There were also significant differences between dosing with 10 and 150 μM NaFe-EDTA.



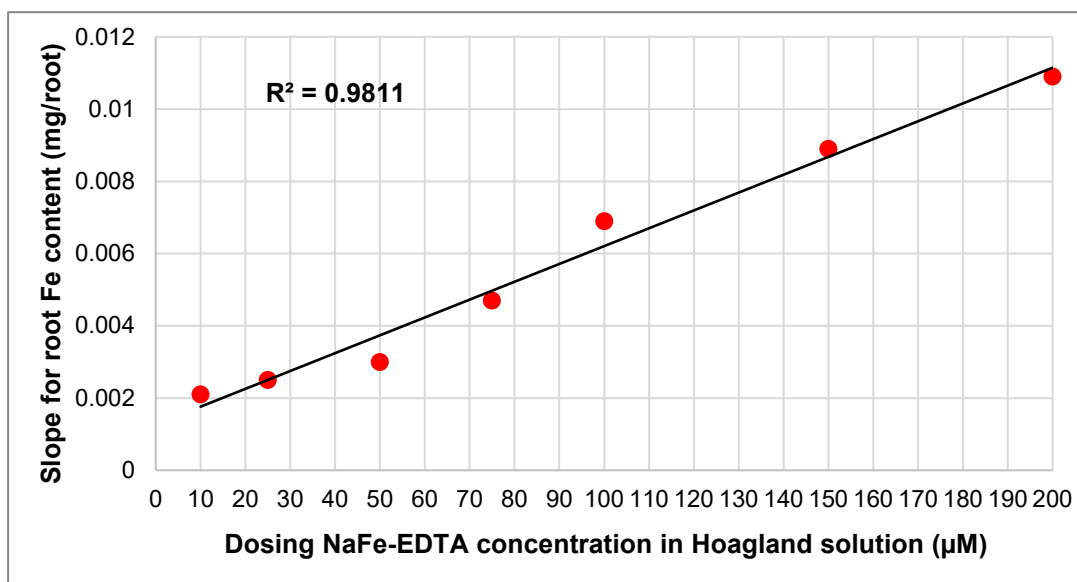
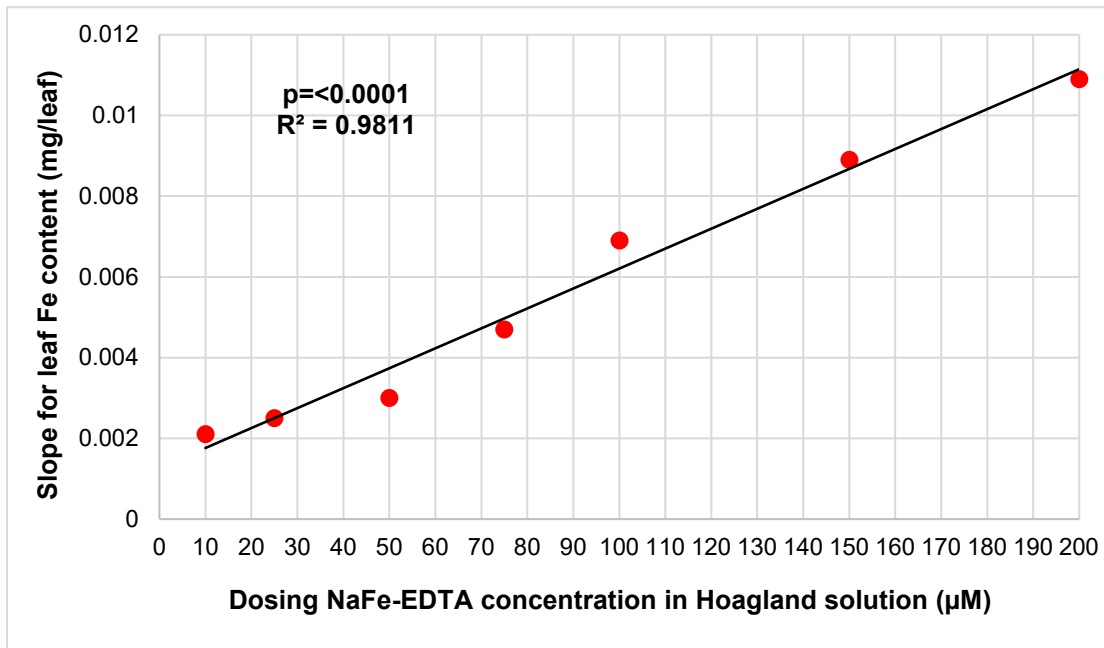
Figures 4.5A—B: Average Fe contents of spinach 4.5A) leaf and B) root material in one plant (in mg Fe/plant part), on the last 21 days of growth (starting from Day 0) after dosing with 10, 25, 50, 75, 100, 150 and 200µM NaFe-EDTA in solution. There were 10 time points in total. Error bars represent SEM and the letters are derived from ANOVA post-hoc Tukey testing ($p < 0.05$) on Minitab 21 software.

Figure 4.5B shows the lowest average Fe contents in roots of one plant after dosing with 10 µM NaFe-EDTA, where it wavered between 0.02 and 0.05 mg Fe/root throughout. However, on Day 2, the root Fe it was lower at 25 µM NaFe-EDTA by 98

approximately 0.01 mg Fe/root. It was the highest after dosing with 100 μM NaFe-EDTA, in which the peak of approximately 0.1650 mg Fe/root was recorded on Day. 16. There was then a reduction in average Fe contents in roots of one plant after dosing, which was most likely attributed to Fe depletion. Their contents reduced after dosing with 150 and 200 μM NaFe-EDTA because of potential toxicity for the roots. There were also significant differences in average Fe contents between dosing with 10 μM N^6Fe -EDTA and all other dosing concentrations.

Similar results were reported by Kumwimba *et al.* (2013) where lettuce root arsenic (As) depletion occurred after prolonged periods of as exposure, between a 10—24 hour period. During the initial period of exposure, root as accumulation was at its peak. Moreover, the nutrient demand of plants changes continuously as they grow, and they seldom remain constant throughout each growth stage (Mankin and Fynn, 1996).

Şimşek and Çelik (2021) reported increasing the dosing concentrations of Fe-EDTA, causing a general increase in internal Fe contents of the spinach leaves and roots. In roots, it peaked at 33.77 mg/root after dosing with the highest concentration of 150 μM Fe-EDTA, and in leaves, 2.23 mg/leaf Fe-EDTA after dosing with 90 μM Fe-EDTA. The highest dose of 150 μM Fe-EDTA caused a significant decrease in all macro and micronutrient contents and their uptake from the roots. This therefore indicated the potential toxicity range being reached. Fe contents were always highest in the roots. Dosing with lower NaFe-EDTA concentrations such as 30 and 60 μM did not only reduce the Fe contents in the spinach root and leaf material, but also, the contents of other macronutrients, especially Mg.



Figures 4.5C—D: Linear regression analysis for slope values for leaf and root Fe contents, after dosing with 10, 25, 50, 75, 100, 150 and 200µM NaFe-EDTA in solution. R² and p-values shown.

Figures 4.5C—D show strong and significant relationships between dosing concentrations of NaFe-EDTA in solution and slope values for leaf and root Fe contents. This is because the p-values are far below 0.05 and R² is closer to 1. They both show that the rate of Fe content accumulation in mg/root and leaf/day is strongly linearly dependent on Fe dosing concentrations (in µM) in Hoagland nutrient solution. This shows that the rate of Fe content in both roots and leaves is strongly linearly

dependent on the Fe in solution. It is even nonlinear for the higher Fe concentrations, suggesting that the saturation point/toxicity limit was not reached.

4.3.4 Residual Fe contents in the spinach growth matrix

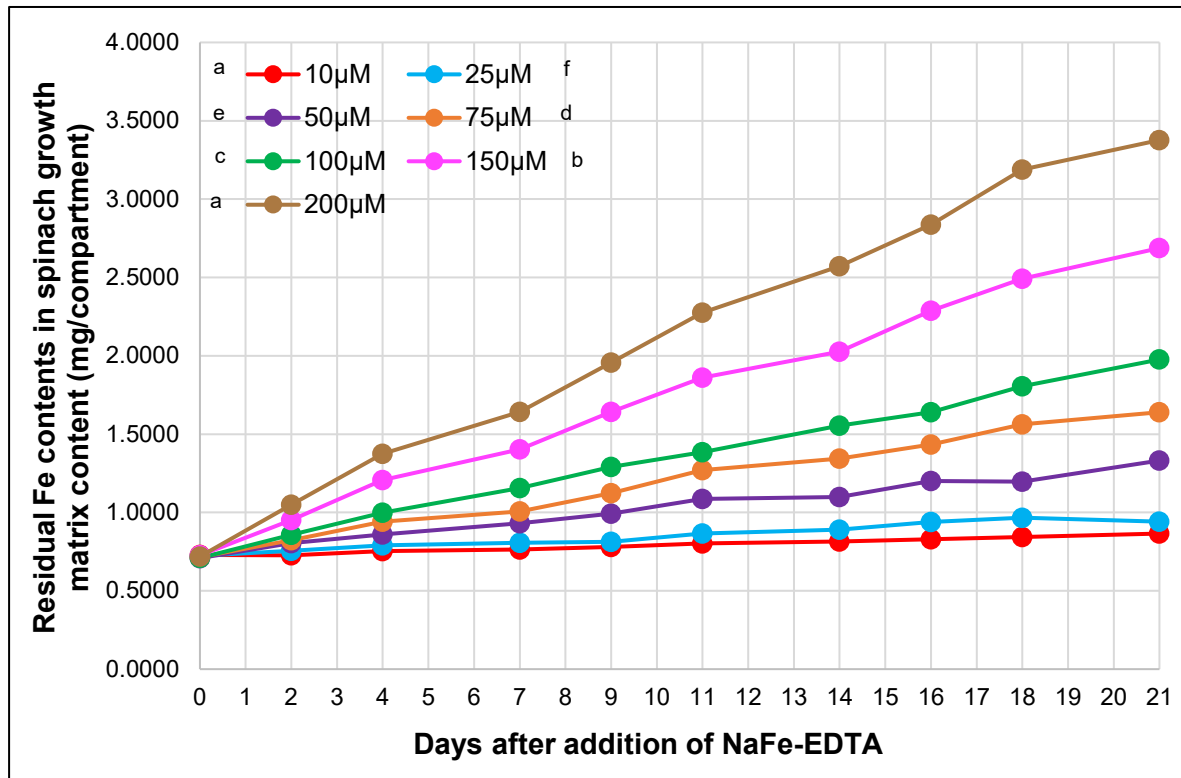


Figure 4.6: Residual Fe contents in the perlite spinach growth matrix (in mg Fe/compartiment), on the last 21 days of growth (starting from Day 0) after dosing with 10, 25, 50, 75, 100, 150 and 200 µM NaFe-EDTA in solution. There were 10 time points in total.

As seen in Figures 4.5A—B, Figure 4.6 shows the lowest residual Fe contents in the spinach growth matrix, after dosing with 10 and 25 µM NaFe-EDTA in solution, where it wavered between 0.75 to 1 mg Fe/compartiment. This was most likely because a majority of the Fe being accumulated by the spinach plant roots, at lower dosing concentrations. Between Days 0—4, the residual Fe growth contents for 10, 25, 50, 75 and 100 µM remained constant throughout. The peak of 3.5 mg Fe/compartiment was reached on Day 21 after dosing with 200 µM external solution concentration. The

second highest of approximately 2.7 mg Fe/compartment was reached on Day 21 after dosing with 150 μM external solution concentration.

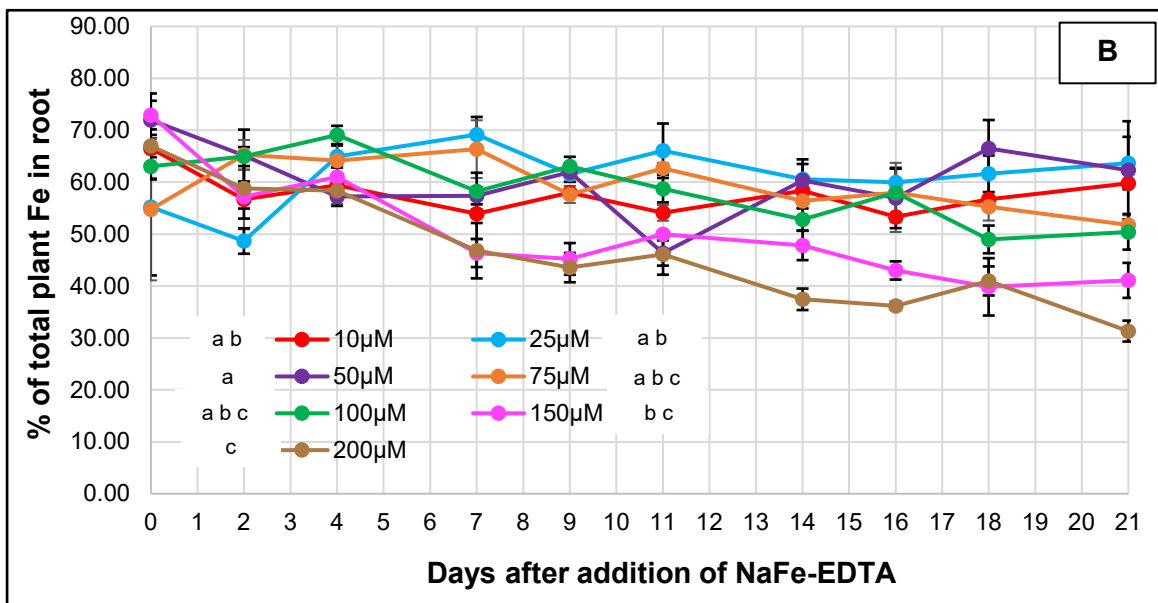
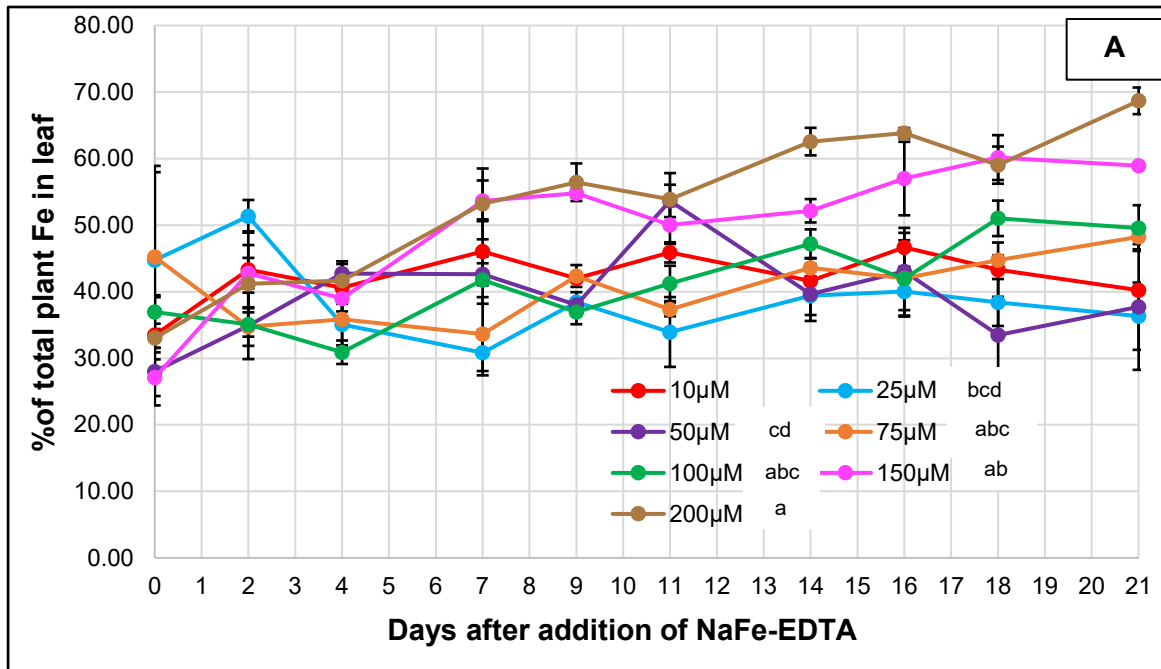
This was most likely attributed to more Fe not being accumulated in the root symplastic pathway and instead, being depleted in the perlite material, especially after dosing with higher solution concentrations (Kumwimba *et al.*, 2013). Similar results were reported by Bar-Tal *et al.*, (1997), who reported reduced LR uptake of P and N at higher soil P and N concentrations.

There were also significant differences in the residual Fe content in the growth matrix after dosing with all external solution concentrations, with the exception to dosing with 10 and 200 μM NaFe-EDTA in solution.

4.3.5 Percentage of plant Fe in spinach leaf and root material

Figure 4.7A shows the highest percentage of total plant Fe in leaves, of 70% on Day 21 after dosing with 200 μM NaFe-EDTA in solution. The lowest percentage of total plant Fe in leaves, of 28% was reached on Day 0 of dosing with 150 μM NaFe-EDTA in solution. From Day 7 onwards, they fluctuated between 50 and 70%, after dosing with 200 μM NaFe-EDTA in solution. There was a strong linear increase for the weekend of Days 4—7, for this concentration, and after dosing with 100 μM NaFe-EDTA in solution.

There were also significant differences between dosing with 10 and 200 μM NaFe-EDTA in solution.



Figures 4.7A–B: Percentage of total plant Fe in spinach (4.7A) leaf and B) root material, on the last 21 days of growth (starting from Day 0) after dosing with 10, 25, 50, 75, 100, 150 and 200 μM NaFe-EDTA in solution. There were 10 time points in total. Error bars represent SEM.

Figure 4.7B shows direct inverse effects of Fe percentage of total plant Fe in root material in comparison to leaf material. For example, after dosing with 200 μM NaFe-EDTA on Day 21, the lowest percentage Fe of total plant Fe in roots, of approximately 103

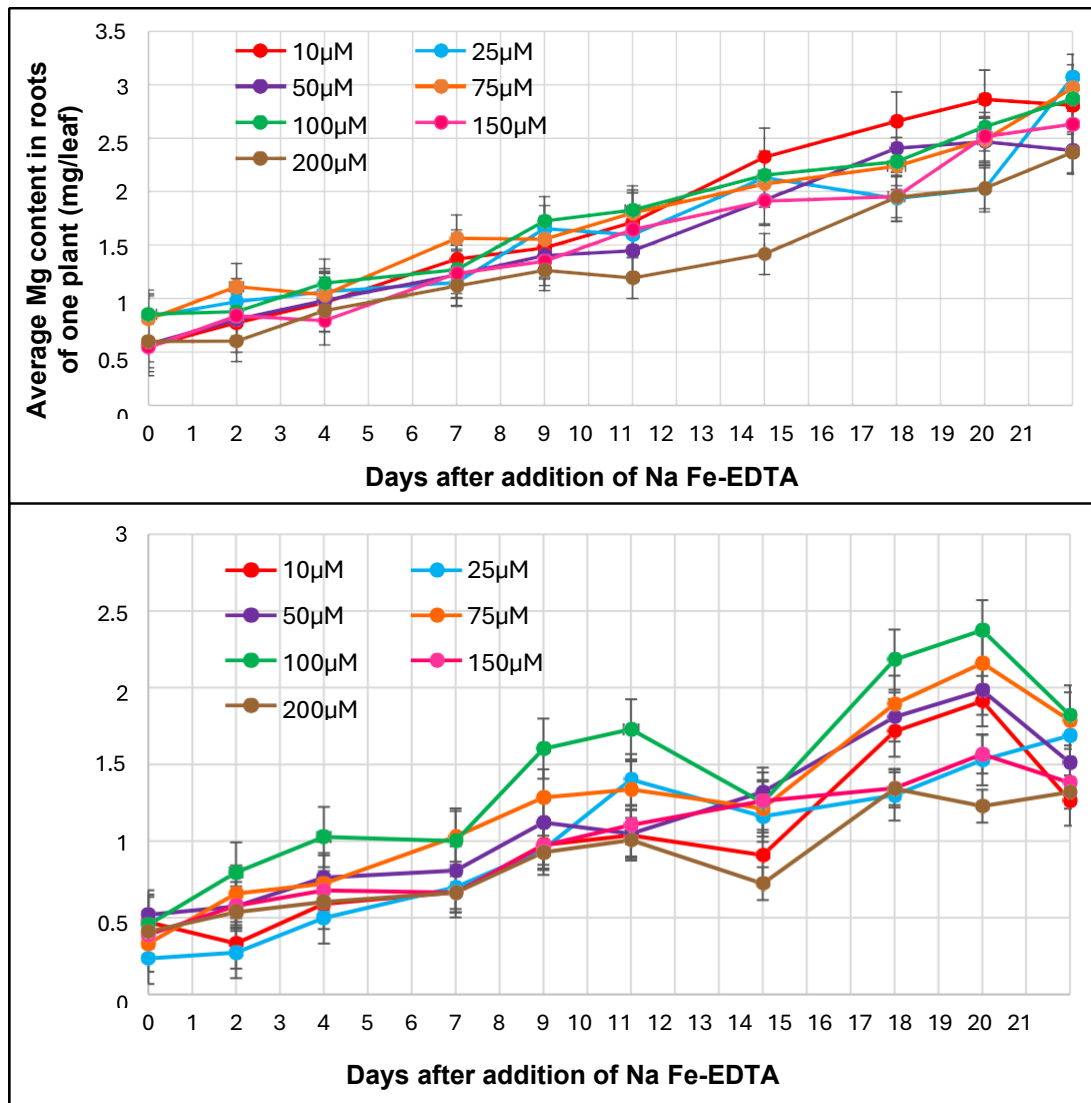
30% was recorded. The peak percentage of approximately 67% was recorded after dosing with 50 μM NaFe-EDTA on Day 18. Past Day 4 of dosing with 200 μM NaFe-EDTA, there was a more noticeable decrease in percentage of total plant Fe in roots, from 60 to eventually 30% on Day 21. The sharpest decline occurred between Days 4—7, the exact opposite of what was noticed in leaf material.

There were also significant differences in percentage root Fe localisation, after dosing with 50 and 200 μM NaFe-EDTA in solution.

4.4 The impact of iron dosing on the content of other minerals in spinach leaf and root material

4.4.1 Magnesium

Figure 4.8A shows Mg contents were highest throughout, after dosing with 100 μM NaFe-EDTA in solution, with the peak of approximately 2.3 mg/leaf being recorded on Day 19. Conversely, the lowest leaf Mg contents were recorded after dosing with 200 μM NaFe-EDTA in solution, with the lowest of 0.5 mg/leaf being recorded on Day 0. For all dosing concentrations, there was a linear increase of Mg contents, with no major peaks or troughs recorded. As the leaves grow, not surprisingly Mg contents also rise, hence the increased amounts of chlorophyll as well.



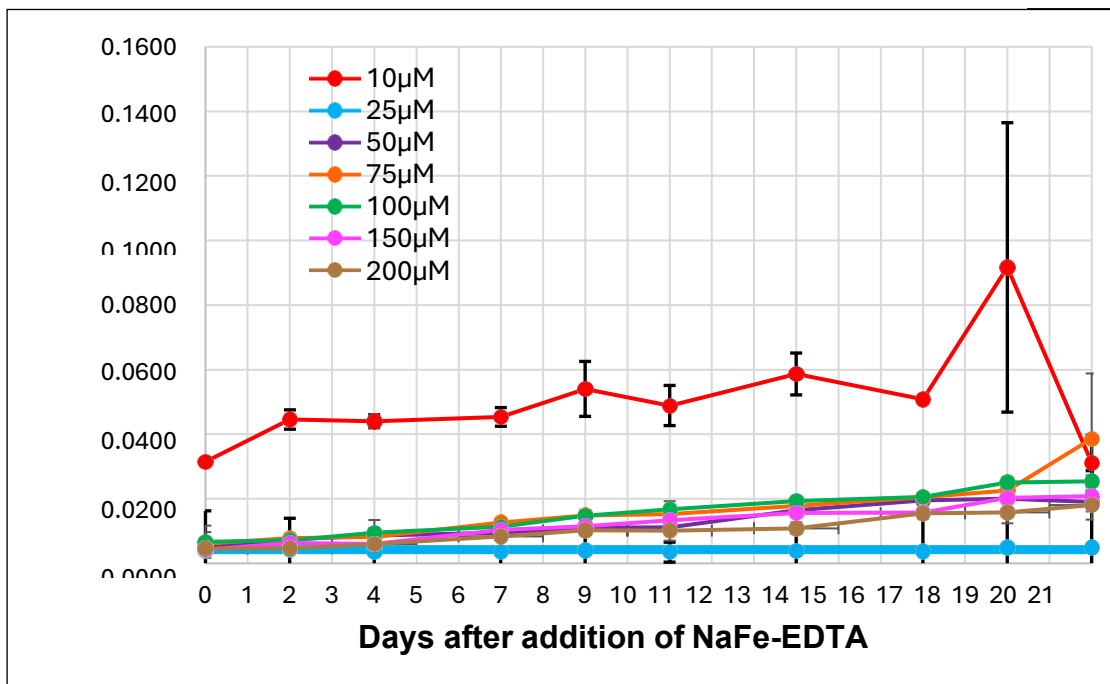
Figures 4.8A—B: Average Mg contents of spinach 4.8A) leaf and B) root material in one plant (in mg Mg/plant part), on the last 21 days of growth (starting from Day 0) after dosing with 10, 25, 50, 75, 100, 150 and 200µM NaFe-EDTA in solution. There were 10 time points in total. Error bars represent SEM.

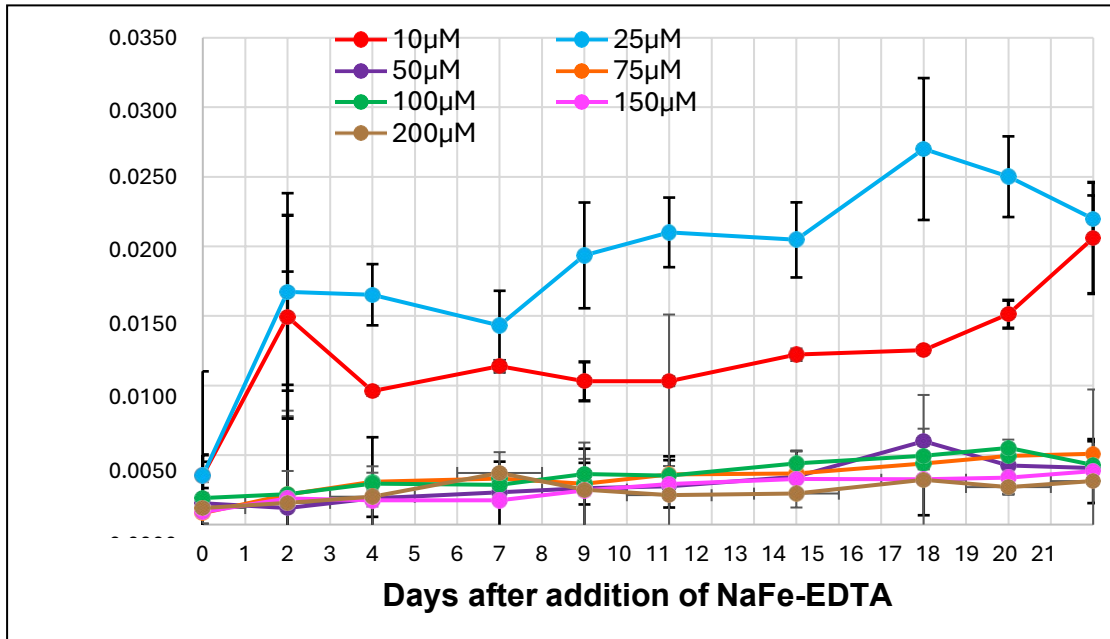
Figure 4.8B shows Mg contents were always the highest after dosing with 100 µM NaFe-EDTA, with the peak of 2.4 mg/root being recorded on Day 19. The lowest root Mg contents were recorded after dosing with 200 µM NaFe-EDTA, with the lowest of 0.4 mg/root being recorded on Day 0 as well. One interesting trend noticed was that during weekends periods, root Mg contents for all dosing concentrations of NaFe-EDTA decreased rapidly before being resupplied by Hoagland nutrient solution on the

upcoming Mondays. The steepest decline was recorded between Days 12—14 after dosing with 100 μM NaFe-EDTA. This shows that there was some form of buffering mechanism taking place in the root architecture after exposure to that one dosing concentration.

4.4.2 Zinc

Figure 4.9A shows Zn contents always a lot higher throughout, after dosing with 10 μM NaFe-EDTA, with the peak of approximately 0.9 mg/leaf being reached on Day 19. Leaf Zn contents upon exposure to the other dosing concentrations remained relatively low, wavering between 0 and 0.2 mg/leaf.





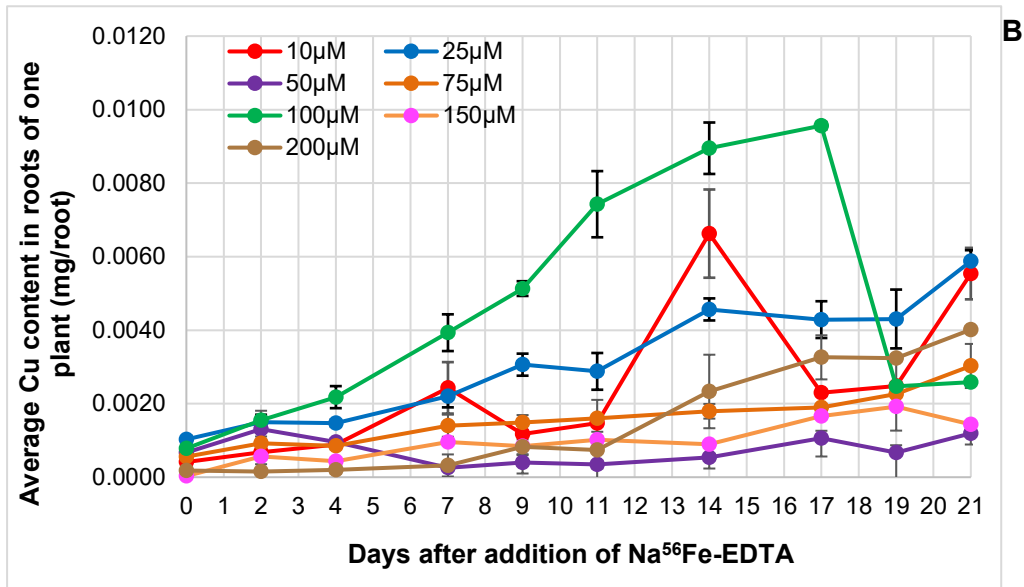
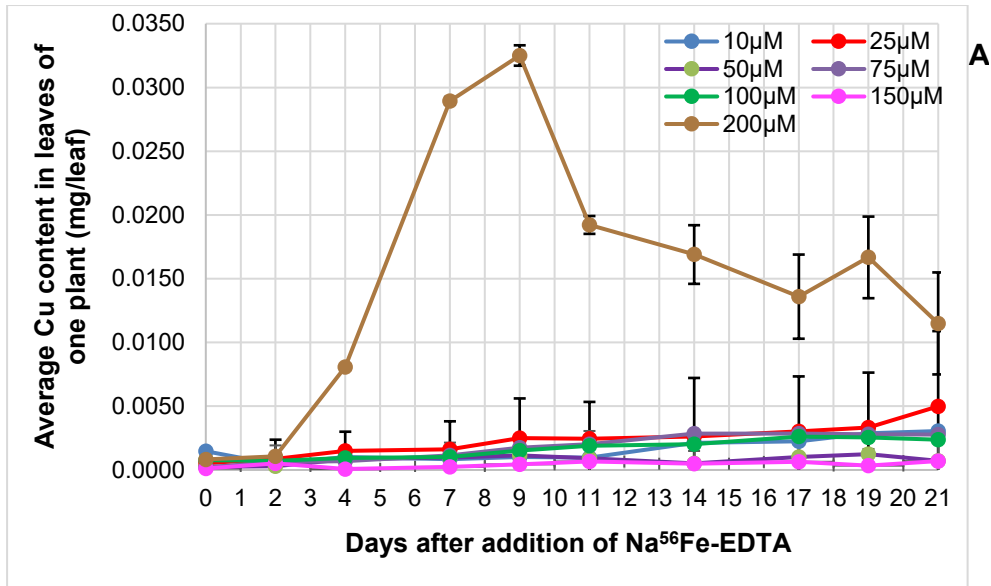
Figures 4.9A—B: Average Zn contents of spinach 4.9A) leaf and B) root material in one plant (in mg Zn/plant part), on the last 21 days of growth (starting from Day 0) after dosing with 10, 25, 50, 75, 100, 150 and 200 μM NaFe-EDTA in solution. There were 10 time points in total. Error bars represent SEM.

Figure 4.9B shows the highest root Zn contents after dosing with 25 μM NaFe-EDTA, with the peak being reached at 0.027 mg/root on Day 17. They were the second highest after dosing with 10 μM NaFe-EDTA, with the peak being reached at 0.02 mg/root, on Day 21.

Furthermore, at higher dosing concentrations between 75 and 200 μM NaFe-EDTA, root Zn contents remained lower throughout, fluctuating between 0 and 0.005 mg/root.

4.4.3 Copper

Figure 4.10A shows leaf Cu contents peaking after dosing with 200 μM NaFe-EDTA, with the peak of 0.032 mg/leaf being reached on Day 9. It is possible that Cu and Fe μM NaFe-EDTA function synergistically with one another.

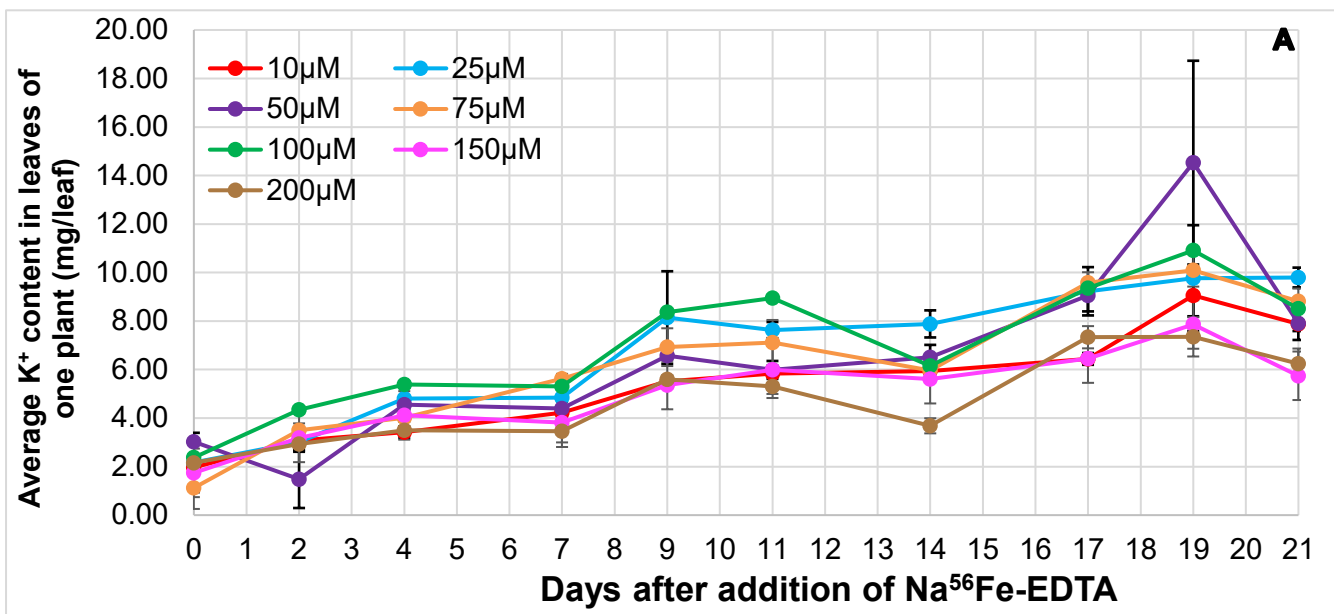


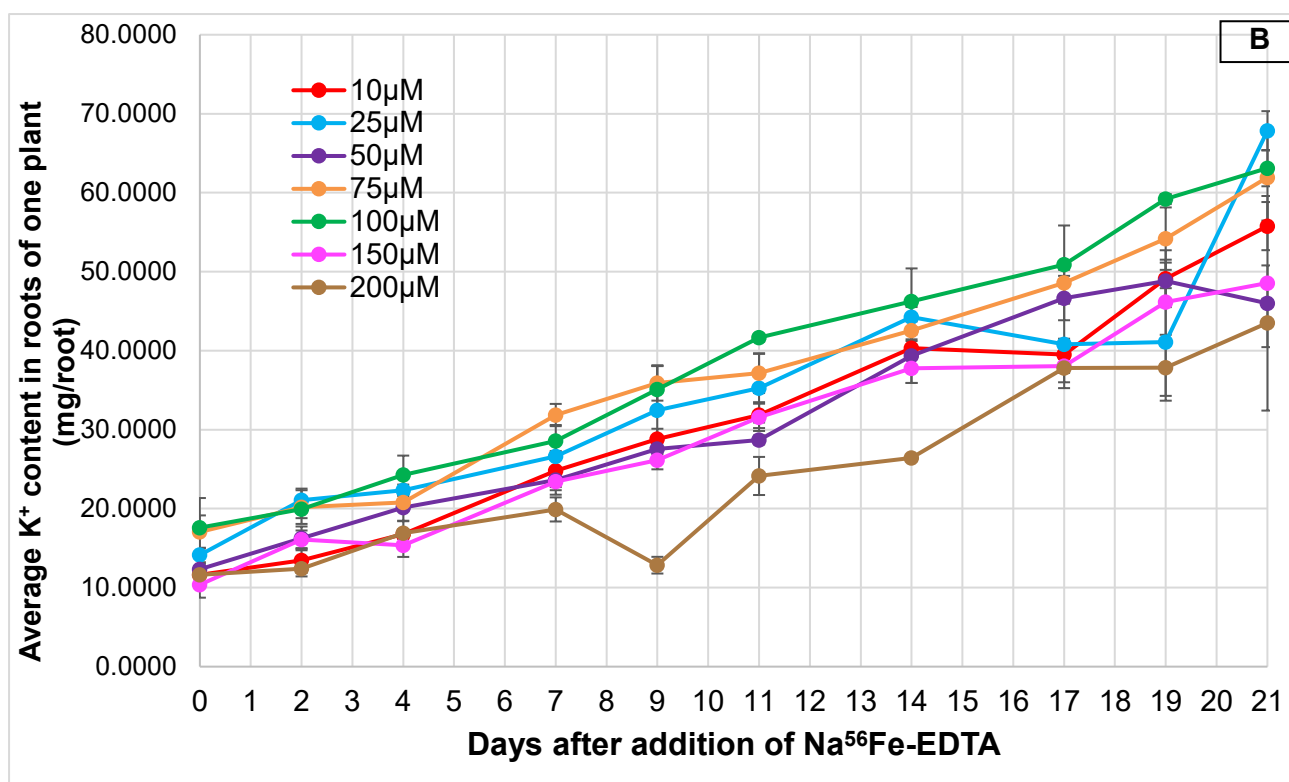
Figures 4.10A—B: Average Cu contents of spinach 4.10A) leaf and B) root material in one plant (in mg Cu/plant part), on the last 21 days of growth (starting from Day 0) after dosing with 10, 25, 50, 75, 100, 150 and 200 μM NaFe-EDTA in solution. There were 10 time points in total. Error bars represent SEM.

Figure 4.10B shows root Cu contents peaking after dosing with 100 μM NaFe-EDTA, with the peak of close approximately 0.009 mg/root being reached on Day 17. However, between Days 17—19, there was a steep decline of root Cu content from 0.01 to 0.002 mg/root. Interestingly, the lowest root Cu contents were recorded after dosing with 50 μM NaFe-EDTA, with the trough being reached on Day 7 with a root Cu content of approaching 0 mg/root.

4.4.4 Potassium

Figure 4.11A shows K^+ content in leaf material was generally highest after dosing with 100 μM Na Fe-EDTA in solution, and lowest, after dosing with 200 μM NaFe-EDTA in solution. These results mirror Figures 4.5A—B for Fe contents where they were also at lowest after dosing with 200 μM NaFe-EDTA in solution.





Figures 4.11A—B: Average K contents of spinach 4.11A) leaf and B) root material in one plant (in mg K/plant part), on the last 21 days of growth (starting from Day 0) after dosing with 10, 25, 50, 75, 100, 150 and 200 μM NaFe-EDTA in solution. There were 10 time points in total. Error bars represent SEM.

In terms of K^+ content in root material, it peaked at 14 mg/root on Day 19, after dosing with 50 μM NaFe-EDTA in solution (see Figure 4.11B). However, it was the exception rather than the rule, and on all the other days, the highest K^+ contents were recorded after dosing with 100 μM NaFe-EDTA in solution. Just as recorded for leaf K^+ content, the lowest root K^+ content of 4 mg/root was recorded on Day 14, after dosing with 200 μM NaFe-EDTA in solution. Finally, K^+ contents in both root and leaf material were higher than Fe, Cu and Zn, because it is a macronutrient that is more prevalent in the growth matrix in comparison to micronutrients. K^+ is also known to have alleviatory effects on root Fe^{2+} stress.

4.5 The Bayesian approach for estimating unknown parameters from the data

4.5.1 Introduction to Bayesian statistics and Markov Chain Monte Carlo (MCMC) method

Bayes' theorem was discovered by the English mathematician, Thomas Bayes (1701 – 61). Bayes' theorem offers a valid method of revising current predictions and theories when new or updated evidence are provided (Foreman-Mackey, 2013). The theorem involves the calculation of conditional probabilities, which is the probability of a hypothesis given that an event has occurred. Unknown parameters get treated as random variables (Harcet *et al.*, 2013). The general formula (see Equation 4.5) is:

$$P(\theta|Y) = (P(Y|\theta) P(\theta))/P(Y) \text{ (Eq. 4.5)}$$

$P(\theta|Y)$ is known as the Bayesian **posterior distribution** of the unknown parameters after model fitting. This shows the probability that the given model parameter values, θ , describe the measured data, Y . This quantifies the knowledge of the model parameter uncertainty after fitting the model to the data. It is useful for evaluating expected events, to make predictions (Bishop, 2006).

The right-hand side of the equation incorporates both the **likelihood function** ($P(Y|\theta)$) and the **prior distribution** $P(\theta)$. These are the two determinants of the final posterior distribution. The prior distribution plugs values into models that act as inputs, through the incorporation of prior knowledge about possible parameter values, before incorporating the data to inform the model (Bishop, 2006; Foreman-Mackey *et al.*, 2013). However, this can just be set to 1 if there are not enough informative priors.

4.5.2 The likelihood function

As seen in Section 4.2.1, the likelihood function is notated as $P(Y|\theta)$, which is the probability of the data given the various model parameter settings (Bishop and Nasrabadi, 2006). It is a distribution that represents our existing beliefs/thoughts/evidence of what the possible values of the parameter can be.

We cannot check every possible value of an unknown parameter, however, we can use the prior distributions, $P(\theta)$, to generate representative samples of possible parameter values. Each value from representative samples is substituted in the model, which generates modelling data, Y_{model} . The difference between the model-produced Fe content values, Y_{model} , and measured Fe content values, Y , is known as the **residual** or **modelling error** (see Equation 4.6).

$$\text{Residuals} = Y_{\text{model}} - Y \quad (\text{Eq. 4.6})$$

Their distribution constitutes the likelihood function. On the other hand, the likelihood function expresses the probability that the observed data set was produced by given model parameter values. The likelihood of time-series data is often expressed as the product of the individual probability distributions of each data point in Y , given the model parameter values, θ .

Given the prior distributions and likelihood function, each as individual values, the **posterior distribution** can then be calculated, which is the outcome of the Bayesian formula (see Equation 4.5). Theoretically speaking, the initial values of Fe contents in the root and leaf material are assumed to be equal to the measurements on Day 0 or added to the set of unknown parameters. Initial values can also be assumed to be unknown, therefore a Gamma prior should be imposed on them and estimated in the same manner as the rates.

Finally, in this experiment, the Bayesian estimation was implemented with Ensemble MCMC, under the assumption of a zero-mean Gaussian likelihood (Foreman-Mackey *et al.*, 2013). The notation was $P(Y|\theta) = N(0, \sigma^2)$

4.5.3 Prior distributions of unknown parameters

The assumed prior distributions of each of the unknown model parameters are shown in Figure 4.12A and the assumed prior distributions of the initial unknown conditions are shown in Figure 4.12B. σ^2 represents the unknown modelling errorvariance and it must also be estimated in this procedure.

Therefore, the final list of unknown parameters consists of r_{MR} , r_{RL} , r_D and K_M .

Additional unknown parameters consist of σ^2 and $x(0)$ but were excluded from the final analysis.

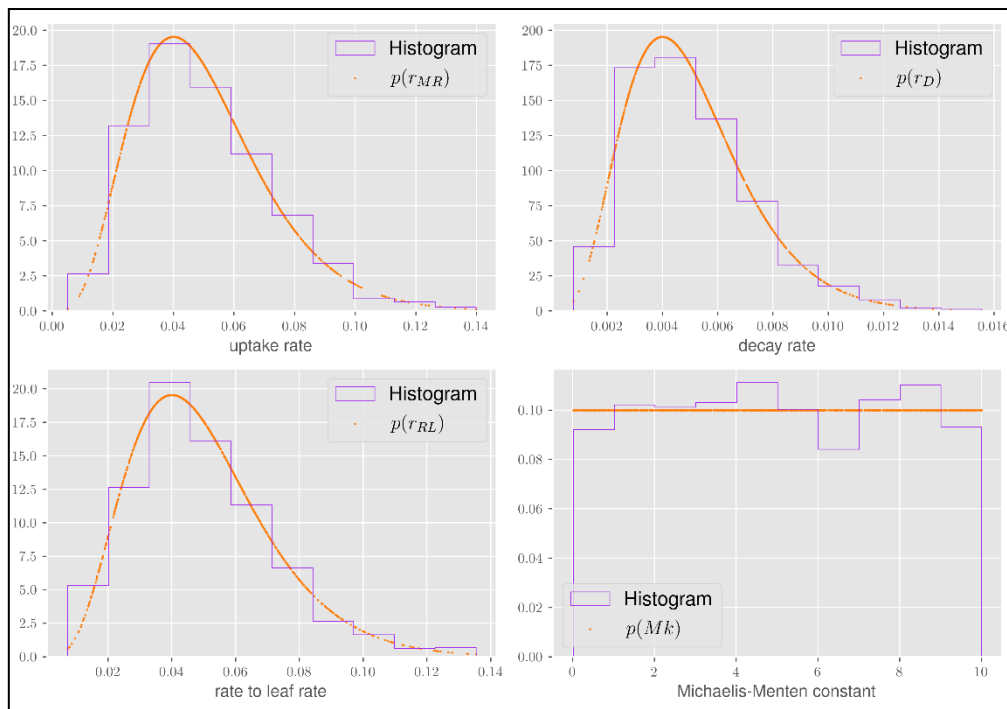


Figure 4.12A: Assumed prior distributions of the unknown parameters, θ , from Equations 4.1A—C. Note that K_M is notated as M_k here.

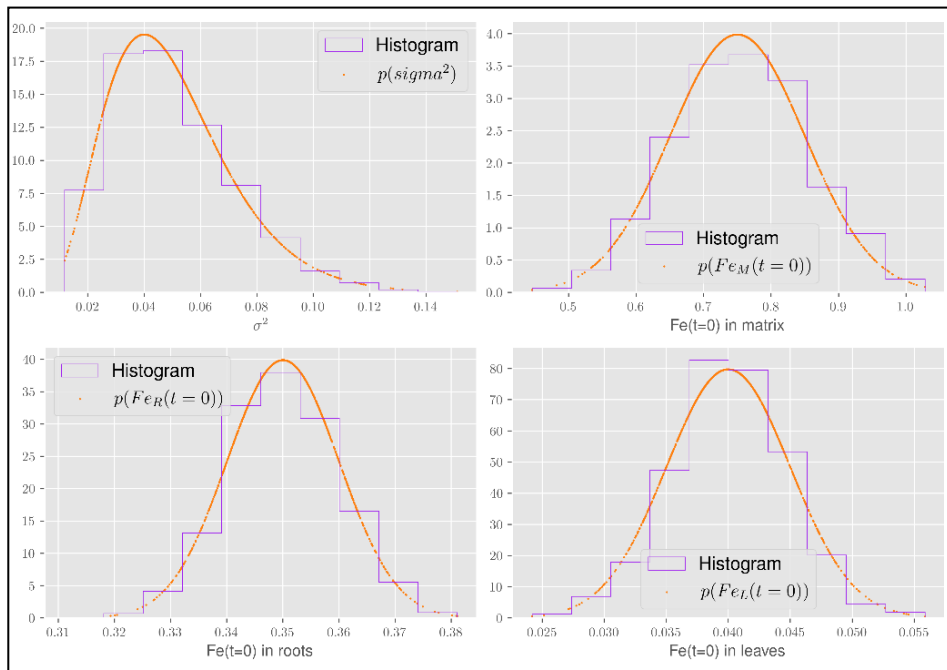


Figure 4.12B: Assumed prior distributions of the initial unknown conditions, modelling error variance, σ^2 and $x(0)$ based on Equation 4.1D.

4.5.4 The Gamma distribution

Based on this data, a multivariate distribution can also be calculated where all the probabilities of the unknown parameters get multiplied together (see Equation 4.7).

$$P(\theta) = P(r_{MR}) \times P(r_{RL}) \times P(K_M) \times P(r_D) \times P(\sigma^2) \times P(x_0) \quad \text{(Eq. 4.7)}$$

Based on Equation 4.7, in this experiment, the rate values r_{MR} , r_{RL} and r_D can never be negative or more than 1. Therefore, Gamma priors were chosen for each of them, a common prior imposed for rate values. Because of this, Gamma priors are assumed with high skewness parameters. The only existing knowledge on K_M is that it is above 0 and is likely to be of the same order of magnitude as the measured Fe contents in the growth matrix. Therefore, a uniform prior distribution of the interval [0 –10], was imposed within which all values of K_M were equally probable. A Gamma prior was

imposed on σ^2 to ensure it remained positive, and for the initial conditions, the normal prior centered around the measurements of Day 1, was selected.

The Gamma distribution is a probability distribution over a range of positive random variables only, excluding the negative ones. These distributions are a two-parameter family of continuous distributions. Values that are not reasonable because of being on their way to infinity, get cut off. Therefore, these cut-off values are parameter specific and are defined by each experiment. They often exist as positive values but favour lower values (Bishop and Nasrabadi, 2006).

4.5.5 The uniform distribution

A continuous random variable, x , is a random variable that can take on infinitely many values, compared to a discrete random variable which can only take on a range of specified values. This can be seen in Figure 4.12A for K_M . The uniform distribution for a continuous random variable is a probability distribution where all outcomes are equally possible. Out of the four parameters seen in Equation 12, one of them exists as a uniform distribution; $P(K_M)$ because although K_M is also never negative, its upper limit is unknown.

4.5.6 Markov Chain Monte Carlo (MCMC) algorithm

All the models were fitted to the data with the Markov Chain Monte Carlo (MCMC) method, which belongs to a family of sampling-based methods to acquire a posterior distribution of unknown model parameters. It has its origins in the field of physics; however, it started having more of a significant contribution in the field of statistics by the end of 1980s. This approximate inference method based on numerical sampling

allows for a large class of distributions and is used to fit a model and draw samples from a joint distribution of unknown model parameters and prior knowledge. Samples are dependent on one another. These constitute the umbrella category of Bayesian statistics (Bishop and Nasrabadi, 2006).

The desirable outcome of Bayesian model fitting is to avoid high residuals, therefore lower likelihood functions and narrower posterior distributions for the unknown parameters. The narrower the distribution is, the more precise the posterior knowledge about the model parameter values. If the posterior distribution is unimodal, with only one peak, then the parameter values corresponding to the distribution peak constitute optimal configuration of the model with respect to the chosen likelihood function. Since in our study very little is known about model parameters prior to the model fitting procedure, the posterior distribution is mainly defined by the likelihood function.

This MCMC method is divided into two core principles. The Monte Carlo principle is all about rejection sampling and is named after the European capital city of the principality of Monaco, famous for its many casinos. Because the iterations are random, it is impossible to control the direction or distances of steps or leaps in the parameter space, represented in the case of a single parameter by the x-axis.

The basis of the Markov Chain is the absence of memory of the previous iterations. It allows for evaluation of model fits to the data and establishment of larger numbers of parameters and possible ranges of parameter values (Foreman-Mackey *et al.*, 2013). Unlike the Monte Carlo component itself which only draws on independent samples, in the Markov Chain, the next sample is always dependent only on the previous one but nothing else prior. This helps to decide on where the next sample should be, forming a chain. If a candidate sample is rejected, another sample will then be randomly drawn from the distribution. However, if the posterior probability of

Student ID: 20194859

the new sample gets improved, then we just leave it at that.

Finally, for all 10 time points, after dosing with all external NaFe-EDTA

concentrations, cubic B-spline interpolation functions were generated on Anaconda

Spyder Software. However, no interpolation functions were generated because it is a

time-invariant parameter.

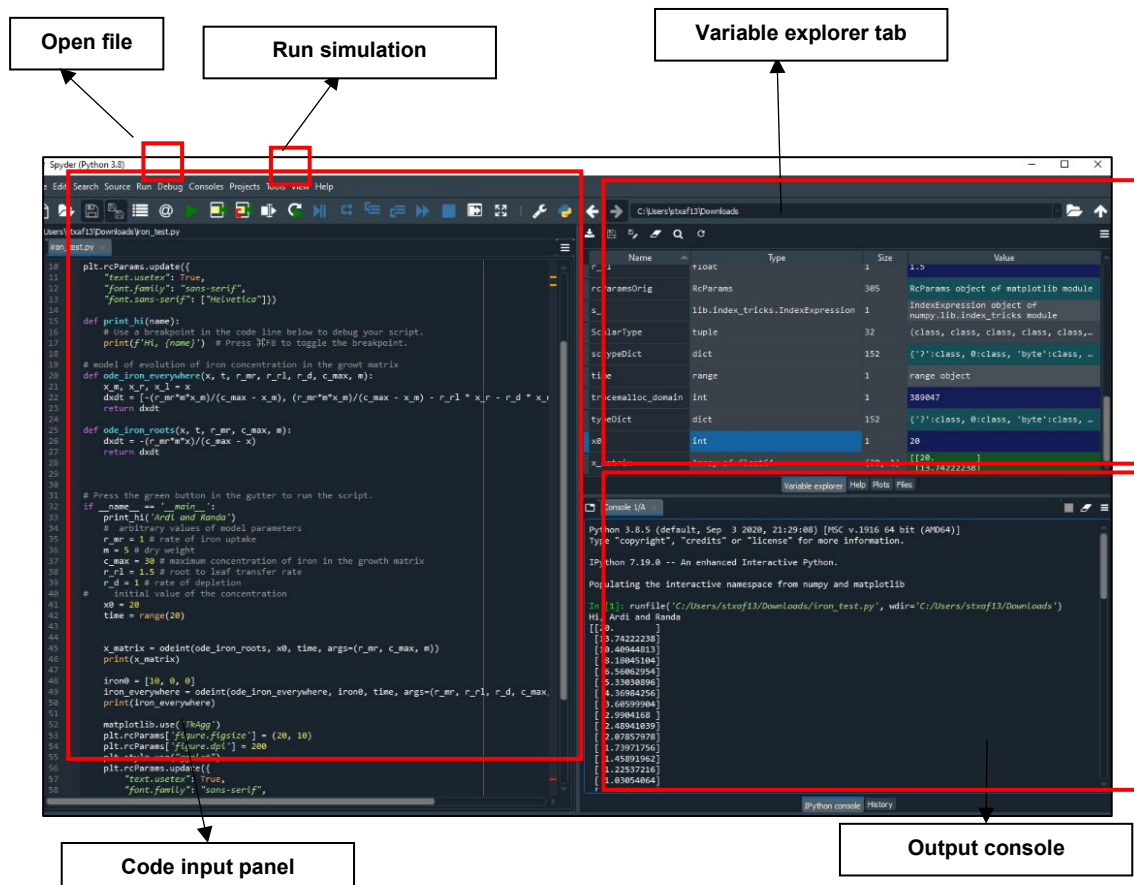


Figure 4.13: Sample representation of the Anaconda Python Spyder simulation software with model code notation in input console and model run in the output console. All key features are clearly labelled.

4.5.7 ODE modelling simulation outputs

The penultimate outputs from MCMC included contour plots, histograms and iteration walker diagrams (see Appendices 7A—D) set to 8000 iterations, with respect to four different versions of the dynamic model; 1) constant decay rate, 2) variable decay rate, 3) minimal Fe in the growth matrix and 4) no inhibition of Fe uptake.

For the sake of brevity, contour plots were only illustrated for model fitting after dosing with 100 μM NaFe-EDTA in solution. Also, final modelling outputs were only illustrated for model fitting after dosing with both 10 and 100 μM NaFe-EDTA in solution, to be at both ends of the experimental range of dosing concentrations.

The final outputs of each iteration until reaching the desired posteriors, were each displayed with MCMC walker diagrams, from the burn-in phases (Roose *et al.*, 2001). The choice of the proposal distribution had a strong influence on the burn-in (Daniel Foreman-Mackey, 2013). Examples are clearly illustrated for in Appendices 7A—D after dosing with 100 μM NaFe-EDTA in solution, for 1) constant decay rate, 2) variable decay rate, 3) minimal Fe in the growth matrix and 4) no inhibition of Fe uptake.

4.6 Results and discussion

4.6.1 Constant decay rate of perlite spinach Fe

The original system of ODEs, Equations 4.1A—C, were based on three equations. However, from the perspective of parameter estimation, all the unknown parameters are already included in Equations 4.1B—C. This therefore resulted in the exclusion of

Equation 4.1A from the final model. Therefore, in this case, x_M became a varying parameter of the model rather than in steady state, therefore its initial state gets removed from the initial Fe content parameters.

The spinach plant root DWs serving as the inhibiting factors in the uptake term of the model are another time-varying parameter (in days). Therefore, both the root DW and growth matrix Fe content quantities for all 10 time points, were used to generate cubic B-spline interpolation functions after dosing with all external NaFe-EDTA solution concentrations. However, no interpolation functions were generated for K_M because of it is a time-invariant parameter.

The cubic B-spline function, shown by Figure 4.14, shows that the Fe contents in the matrix increased linearly after dosing with all Na Fe-EDTA solution concentrations. There is more variability in the root DWs but there is a constant rate of increase. The negative changes in DW after dosing with 50 μM and 200 μM , between Days 18 and 21 are most likely attributed to measurement errors and plant-to-plant variability, especially the fact that they were taken in triplicates.

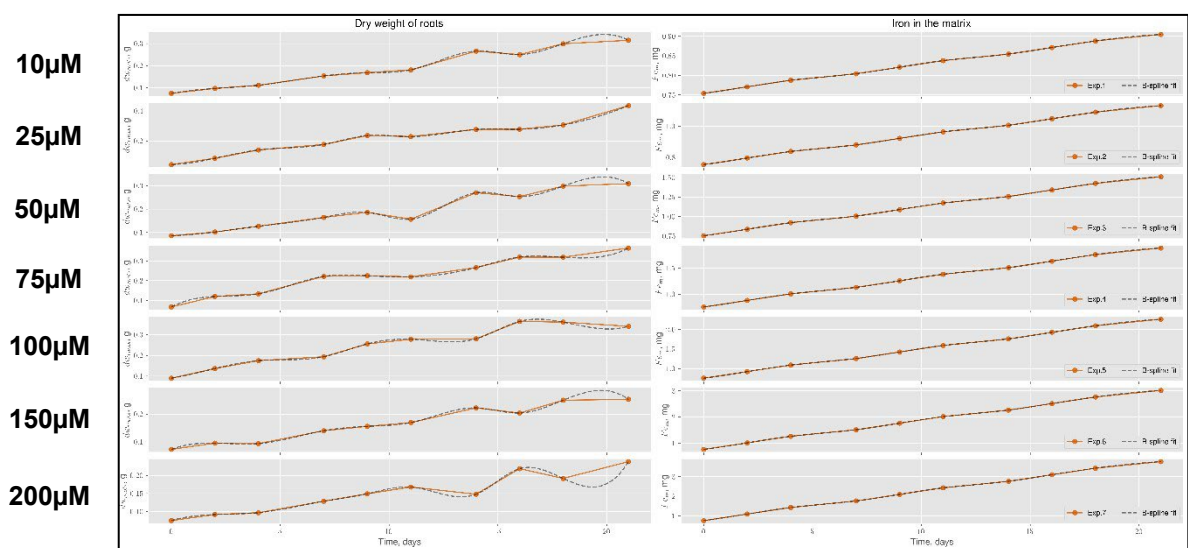


Figure 4.14: Cubic B-spline interpolation function of perlite spinach root DWs (left column) and growth matrix Fe contents (right column), after dosing with all seven NaFe-EDTA

concentrations. The measured values for all 10 time points are shown in orange and the approximation function in dashed grey.

The model was initially designed for the replicates for the different external dosing solution concentrations of Na Fe-EDTA separately. This was done to observe potential changes in the five model parameter values after feeding with higher dosing concentrations. The similarity of the best-fit models was assessed through comparison of the shapes of the final posterior distributions. The end-result of the ensemble MCMC algorithm, is a collection of Markov chains corresponding to individual unknown parameters, $\theta_{i(j)}$, where $j = 1$ and N is the number of unknown parameters within each model. Each chain contains M possible values, of the individual parameter, $\theta_{i(j)}$, and is then displayed by $(\theta_{i(j)}^{\Sigma^M})$, where $i=1$, and M represents an individual value.

Posterior distributions of the unknown parameter values were constructed as the distribution of M points in the Markov Chain, therefore the shapes of the posterior distributions were quantified using sample statistics, based on the following four central moments and their accompanied formulae (see Equations 4.8A—D).

- **Sample mean** is the expected value of the posterior distribution of possible parameter values.

$$\bar{\theta}^{(j)} = \frac{1}{M} \sum_{i=1}^M \theta_{i(j)} \quad (\text{Eq. 4.8A})$$

- **Sample variance** quantifies the general spread of possible parameter values. It is technically the standard deviation, squared (σ^2).

$$\text{Var}[\theta^{(j)}] = \frac{1}{M-1} \sum_{i=1}^M (\theta_{i(j)} - \bar{\theta}^{(j)})^2 \quad (\text{Eq. 4.8B})$$

- **Sample skewness** quantifies the asymmetry of the possible parameter values around the mean value.

$$\text{Skew}[\theta^{(j)}] = \frac{\frac{1}{M} \sum_{i=1}^M (\theta_{i(j)} - \bar{\theta}^{(j)})^3}{\text{Var}[\theta^{(j)}]^{3/2}} \quad (\text{Eq. 4.8C})$$

- **Sample kurtosis** quantifies the heaviness of the tails of a normal distribution.

$$\text{Kurt}[\theta^{(j)}] = \frac{\frac{1}{M} \sum_{i=1}^M (\theta_{i(j)} - \bar{\theta}^{(j)})^4}{\text{Var}[\theta^{(j)}]^2} - 3 \quad (\text{Eq. 4.8D})$$

Sample statistics of these parameters from Equations 4.8B—C were applied to each sample chain for the four estimated model parameters; r_{MR} , r_{RL} , r_D and K_M . Sample statistics for the four central moments for the posterior distributions of constant decay rates, are clearly shown in Tables 4.1A—D after dosing with all seven external Na Fe-EDTA solution concentrations.

Tables 4.1A—D: Sample statistics of the estimated values of 4.1A) r_{MR} , B) r_{RL} , C) r_D and D) K_M , based on Equations 4.1B—C, for all dosing concentrations. The four central moments are mean, variance, skewness and kurtosis.

4.1A) r_{MR}	Experiment	Mean	Variance	Skewness	Kurtosis
R 1	10 μ M	0.624888555	0.036399924	0.360298646	0.239156855
2	25 μ M	0.62244163	0.033904785	0.4140219	0.307914654
3	50 μ M	0.620993817	0.038145697	0.582236503	0.292143379
4	75 μ M	0.556760093	0.02734826	0.400173151	0.254237653
5	100 μ M	0.480072942	0.029007501	0.489159805	-0.11464295
6	150 μ M	0.504116606	0.014060666	1.147586344	2.583625584
7	200 μ M	0.563794749	0.012901404	0.524935409	0.522077184

4.1B) r_{RL}	Experiment	Mean	Variance	Skewness	Kurtosis
1	10 μ M	0.028427346	0.0000570941	1.013515463	3.537126611
2	25 μ M	0.038026021	0.000119429	0.992712187	1.909107158
3	50 μ M	0.042560575	0.000143516	0.788760138	1.181183989
4	75 μ M	0.032867912	0.0007151505	1.010271486	2.268833962
5	100 μ M	0.038575832	0.000133635	1.179153886	2.399800733
6	150 μ M	0.070663958	0.000251844	0.517216104	0.541868459
7	200 μ M	0.090293208	0.000292658	0.524299044	0.317971526

4.1C) r_D	Experiment	Mean	Variance	Skewness	Kurtosis
1	10 μ M	0.065799131	0.000264265	0.463524616	0.661247677
s2	25 μ M	0.071514593	0.000566654	0.715770259	0.846388745
3	50 μ M	0.082733157	0.000659513	0.619342982	0.696683774
4	75 μ M	0.055764316	0.000384505	1.021705549	1.867054257
5	100 μ M	0.053065536	0.000788725	1.287780096	1.989120414
6	150 μ M	0.078153285	0.000803371	0.422650925	0.291527231
7	200 μ M	0.076004878	0.000658071	0.497643498	0.293669909

4.1D) K_M	Experiment	Mean	Variance	Skewness	Kurtosis
1	10 μ M	4.814148875	4.209794899	0.373887639	-0.429188905
2	25 μ M	4.81113774	4.75391871	0.338322526	-0.619383939
3	50 μ M	3.159729149	3.668844365	0.852234389	0.532101738
4	75 μ M	5.580124207	5.79255015	-0.106593552	-0.841859381
5	100 μ M	4.2539816	8.087731053	0.187161599	-1.084474881
6	150 μ M	0.712187856	1.207500913	3.474748364	15.518587
7	200 μ M	0.238649299	0.089653567	4.512670594	41.32627514

4.6.2 Variable decay rate

The first modification to the original model was made by abandoning the assumption of constant Fe decay rates in the spinach plant parts. It was anticipated to result in a better model fit in experiments after dosing with higher NaFe-EDTA solution concentrations. The physiological process behind the decay model term was the reduction of Fe contents in plant parts, following their growth. This experiment allowed tracing of growth of both root and leaf material and thus using their time-varying rates of growth in Equations 4.9A—C on the following page.

$$\frac{dx_R}{dt} = r_{MR} \frac{dw(t)}{(x_M + K_M)} x_M - r_{RL} x_R - r_{RG}(t) x_R \quad (\text{Eq. 4.9A})$$

$$\frac{dx_L}{dt} = r_{RL} x_R - r_{LG}(t) x_L \quad (\text{Eq. 4.9B})$$

$$x(0): 1) x_{R_{t=0}} = x_R(0), 2) x_{L_{t=0}} = x_L(0) \quad (\text{Eq. 4.9C})$$

where:

- $r_{RG}(t)$ is the time-varying rate of root growth.
- $r_{LG}(t)$ is the time-varying rate of leaf growth.

These values were computed from the preliminary DW values of both root and leaf material (see Figures 4.3A—B). Firstly, the differences between their DWs on consecutive days were calculated. This was followed by dividing the number of days between each harvesting day to obtain values for rates of change, in grams per day (g/day). Another cubic B-spline interpolation function was generated for the interpolation results of all NaFe-EDTA external solution concentrations (see Figure 31). The same unknown parameters as Equations 4.1B—C were applied here, however, r_D was excluded from the set of unknown parameters.

The posterior sample statistics for three unknown parameters in Equations 4.9A—C;

1) r_{MR} , 2) r_{RL} and 3) K_M are summarised in Tables 4.2A—C.

Tables 5A—C: Sample statistics of the estimated values of 4.2A) r_{MR} , B) r_{RL} , and C) K_M , based on Equations 4.9A—B, for all dosing concentrations.

4.2A) r_{MR}	Experiment	Mean	Variance	Skewness	Kurtosis
1	10 μ M	0.646092573	0.037217764	0.384177233	0.351774365
2	25 μ M	0.640999103	0.036552512	0.405514825	0.569123054
3	50 μ M	0.658230803	0.038893982	0.435848287	0.353919224
4	75 μ M	0.633702491	0.034715493	0.349729922	0.208977251
5	100 μ M	0.617027348	0.038463058	0.502745231	0.199950764
6	150 μ M	0.580086434	0.037088266	0.718030328	0.758122388
7	200 μ M	0.413966249	0.025854783	1.320508641	1.804805556

4.2C) K_M	Experiment	Mean	Variance	Skewness	Kurtosis
1	10 μ M	14.87711208	31.06523886	0.429014649	-0.294848417
2	25 μ M	14.61387734	33.19090732	0.505904364	-0.323386716
3	50 μ M	11.27390032	23.69666711	0.943618238	0.929827903
4	75 μ M	15.5083515	32.88406901	0.336370433	-0.433976524
5	100 μ M	10.62850324	19.25905	0.741143696	0.768044267
6	150 μ M	4.194325994	5.01049888	0.804965998	0.828256138
7	200 μ M	1.990830199	3.60392337	1.553391443	2.89802557
4.2B) r_{RL}	Experiment	Mean	Variance	Skewness	Kurtosis
1	10 μ M	0.022925399	0.0000241616	0.477102566	0.568329544
2	25 μ M	0.027954365	0.000039519	0.446252959	0.665542563
3	50 μ M	0.02948692	0.000043078405	0.40080221	0.468638408
4	75 μ M	0.027931546	0.00002878222	0.277281355	0.199289796
5	100 μ M	0.033963896	0.0000359716	0.220814165	0.221294147
6	150 μ M	0.047688573	0.000035221	0.187440544	0.108260859
7	200 μ M	0.055614954	0.0000375227	0.177793686	0.218085948

The mean values of all three model parameters demonstrate clear patterns with increasing dosing concentrations of NaFe-EDTA in solution. However, the higher moments of K_M posteriors at lower dosing concentrations indicate that this parameter cannot be reliably inferred from the measured experimental data (see Table 4.2C). For example, dosing between 10–100 μ M NaFe-EDTA in solution resulted in lower skewness and kurtosis as compared to 150–200 μ M. This is further substantiated visually in Figure 4.4. This was probably because of the considered inhibition factor not including enough detail about the complex kinetics of r_{MR} from the growth matrix. Also, the r_{MR} inhibition limit was not yet reached in the conducted experiments.

Figure 4.15 shows the contour plot of the posterior distributions of all unknown parameters after dosing with 100 μ M NaFe-EDTA in solution. The plots show that the posterior distribution of K_M for variable decay rate is better informed. This is because of its lower kurtosis and its peak being surrounded around the mean. Therefore,

despite limited evidence on values of K_M , the model output captures the general trends of Fe content. All the other estimates are just as precise.

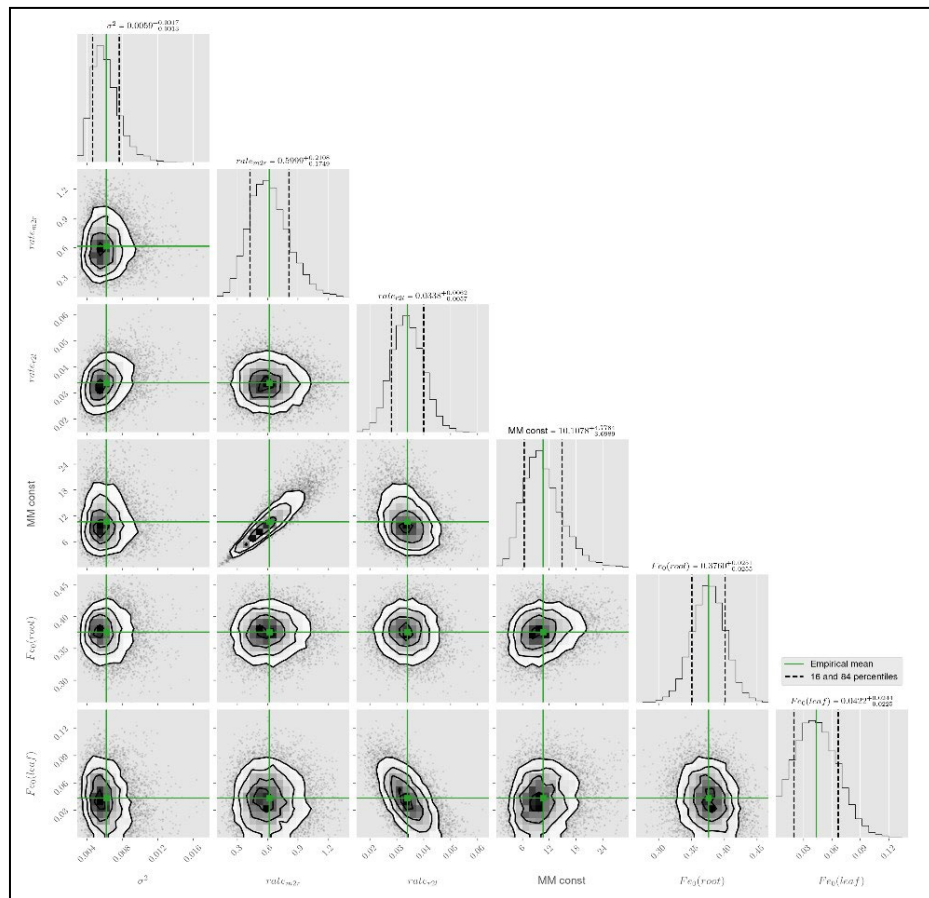


Figure 4.15: Contour plot of posterior distributions of Equations 4.9A–B after dosing with 100 μ M NaFe-EDTA in solution – variable decay rate.

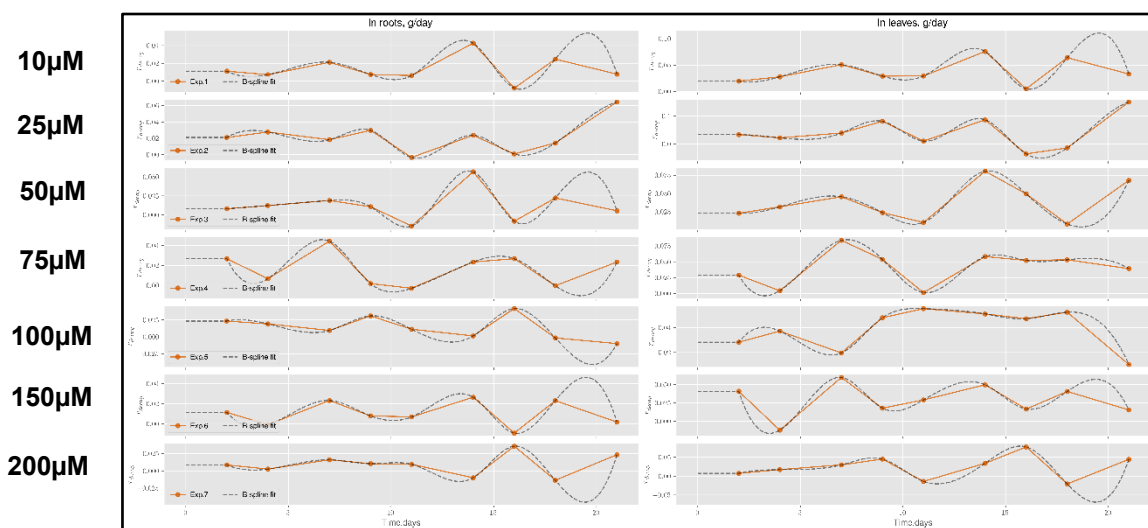
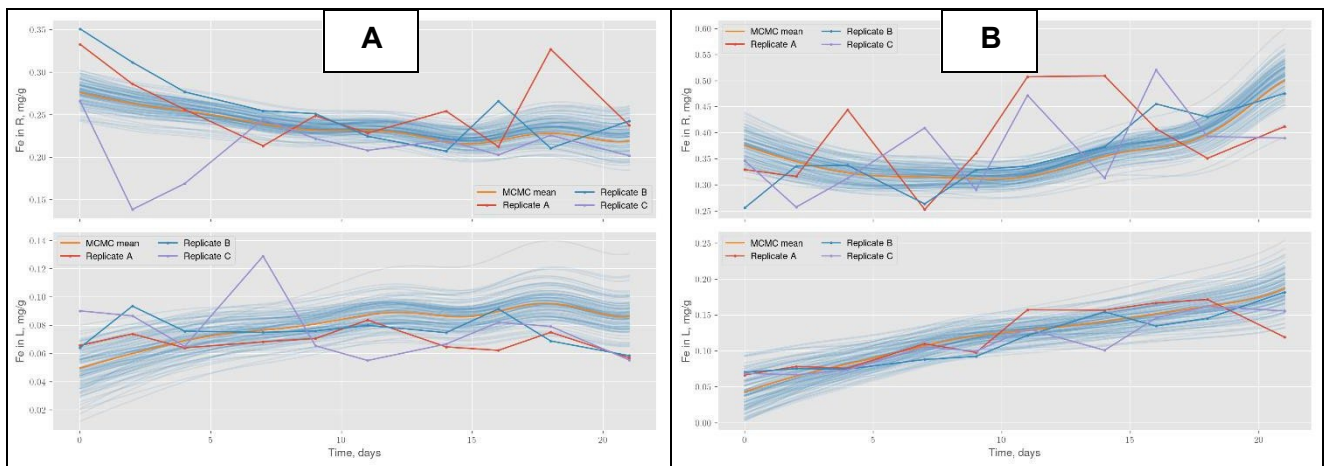


Figure 4.16: Cubic B-spline interpolating function of root (left column) and leaf(right column) growth rates after dosing with all seven NaFe-EDTA concentrations. The measured values for all 10 time points are shown in orange and the approximation function in dashed grey.

Based on Figure 4.16, compared to the spinach root DWs and growth matrix Fe contents, root and leaf growth rates did not increase linearly after dosing with higher NaFe-EDTA concentrations over the growth period. There was more variability overall which indicates that the data did not fit to the model outputs as closely as seen in Figure 4.17.

Figures 4.17A—B compare the output of the fitted models of Equations 13A—B. The model predictions followed dosing with 10 and 100µM NaFe-EDTA in solution.



Figures 4.17A—B: Modelling output corresponding to the 500 samples and MCMC posterior mean from Equations 4.9A—B, after dosing with 4.17A) 10 and B) 100µM NaFe-EDTA in solution.

4.6.3 Minimal Fe content in the growth matrix

Inconsistent estimates for K_M , from experiment to experiment led to another model variation of the inhibition term. The form by Nielsen (1976), was introduced in Equations 4.10A—C.

$$\frac{dx_R}{dt} = r_{MR} \frac{dw(t)}{(x_M - C_{min} + x_M)} (x_M - C_{min}) - r_{RL}x_R - r_{RG}(t) x_R \quad \text{(Eq. 4.10A)}$$

$$\frac{dx_L}{dt} = r_{RL}x_R - r_{LG}(t)x_L \quad (\text{Eq. 4.10B})$$

$$x(0): 1) x_{R_{t=0}} = x_R(0), 2) x_{L_{t=0}} = x_L(0) \quad (\text{Eq. 4.10C})$$

where:

- C_{\min} denotes the minimal Fe in the growth matrix at which the uptake rate is equal to 0 (Nielsen, 1976).

It was anticipated that this form of inhibiting factor was enough to describe the initial decreases of Fe contents, especially for lower dosing concentrations of NaFe-EDTA in solution. All other notations remain the same as Equations 4.9A—C.

For the sake of brevity, the only the posterior sample statistics of r_{MR} (see Table 4.3A) and K_M (see Table 4.3B) were documented.

While the C_{\min} posteriors were consistent for all dosing concentrations of NaFe-EDTA, in terms of means, skewness and low numbers of outliers (see Table 4.3A), the estimates for K_M (see Table 4.3B) remained unreliable with no clear pattern, especially for the skewness, and precision was worse than for variable decay rate, illustrated by Equations 4.9A—C. Nielsen (1976) also reported C_{\min} being completely unaffected by variation in K_M . The estimations of rates were close to the previous values and were therefore omitted here.

Tables 4.3A—B: Sample statistics of the estimated values of 4.3A) C_{min} and B) K_M , based on Equations 14A—B, for all dosing concentrations.

4.3A) C_{min}	Experiment	Mean	Variance	Skewness	Kurtosis
1	10 μ M	0.252333198	0.027459895	0.321667034	-1.007991777
2	25 μ M	0.257324249	0.027695134	0.297003219	-1.038771978
3	50 μ M	0.283278445	0.029688443	0.11299593	-1.173603066
4	75 μ M	0.246593246	0.027354498	0.368255782	-0.970335238
5	100 μ M	0.192196327	0.022050344	0.755883009	-0.333395794
6	150 μ M	0.235947904	0.026930978	0.458712455	-0.866219453
7	200 μ M	0.235295465	0.027449599	0.41873291	-0.94959602

4.3B) K_M	Experiment	Mean	Variance	Skewness	Kurtosis
1	10 μ M	11.19520942	55.04622907	3.963359915	31.02626235
2	25 μ M	12.29910032	73.89536763	3.635612528	22.57821641
3	50 μ M	8.56440751	23.88428255	3.631546538	35.87533084
4	75 μ M	14.28250255	51.75726865	2.253093127	12.40432029
5	100 μ M	9.418652151	17.26643886	0.913842015	1.494447768
6	150 μ M	3.549037217	4.158970182	0.894239235	1.12970194
7	200 μ M	1.657327938	3.246004471	1.841253173	4.385783173

An example contour plot after dosing with 100 μ M NaFe-EDTA in solution can be seen in Figure 4.18 and demonstrates the joint distributions of all estimated parameters. Despite the poor estimation results, especially for C_{\min} with higher kurtosis and the empirical mean being nowhere near the peak, the model can predict the general trend captured by the measurements (see Figures 4.19A—B). Figure 4.19, in general, also shows that this model was not sensitive to K_M , which fit perfectly with the empirical mean value. Therefore, it was completely excluded in further analysis in Section 4.3.5.4.

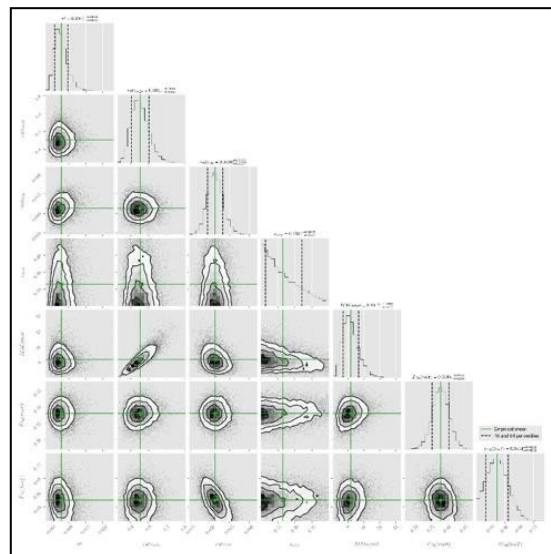
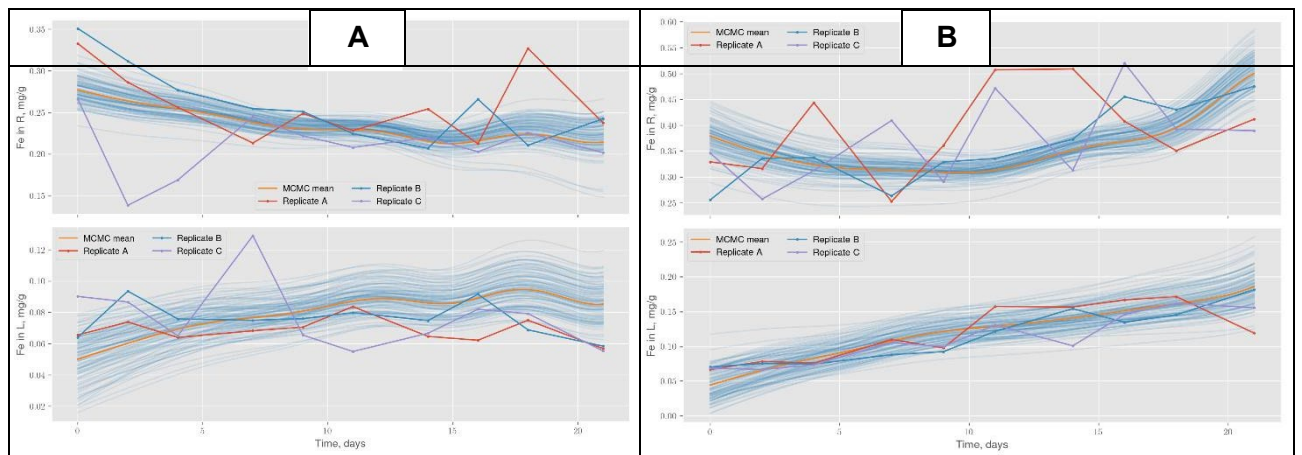


Figure 4.18: Contour plot of posterior distributions of Equations 4.10A—B after dosing with 100 μ M Na Fe-EDTA in solution – minimal Fe content in the growth matrix



Figures 4.19A—B: Modelling output corresponding to the 500 samples and MCMC posterior mean from Equations 4.10A—B, after dosing with 4.19A)10 and B)100 μM NaFe-EDTA in solution.

Finally, the C_{\min} values were generally unaffected by increases in K_M . However, sometimes there are disagreements with this theory because r_{MR} was generally greater than 0 (Nielsen, 1976).

4.6.4 No inhibition of uptake

Previous analysis of the other three models showed that upon dosing with all external NaFe-EDTA solution concentrations, the conditions for noticeable uptake inhibition, in the growth matrix were never fully reached. For this reason, for Equations 4.11A—C, the assumption of inhibited Fe uptake from the growth matrix was eliminated, and the model was further simplified by removing r_D , K_M and C_{\min} .

$$\frac{dx_R}{dt} = r_{MR}x_M - r_{RL}x_R - r_{RG}(t)x_R \quad (\text{Eq. 4.11A})$$

$$\frac{dx_L}{dt} = r_{RL}x_R - r_{LG}(t)x_L \quad (\text{Eq. 4.11B})$$

$$x(0): 1) x_{Rt=0} = x_R(0), 2) x_{Lt=0} = x_L(0) \quad (\text{Eq. 4.11C})$$

Here, the linear uptake of Fe from the growth matrix to the root material was inhibited by C_{\max} of the root and leaf material. The C_{\max} was unidentifiable and could not be determined based on the data currently collected.

Tables 4.4A—B show the sample statistics computed for r_{MR} and r_{RL} . For both parameters, the variance with respect to the mean values, were extremely low and far lower than in Tables 4.3A—B, for minimal content in the growth matrix. This, therefore, indicates very high precision for the posterior estimates. The kurtosis remained consistently positive, and below 0.25, suggesting a lower chance for outliers. The skewness varied for each dosing solution concentration of Na Fe-EDTA without any clear pattern, they remained close to 0 throughout. Therefore, the low kurtosis, skewness and variance suggests that samples of all parameter values were well-centred around the mean value. It was also noticed that the means for r_{MR} after dosing with 10—75 and 100—200 μM NaFe-EDTA formed two separate clusters. Section 4.4.6 will explore these subsets of NaFe-EDTA concentrations to assess the strength of a single model. The mean r_{RL} also increased as the dosing concentrations of Na Fe-EDTA steadily increased.

Tables 4.4A—B: Sample statistics of the estimated values of 4.4A) r_{MR} and B) r_{RL} , based on Equations 4.11A—B, for all dosing concentrations.

4.4A) r_{MR}	Experiment	Mean	Variance	Skewness	Kurtosis
1	10 μM	0.624888555	0.036399924	0.360298646	0.239156855
2	25 μM	0.62244163	0.033904785	0.4140219	0.307914654
3	50 μM	0.620993817	0.038145697	0.582236503	0.292143379
4	75 μM	0.556760093	0.02734826	0.400173151	0.254237653
5	100 μM	0.480072942	0.029007501	0.489159805	-0.11464295
6	150 μM	0.504116606	0.014060666	1.147586344	2.583625584
7	200 μM	0.563794749	0.012901404	0.524935409	0.522077184

4.4B) r_{RL}	Experiment	Mean	Variance	Skewness	Kurtosis
1	10 μ M	0.018682369	2.22633E-05	0.369040699	0.325680642
2	25 μ M	0.021637481	3.29602E-05	0.290154111	0.200938433
3	50 μ M	0.022315624	3.62192E-05	0.287987747	0.135069992
4	75 μ M	0.023774539	2.64181E-05	0.146075284	0.019268737
5	100 μ M	0.029350938	2.79539E-05	0.14407607	0.060664922
6	150 μ M	0.042785637	2.94132E-05	0.005188198	0.186465981
7	200 μ M	0.049892897	3.01912E-05	0.086570452	0.16597179

The example contour plot after dosing with 100 μ M NaFe-EDTA can be seen in Figure 4.20. The modelling outputs after dosing with 10 and 100 μ M NaFe-EDTA in solution are presented in Figures 4.21A—B and clearly demonstrate that the simplified models of Equations 4.11A—B clearly captured the dynamics of Fe in both roots and leaves. Together with the high precision estimates from the sample statistics of the model parameters (see Tables 4.4A—B), the conclusion was that models without inhibition from C_{max} or K_M were better informed by all the data generated for the experiments.

As seen in Figure 4.18 and Tables 4.4A—B, for no inhibition of uptake, of all maximum values for all parameters were centred across the empirical mean and had far lower skewness and kurtosis compared to Figure 4.17, and Tables 4.3A—B, for minimal Fe content in the growth matrix. However, this does not mean that this was the best model for describing the data, rather it indicates that if the inhibition of r_{MR} at lower dosing concentrations of NaFe-EDTA did occur, it was not attributed to K_M . Therefore, a better model of Fe uptake inhibition requires further elucidation, however, it remains beyond the scope for this current project.

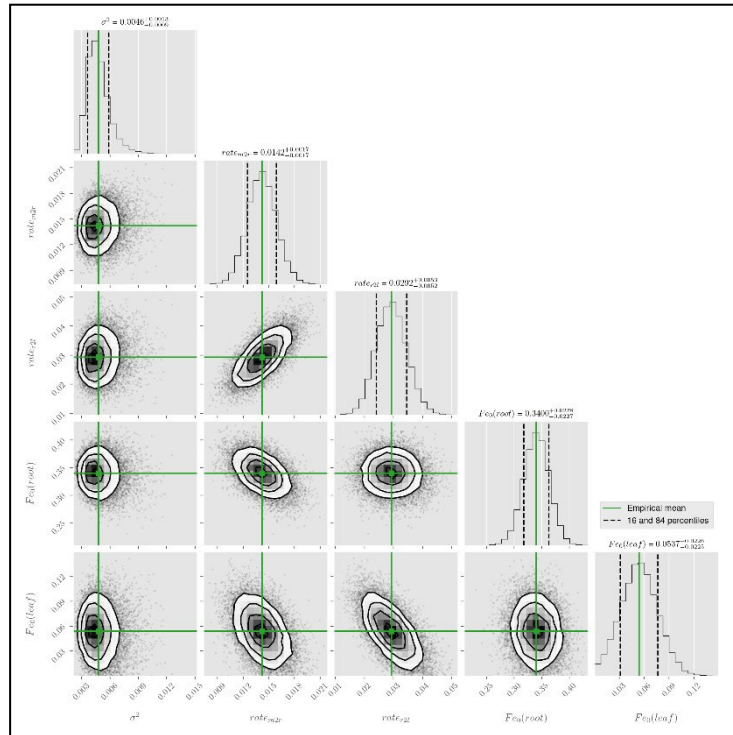
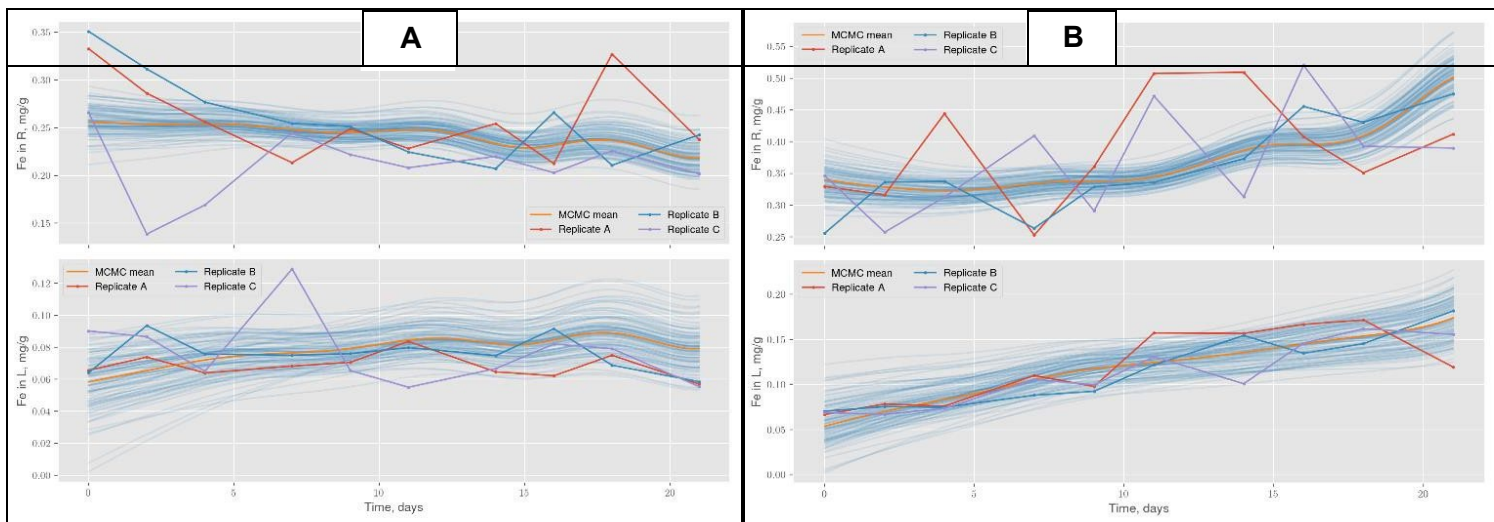


Figure 4.20: Contour plot of posterior distributions of Equations 4.11A—B after dosing with 100 μ M NaFe-EDTA in solution – no inhibition of Fe uptake



Figures 4.21A—B: Modelling output corresponding to the 500 samples and MCMC posterior mean from Equations 4.11A—B, after dosing with 4.21A)10 μ M and B)100 μ M NaFe-EDTA in solution.

4.6.5 Fitting models to several experiments simultaneously

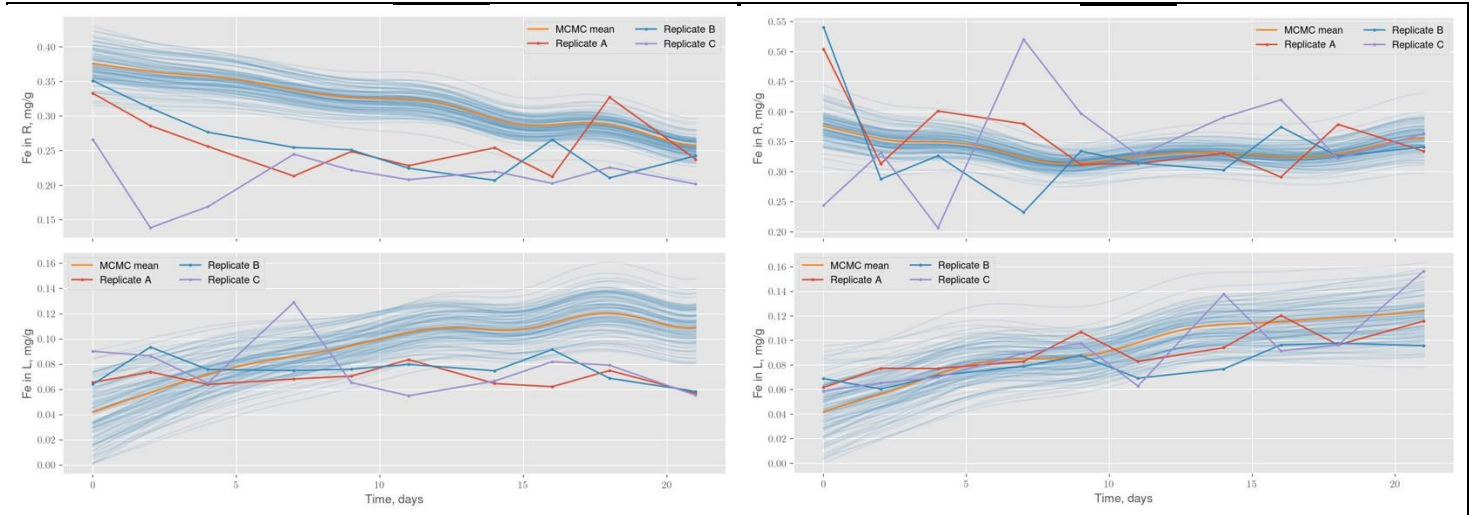
The estimated parameter values (see Tables 4.4A—B) of the model described by Equations 15A—B indicated that the data could be explored with two separate subsets, after dosing with 10—75 and 100—200 μM NaFe-EDTA in solution. Therefore, the models from Section 4.3.2.4 were fitted towards them. The posterior sample statistics for Equations 15A—B were summarised in Tables 4.5 and 4.6. The model outputs fitted to the measurements from 10—75 μM NaFe-EDTA can be seen in Figures 4.22A—B. The model outputs fitted to the measurements from 100—200 μM NaFe-EDTA can be seen in Figures 4.23A—B. It can clearly be shown that for the accuracy of prediction of the lower dosing concentrations of NaFe-EDTA decreased, therefore suggesting that the parameter estimates were biased towards higher concentrations. This can be clearly seen in Figure 4.23B, where the blue model fitting lines closely resembled the data for leaf material, including the MCMC posterior mean, after dosing with 200 μM NaFe-EDTA in solution.

Table 4.5: Sample statistics of r_{MR} values inferred from subsets of dosing concentrations of 10—75 and 100—200 μM NaFe-EDTA in solution.

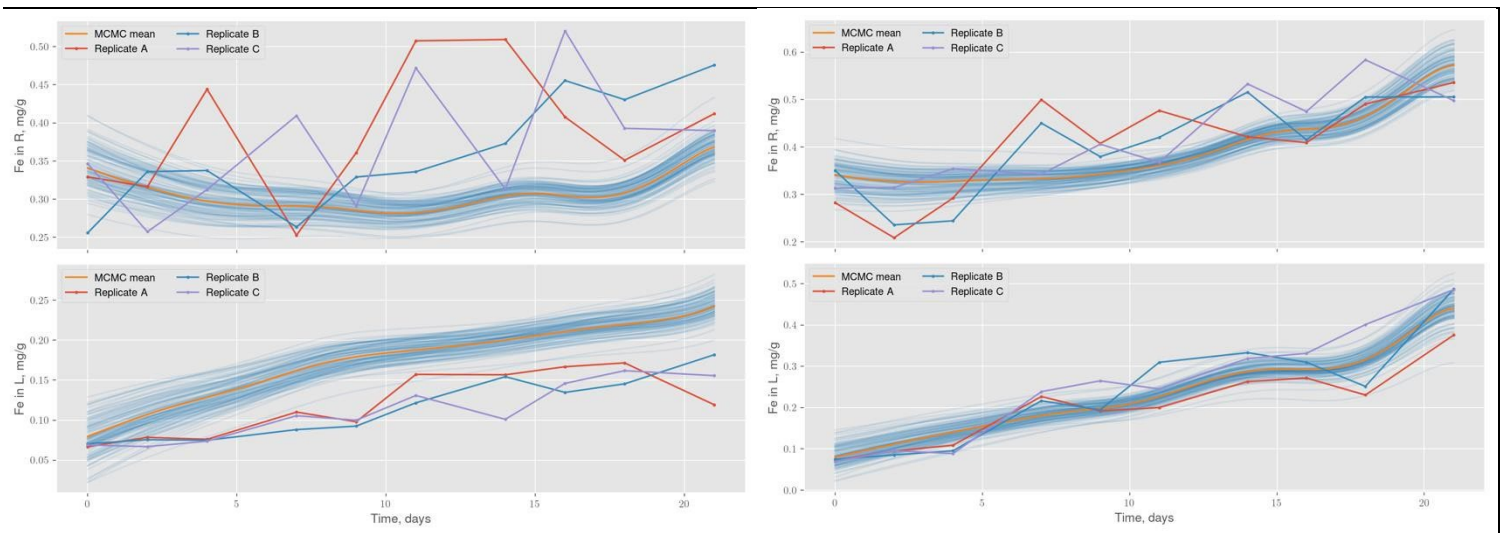
4.5) r_{MR}	Experiment	Mean	Variance	Skewness	Kurtosis
0	10—75 μM	0.009915807	0.00000348222	0.119648134	0.191109773
1	100—200 μM	0.014406828	0.00000158177	0.046265795	0.125096048

Table 4.6: Sample statistics of r_{RL} values inferred from subsets of dosing concentrations of 10—75 and 100—200 μM NaFe-EDTA in solution.

4.6) r_{RL}	Experiment	Mean	Variance	Skewness	Kurtosis
0	10—75 μM	0.023682591	0.0000269313	0.139618138	0.338150176
1	100—200 μM	0.049887883	0.00003048	0.056844284	0.152047788



Figures 4.22A—B: Modelling output represented by Equation 15, fitted to the data after dosing with 10—75 μM NaFe-EDTA in solution; Figure 4.22A) 10 and B) 75 μM NaFe-EDTA in solution.



Figures 4.23A—B: Modelling output represented by Equation 15, fitted to the data after dosing with 100—200 μM Na Fe-EDTA in solution; Figure 4.23A) 100 and B) 200 μM Na Fe-EDTA in solution.

4.7 Discussion and evaluation

This chapter introduces a quantitative analytical framework that can calibrate candidate models of micronutrient uptake against the content of this nutrient in both root and leaf material of plant parts, using the ICP-MS data. While presented specifically for the iron data, it can be readily applied to any element of interest, if their contents and concentrations and contents are tracked throughout the plant parts. To the best of knowledge, this is the first study to incorporate mathematical modelling for the analysis of spinach plants. The framework can be extended by incorporating more detailed models of the uptake mechanisms if enough data is available to inform these models.

In this experiment, the pH of Hoagland nutrient solutions, for all dosing concentrations, were maintained at 5.8, which was the optimal for Fe accumulation in perlite spinach. This was also reported by Tudoreanu and Phillips, (2004), who reported a similar pH for spinach cultivation.

From Equations 15A—B, C_{\max} was unidentifiable and could not be determined based on the data currently collected. Further research on complex spinach root geometry is also required together with incorporating degradation and chemical transformation rates in the rhizosphere. K_M was difficult to identify from the experimental data, because the limiting sections in the growth matrix were never fully reached.

From Figures 4.5A—B, it could be seen that spinach root and leaf Fe contents were lower at higher dosing concentrations of NaFe-EDTA, potentially indicating some form of inhibition taking place to regulate the uptake. This was maybe attributed to underlying mechanisms inside the plants, or changes in root morphology. *Bar-Tal et al.*, (1997) reported significant decreases in elongation of tomato root tips, at higher

concentrations of other elements such as N and P. This indicated that the root architecture could be altered by the micronutrient composition of the environment. The same was true for *Arabidopsis*, with total root length increasing following mild N deficiency but root length being stunted following severe deficiency. To our best knowledge, no other studies have reported the effect of Fe concentration on root architecture in plants, or the order in which the spinach belongs to. Exploring this effect in more targeted experiments with perlite, could be a potential direction for inquiry.

Therefore, for future enquiry, a more targeted experiment must be designed, to include more measurable variables of plant morphology in terms of root system architecture (RSA) – these include the length, thickness and angles of the primary roots (PR) and lateral roots (LR). Baligar *et al.*, (1998) reported RSA being highly determined by the number, diameter, length, surface area and distribution in the soil. A mathematical model will need to be designed and informed by this data, which would then include the logistic term in the uptake equation, with the interpretation being that there is some maximal concentration that the roots can take up because of limited surface contact with other nutrients.

In the context of Fe, their increased concentrations result in morphological changes including inhibition of root elongation, increased diameter of apical root zones and abundant root hair formation. Proteoid roots also begin to form (Giehl and von Wirén, 2014). Carbon flow can also facilitate directional root elongation to areas with more favourable conditions. Excess soil Fe is also known to inhibit lateral root (LR) initiation, however, not the subsequent elongation process. These inhibitory effects are not seen in the PR. In fact, the physical contact of PR to excess soil Fe is necessary as a warning for inhibition of LR development and elongation (Li *et al.*, 2013). These parallel with Equations 15A—B which assumed no inhibition of Fe uptake. The fitting results

for the model described by Equations 15A—B elucidate an unexpected pattern of Fe uptake by the spinach plants, following an increase of Fe in the Hoagland nutrient solution. The dynamics of Fe transfer do not change significantly, at previously reported toxicity levels.

Şimşek and Çelik, (2021) reported dosing with 150 μM Fe-EDTA resulting in a significant decrease in macro and micronutrient uptake in hydroponic spinach uptake in roots. However, nothing drastic happened for that exact concentration. Based on Tables 7A—B, the rate of Fe uptake was the lowest after dosing with 10 μM Na Fe-EDTA, followed by a steady increase after dosing with 200 μM Fe-EDTA, to match the rate of uptake corresponding to lower dosing concentrations.

Li *et al.* (2016) reported that at adverse toxic concentrations of Fe, Arabidopsis can take on board adaptation strategies including reduced Fe accumulation at the root level, immobilisation of active Fe which has already reached the leaves or leaf tissue, and through enhancement of high-tolerance mechanisms including enzymatic detoxification. Potassium (K^+) has also been known to play a critical role in regulation of RSA during moments of Fe toxicity. Morphologically speaking, the suppression of PR and LR growth at the higher dosing concentrations of 250—350 μM Fe, is significantly alleviated by addition of 8 mM K^+ . The hypothesis states that K^+ may reduce the activity of excess Fe^{2+} in the root medium and target Fe^{2+} -mediated root elongation, or the enzymatic systems which control Fe^{2+} immobilisation and detoxification. This rescue effect closely mirrors the alleviation effects of K^+ following NH_4^+ toxicity. Therefore, this alleviation process offers a decent agricultural strategy of reduction of manifestation of cation toxicity in the field. After dosing at higher NaFe-EDTA concentrations, the estimated rate of Fe uptake was lower for plants dosed with lower dosing concentrations. On the other hand, the rate of Fe transfer from roots to

leaves monotonously increased, following higher dosing concentrations. Furthermore, there was a clear decrease in DWs for both root and leaf concentrations, after dosing with 150 and 200 μM NaFe-EDTA in solution (see Figures 4.5A—B).

It was possible that the spinach plants engaged in intrinsic mechanisms, impacting plant physiology, such as inhibition of root elongation. An elaborate conclusion cannot be made on the reduction of DWs being a physiological response to Fe toxicity levels, because only the influence of FW on rates were incorporated and not the dynamical changes of the DWs themselves. Another potential avenue of future research would be to incorporate the complex dynamics of root growth in terms of DWs.

Conversely, Clark (1970) also performed an extensive study and concluded that higher levels of Fe did not have a profound impact on root:shoot ratios. Finally, low pHs significantly reduce root mass, length, and root hair formations. Therefore, future experiments should further investigate which exact mechanisms will govern these internal inhibition processes.

Finally, the main shortcoming of this project was limited observed variables, such as DWs, as an indication of growth, led to very simplistic models built around the assumption that only DW of the roots led to inhibition of their uptake. One suggested improvement to the experiment and the final models could be accounting for more aspects of plant physiology, ranging from root morphology, mineral concentrations, NO_3^- concentrations, and chlorophyll and carotenoid contents.

4.8 Conclusions

- Fe toxicity limits and C_{\max} were never reached.
- Fe contents were always higher in root, rather than leaf material.
- The maximum yields and Fe contents for both root and stem material were reached after dosing with both 50 and 100 μM NaFe-EDTA in solution.
- At higher dosing concentrations of NaFe-EDTA in solution, internal concentrations of Fe, in both leaves and roots were higher.
- It is possible that the toxicity limits were reached at 150 and 200 μM NaFe-EDTA in solution, and the roots experienced Fe stress.
- Finally, the MCMC, is a suitable method for determining the posterior distribution, which in turn compares the actual data to any given model. One iteration is only dependent on the previous one and nothing else.
- For further inquiry and logic, more variables should be incorporated in the ODEs, including the ones for plant morphology, NO_3^- concentrations and chlorophyll concentrations

Chapter 5: Tracing iron distribution in spinach leaves and the bioaccessibility of iron from spinach leaves and their Chloroplast Rich Fractions (CRFs)

5.1 Introduction to bioaccessibility from plant-based food sources

Digestion studies of nutrient components include three terms; bioaccessibility, bioavailability and bioactivity, each of them has various methods of assessment. Bioaccessibility is the amount of ingested food or nutrient material potentially available for absorption in the duodenal section of the small intestine (Eriksen *et al.*, 2017; Rodriguez-Ramiro *et al.*, 2019). The term, 'bioavailability' extends to include the utilisation of the bioaccessible nutrient which gets assimilated in the bloodstream. This is followed by 'bioactivity' which includes the specific effect of this nutrient upon its uptake by certain tissues and its physiological response.

Bioaccessibility of food material is often determined using in vivo and in vitro digestion methods. However, the in-vivo methods are costly, resource intensive and ethically disputable (Cai *et al.*, 2017; Etcheverry *et al.*, 2012). Generally, in vitro experiments based on solubility/dialysability are tools to understand factors that may affect subsequent mineral absorption (Sandberg, 2005). Therefore, less-labour intensive in vitro studies have been established, which study the interactions between nutrients and food components, pH and enzymatic activity, food preparation and processing procedures (Minekus *et al.*, 2014).

In vitro digestion trials also include dynamic and static mode of digestion. Static digestion methods also have their limitations because they fail to mimic the complex dynamics of the digestion processes, in terms of pH fluctuations, enzyme activities

and microbial content. However, the alternative dynamic digestion methods were not used, because of high running and maintenance costs (Brodkorb *et al.*, 2019).

Many researchers have studied the bioaccessibility of iron from plant sources, using simulated gastrointestinal (GI) digestion followed by some methods to assess the solubilisation of iron in the digested food. The GI digestion methods consist of simulated GI phases and intestinal phase with some variation of experimental conditions (pH, time, enzyme type and amount). Bioaccessibility assessment also varies between different studies, trying to separate bioaccessible iron, either by the means of centrifugation or filtration, using the equilibrium dialysis technique (dialysability). Experiments based on solubility/dialysability are considered as representative tools to understand factors that may impact subsequent mineral absorption.

Dialysability was first developed by Miller *et al.* (1981) who used it to evaluate minerals availability as he described it. The method aimed to measure the soluble and low molecular iron in food samples following in vitro gastrointestinal digestion. He measured it by inserting a dialysis membrane fraction filled with buffer solution in the digestion mix during the intestinal phase, the last part of the GI digestion. This allows the lower molecular weight iron to diffuse into a semi-permeable membrane with 6000 to 10000 molecular weight cut-off in a process mimicking the differential epithelial uptake (Miller *et al.*, 1981).

The iron content of foods does not indicate its bioavailability because iron absorption depends on some factors, mainly the form of iron and the physiological state of the individual consumer. Because plants mainly contain non-haem iron, even if its iron content is high, absorption of iron is low due to plant-based molecule–iron interactions.

The bioavailability of iron from vegetables is low and variable and influenced by food composition and matrix. The absorption of iron has been reported as 25–30% from animal flesh/organs, 7–9% from green leafy vegetables, 4% from grains, and 2% from dried legumes, indicating that different food types or other dietary factors might also influence iron bioavailability. The presence of plant cell walls is known to affect the bioaccessibility of nutrients (Holland *et al.*, 2020). Therefore, we hypothesised that releasing chloroplasts (the major location of plant leaf iron) from its cell wall confines will increase the bioaccessibility of iron from a green leaf source.

This chapter aimed to:

- 1) Optimise the process of samples preparation including heat treatment of spinach leaves and CRF isolation and tracing the iron distribution in each fraction along with the biomarker pigments.
- 2) Optimise the method of in-vitro digestion for the purpose of iron bioaccessibility measurement through iron dialysability method.
- 3) Determine the iron bioaccessibility of powdered Leaf Material (PLM) (heated and fresh) versus Chloroplast Rich Fraction (CRF) (isolated from both heat treated and fresh leaves).
- 4) Repeat the in-vitro digestion work using plant materials enriched with ^{57}Fe stable isotope.

5.2 Materials and methods

5.2.1 CRF preparation from commercial spinach leaves – juicing procedure

5.2.1.1 Leaf pretreatment and preparation

For the first and second parts of the experiment, spinach (*Spinacia oleracea*) was purchased from Tesco PLC, UK – labeled as ‘baby spinach’. All leaf samples were washed in MQ H₂O (18.2 MΩ), to remove all debris and were then laid on tissue (10 mins) to remove the excess water. At this stage, portion of the leaves was left as fresh for further extracting fresh chloroplast rich fraction from them and to prepare the fresh powdered leaves materials (PLM) from them (see Figure 5.1). The other portion of the washed leaves was heat treated as in section (5.2.1.2) to prepare heat treated chloroplast rich fraction (HTCRF) and heat-treated leaves materials (HTLM), see Figure 5.1).

5.2.1.2 Heat treatment

A portion of the washed leaves were heat-treated (HT), known as blanching, by placing 200 g of washed spinach leaves in boiling (100°C) MQ H₂O for 30 seconds, before being placed in ice cold water, for 15 seconds, to prevent further cooking. The leaves were then spun in a salad spinner and laid on tissue once again, before being juiced to obtain the heat-treated CRF (HTCRF), seen in Figure 5.1.

5.2.1.3 CRF isolation

Both fresh and blanched leaves were juiced using a twin-screw juicer (Angelia 7500) as shown in Figure 5.1 and 5.2, which separated the fiber and juice. The fibrous part

was immediately discarded, except for when freeze-drying for subsequent Fe analysis. To standardise and remove any remaining fiber, the juice was poured in a 75 μm stainless steel sieve. The filtered juice was then centrifuged (Beckman Avanti JXN-26) at 10,000 RPM, 4°C for 10 minutes.

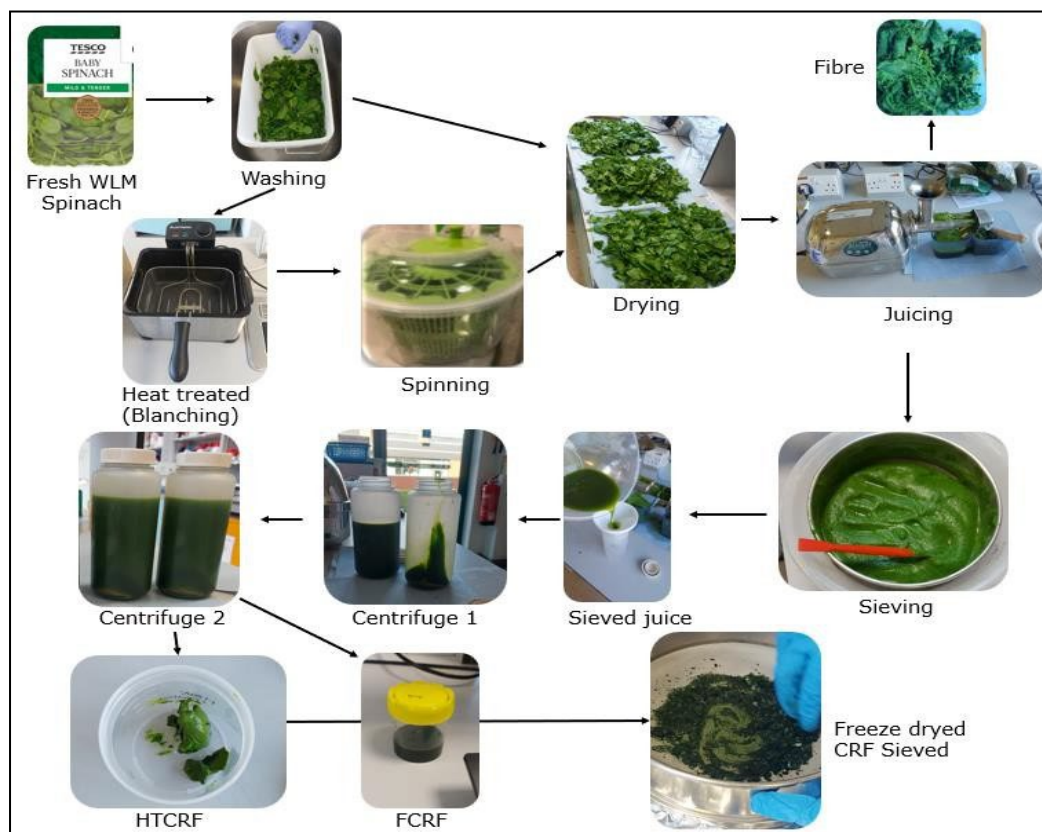


Figure 5.1: Flowchart of blanching process and chloroplast rich fraction (CRF) preparation via juicing for heat-treated (HTCRF) and fresh CRF (FCRF).

The supernatant was decanted and re-centrifuged using the same parameters and the CRF was collected from both centrifugation rounds, frozen at -80°C, ready for freeze-drying to obtain either fresh CRF (FCR) or heat treated CRF (HTCRF). Some of the juice was incubated in the cold room, at 4°C, for 24 hours followed by double

centrifugation and separation of CRF as previously completed. These samples were then labeled as incubated CRF (ICRF).

5.2.1.4 Heat treatment of CRF

To map the Fe distribution in different parts of spinach leaves, fresh leaves were fractionated using a twin-screw juicer as seen in Figure 5.2. The yield of each fraction from 1 kg of fresh leaves was measured along with the amount of Fe in each fraction as content and percentage.

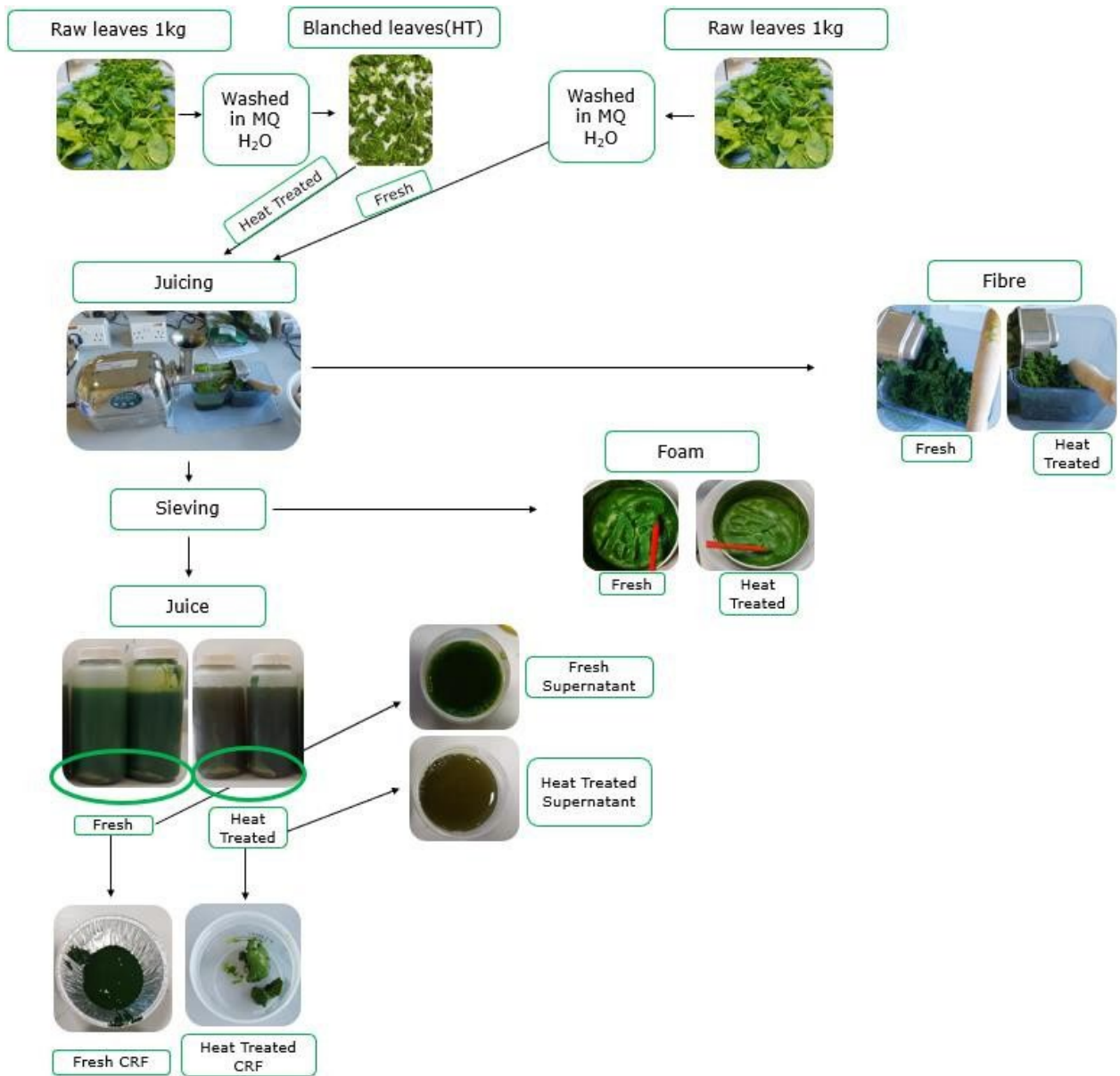


Figure 5.2: Flowchart illustrating the process and distribution of Fe in the three main spinach leaf fractions collected, circled in green is the chloroplast rich fraction (CRF) taken from the centrifuged juice. Mass distribution (%) and Fe distribution (mg/kg) are shown in Table 5.1 for each fraction.

5.2.1.5 Pre-digestion sample preparation

All freeze-dried samples from previous treatments (FCRF, HTCRF, ICRF, PLM, HTPLM) were frozen at -80°C for 24 hours before freeze-drying (Edwards Freeze dryer Super Modulyo) for one week. Once all samples were dry, they were filtered through a 250 µm stainless steel sieve while applying gentle hand pressure on them, followed by storage plastic containers, at -20°C. Samples were then labeled as 1) fresh Powdered leaf material (PLM), 2) heat-treated powdered leaf material (HTPLM), 3) fresh CRF (FCRF), 4) heat treated CRF (HTCRF) and 5) incubated CRF (ICRF). Aliquots of each sample were separated at this stage to be analyzed for initial Fe content.

5.2.2 Static *in vitro* digestion procedure

A static *in vitro* digestion was run according to INFOGEST¹ 2.0 with some modification related to Fe bioaccessibility based on observations and literature (Brodkorb *et al.*, 2019). Salivary amylase was omitted, as spinach is a non-starchy vegetable, and it was therefore replaced with MQ H₂O (0.5 mL) to compensate for this loss.

5.2.2.1 Pre-digestion preparation

Simulated electrolyte fluids for digestion were first prepared; Simulated Salivary Fluid (SSF), Simulated Gastric Fluid (SGF) and Simulated Intestinal Fluid (SIF). Piperazine-N,N'-bis (2-ethanesulfonic acid

¹ INFOGEST – An international network of excellence on the fate of food in the gastrointestinal tract. It is a network of scientific study into the effects of food on human health specifically during digestion, which aims to harmonise research. A specific set of static *in-vitro* digestion parameters is set out in the INFOGEST method, improved in 2019 INFOGEST 2.0 (Brodkorb *et al.*, 2019).

solution (PIPES) was prepared (0.15N) along with acid adjustment solutions, HCl (1M) and NaOH (1M) as well as $\text{CaCl}_2 \cdot (\text{H}_2\text{O})_2$ (0.3 M). These solutions were stored at -4°C and used within a three-month period. Digestion fluids were all brought up to 37°C before *in vitro* digestion was conducted and enzymes were kept frozen until use, as this is a critical step in the INFOGEST 2.0 protocol (Brodkorb *et al.*, 2019).

The following enzymes were purchased, and their activities were assayed as seen in INFOGEST 2.0 (Brodkorb *et al.*, 2019):

- Rabbit Gastric Lipase from Rabbit Gastric Extract (RGE) (Lipolytech, France) (lipase activity of 24.9 U/mg and pepsin activity of 1168.2).
- Pepsin (from porcine gastric mucosa, Sigma- Aldrich, UK) (activity of 3734.7 U/mg).
- Pancreatin (Pancreatin from porcine pancreas, Sigma, UK), (trypsin activity of 2.29), bile extract (0.78 mmol of bile salts/g bile mixture).

The amount of each enzyme was then calculated to achieve an activity of; 60 U/mL for gastric lipase (4.08 mg in 0.5 mL MQ H_2O), 2000 U/mL for the pepsin (5.59 mg in 0.5 MQ H_2O), 100 U/mL for trypsin activity in the pancreatin enzyme mix (1746.725 of pancreatin in 5 mL SIF) and 10 mmol/L of bile salt (514 mg of bile extract in 2.5 mL MQ H_2O).

5.2.2.2 *In vitro* digestion

The static *in vitro* digestion was conducted based on three main digestive phases; oral, gastric, and intestinal, following Figure 5.3 as a guide.

- **Oral phase** – a 0.5 mL salivary α -amylase solution (1500 U/mL) made up in SSF electrolyte stock solution (α -amylase from human saliva Type IX-A, 1000–3000U mg⁻¹ protein, Sigma) was added followed by 25 μ L of 0.3 M CaCl₂ and 0.475 mL of distilled water to make the total volume up to 10 mL, thoroughly mixed, and shaken (150 RPM, 2 min at 37°C).
- 1) **Gastric phase** – the digestate from the oral bolus (10 mL) were mixed with 8.0 mL of simulated gastric fluid (SGF) electrolyte stock solution, 1.0 mL of porcine pepsin (EC 3.4.23.1) and 5.0 μ L of CaCl₂ were then added to achieve 2000U /mL and 0.075 mM, respectively in the final digestion mixture. The pH was then reduced to 3, by using 1 M HCl by direct measurement, accordingly. Distilled water was then added to complete the volume to 20 mL and samples were returned to the shaking incubator (Microtitre plate shaker incubator, SI505) (150 RPM, 2h, 37°C). Ascorbic acid (0.0315g) (L-Ascorbic acid SIGMA-Aldrich UK) was also added at the gastric phase as a step of optimizing our procedure for iron bioaccessibility measurement. The addition was based on 10 times higher than the absolute amount of iron in our samples.
- **Intestinal phase** – the digestate from gastric chyme (20 mL) was mixed with 11 mL of simulated intestinal fluid (SIF), electrolyte stock solution, 5.0 mL of a pancreatin solution of 800 U/mL made up in SIF (pancreatin from porcine pancreas, Sigma, UK), 2.5 mL fresh bile extract (160 mM), 40 μ L of 0.3 M CaCl₂. The pH was then adjusted to 7 with 1 M NaOH and accordingly distilled water was added to make the total volume up to 40 mL. Samples were once more returned to the shaking incubator (150 RPM for 2h at 37°C).

The amount of HCl/NaOH added in gastric and intestinal phases, occasionally varied depending on the sample nature, thus it was adjusted for each sample along with distilled water.

Enzyme inhibitors were added to the digested samples. Orlistat² (Sigma-Aldrich, UK) dissolved in ethanol at 100 mM was added 1% by volume to digestate, to arrest lipase activity. Pefabloc³ (Sigma-Aldrich, UK) made up in water to 5 mM, was also added to arrest protease activity, to make up to 1 mM final concentration. After that digested, spinach samples were stored at -80°C, for a maximum of one week, until further analysis (Minekus *et al.*, 2014).

5.2.2.3 Dialysability procedure

The procedure of mineral dialysability was adapted from Garcia-Sartal *et al.* (2011). The procedure includes inserting a buffer containing dialysis bag during the intestinal phase of digestion and assessing the minerals fractions which enter the bag (García-Sartal *et al.*, 2011). CRF samples and PLM samples (0.5 g) of each treatment were weighted in separate 100 mL Duran bottles. The in-vitro digestion procedure was simply carried out, based on Section 5.2.2.2, with some modifications, as represented by Figure 5.3.

After adjustment of the intestinal stage, a dialysis membrane with 8-10 kDa MWCO (Molecular weight cut-off), filled with 10 mL of a 0.15 N PIPES solution (pH = 7.5) was placed inside each Duran bottle containing the digested mix. Intestinal digestion along with a dialysing process took place in the shaker (150 RPM, 2 h, 37 °C).

² (-)-Tetrahydrolipstatin, N-Formyl-L-leucine (1S)-1-[[[(2S,3S)-3-hexyl-4-oxo-2-oxetanyl]methyl]dodecyl ester. Orlistat, used in obesity research, is a pancreatic lipase inhibitor that acts locally in the gastrointestinal tract to inhibit lipase activity.

³ 4-(2-aminoethyl)-benzene-sulfonyl fluoride, aebfsf, aminoethyl-benzene-sulfonyl fluoride, 4-2-, proteinase k inhibitor. Pefabloc SC is a specific, potent, and irreversible inhibitor of serine proteases.

The order of addition during the intestinal phase was improved based on our observations where the gradual increase of the digestion mix pH was needed to avoid any dramatic changes which might affect the iron solubility. This was achieved by adding an equilibrium step so that the dialysis tubing with PIPES and digestion mix pH could equilibrate. This meant that no HCl addition was needed to reduce the pH before intestinal digestion, which had been found to coagulate the enzymes. Addition of SIF before equilibrium increased the pH rapidly, however enzymes coagulation did not occur. Dialysis membranes were added to each sample so that the knotted ends were pressed against the Duran bottle walls. Samples were left for an hour in the shaking incubator at 100 RPM, 37°C to equilibrate. After an hour, enzymes and CaCl₂ (40 µL) were added, and the final volume was made up to 40 mL with MQ H₂O (as shown in Figure 5.3). Because of the equilibration step, the final pH was already around 7 and no further pH adjustments, neither with HCl, nor NaOH, were required.

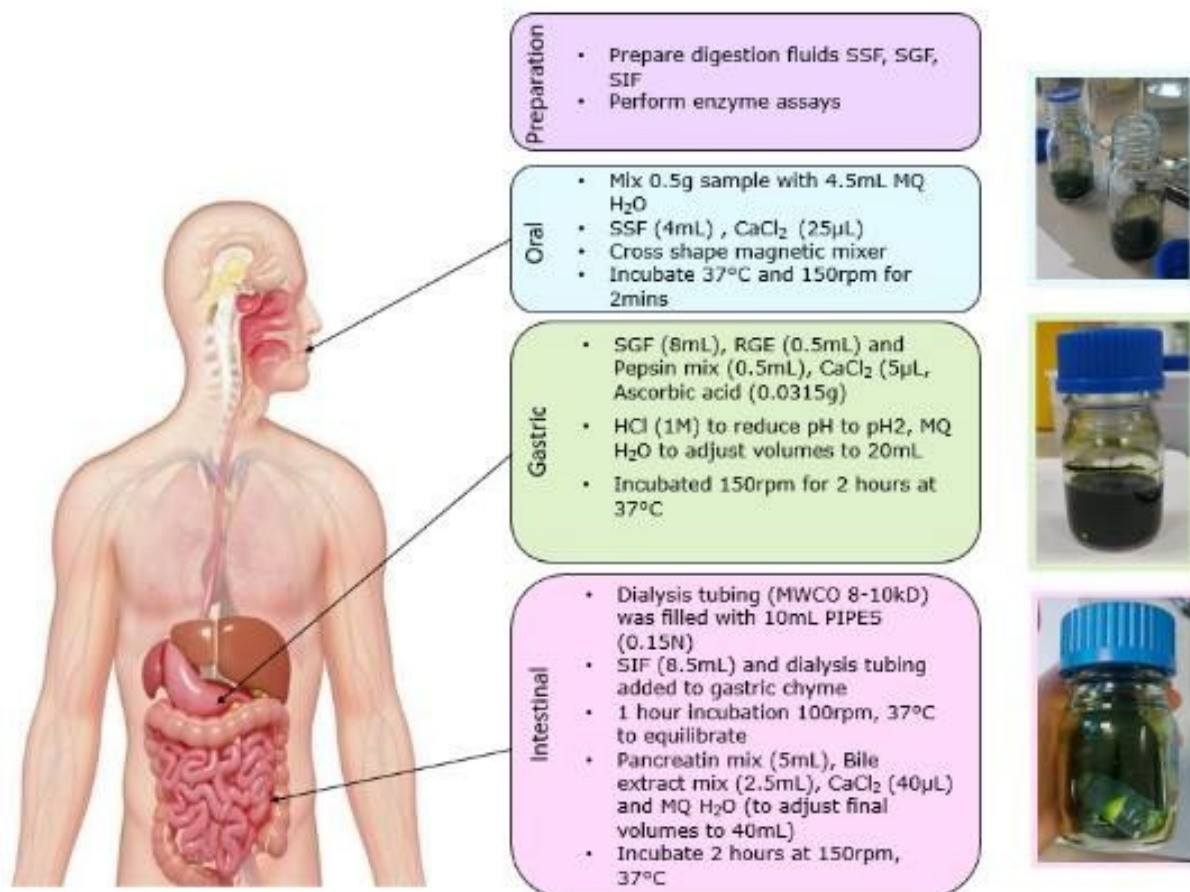


Figure 5.3: Overview of the four key stages, timings and volumes used during the in vitro digestion procedure. A human digestive system illustration (left) corresponding to each stage and in vitro images (right) at three key stages; oral, gastric, and intestinal. Adapted from Brodkorb *et al.* (2019)

5.2.2.4 Post digestion fractionation

Dialysis bags were removed from the digestion bolus using tweezers, washed in MQ H₂O and then the dialysate (the solution inside the dialysis bag containing the buffer and the dialysable Fe) was transferred to a glass container using a syringe and needle attachment to avoid any contamination.

3 mL of the digestate samples (the fraction left in the Duran bottle post digestion) were also transferred into separate containers for analysis. The remaining

digestate was then centrifuged (Rotina 380R, Hettich Zentrifugen) (15 min, 3000 RPM, 4°C) to separate the digestate micelle phase (supernatant) from the pellet. All centrifuged samples were collected in Bijou bottles, labelled and frozen at -20°C until further mineral analysis.

5.2.3 Mineral analysis

5.2.3.1 Sample preparation using microwave acid digestion.

As reported in Section 3.2.1, for all solid, dry samples, around 0.2 g was added to high-pressure Teflon vessels along with 6 mL of HNO₃ (>68% Primar Plus™ trace reagent grade). In case of liquid samples, 3 ml were taken in Teflon vessels added to 3 ml of HNO₃.

The Teflon tubes were then digested as in Section 3.2.1.

5.2.3.2 ICP-MS analysis

The same procedures seen in Section 2.8.4, were performed here.

5.2.4 Final calculations – dialysability and solubility

Dry aliquots of all samples; FLM, HTLM, FCRF, HTCRF and ICRF were sent for mineral analysis, to analyse total amount of both total Fe and ⁵⁷Fe, in each fraction. 3 mL aliquots of each digestion fraction (dialysate and micelle) were also taken for

mineral analysis. The amount of Fe in the spinach leaf samples and in total dialysate (10 mL), and micelle fraction (38 mL) was calculated. The amount of Fe coming from the enzymes and the reagents were also considered by using enzyme blank samples, that had undergone in-vitro digestion, followed by calculations.

Fe solubility and dialysability were determined using Equations 5.1 and 5.2, as indicators of Fe bioaccessibility from the static in vitro digestion model.

$$\text{Fe solubility \%} = \frac{\text{Fe in total the micellar fraction} + \text{Fe in dialysate}}{\text{Total Fe}} \times 100 \quad (\text{Eq. 5.1})$$

$$\text{Fe dialysability \%} = \frac{\text{Fe in total dialysate}}{\text{Total Fe}} \times 100 \quad (\text{Eq. 5.2})$$

5.2.5 Statistical analysis

Data were always presented as mean values. The statistical analysis was performed via statistical software (IBM SPSS Statistics 28.0) and analysed as a one-way ANOVA with a Tukey post-hoc test to determine any significant differences ($p < 0.05$) between samples.

5.3 Results and discussion

5.3.1 The distribution of Fe after fractionating spinach leaves with an extrusion juicer

During the initial fractionation process of the commercial spinach leaf as in Figure 5.2, Fe concentrations were measured for five separate fractions/components. Figure 5.4 represents the total Fe content of each of these fractions' namely, PLM, fibre, supernatant, juice and CRF.

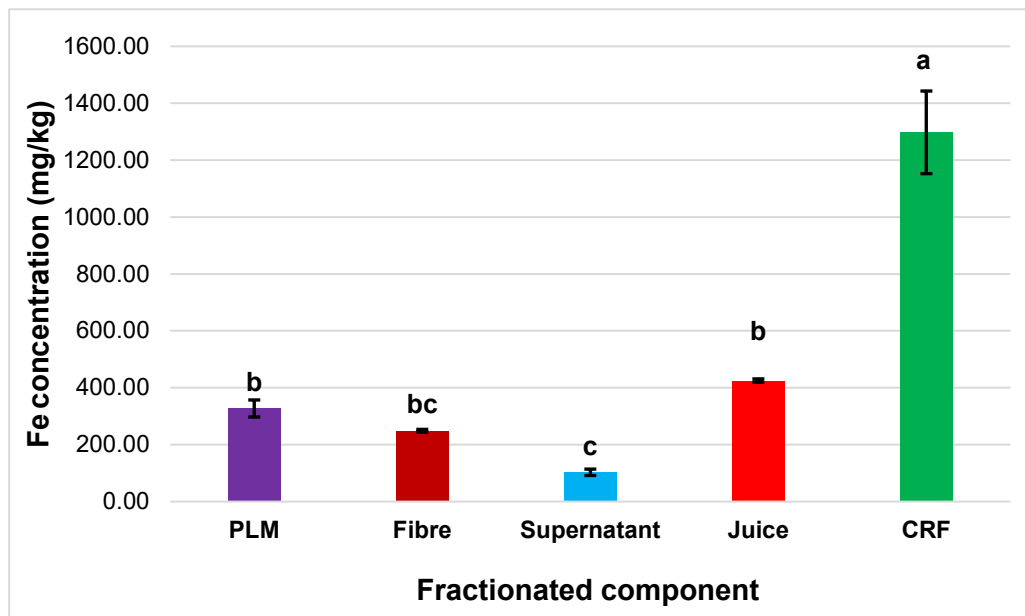


Figure 5.4: Fe concentrations (mg/g DW) of five fractionated components of Tesco baby spinach leaves; Powdered leaf material (PLM), fibre, supernatant, juice, chloroplast rich fraction (CRF). Error bars show SEM and letters are derived from ANOVA post-hoc Tukey testing to compare fractionated components ($p < 0.05$).

Figure 5.4 shows the highest Fe concentration of 1300 mg/kg DW was most significantly concentrated in the CRF and was significantly higher than the other four fractionated components. The supernatant had the lowest Fe concentration of approximately 100 mg/kg DW. These results again parallel with Gedi *et al.*, (2017),

who reported significantly higher Fe concentrations for spinach CRF, compared with PLM, after using an alternative blender sucrose extraction technique (Gedi *et al.*, 2017). The higher iron concentrations in the CRF material (rich in chloroplasts) were anticipated, as chloroplasts represent the organelle with the highest requirement of Fe in plant cells. The literature indicates that chloroplasts contain about 80% of the iron in the entire leaves (Solti *et al.* 2012).

More fractionation trials were conducted to calculate the mass, and the Fe distribution between different leaf fractions. We also compared this distribution between fresh leaves and heat-treated leaves. Data are shown in Table 5.1 and 5.2.

Table 5.1: Mean percentage of mass distribution on a dry-weight (DW) basis, from 1kg of raw spinach leaves \pm Standard deviation (SD) and mean mg/kg Fe relative to whole leaf DW \pm Standard deviation (SD) and percentage distribution between the main leaf fractions: juice, fibre and foam. The presence of different letters a, b, c, d, e and f denote a significant difference between samples at $p < 0.05$ for mass distribution data. The presence of different letters v, w, x, y and z denote a significant difference between samples at $p < 0.05$ for Fe distribution data.

Leaf Fraction	Mass distribution (%) of leaves DW		Fe distribution mg/kg DW of each fraction and (% of the total iron content in leaves DW)	
	Fresh	Heat-treated	Fresh	Heat-treated
Juice	53.12 \pm 0.86 ^e	25.52 \pm 0.2 ^c	16.98 \pm 0.39 ^z (66.77%)	10.33 \pm 0.35 ^y (51.36%)
Fibre	40.65 \pm 0.2 ^d	70.23 \pm 0.96 ^f	6.11 \pm 0.34 ^w (24.04%)	8.33 \pm 0.26 ^x (41.42%)
Foam	6.24 \pm 0.03 ^b	4.24 \pm 0.17 ^a	2.34 \pm 0.11 ^v (9.19%)	1.45 \pm 0.07 ^v (7.21%)

*Fe in whole fresh leaf was 25.44mg/kg and Fe in whole heat-treated leaves was 20.12mg/kg, due to some loss in the blanching process.

Table 5.2: Mass (g DW) and percentage mass (%) from the juice fraction in dry weight (DW), mg/kg Fe on a DW basis from juice and as a percentage of the juice and the total Fe recovery mg/kg and % in CRFs from the whole leaf. Fe percentage was calculated based on the (Total Fe in each CRF from 1kg leaves*100)/ Total Fe content of the 1 kg leaves.

	CRF mass recovered from 1kg leaves (g DW and % of juice DW)		Fe recovered from juice to CRF in (mg DW) and (% of Fe recovered from the juice)		Fe in the recovered CRF (mg/kg DW) and % Fe recovered from 1kg fresh leaves	
	Fresh	Heat-treated	Fresh	Heat-treated	Fresh	Heat-treated
CRF	5.27 21.19%	1.07 8.73%	8.49 (49.96%)	6.77 (65.53%)	1609.42 (33.36%)	6275.71 (33.67%)

The distribution of mass and Fe during the CRF isolation process was analysed to understand how much Fe was in each fraction during CRF isolation using the juicer method and the impact of HT on Fe distribution. Table 5.1 shows that for both mass distribution and Fe distribution, all sample sets were significantly different except for Fe distribution within the foam fraction.

Once juiced, the leave mass was mainly distributed between juice, fibre and foam (foam is formed once the juice is sieved). In fresh leaves, about 53% of the mass went to the juice and 40% to the fibre fraction, while in the case of HT leaves, only 25% of the mass went to the juice and 70% was transferred to the fibre. This can be attributed to the textural changes in the leaves as subject to the high temperature of blanching. The leaves were softened by blanching and became thinner (as shown in Figure 5.5 bellow), thus they slipped through the twin screw of the juicer leading to less efficiency of the mechanical forces of the

screws and less juice, by half, was produced compared to fresh leaves.

More juice was derived from fresh leaves compared with HT leaves, and a significantly higher percentage of Fe was retained in the juice (fresh and HT) than from both the foam and fibre fractions. HT samples showed that a significantly higher amount of Fe went to the fibre fraction along with the mass.

The juice from both fresh and HT leaves was further fractionated into CRF and supernatant and the mass and Fe distribution was analysed, calculated and presented in Table 5.2. The total mass and Fe recovered from leaves to CRF, indicating that for fresh samples a dry mass of 5.27g CRF was recovered containing a total of 8.49 mg of Fe. For the HT samples, 1.07 g of DW CRF was recovered containing a total Fe of 6.77 mg. A higher mass recovery (as percentage) is shown in fresh CRF, but about 4 higher iron recovery (as percentage of total dry weight) was recorded in HTCRF means overall both fresh and heat-treated CRF have a comparable iron recovery percentage at 33.4% and 33.7% respectively from the original 1 Fe kg leaves. However, the literature states that 80% of Fe in the leaves is located within the chloroplast (Solti et al. 2012). This difference is justified due to the nature of our CRF isolation process, which depends on physical fractionation and there is a loss of CRF mass in foam, fibre, and supernatant fraction. Thus, it would be useful in further studies to consider an extra juicing step to recover the juice from the fibre part, especially in the case of heat treated leaves.

To better understand the changes of the leaves' ultrastructure as affected by heating, our colleague, Chao Chi (2023) has produced detailed images using transmission electronic microscope (TEM) of fresh vs heat treated leaves

(leaves were blanched in the same method at 100°C for 30 Sec). Those images are presented in Figure 5.5 below. The ultrastructure of blanched (HT) spinach leaves is shown in (Figure 5.5 d, f and h) and compared to that of fresh spinach leaves (Figure 5.5 c, e and g).

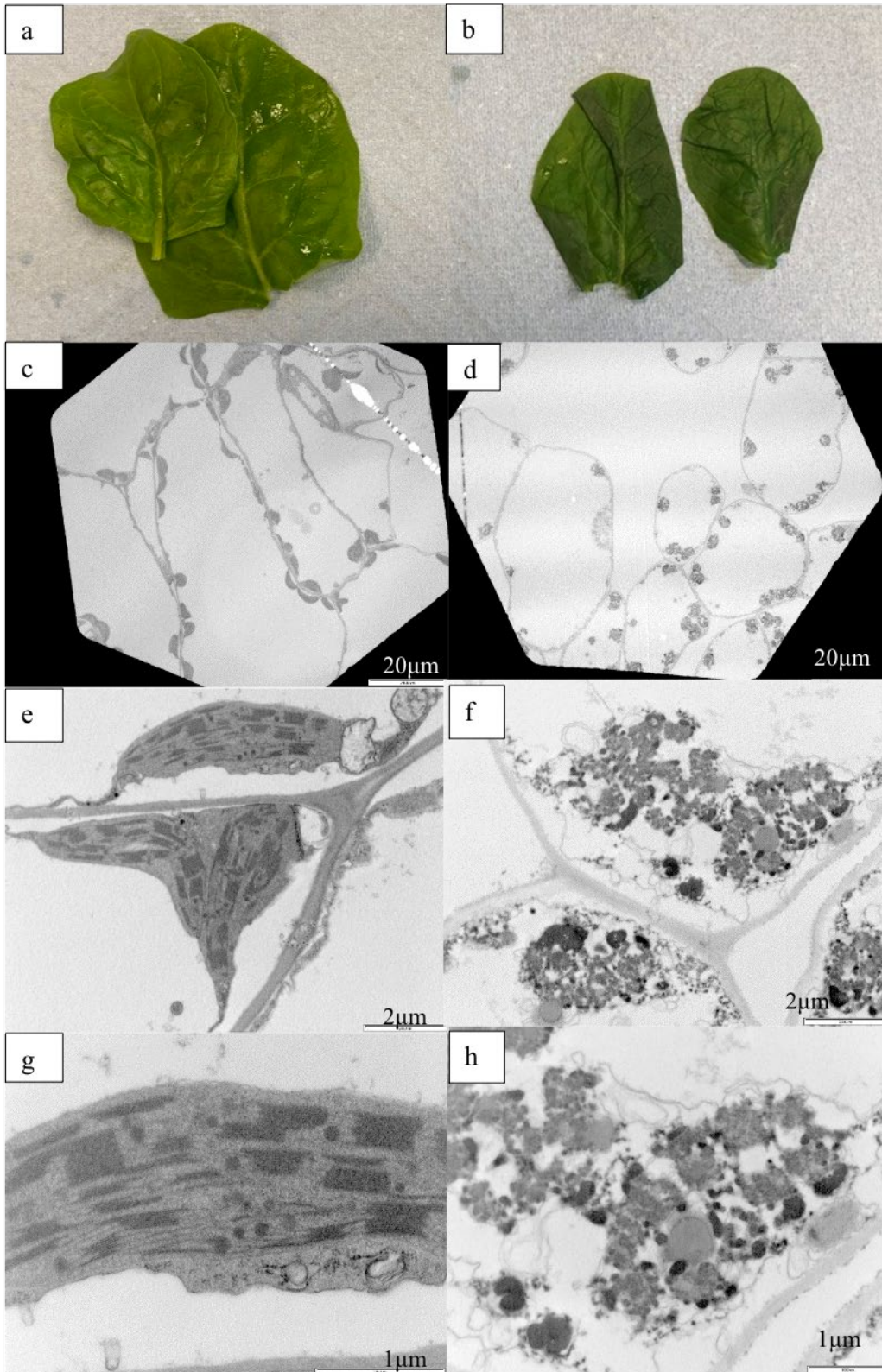


Figure 5.5: TEM images of fresh/blanched spinach leaves at different magnifications a) Fresh spinach leaves, b) blanched spinach leaves (100 °C 30s), c, e, g) were fresh leaves at magnification of 800×, 8200× 27000×; d, f, h) were blanched leaves at magnification of 800×, 1700×, 8200×.

As shown in Fig 5.5 a and b, blanched leaves showed textural shrinkages, softening and colour differences. Blanching leads to replace the air space in the cells with hot water and this reduce cells' opacity and cause shrinking of the leaves' tissues and membrane deterioration accompanied with a release of intercellular fluids. Moreover, it is noted that the colour of the blanched leaves became brighter (Figure 5.5 a, b) as heating encourage the conversion of colourless precursors into bright green compounds which increase the green colour intensity just after blanching and before drying, while chlorophylls pigments get degraded (Gunawan *et al.*, 2000; Tijskens *et al.*, 2001).

The chloroplasts of fresh leaves maintain their integrity with defined thylakoids (figure 5.5 e,g). Ideally, chloroplasts in fresh leaves have lens shape and they are (3-10µm in diameter and 1-3µm thick) located around the edges of cell, or slightly twisted bands at the cell edges (Burrows *et al.*, 2020), which can be seen in (Figure 5.5 e,g) as well. While after leaves being blanched, the integrity of the chloroplast was destroyed, and the ultrastructure was not following the typical shape and volume of the chloroplast. Moreover, the plant cells were ruptured, leaving cell contents indistinguishable and disorganized.

Blanching does affect the internal structure of the thylakoid membranes inside the chloroplast. This effect has been studied in terms of the thylakoids emulsifying properties after being heat treated. A study by Ostbring *et al.*, 2020 Reported a loss of emulsifying capacity because of heat treatment during drying. The same study explained that chlorophyll degradation was induced by heat treatment and its severity is correlated with the heating temperature and duration. Chlorophyll in turn is the main pillar of the thylakoids and hence the

chloroplast structure. Chlorophyll is the main supporter of the light harvesting complex and its alpha helices. Thus, the degradation of chlorophyll facilitates the aggregation of the thylakoid membranes which leads to reduced emulsifying capacity as the interfacial properties are reduced. Consequently, the ability of the thylakoid membrane to inhibit the lipid digestion by hindering the lipase/co-lipase activity is reduced by heat treatment.

In our study, it was reported in table 5.1 and 5.1 that while the mass of CRF produced from blanched leaves is 5 times less, the absolute amount of iron recovered from 1 kg of both fresh and heat-treated leaves was almost equivalent. This suggests a selective recovery of the iron and/or exclusive separation of iron concentrating organelles/components within the chloroplast itself. As it was mentioned in the introduction, 80% of the iron in green leaves is localized in the chloroplast and of this 60- 80% are localized in the thylakoid membrane and 20 % in the chloroplast stroma (Giovanni *et al.*, 2015). Moreover, the images shown in figure 5.5 clearly show damage in the chloroplast structure, this together might lead to a rupture in the chloroplast, release of aggregated thylakoids which facilitates its recovery from the juice by centrifugation. So, it is believed that the CRF fractionated from the blanched leaves contains fragments of thylakoids which are richer in iron than a whole intact chloroplast which contains starch, lipids and other components.

Overall mapping mass and Fe distribution showed that CRFs contain a higher Fe proportion of its mass than leaves agreeing with current literature in principle. This has led us to further investigate the bioaccessibility of iron in leaves vs CRF fraction to unlock the potential of CRF as a concentrated iron storage.

5.3.2 The distribution of chloroplast-marker pigments after fractionating spinach leaves with an extrusion juicer.

Measurements of chloroplast-marker pigments provide an indirect relationship between the chloroplast and the Fe distribution within all five spinach leaf fractions. The pigments included chlorophyll-a, chlorophyll-b, total chlorophyll (see Equation 4D), and total carotenoids.

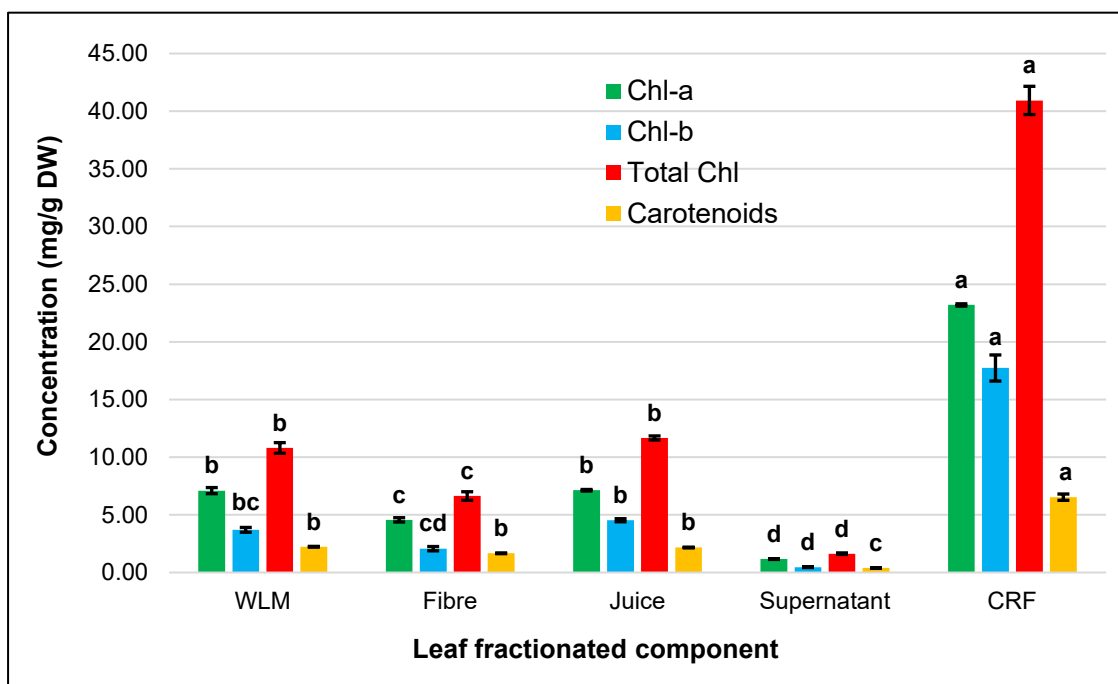


Figure 5.6: Concentrations of chloroplast-marker pigments (mg/g DW) of five fractionated components of fresh baby spinach leaves; whole powdered leaf material (WLM), fibre, supernatant, juice, chloroplast rich fraction (CRF). Error bars show SEM and letters are derived from ANOVA post-hoc Tukey testing to compare each pigment content in fractionated components ($p < 0.05$). Statistical analysis is made between the same pigment (share the same bar colour) in each fraction.

The highest concentration of chl-a was in the CRF with its peak of roughly 23 mg/g DW being reached in the CRFs. This was expected because the chlorophylls are entities unique to the chloroplast organelle. Chlorophyll concentrations provide an indirect indication of the concentration of chloroplasts

compared to more direct measurements of actual chloroplast material (Gedi *et al.*, 2017).

Based on Figure 5.6, the concentrations of chl-a were also significantly different between CRFs, PLMs and other fractionated components. The supernatants generally had the lowest concentrations of all three pigments and total-chl. Total-chl, chl-b and carotenoid concentrations also peaked in the CRFs with values of approximately 41, 18 and 6.5 mg/g DW, respectively. These concentrations were also significantly different from PLMs and the other three fractionated components.

These results are consistent with Gedi *et al.*, (2017) who reported the highest concentration of 73.8 mg/g DW of total-chl in spinach CRFs in comparison to only 7.8 mg/g DW for PLM. However, in his experiment, CRFs were recovered with an alternative blender sucrose extraction technique. All fractionated components had lower concentrations of carotenoids compared with total chlorophyll and were significantly different, for CRF and PLM. Chlorophyll and carotenoids are markers for chloroplasts, so it is clear from these results that the extrusion juicer fractionation procedure is as effective as the blending method at releasing chloroplasts from cells prior to a centrifugation step to concentrate the chloroplasts in the CRF material.

The results in this section, along with the Fe distribution data support the idea of using CRF material to measure the bioaccessibility of Fe localised in chloroplasts using an in-vitro digestion method.

5.3.2.1 Chlorophyll distribution between CRF and juice from fresh and HT leaves.

The difference between pigments content between CRF and juice produced by blanched and fresh spinach leaves, was studied in collaboration with our colleague Chao Chi and Figure 5.7 below represents the pigments (chlorophylls and carotenoids) content in each fraction.

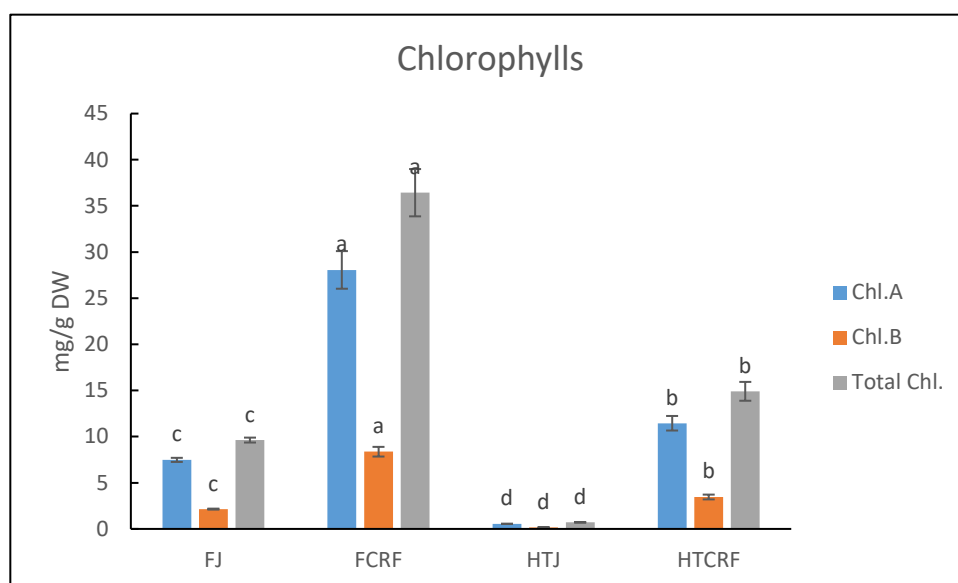


Figure 5.7 : Chlorophylls content of fresh/blanched spinach juice and CRF. a) mg/g DW. Results are expressed as means \pm SD (n=3). Error bars show SEM and letters are derived from ANOVA post-hoc Tukey testing to compare each pigment content in fractionated components ($p < 0.05$).

As expected, Chlorophyll content was higher in CRF than corresponding juice in both fresh and blanched extracts, while chlorophyll a was higher than chlorophyll b in all samples. Chlorophylls a and b content decreased after blanching both in juice and CRF samples. Approximately 93% and 59% (based on dry weight) of the total chlorophylls were lost following blanching in juice and CRF samples respectively. These changes can be explained at the molecular level by understanding the function and location of chlorophyll in green leaves.

The intrinsic of the thylakoid membrane consists of photosynthesis I and II which contain

proteins called light harvesting complex (LHC) I and II which in turns comprise both chlorophyll a and b. Chlorophyll is an amphiphilic molecule with a hydrophobic phytol chain and hydrophilic porphyrin. Chlorophyll thereby interacts with hydrophobic helices, of the light harvesting complex I and II inside the thylakoid membrane. Thereby, the helical structure is supported by the amphiphilic chlorophyll molecules both within the helices through chlorophyll a (which is required in larger quantity) and in between the helices via Chlorophyll b. In higher plant chlorophyll a is more important for the internal structural stability of the photosynthetic system and hence to the thylakoid membrane. Thus, the concentration of chlorophyll a is higher compared to b in both PSI and PSII (the ration of chlorophyll a/b is 4.0 in PS I and 2.2 in PS II).

Chlorophyll is a green pigment which is sensitive to light, enzymatic degradation, acidity, and heat. During heat treatment, like blanching, and/or enzymatic removal of the phytol group, chlorophyll is degraded to pheophytin or pheophorbide by replacement of Mg^{2+} with $2H^{+}$. Both degrading molecules of chlorophyll absorb light at 409 nm resulting in an olive-green colour. Moreover, the new degraded molecules have less hydrophobicity and by removing of the phytol chain, the amphiphilic properties are lost due to removal of the entire hydrophobic part.

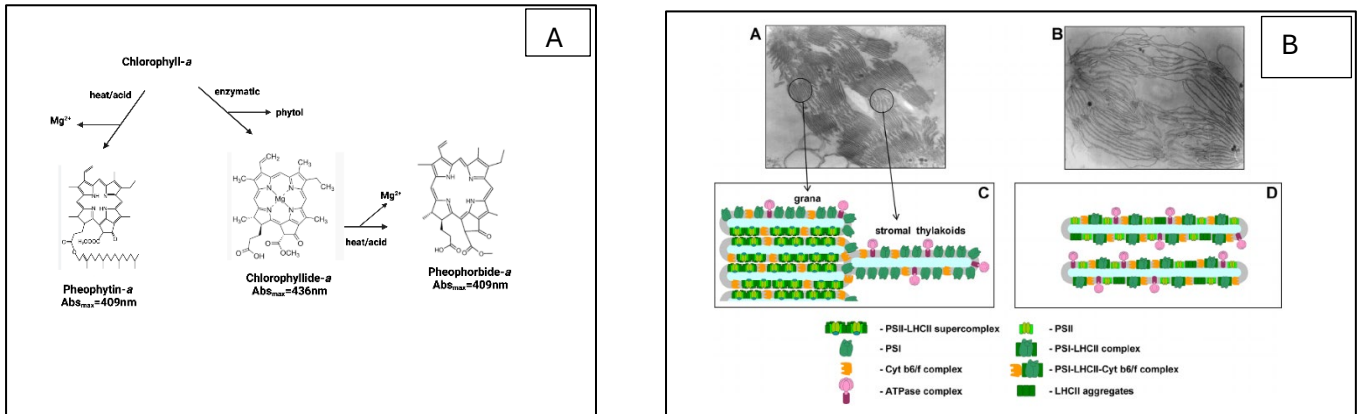


Figure 5.8 A-B: A) The changes in chlorophyll molecule as induced by heat treatment and/or enzymatic treatment. B) the changes in the thylakoid membrane properties as affected by heat treatment (Ivanov *et al.*, 2017).

As a result, chlorophyll loses its ability to stabilise and support the pigment/proteolipid complexes causing aggregation in the thylakoid membranes due to the association between the hydrophobic regions/ domains (Heaton *et al.*, 1996). In accordance, Zhang *et al.* (2012) reported that heating green leaves to above 70°C cause a complete rupture of the thylakoids structure.

5.3.3 Observations during CRF isolation and in vitro digestion.

During samples preparation, noticeable differences between F and HT samples were observed in terms of morphology, the mass recovered and the amount of iron in each sample, as shown in Table 5.1 and 5.2. FCRF and fresh digestate had a much deeper green colour compared to the olive toned HTCRF and HT digestate. This is because the chlorophyll molecules break down when thermally degraded and form pheophytins, resulting in an olive tone shown in Figure 5.9 (Kaiser *et al.*, 2012).

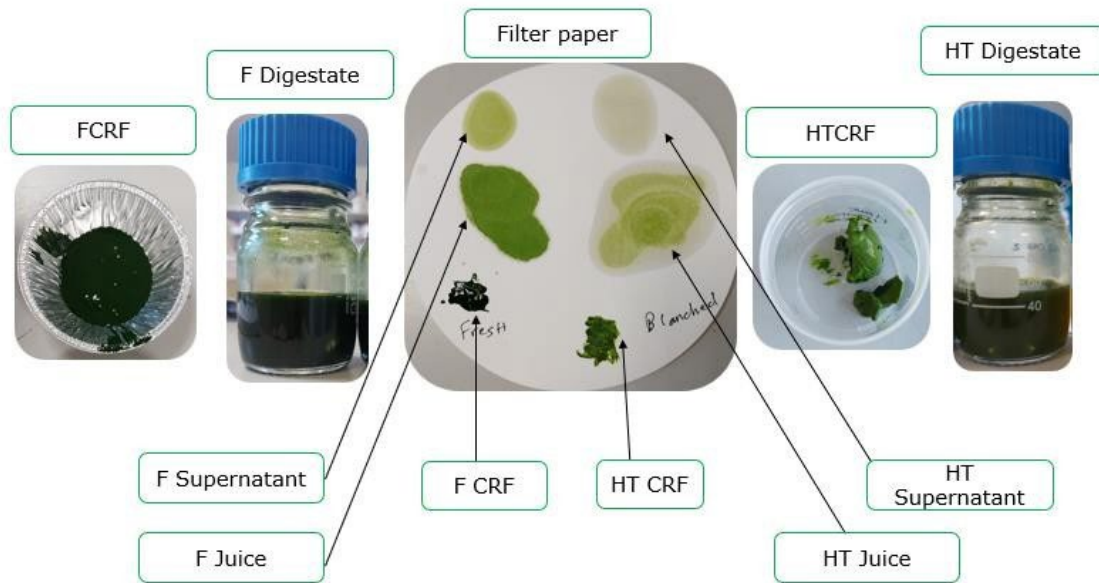


Figure 5.9: Images of the colour differences between fresh (F) and heat-treated (HT) samples from left to right; FCRF, fresh digestate, filter paper showing the colour differences between F and HT juice, supernatant (post-centrifugation and CRF removal) and CRF, HPCR and HT digestate.

Figure 5.9 also reflects observations of the morphological and density differences between the products of HT leaves compared with F leaves. The resulting juice from fresh leaves is denser and rich in CRF components. After centrifugation, the pellets separated from fresh juice (FCRF) samples were more of a liquid compared with the pellets separated from heat treated juice (HPCR) juice which was thicker and came out in one integrated piece. The left supernatant was also clearer in the heat-treated juice indicating a better CRF separation from the heat-treated juice than the fresh juice.

Whilst testing and refining the *in vitro* digestion method, materials were seen to coagulate in the enzyme-only control at pH 5.5, coagulation was observed when adjusting the pH of the intestinal phase using HCl (0.1 M) (see Figure 5.10). Coagulation is a process where liquids change to semi-solid or solid state. The addition of HCl was needed initially as after the addition of the SIF the pH of the digestate at the intestinal

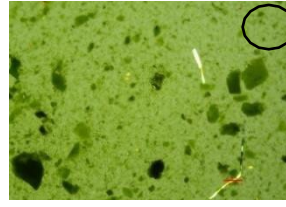
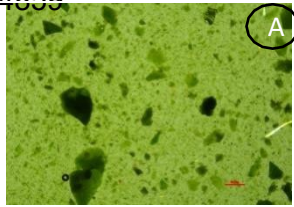
phase went up to around 7 and we wanted to lower the pH to 6.5 based on the previous work in our group with the CRF materials. However, this step was amended later. HCl is a strong acid which denatures proteins, such as pancreatic enzymes, by breaking the hydrogen bonds which in turn means the protein unfolds. The addition of HCl via pipetting caused a fast localized pH change resulting in coagulation and likely deactivation of some of the pancreatic enzymes. To prevent this rapid pH change, SIF (8.5 mL) and dialysis tubing (with PIPES (0.15N)) were added to the gastric chyme and incubated for an hour (equilibrium time) before adding the enzymes and adjusting the volume to 40 mL. The equilibrium step has also helped to improve iron dialysability and to reduce the variation resulting from the dropwise pH adjustment (Teucher *et al.*, 2013).



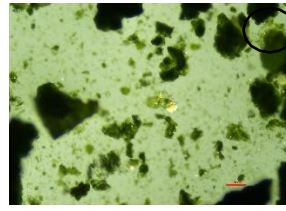
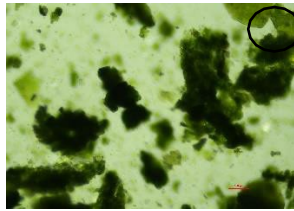
Figure 5.10: Enzyme-only digestate showing coagulation of proteins when adding HCl to adjust the pH.

Images from light microscopy (Nikon Eclipse Ci) were taken before and after static in-vitro digestion of fresh (F), heat-treated (HT) CRF and F and HTPLM, as shown in Figure 5.11.

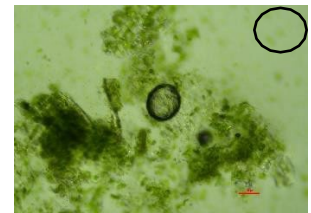
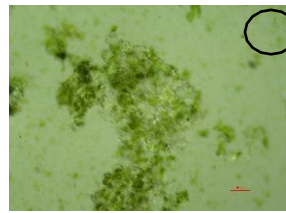
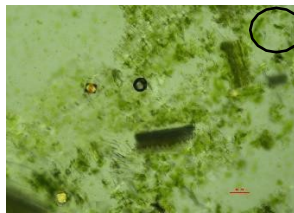
FCRF



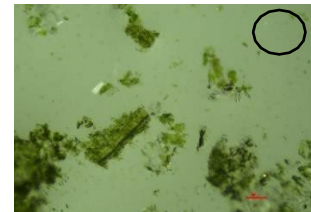
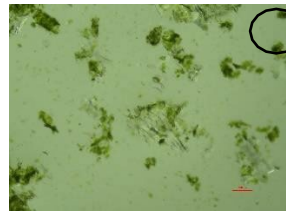
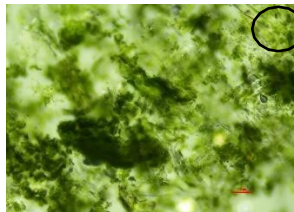
HTCRF



PLM

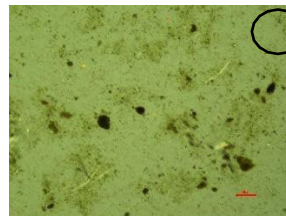
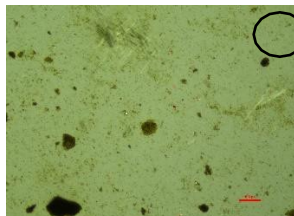


HTPLM



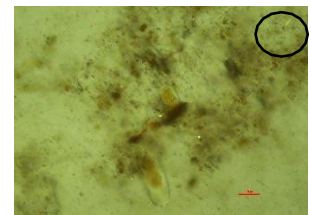
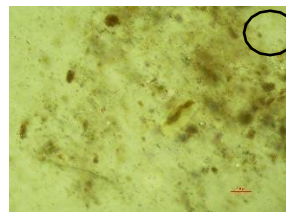
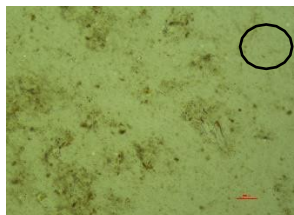
FCRF

digestate



HTCRF

digestate



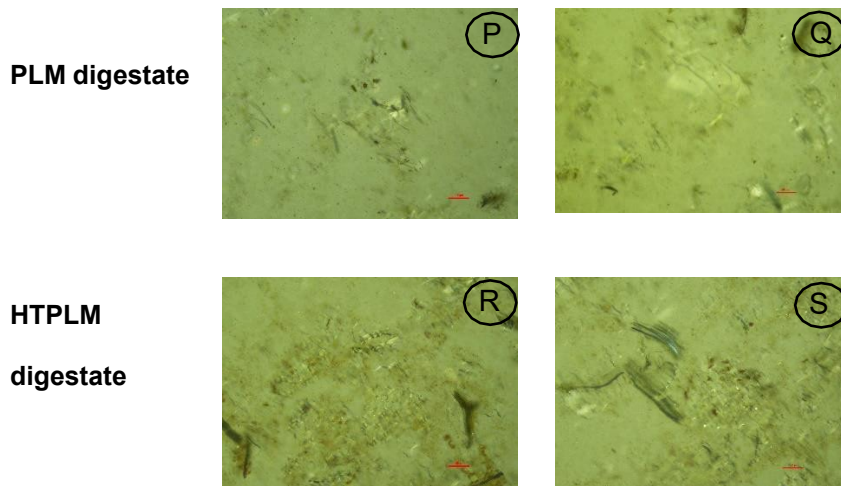


Figure 5.11: Light micrographs of spinach material before and after digestion. Light micrographs taken on a Nikon Eclipse Ci of different samples for *in vitro* digestion as follows: (A, B) FCRF, (C, D) HTCRF, (E, F, G) PLM, (H, I, J) HTPLM, (K, L) digestate from FCRF, (M, N, O) digestate from HTCRF, (P, Q) digestate from PLM and (R, S) digestate from HTPLM. Scale bar:100px.

The microscope images show that undigested samples have a stronger, brighter green colour compared with all digestates under the microscope, with F samples illustrating the same as Figure 5.6, with deeper green and HTs having a more yellowish to olive tone. This is due to the change in chlorophyll (a and b) colour and the loss of their greenness under acidic pH of gastric phase. This is mainly because under acidic pH and prolonged heating, chlorophyll lose its central magnesium ion and get substituted by two hydrogen ions resulting in the formation of pheophytin which are olive brown in colour. The chlorophyll derivatives are not reversible thus the yellow-olive green colour remains even after adjusting the pH to 7 in the intestinal phase. (Agellon, 2002). Also, the addition of bile extracts in the intestinal phase in both control and sample participate in colour changes as bile salts have dark green to yellowish brown colour.

Cell walls are visible in all samples but particularly defined the PLM, both F and HT, pre and post-digestion. Undigested samples have a dense assembly of cells and material compared with the more dispersed material in the digested samples. This could be due to digestion time and the addition of a magnetic stirrer, which could have dispersed cells more in digested CRF and PLM.

5.3.4 Protocol optimisation

5.3.4.1 The impact on Fe dialysability of the addition of oil or ascorbic acid, and of altering gastric pH.

During experimentation, the in vitro digestion method was optimised to release the maximum amount of Fe from FCRF. Optimisation experiments were based on previous work, as well as the literature, and were carried out sequentially as follows.

- 2) Addition of sunflower oil (gastric pH 5.5+sunflower oil), which was purchased from Tesco the same morning of preparation.
- 3) Changes in gastric pH (pH 5.5, pH 5.5+oil, pH 3.5, pH 2)
- 4) Addition of ascorbic acid to the gastric pH which allowed for improved dialysability, yet not significantly (gastric pH 2 +Ascorbic acid).

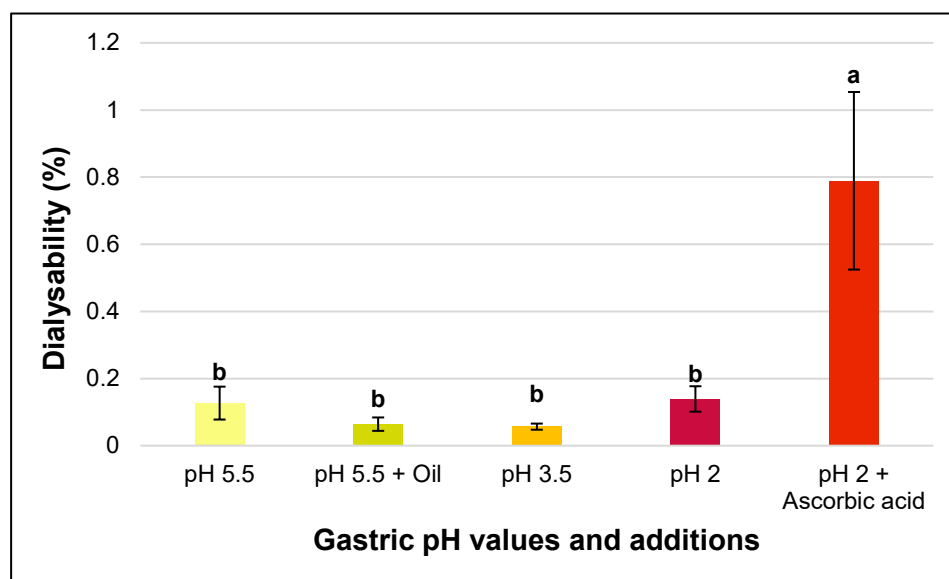


Figure 5.12: Mean percentage of Fe dialysability from FCRF, subjected to different gastric changes as follows: pH 5.5, pH 5.5 + sunflower oil, pH 3.5, pH 2 and pH 2 + ascorbic acid. Error bars represent SEM and the presence of different letters a and b denote a significant difference between samples at $p < 0.05$ using Tukey post-hoc test.

Data from Figure 5.12 showed no significant difference in the % dialysable Fe between the different gastric pH changes including the addition of sunflower oil at $p < 0.05$. However, the addition of ascorbic acid to the pH 2 treatment has resulted in significant improvement (denoted by “a”) in the % dialysable Fe which has increased by 5-fold over the pH 2 treatment without the addition of ascorbic acid. Similar results were shown by Miller *et al.* (1981) who reported that the addition of ascorbic acid to an albumen meal increased the dialysable Fe by 4-fold.

Sunflower oil was added and homogenised with the oral bolus to mimic a meal, where a mixture of components is consumed at once. The reason why the addition of oil was considered is that previous research within our group published by Wattanakul *et al.* (2022), showed that the presence of oil increased the bioaccessibility of some lipophilic nutrients. The digestion of lipophilic components in the thylakoid membrane would help to destroy their structure within the chloroplast and thus release the iron binding components making them more available for the digestive enzymes. However,

according to the results of this study so far, the addition of oil did not help with the release of Fe from the chloroplast, although it did help with the bioaccessibility of β -carotene and galactolipids from FCRF.

Gastric pH can vary in-vivo due to fed and fasted states. A pH of 2 has been recorded in the fasted state and in the pylori region of the stomach (Eyerly, 1940). The standardised INFOGEST protocol recommends pH 3 as a gastric pH while a higher pH, around 5, emulating the fed state (Mennah-Govela *et al.*, 2020).

Pepsin is an aspartic protease that acts in food digestion in the mammalian stomach. Pepsin is mostly active at the optimal pH of 3 which allows pepsin to operate in its natural acidic environment, while at neutral pH the enzyme gets denatured, and becomes inactive (Campos and Sancho, 2003). However, in-vivo studies on the human stomach recorded that due to gastric emptying, most food encounters a variety of pHs at the gastric phase (Sams *et al.*, 2016). These variations range from pH 5.5 at the full stomach of solid food to pH 2 at 95% emptying state which takes place at around 2 hours of gastric digestion. The same study reported that 53% of digestion studies use the pH 2, at gastric phase. The pH of the intestinal phase has been also reported to fluctuate between 3.8 to 7.8, when samples were taken from the proximal to distal ends of human duodenum (Sams *et al.*, 2016). The rate of gastric emptying in its turn is modulated by many factors including neuromuscular factors, meal-related factors, and other factors. Meal-related factors that affect gastric emptying include the digestible components of the solids and liquids, fat content (nutrient density), viscosity, acid content, volume, and indigestible foodstuffs.

For this study, a range of gastric pHs were assessed to see if changing the pH influences Fe release. Changing the gastric pH had no significant effect on the dialysability of Fe, but pH 2 displayed the highest mean value which agrees with many studies on iron bioaccessibility, where lower pH displayed better bioaccessibility, and so was the chosen pH for the gastric stage for the rest of our experiments.

This addition ratio of ascorbic acid was based on the Miller *et al.* (1981) study and on his recommendation that the addition of ascorbic acid needs to exceed 4:1 (ascorbic acid: iron) ratio to be most effective especially where iron absorption inhibitors exist. For example, phytates, tannins and oxalic acid were present in spinach (Germano and Canniatti, 2011). The enhancement of iron absorption by the addition of ascorbic acid is more pronounced in meals containing non-haem iron such as vegetables and cereals or with the added inorganic iron salts, rather than the meals containing haem iron such as meat (Teucher and Olivares, 2004). The mechanism of this enhancement involves two actions; (1) the prevention of the formation of insoluble iron compounds by forming a chelate with ferric iron (Fe^{+3}) at acid pH that remains soluble, and thus more bioavailable, later at the alkaline pH of the duodenum and (2) the reduction of ferric Fe^{3+} to the more stable and soluble form of ferrous iron Fe^{2+} at acidic and neutral pHs, which seems to be a requirement for the uptake of iron into the mucosal cells as demonstrated in Figure 1.2, in Chapter 1 (Hallberg, 1981; Lynch and Cook, 1980; Timoshnikov *et al.*, 2020; Ems *et al.*, 2022; Piskin *et al.*, 2022).

The benefit of ascorbic acid addition to the bioaccessibility of iron has been reported as early as 1972 by Sayers *et al.* (1972). They proved that the addition of ascorbic acid to maize porridge enhanced the absorption of both intrinsic and the added iron measured in vivo by the red cell utilisation method in iron deficient subjects (adults, males, and females). However, the same study recommended that the use of ascorbic.

acid should be considered with caution as some cooking methods, such as baking, can oxidize the ascorbic acid and prevent its effect.

Moreover, it is worth noting that the interaction between ascorbic acid and some transition metal ions such as Fe and Cu has pro-oxidative activity (Każmierczak *et al.*, 2020) However, this activity requires a high concentration of ascorbic acid in the range of millimolar, while the concentration of the added ascorbic acid in the final digestate in this experiment is 0.178 mM. Moreover, this pro-oxidation ability of ascorbic acid along with transition metals has only been proven in-vitro, while there is no convincing evidence of this activity in vivo. Also, thylakoid membranes have emulsifying characteristics (which is higher in fresh CRF than HTC RF as explained in section (5.3.2.1). and this is well known to hinder lipid digestion in vivo and thus thylakoid membrane is a candidate material to be used to control lipid digestion and to be used in appetite regulation (Rayner *et al.*, 2011). This makes the thylakoid membrane in the CRF extract an active barrier in vivo to protect the lipid droplets in vivo from being affected by the free radicals or any pro-oxidation factor. Thus, CRF materials (fresh and heated) with added ascorbic acid could be a dietary material with a better potential as iron supplement. This added to their established role in reducing lipid digestion and thus it can be used to alleviate obesity (Rayner *et al.*, 2011).

To ensure optimum Fe release which allows us to get measurable dialysable iron, all subsequent experiments were optimised by lowering the gastric pH to 2, also by adding 10-fold ascorbic acid.

5.3.5.3 Iron bioaccessibility of different spinach leaf treatments

Firstly, the amount of Fe in the digestion system is presented in Figure 5.13, to give an insight into the initial Fe content introduced to the digestion system by each of the five spinach leaves treatments: FCRF, HTCRF, ICRF, PLM and HTPLM.

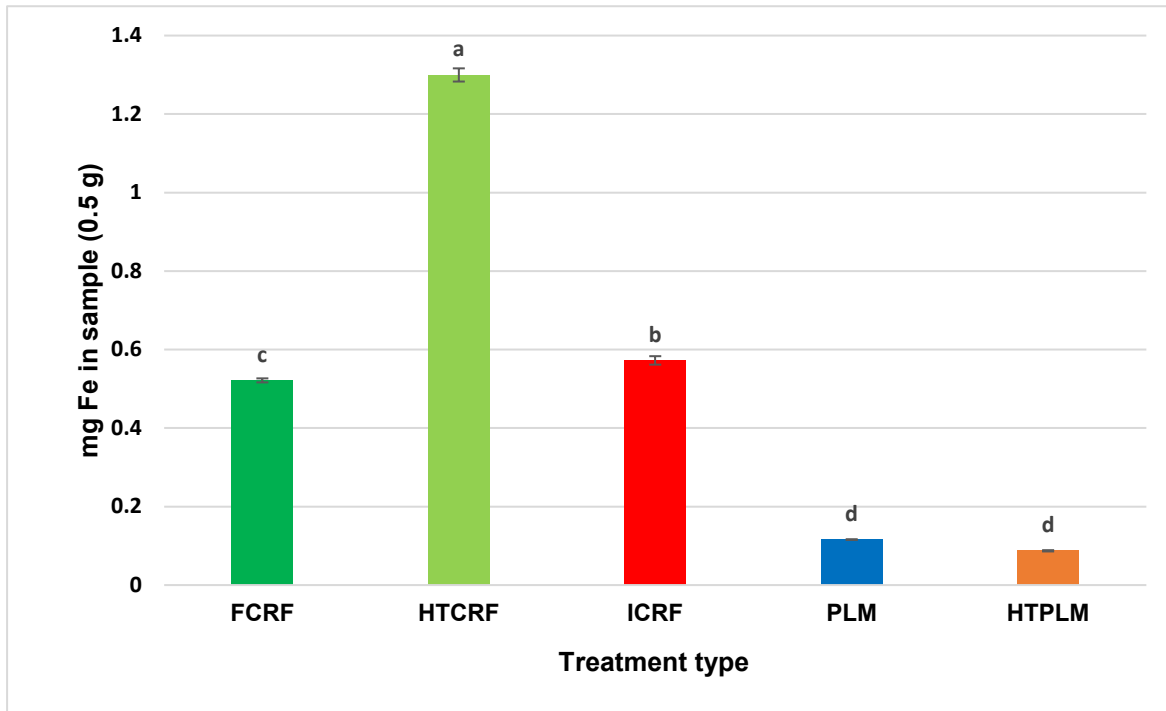


Figure 5.13: Amount of iron in each sample introduced to the digestive system, 0.5g of DW of each sample treatment FCRF, HTCRF, ICRF, PLM and HTPLM. Error bars represent SEM and the presence of different letters a and b denote a significant difference between samples at $p < 0.05$ using Tukey post-hoc test.

As mentioned earlier in this chapter that the CRF extract contains a significantly higher amount of iron than the powdered leaves which is whole leaves. In case of heat treatment, the CRF extract contains an even higher amount of iron which is between (2.5 to 3.8) times of the CRF isolated from fresh/non heated leaves (both FCRF and ICRF) according to our results. Gedi *et al.*, (2017) shows similar results with spinach CRFs showing larger concentrations of Fe compared with PLM.

It is also important to redemonstrate the whole process of digestion followed by the separation of dialysable and soluble fractions for subsequent mineral analysis. Figure 5.14 represents a schematic diagram of the whole digestion and bioaccessibility process.

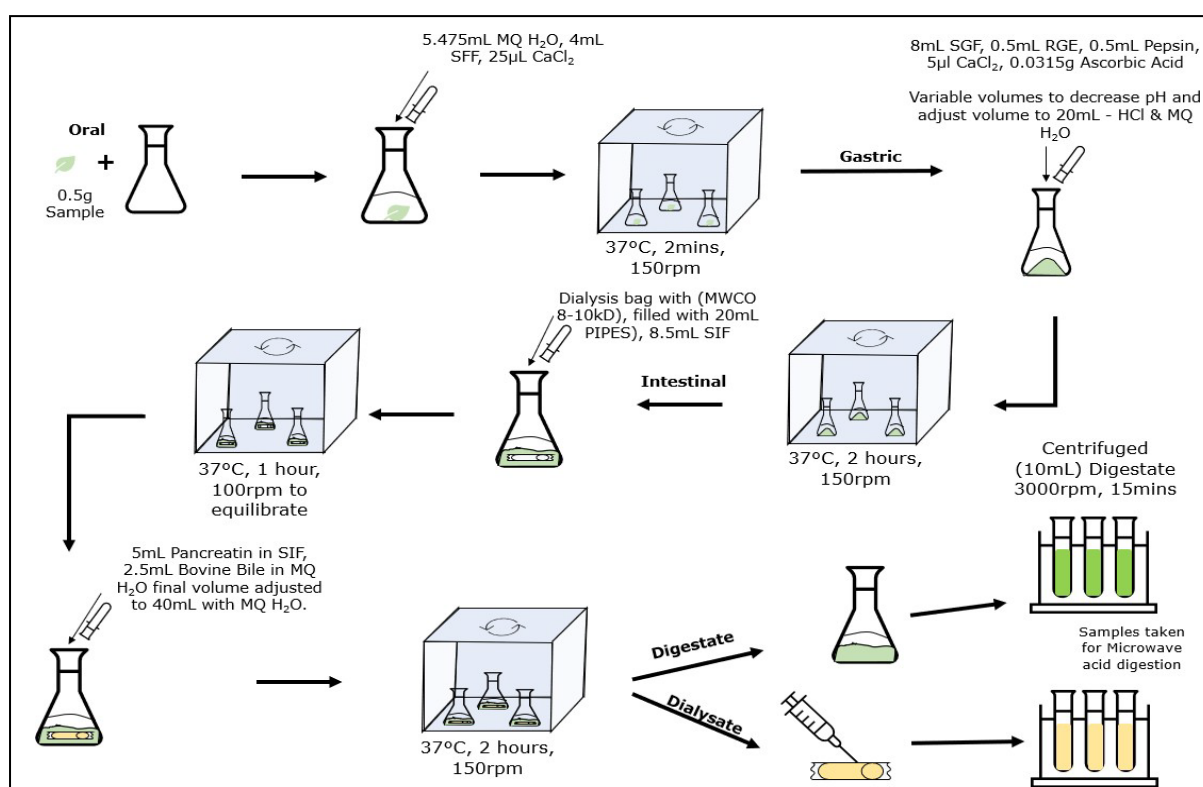
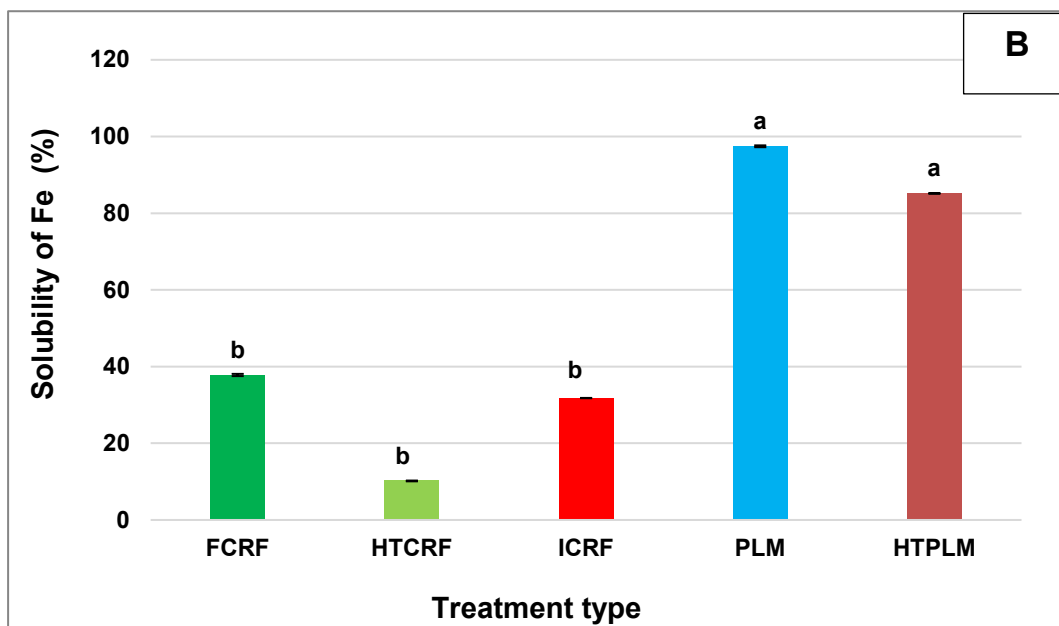
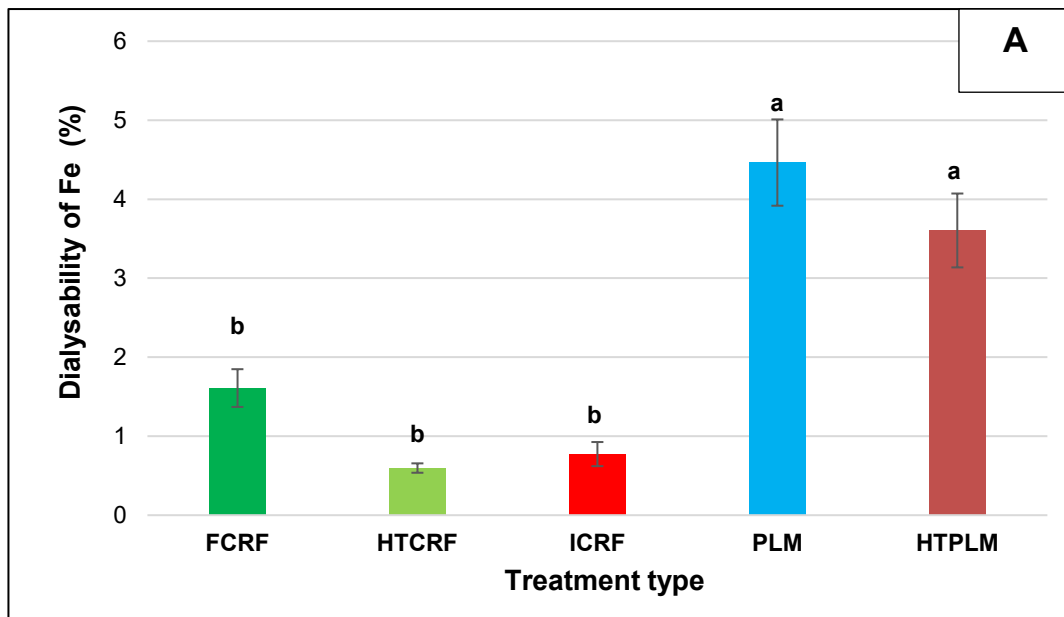


Figure 5.14: Illustration of in-vitro digestion process, post digestion treatments and separation of dialysable and soluble fraction for mineral analysis. SSF, simulated salivary fluid; SGF, simulated gastric fluid; SIF, simulated intestinal fluid; RGE, rabbit gastric enzyme.

Total Fe content was measured in the initial samples as dry powdered materials then in the dialysis bag fractions and soluble fractions as well as the enzymes and bile extracts added during the digestion steps. Calculations were made and data presented as % dialysability (figure 5.15A), and % solubility of Fe (see Figure 5.15C) absolute dialysable (amount of dialysable iron in mg Figure 5.15C) in the same five sample treatments.



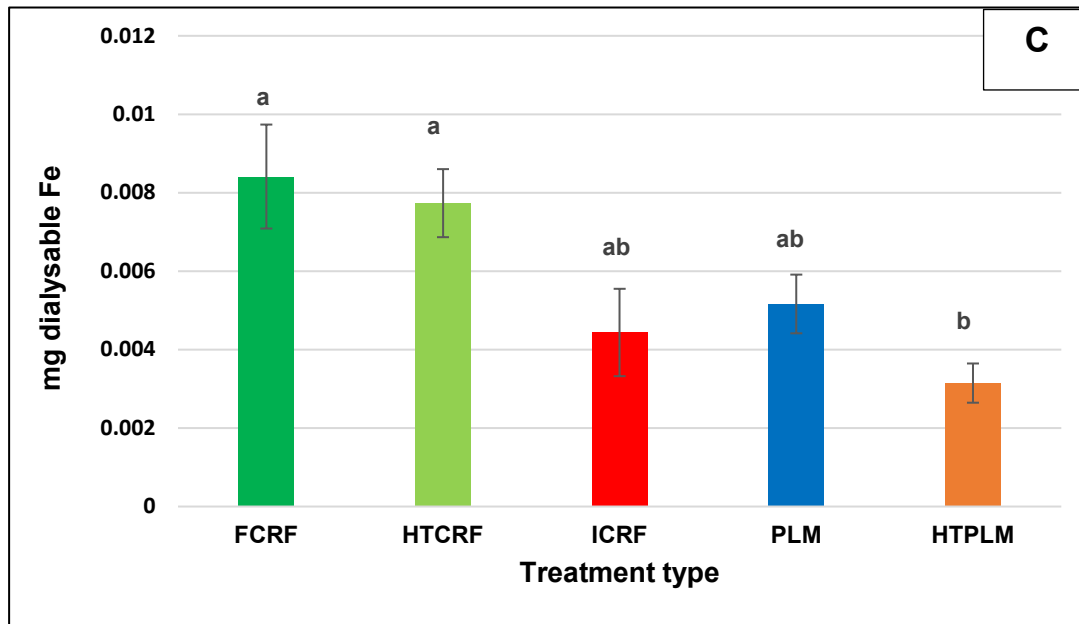


Figure 5.15 A—C: A) % dialysable Fe, B) % solubility, C) mg dialysable Fe in a 0.5g sample for 5 different treatment types; (FCRF), (HTCRF), (ICRF), (PLM) and (HTPLM). Error bars represent SEM and the presence of different letters a and b denote a significant difference between samples at $p < 0.05$ using Tukey post-hoc test.

From Figure 5.16A, there were no significant differences between fresh PLM and HTPLM, in terms of percentage of dialysable Fe. However, there were significant differences between the % dialysable iron released from both PLM and HTPLM vs all CRF samples (FCRF, HTCRF and ICRF). HTCRF recorded the lowest dialysability of 0.59mg/100g, whilst FCRF recorded just half the amount in both FPLM and HTPLM. This difference can be attributed to the differences in iron bound compounds between leaf and isolated chloroplast.

Haem iron (Fe^{+2}) exists in leaves as only 9% of total iron and it is mainly associated with the Fe-storage protein, ferritin (White and Broadley, 2009). Ferritin is localised in the non-green plastids (leucoplasts and chromoplasts), where it plays a role as a buffer between iron homeostasis and the redox balance by taking up iron in ferrous (Fe^{2+}) form and preventing toxic levels from being reached by converting it, via ferroxidase activity, to ferric (Fe^{3+}) form for storage. Ferritin then releases iron depending on the

cellular requirement (Zhao, 2010, Malhotra *et al.*, 2020). Thus, Ferritin may contain both form of iron (Fe^{+2} and Fe^{+3}).

The non-haem form, with most of this iron found in protein complexes (63%). Non-haem iron protein includes mainly ferritin, ferredoxin, thylakoid complexes, mitochondrial complexes, aconitase, nitrite reductase and sulphite reductase (Hewitt, 1983).

Plant ferritin (phytoferritin) is known to be a form of bioavailable iron in plants and found in high concentrations in peas, beans, soybeans, and other pulses. Research by Perfecto *et al.* (2018) showed that in garden pea, ferritin (present in the cytoplasm not chloroplasts of pea and leaf cells) exposed to a low pH resulted in complete protein degradation and led to the significant release of soluble iron from the iron core (Perfecto *et al.*, 2018). Three possible mechanisms for iron uptake from plant ferritin have been proposed: full hydrolysis of iron to Fe^{2+} and Fe^{3+} and subsequent Fe^{2+} uptake via DMT⁻¹, Fe^{3+} core uptake, and plant ferritin protein/receptor-bound uptake (Perfecto *et al.*, 2018). PLM used within this experiment could have a store of excess Fe bound to ferritin, and was therefore released during gastric digestion, resulting in a significantly higher percentage of dialysable iron than CRF.

Differences of iron dialysability % between the HTCRF and FCRF verify that blanching impacts the nature and digestibility of chloroplast Fe in CRF but not in PLM preparations.

Table 5.15B shows the solubility (% of Fe released into the micelle phase) of each of the five samples. Both solubility and dialysability follow the same trend, where CRF indicates a significantly lower percentage of soluble iron than PLM. The solubility of Fe in samples shows that there is a higher percentage of Fe released in the in-vitro digestion model, but not much is low molecular weight as the dialysable fraction shows notably lower values.

Although a higher percentage of Fe bioaccessibility is shown in both soluble and dialysable fractions from fresh and heat-treated leaves materials, the absolute amount of Fe in mg which passed to the dialysable membrane from CRF is higher and that is because the amount of Fe per dry weight of CRF samples is significantly higher than that of PLM. So, although the percentage dialysability of iron from CRF is lower than PLM, the absolute or net amount which is dialysable from the same dry biomass of CRF is significantly higher and thus, there still is a significant benefit of extracting CRF.

Significant differences between the HTCRF and fresh CRF verify that blanching impacts the nature and digestibility of chloroplast Fe in CRF but not in PLM preparations. Thus, more research into the role and the activity of endogenous enzymes in CRF and why more Fe is released from the fresh chloroplasts compared to the heat treated one was conducted. Therefore, the activity of the endogenous enzymes was encouraged by incubating the juice for 24 hours before extracting the CRF. However, the data in Figure 5.15 A showed no significant differences of the % dialysable Fe between FCRF and the incubated CRF.

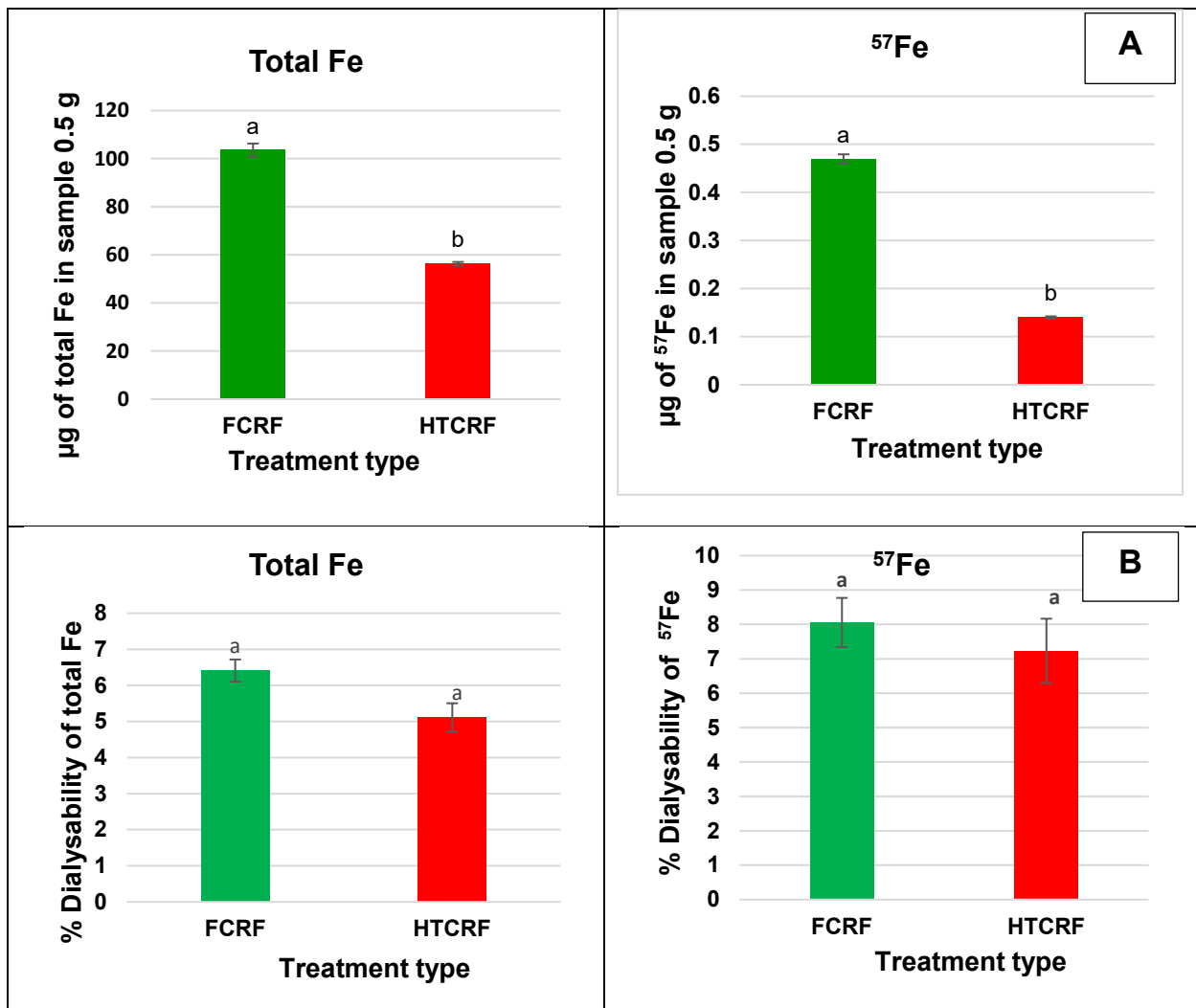
Dialysability as a method has been extensively used in assessing the bioaccessibility of some minerals including zinc and iron either from single food ingredient or from a whole meal. A study by Chiplonkar *et al.* (1999) found a good correlation between the iron bioavailability of iron from various meals through the day using human absorption of iron as indication and the dialysability of iron from the same meals using in-vitro digestion model followed by dialysability assessment. The correlation between in-vitro percent dialysability and human absorption was 0.96 for iron and 0.92 for zinc and both were statistically significant ($p = 0.0001$). which proves that in-vitro digestion followed by dialysability as a method provides a good index for the iron bioavailability from meals generally (Chiplonkar *et al.* 1999). Generally, in-vitro experiments based on solubility/dialysability are useful tools to understand factors that may affect

subsequent mineral absorption (Sandberg, 2005).

However, one of the drawbacks of the dialysability methods is that they exclude iron bound to large molecules, which in some cases is available and include iron bound to small molecules, which is not always available.

Iron bioaccessibility using CRF materials labelled with ⁵⁷Fe.

The in vitro bioaccessibility of iron was also examined using the hydroponically grown spinach which were labelled with ⁵⁷Fe.



The results show a bioaccessibility

of total iron of (6.4% of FCRF and 5.1 of the HTCRF. While the % dialysability of ^{57}Fe was 8.1 for the CRF 7.2 for the HTCRF. The bioaccessibility values of both total iron and ^{57}Fe comes in agreement in terms of having better bioaccessibility for the fresh CRF than the HTCRF. The data of the ^{57}Fe bioaccessibility confirm that this iron is coming from spinach CRF rather than from the enzymes and reagents used in the experiment.

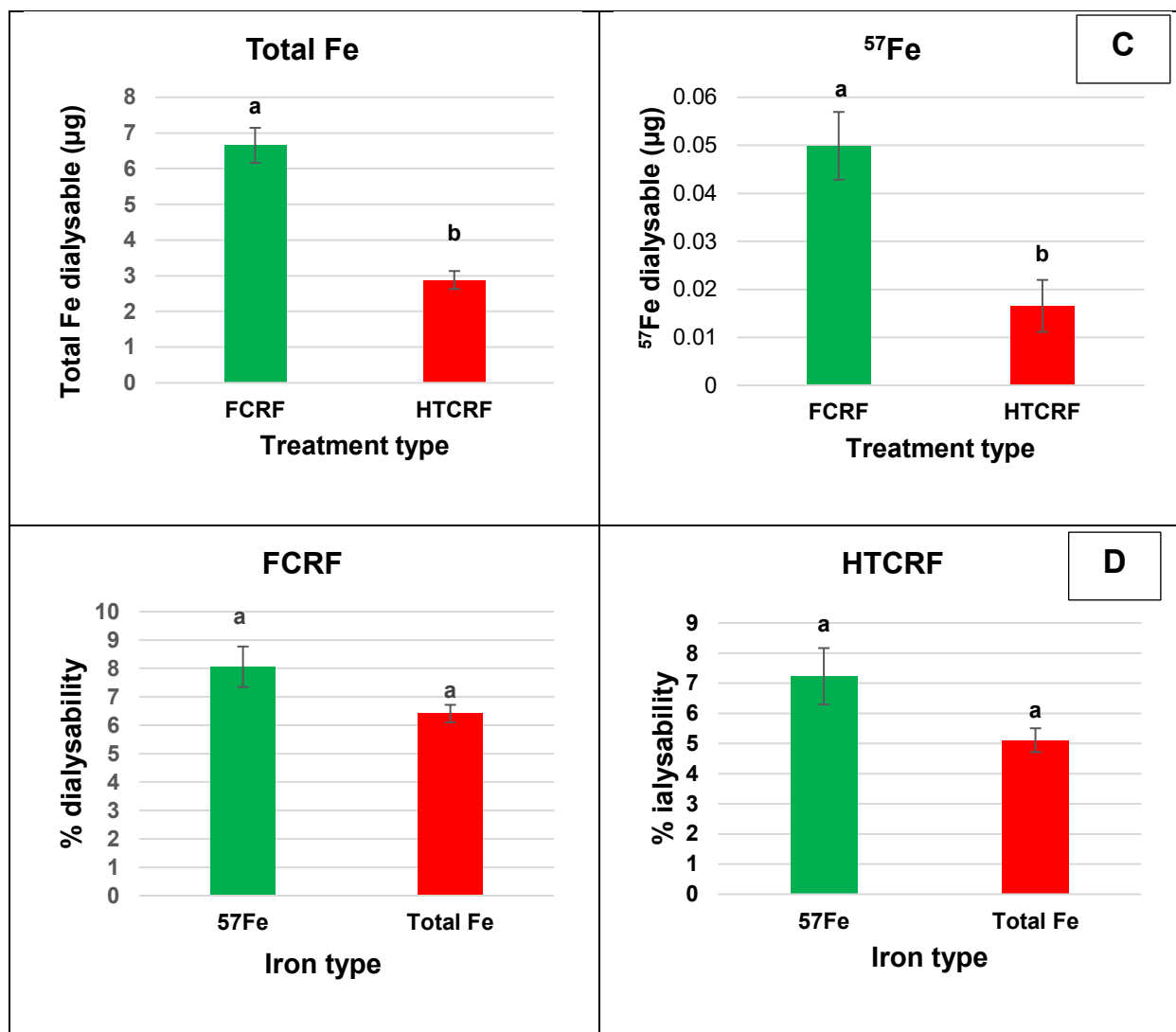


Figure 5.16 A—D: A) µg total Fe to the left and ⁵⁷Fe to the right in a 0.5g sample, B) % dialysability of total Fe to left and ⁵⁷Fe to the right, C) µg dialysable of total Fe to left and ⁵⁷Fe to the right, D) % of dialysable 57Fe and total iron from the FCRF to the left and the % of dialysable ⁵⁷Fe and total Fe from HTCRF to the right. Error bars represent SEM and the presence of different letters a and b denote a significant difference between samples at p < 0.05 using Tukey post-hoc test.

The iron content of fresh CRF is significantly higher than the HTCRF, unlike the results shown in Table 5.2. This is because the heat treatment for the CRF in this experiment was done by pasteurising the juice (at 90°C for 20 Sec) rather than blanching the leaves before juicing them to produce the juice then the HTCRF. This has led to much more extra debris and cell walls materials to pass through the HTCRF fraction, again in this experiment only. This has been a limitation of this study which should be

avoided in future work. The bioaccessibility as % dialysability, of the iron from FCRF Isolated from the hydroponically grown spinach showed a 4-fold increase over the FCRF from the spinach bought from the supermarket which is soil grown.

However, the initial amount of iron in the FCRF isolated from Tesco Spinach sample was 5 times higher and the absolute dialysable iron was 8.4ug for the CRF from Tesco spinach and 6.6 ug of the hydroponically grown spinach. This might indicate that the form of iron provided to the spinach in our hydroponic system resulted in spinach leaves with more bioaccessible iron.

5.4. Limitations and further study suggestions

During this project we encountered some difficulties and limitations which includes;

- In case of CRF isolation from blanched leave, it would be useful to recover the juice which went to the fibre part. This could be achieved by reinserting the fibre in the juicer or to juice it by squeezing it in cheese cloth. However, this requires more detailed study to understand the nature of the juice left in the fibre part.
- The addition of ascorbic acid should have been applied to all three pHs as well as taking more than three replicates. This could have expanded the understanding of these changes and provided more representative data.
- Further investigated to understand the impact of different amounts of ascorbic acid at varying gastric pHs on Fe bioaccessibility could be useful as well. Ascorbic acid addition could also have been added at different masses as Miller *et al.*, (1991) acknowledged that dialysability is dependent on the amount and the form of ascorbic acid applied.
- The bioaccessibility and bioavailability of Fe from ferritin stored within leaves and the vascular tissue is worth of further investigation. Further research can emphasize the understanding of ferritin stores from plants grown in Fe excess.

or deficit, and the bioaccessibility and bioavailability of Fe through in vitro digestion and Caco-2 cell plating.

- Measuring chlorophyll content could have added value to our work as it is a direct indication of spinach growth. Chlorophyll and carotenoid contents in the leaves of spinach plants were increased by Fe-EDDHA chelate supplementation.
- More work could also be conducted to assess the effect of iron sources in hydroponic system using different iron chelates and salts on the bioaccessibility of this iron from the spinach leaves.
- Bioaccessibility of Fe using the dialysable membrane/bag could be improved by replenishing the buffer inside the dialysis bag halfway through the incubation time to avoid reaching a saturation point and the keep the momentum for selective and passive diffusion of the molecules.

5.5 Conclusions

- Addition of ascorbic acid increased dialysability and bioaccessibility, far more than the addition of oils, or increase of gastric pH.
- % dialysability of Fe from PLM is significantly higher than CRF (Fresh, heated, and incubated). However due to the much higher initial iron content in CRF, the dialysable amount of Fe is higher in CRF (FCRF < HTCRF and ICRF).
- % dialysability of labeled FCRF was higher than HTCR using ⁵⁷Fe as biomarker.
- % dialysability of ⁵⁷Fe was a bit higher than total Fe, however not significantly, which validate our results and prove that the dialysable iron is mostly coming from the intracellular iron either from CRF or PLM.

6.0 Grand discussion

6.1 Introduction

Iron has an essential biological role in a wide range of metabolic processes and is thus a vital component for all living organisms, including plants, humans, animals and prokaryotes. It is a micronutrient, however, required at slightly higher amounts compared to others, such as Zn and Cu (Abbaspour *et al.*, 2014). For example, it is involved in the synthesis of nucleotides, chlorophyll and respiration, where it participates in electron transfer between the two redox states; ferrous (II) Fe^{2+} and ferric (III) Fe^{3+} (Roschztardt *et al.*, 2013). The deficiency of Fe has been emphasised on a global scale, and currently impacts more than three billion people worldwide (Roose *et al.*, 2001). McLean *et al.*, (2009) reported this issue being significant in children, pregnant and childbearing women. It has had a profound impact on children's psychomotor development and cognitive abilities and has also resulted in fatigue and lowered immunity (Brown and Ford, 2008). Plants have adapted two main pathways to adapt to Fe deficiency; Strategy I used by all the non-graminaceous higher plants, in this case spinach, and Strategy II is used by the graminaceous cereal plants. Strategy I is reduction-based, and Strategy II is chelation-based (Krohling *et al.*, 2016). Plants have evolved important buffering mechanisms, following poor root growth, resulting from Fe toxicity (Morrissey and Guerinot, 2009). 80—90% of plant Fe in the entire leaf material, gets confined in chloroplasts. However, the exact mechanisms involved in chloroplast Fe uptake still require further investigation.

Out of a majority of Green Leafy Vegetables (GLVs), spinach is the highest in terms of mineral, vitamin, phytochemicals, and have exceptionally high antioxidant capacities. Alvino and Barbieri, (2015) reported these phytochemicals being linked to

a reduction in chronic disease, cancer, obesity, inflammatory and neurological diseases.

6.2 Methodology

A broad range of growth locations and substrates were tested on Sutton Bonington Campus, to determine the most optimal option, based on final spinach yields and Fe contents. The soil method involved Levington M4 compost, and the hydroponic methods included rockwool cubes and perlite. Compost produced the highest yields and leaf sizes; however, the nutrient compositions were not always consistent. The yields from the rockwool cubes were a lot lower, because of dissolution, which significantly raised the pHs of the nutrient feed, hindering their growth (Blok and Kaarsemaker).

Perlite gave the most consistent growth rates and in terms of germination and yield. Because it is more sterile with no carcinogenic implications, it was chosen as the final choice to grow Trombone F1 spinach (Nicola *et al.*, 2004).

A standard modified Hoagland nutrient solution formulated in the laboratory facilities and was composed of all essential macro and micronutrients ranging from K, P, Na, Ca, Mg, Fe and Zn (Søberg, 2016). The Fe was in the form of Na Fe-EDTA to prevent the damaging photooxidation reactions (Şimşek and Çelik., 2021). \cong 0.78g of MES powder was also used to maintain the optimal germination pH of approximately 5.8.

Finally, the total Fe and ^{57}Fe contents of spinach root and leaf material were measured after microwave acid digestion and ICP-MS analysis. The novelty of this project was dosing spinach plants with ^{57}Fe . Measurement of biomarker photosynthetic pigments

in lipid extracts was performed using spectrophotometry, followed by calculations in the equations by Lichtenthaler and Buschmann (2001).

6.3 Mathematical modelling

Results in Figures 4.2 and 4.3 show the highest root and leaf DWs after dosing with 100 μM Na Fe-EDTA in solution. The toxicity range was reached beyond 150 μM , and this agrees with Şimşek and Çelik (2021), who reported spinach leaf material having the highest DW, after dosing with 120 μM Fe-EDTA, followed by a decrease at the highest dosing concentration of 150 μM in solution. In terms of Fe contents, the peaks were reached after dosing with 200 μM NaFe-EDTA in leaf material, and 150 μM in root material. Excess Fe is known to inhibit lateral root (LR) elongation, and morphology, therefore, reducing the uptake at higher concentrations (Li *et al.*, 2013).

In the context of mathematical modelling, the key concept in ODEs is time, t , and rates of change of different entities are measured through time, in our case, concentrations of molecules (Harcet *et al.*, 2013). In this experiment three ODEs were generated for the concentrations of Fe: the growth matrix, roots and leaves. Equation 4.4 was used to indirectly calculate the concentrations of Fe in the growth matrix. Four different versions of the dynamic model were generated, based on Bayesian statistics. These included 1) constant decay rate, 2) variable decay rate, 3) minimal Fe in the growth matrix and 4) no inhibition of Fe uptake. Different model parameters were added and removed within each of these. The unknown model parameters included K_M , r_{MR} , r_{RL} and r_D and were included as part of the final model.

Final analysis of the Bayesian statistics showed that C_{\max} was unidentifiable and could not be determined based on the data already collected. Further inquiry is needed on

the complex spinach root geometry, and K_M was difficult to identify from the experimental data, because limiting sections in the growth matrix were never fully reached. Future models could account for more aspects of plant physiology, ranging from plant morphology, mineral concentrations, NO_3^- concentrations, and chlorophyll and carotenoid contents.

6.4 Bioaccessibility

Fresh and heat-treated spinach leaves were fractionated using a physical of juicing and centrifugation to produce chloroplast rich fractions (FCRF and HTCRF). CRF is a nutrient dense organelle which have been released from the confined cell walls, so the hypothesis that they can release their nutrients and micronutrient more easily in the gastrointestinal track. The focus of this project was on the bioaccessibility of iron from CRF vs whole leaves and to use the CRF which has been labelled with ^{57}Fe to further support our findings and distinguish Fe in spinach from Fe carried over into the digestion simulations from reagents and enzyme cocktails or any other extracellular source.

Mass distribution and Fe distribution data established that Fe in CRF extracted from both heat-treated and fresh leaves had similar recovery rates. This shows that blanching spinach did not have a significant effect on the recovery of Fe although it did have a significant effect on the amount of CRF mass recovered.

The % bioaccessibility of Fe in spinach from CRF (cell free) compared to PLM (cell bound) has been established, using an optimized in-vitro digestion model adapted from (Brodkorb *et al.*, 2019). This was followed by testing the % of iron dialysability using a dialysis membrane of 8-10 kDa MWCO (Molecular weight cut-off). This dialysis

membrane was used to filter out the iron which is bound to small molecules with lower molecule weight than (10 kDa), assuming these molecules are bioaccessible which based on many dialysability studies has high correlation with the bioavailability of this iron in human gastrointestinal track (Sandberg, 2005).

Optimization of the in-vitro model showed that addition of oil had no effect on the bioaccessibility of Fe, on the other hand, addition of ascorbic acid had a five-fold increase in Fe dialysability at pH 2. Henceforward ascorbic acid was added to the in-vitro methodology and the gastric pH was adjusted to 2. HTCRF showed significantly lower percentage bioaccessibility Fe compared to FCRF and PLM. The data also concluded that on a dry weight basis FCRFs and HTCRFs contained higher amounts of Fe in both fractions than PLM. Concluding that within this research bioaccessibility of Fe is greater from whole leaf material than cell-free spinach chloroplasts (CRF) and that fresh material has a greater Fe bioaccessibility compared to heat-treated. The absolute or net amount of dialysable Fe in both FCRF and HTCRF was significantly higher than that of PLM and HTPLM. This might be due to the limitation of our method where it might be that the amount of Fe bound molecule inside the dialysis bag has reached its saturation level and a renewal of the buffer inside the membrane after one hour of incubation might give a better dialysability. Moreover, the Fe in CRF might be linked with larger molecule than 10KDa, which cannot pass through the dialysable membrane but still can be released in the gastrointestinal tract.

This will establish a better understanding of the Fe available within spinach and recovered chloroplasts and whether they could be nutritionally beneficial for an individual through fortification.

7.0 Grand conclusion

- As many methods to grow spinach for this experiment were tried, growing spinach hydroponically using perlite as a growing medium in a well- controlled growing room (19 – 24°C, relative humidity between 50 – 70%, and light intensity of 17—22 mol/m²/d) gave us the best settings. This has helped to get a consistent produce with the germination rate, yield, constancy of plant quality and the practicality of plants harvesting and roots separation.
- Spinach plants grown on perlite in a growth room provided an effective way to measure the rate of iron uptake into roots and leaves. They also yielded enough leaf material to recover Chloroplast Rich Fraction (CRF), for the bioaccessibility trials.
- ⁵⁷Fe enrichment was achieved through watering mature spinach plants (grown for 21 days), a further 3 consecutive times with Hoagland nutrient solution containing 3 μM ⁵⁷Fe.
- In the iron uptake kinetic experiment using a series of iron concentration in the Hoagland feed solution of (10,25,50,75,100,150,200 μM), Fe toxicity limits and C_{max} were never reached.
- Fe contents were always higher in root, rather than leaf material.
- The maximum yields and Fe contents for both root and stem material were reached after dosing with 100 μM NaFe-EDTA in solution and Fe contents (mg/Kg) were always higher in root, rather than leaf material.
- The MCMC, is the most effective way in determining the posterior distribution, which in turn compares the actual data to any given model. One iteration is only dependent on the previous one and nothing else.

- Iron bioaccessibility measured as % dialysability using modified in-vitro digestion model was optimised by using gastric pH of 2 with added ascorbic acid)
- Percentage dialysable iron was significantly better for the PLM than CRF material with fresh leaves being higher than heat treated leaves and Fresh CRF higher than HTCRF.
- Percentage dialysability of ^{57}Fe was a bit higher than total Fe, however not significantly, which validate our results and prove that the dialysable iron is mostly coming from the intracellular iron either from CRF or PLM.
- Absolute dialyzable iron value was higher for CRF materials than PLM, which requires further investigation and improvement of the dialysability technique.

8.0 References

Abbaspour, N., Hurrell, R. & Kelishadi, R. (2014) Review on iron and its importance for human health. *J Res Med Sci*, 19(2), 164-74.

Alvino, A. & Barbieri, B. (2015) Vegetables of temperate climates: leafy vegetables.

Ancuceanu, R., Dinu, M., Hovanet, M.V., Anghel, A.I., Popescu, C.V., Negres, S., (2015) A Survey of Plant Iron Content—A Semi-Systematic Review. *Nutrients*, VII(1), p. 10320–10351.

Anderson, G. J., Frazer, D. M., McKie, A. T., Vulpe, C. D. & Smith, A. (2005a) Mechanisms of haem and non-haem iron absorption: lessons from inherited disorders of iron metabolism. *Biometals*, 18(4), 339-48.

Anderson, G. J., Frazer, D. M., McKie, A. T., Vulpe, C. D. & Smith, A. (2005b) Mechanisms of Haem and Non-Haem Iron Absorption: Lessons from Inherited Disorders of Iron Metabolism. *Biometals*, 18(4), 339-348.

Baligar, V. C., Fageria, N. K. & Elrashidi, M. A. (1998) Toxicity and nutrient constraints on root growth. *HortScience*, 33(6), 960-965.

Bar-Tal, A., Ganmore-Neumann, R. & Ben-Hayyim, G. (1997) Root architecture effects on nutrient uptake, *Biology of root formation and development* Springer, 39-45.

Bermejo, F. & García-López, S. (2009) A guide to diagnosis of iron deficiency and iron deficiency anemia in digestive diseases. *World J Gastroenterol*, 15(37), 4638-43.

Bhattacharjee, S., Dasgupta, P., Paul, A. R., Ghosal, S., Padhi, K. K. & Pandey, L. P. (1998) Mineral element composition of spinach. *Journal of the Science of Food and Agriculture*, 77(4), 456-458.

Bishop, C. M. (2006) *Pattern Recognition and Machine Learning*. Cambridge, England: Springer Science.

Bishop, C. M. & Nasrabadi, N. M. (2006) *Pattern recognition and machine learning*, 4Springer.

Borowski, E. (2013) Uptake and transport of iron ions (Fe²⁺, Fe³⁺) supplied to roots or leaves in spinach (*Spinacia oleracea* L.) plants growing under different light conditions. *Acta Agrobotanica*, 66(2).

Brechner, M. & De Villiers, D. (2013) Cornell controlled environment agriculture. Hydroponic Spinach Production Handbook. *Cornell University CEA Program*.

Brodkorb, A., Egger, L., Alminger, M., Alvito, P., Assunção, R., Ballance, S., Bohn, T., Bourlieu-Lacanal, C., Boutrou, R. & Carrière, F. (2019) INFOGEST static in vitro simulation of gastrointestinal food digestion. *Nature protocols*, 14(4), 991-1014.

Brown, M., Ford, M., 2008. *Chemistry for the IB Diploma*. 1st ed. Harlow, Essex: Pearson Education Limited.

Bryszewska, M. A. (2019) Comparison study of iron bioaccessibility from dietary supplements and microencapsulated preparations. *Nutrients*, 11(2), 273.

Burrows GE, Connor C. Chloroplast Distribution in the Stems of 23 Eucalypt Species. *Plants*. 2020; 9(12):1814.

Cai, X., Chen, X., Yin, N., Du, H., Sun, G., Wang, L., Xu, Y., Chen, Y. & Cui, Y. (2017) Estimation of the bioaccessibility and bioavailability of Fe, Mn, Cu, and Zn in Chinese vegetables using the in vitro digestion/Caco-2 cell model: the influence of gut microbiota. *Food & function*, 8(12), 4592-4600.

Carpenter, C. E. & Mahoney, A. W. (1992) Contributions of heme and nonheme iron to human nutrition. *Critical Reviews in Food Science & Nutrition*, 31(4), 333-367.

Connorton, J. M., Balk, J. & Rodríguez-Celma, J. (2017) Iron homeostasis in plants—a brief overview. *Metallomics* 9: 813–823.

Conrad, M. E. & Umbreit, J. N. (2000) Iron absorption and transport—an update. *American journal of hematology*, 64(4), 287-298.

Damon, A., McGonegal, R., Tosto, P. & Ward, W. (2007) *Higher level Biology: developed specifically for the IB diploma* Harlow (Reino Unido): Pearson Education, 2007.

Daniel Foreman-Mackey, D. W. H., Dustin Lang, Jonathan Goodman (2013) The MCMC Hammer. *Publications of the Astronomical Society of the Pacific*, 125(1), 306-312.

Dasa, F. & Abera, T. (2018) Factors affecting iron absorption and mitigation mechanisms: A review. *Int. J. Agric. Sci. Food Technol*, 4, 24-30.

Di Marzio, W. D., Sáenz, M., Alberdi, J., Tortorelli, M. & Silvana, G. (2005) Risk assessment of domestic and industrial effluents unloaded into a freshwater environment. *Ecotoxicology and environmental safety*, 61(3), 380-391.

Divol, F., Couch, D., Conéjéro, G., Roschztardt, H., Mari, S. & Curie, C. (2013) The Arabidopsis YELLOW STRIPE LIKE4 and 6 transporters control iron release from the chloroplast. *The Plant Cell*, 25(3), 1040-1055.

Eid, E. M., Alrumman, S. A., Galal, T. M. & El-Bebany, A. F. (2018) Prediction models for evaluating the heavy metal uptake by spinach (*Spinacia oleracea* L.) from soil amended with sewage sludge. *International journal of phytoremediation*, 20(14), 1418-1426.

Etcheverry, P., Grusak, M. A. & Fleige, L. E. (2012) Application of in vitro bioaccessibility and bioavailability methods for calcium, carotenoids, folate, iron, magnesium, polyphenols, zinc, and vitamins B6, B12, D, and E. *Frontiers in physiology*, 3, 317.

Eyerly, J. B. (1940) Comparative pH values within the stomach, pylorus and duodenum in antacid therapy. *American Journal of Digestive Diseases*, 7, 431-434.

Finazzi, G., Petroustos, D., Tomizioli, M., Flori, S., Sautron, E., Villanova, V., Rolland, N. & Seigneurin-Berny, D. (2015) Ions channels/transporters and chloroplast

Student ID: 20194859

regulation. *Cell calcium*, 58(1), 86-97.

Foreman-Mackey, D., Hogg, D. W., Lang, D. & Goodman, J. (2013) emcee: the MCMC hammer. *Publications of the Astronomical Society of the Pacific*, 125(925), 306.

Francis Kweku Amagloh, R. A. A., Richard McBride, Edward Ewing Carey, Tatiana Christides (2017) Nutrient and Total Polyphenol Contents of Dark Green Leafy Vegetables, and Estimation of Their Iron Bioaccessibility Using the In Vitro Digestion/Caco-2 Cell Model. *Foods*, VI (54), 1-12.

Gedi, M. A., 2017. Nutrient Composition and Digestibility of Chloroplast Rich Fractions from Green Leaf Materials, Nottingham, England: University of Nottingham.

Gedi, M. A., Briars, R., Yuseli, F., Zainol, N., Darwish, R., Salter, A. M. & Gray, D. A. (2017) Component analysis of nutritionally rich chloroplasts: recovery from conventional and unconventional green plant species. *Journal of food science and technology*, 54, 2746-2757.

Gedi, M.A., Magee, K.J., Darwish, R., Eakpatch, P., Young, I., Gray, D.A., 2019. Impact of the partial replacement of fish meal with a chloroplast rich fraction on the growth and selected nutrient profile of zebrafish (*Danio rerio*). *Food & Function*, X(1), pp. 733-745.

Gong, X., Guo, C., Terachi, T., Cai, H. & Yu, D. (2015) Tobacco PIC1 mediates iron transport and regulates chloroplast development. *Plant Molecular Biology Reporter*, 33, 401-413.

Gulec, S., Anderson, G. J. & Collins, J. F. (2014) Mechanistic and regulatory aspects of intestinal iron absorption. *American Journal of Physiology-Gastrointestinal and Liver Physiology*, 307(4), G397-G409.

GUNAWAN, M.I. and BARRINGER, S.A. (2000), GREEN COLOR DEGRADATION OF BLANCHED BROCCOLI (*BRASSICA OLERACEA*) DUE to ACID and MICROBIAL GROWTH. *Journal of Food Processing and Preservation*, 24: 253-263.

Gupta, K., Barat, G. K., Wagle, D. S. & Chawla, H. K. L. (1989) Nutrient contents and antinutritional factors in conventional and non-conventional leafy vegetables. *Food chemistry*, 31(2), 105-116.

Hallberg, L. (1981) Bioavailability of dietary iron in man. *Annual review of nutrition*, 1(1), 123-147.

Harcet, J., Heinrichs, L., Seiler, P. M. & Skoumal, M. T. (2013) *Oxford IB Diploma Programme: Mathematics Higher Level Course Companion* Oxford University Press-Children.

Heaton, J. W., & Marangoni, A. G. (1996). Chlorophyll degradation in processed foods and senescent plant tissues. *Trends in Food Science & Technology*, 7(1), 8-15.

Hell, R. & Stephan, U. W. (2003) Iron uptake, trafficking and homeostasis in plants. *Planta*, 216, 541-551.

Hess, S. Y., Zimmermann, M. B., Arnold, M., Langhans, W. & Hurrell, R. F. (2002) Iron deficiency anemia reduces thyroid peroxidase activity in rats. *The Journal of nutrition*, 132(7), 1951-1955.

Jain, A., Wilson, G. T. & Connolly, E. L. (2014) The diverse roles of FRO family

Student ID: 20194859

metalloreductases in iron and copper homeostasis. *Frontiers in Plant Science*, 5, 100.

Ivanov, A.G., Velitchkova, M.Y., Allakhverdiev, S.I. *et al.* Heat stress-induced effects of photosystem I: an overview of structural and functional responses. *Photosynth Res* **133**, 17–30 (2017).

Jin, C.-W., Liu, Y., Mao, Q.-Q., Wang, Q. & Du, S.-T. (2013) Mild Fe-deficiency improves biomass production and quality of hydroponic-cultivated spinach plants (*Spinacia oleracea* L.). *Food chemistry*, 138(4), 2188-2194.

Jones Jr, J. B. (2016) *Hydroponics: a practical guide for the soilless grower* CRC press.

Kaźmierczak-Barańska J, Boguszevska K, Adamus-Grabicka A, Karwowski BT. Two Faces of Vitamin C-Antioxidative and Pro-Oxidative Agent. *Nutrients*. 2020 May 21;12(5):1501.

Krohling, C. A., Eutrópico, F. J., Bertolazi, A. A., Dobbss, L. B., Campostrini, E., Dias, T. & Ramos, A. C. (2016) Ecophysiology of iron homeostasis in plants. *Soil Science and Plant Nutrition*, 62(1), 39-47.

Kumwimba, M. N., Xibai, Z. & Lingyu, B. (2013) Uptake kinetics of arsenic by lettuce cultivars under hydroponics. *African Journal of Environmental Science and Technology*, 7(5), 321-328.

Lee, S.-R., Oh, M.-M. & Park, S.-A. (2016) Ferric-chelate reductase activity is a limiting factor in iron uptake in spinach and kale roots. *Horticulture, Environment, and Biotechnology*, 57, 462-469.

Li, W. & Lan, P. (2017) The understanding of the plant iron deficiency responses in strategy I plants and the role of ethylene in this process by omic approaches. *Frontiers in plant science*, 8, 40.

Liu, D. H., Adler, K. & Stephan, U. W. (1998) Iron-containing particles accumulate in organelles and vacuoles of leaf and root cells in the nicotianamine-free tomato mutant chloronerva. *Protoplasma*, 201, 213-220.

Lynch, S. R. & Cook, J. D. (1980) Interaction of vitamin C and iron. *Ann NY Acad Sci*, 355(1), 32-44.

Lysenko, E. A., Klaus, A. A., Kartashov, A. V. & Kusnetsov, V. V. (2020) Specificity of Cd, Cu, and Fe effects on barley growth, metal contents in leaves and chloroplasts, and activities of photosystem I and photosystem II. *Plant Physiology and Biochemistry*, 147, 191-204.

López-Millán, A. F., Duy, D. & Philippar, K. (2016) Chloroplast iron transport proteins—function and impact on plant physiology. *Frontiers in plant science*, 7, 178.

M. Minekus, M. A., P. Alvito, S. Ballance, T. Bohn, C. Bourlieu, F. Carriere, D. Dupont, D. Dufour (2014) A standardised static in vitro digestion method suitable for food – an international consensus. *Food & Function*, V(1), 1113-1124.

Machado, R. M. A., Alves-Pereira, I. & Ferreira, R. M. A. (2018) Plant growth, phytochemical accumulation and antioxidant activity of substrate-grown spinach. *Heliyon*, 4(8).

Malhotra, H., Pandey, R., Sharma, S. & Bindraban, P. S. (2020) Foliar fertilization: possible routes of iron transport from leaf surface to cell organelles. *Archives of Agronomy and Soil Science*, 66(3), 279-300.

Mankin, K. R. & Fynn, R. P. (1996) Modeling individual nutrient uptake by plants: relating demand to microclimate. *Agricultural Systems*, 50(1), 101-114.

Maréchal, E. (2018) *Plastids: Methods and Protocols*. Grenoble, France: Springer Ltd.

Student ID: 20194859

Maunder, E. M. W. & Meaker, J. L. (2007) The current and potential contribution of home-grown vegetables to diets in South Africa. *Water SA*, 33(3), 401-406.

McDowell, L. R. (1992) *Minerals in animal and human nutrition* Academic Press Inc.

McLean, E., Cogswell, M., Egli, I., Wojdyla, D. & De Benoist, B. (2009) Worldwide prevalence of anaemia, WHO vitamin and mineral nutrition information system, 1993–2005. *Public health nutrition*, 12(4), 444-454.

Mennah-Govela, Y. A., Cai, H., Chu, J., Kim, K., Maborang, M.-K., Sun, W. & Bornhorst, G. M. (2020) Buffering capacity of commercially available foods is influenced by composition and initial properties in the context of gastric digestion. *Food & function*, 11(3), 2255-2267.

Miller, G. W., Huang, I. J., Welkie, G. W. & Pushnik, J. C. Function of iron in plants with special emphasis on chloroplasts and photosynthetic activity 1995. Springer.

Milman, N. T. (2020) A review of nutrients and compounds, which promote or inhibit intestinal iron absorption: making a platform for dietary measures that can reduce iron uptake in patients with genetic haemochromatosis. *Journal of Nutrition and Metabolism*, 2020.

Minekus, M., Alming, M., Alvito, P., Ballance, S., Bohn, T., Bourlieu, C., Carrière, F., Boutrou, R., Corredig, M. & Dupont, D. (2014) A standardised static in vitro digestion method suitable for food—an international consensus. *Food & function*, 5(6), 1113-1124.

Miret, S., Tascioglu, S., van der Burg, M., Frenken, L. & Klaffke, W. (2010) In vitro bioavailability of iron from the heme analogue sodium iron chlorophyllin. *Journal of agricultural and food chemistry*, 58(2), 1327-1332.

Morrissey, J. & Guerinot, M. L. (2009) Iron uptake and transport in plants: the good, the bad, and the ionome. *Chemical reviews*, 109(10), 4553-4567.

Natesh, H. N., Abbey, L. & Asiedu, S. K. (2017) An overview of nutritional and antinutritional factors in green leafy vegetables. *Horticult Int J*, 1(2), 00011.

Nielsen, N. E. (1976) A transport kinetic concept for ion uptake by plants: III. Test of the concept by results from water culture and pot experiments. *Plant and Soil*, 45, 659-677.

Odhav, B., Beekrum, S., Akula, U. S. & Baijnath, H. (2007) Preliminary assessment of nutritional value of traditional leafy vegetables in KwaZulu-Natal, South Africa. *Journal of Food Composition and Analysis*, 20(5), 430-435.

Oki, H., Kim, S., Nakanishi, H., Takahashi, M., Yamaguchi, H., Mori, S. & Nishizawa, N. K. (2004) Directed evolution of yeast ferric reductase to produce plants with tolerance to iron deficiency in alkaline soils. *Soil science and plant nutrition*, 50(7), 1159-1165.

Oliveira, S.R., Menegário, A.A., Arruda, A.Z., (2014) Evaluation of Fe uptake and translocation in transgenic and non-transgenic soybean plants using enriched stable Fe⁵⁷ as a tracer. *Metallomics*, VI(1), pp. 1832--1840.

Orech, F. O., Akenga, T., Ochora, J., Friis, H. & Aagaard-Hansen, J. (2005) Potential toxicity of some traditional leafy vegetables consumed in Nyang'oma Division, Western Kenya. *African Journal of Food, Agriculture, Nutrition and Development*, 5(1).

Orera, I., Rodriguez-Castrillón, J.A., Moldovan, M., García-Alonso, J.I., Abadía, A., Abadía, J., Álvarez-Fernández, A., (2010) Using a dual-stable isotope tracer method to study the uptake, xylem transport and distribution of Fe and its chelating agent from stereoisomers of an Fe(III)-chelate used as fertilizer in Fe-deficient Strategy I plants. *Metallomics*, 11(1), pp. 646-657.

Östbring K, Sjöholm I, Rayner M, Erlanson-Albertsson C. Effects of Storage Conditions on Degradation of Chlorophyll and Emulsifying Capacity of Thylakoid Powders Produced by Different Drying Methods. *Foods*. 2020 May 22;9(5):669. doi: 10.3390/foods9050669. PMID: 32455958; PMCID: PMC7278877.

Oztekin, G.B., Uludag, T., Tuzel, Y., (2018) Growing spinach (*Spinacia oleracea* L.) in a floating system with different concentrations of nutrient solution. *Applied ecology and environmental research*, 16(3), pp. 3333-3350.

Pasricha, S.-R., Drakesmith, H., Black, J., Hipgrave, D. & Biggs, B.-A. (2013) Control of iron deficiency anemia in low-and middle-income countries. *Blood, the Journal of the American Society of Hematology*, 121(14), 2607-2617.

Raes, K., Knockaert, D., Struijs, K. & Van Camp, J. (2014) Role of processing on bioaccessibility of minerals: Influence of localization of minerals and anti-nutritional factors in the plant. *Trends in Food Science & Technology*, 37(1), 32-41.

Rajapitamahuni S, Kang BR, Lee TK. Exploring the Roles of Arbuscular Mycorrhizal Fungi in Plant–Iron Homeostasis. *Agriculture*. 2023

Ratan Das, D. S., Tapas Paul (2019) Anti-Nutritional Factor of Vegetables and their Effect on Human Body- A Review. *International Journal of Agriculture, Environment and Biotechnology*, XII(1), 209-212.

Rayner, M., Emek, S. C., Gustafssona, K., Erlanson-Albertsson, C., & Albertsson, P. Å. (2011). A novel emulsifier from spinach with appetite regulation abilities. *Procedia Food Science*, 1, 1431-1438.

Rebeiz, C. A., Benning, C., Bohnert, H. J., Daniell, H., Hooper, J. K., Lichtenthaler, H. K., Portis, A. R. & Tripathy, B. C. (2010) *The chloroplast: basics and applications*, 31Springer Science & Business Media.

Reinhardt, W., Albright, L. D., de Villiers, D. S., Langhans, R. W., Shelford, T. J. & Rutzke, C. F. (2007) Root Disease Treatment Methods for Commercial Production of Hydroponic Spinach. *Final Report Prepared for the New York State Energy Research and Development Authority by Cornell University Department of Biological and Environmental Engineering—Feb.*

Riaz, N. & Guerinot, M. L. (2021) All together now: regulation of the iron deficiency response. *Journal of Experimental Botany*, 72(6), 2045-2055.

Roberts, J. L. & Moreau, R. (2016) Functional properties of spinach (*Spinacia oleracea* L.) phytochemicals and bioactives. *Food & function*, 7(8), 3337-3353.

Rodriguez-Ramiro, I., Dell'Aquila, C., Ward, J. L., Neal, A. L., Bruggraber, S. F. A., Shewry, P. R. & Fairweather-Tait, S. (2019) Estimation of the iron bioavailability in green vegetables using an in vitro digestion/Caco-2 cell model. *Food chemistry*, 301,

Student ID: 20194859
125292.

Roose, T., Fowler, A. C. & Darrah, P. R. (2001) A mathematical model of plant nutrient uptake. *Journal of mathematical biology*, 42, 347-360.

Roschttardt, H., Conéjéro, G., Divol, F., Alcon, C., Verdeil, J.-L., Curie, C. & Mari, S. (2013) New insights into Fe localization in plant tissues. *Frontiers in plant science*, 4, 350.

Rutherford, J. (2009) *Environmental Systems and Societies for IB Diploma*. Oxford, England: Oxford University Press.

Salgado, J. C., Olivera-Nappa, A., Gerdtzen, Z. P., Tapia, V., Theil, E. C., Conca, C. & Nuñez, M. T. (2010) Mathematical modeling of the dynamic storage of iron in ferritin. *BMC Systems Biology*, 4, 1-15.

Sams, L., Paume, J., Giallo, J. & Carrière, F. (2016) Relevant pH and lipase for in vitro models of gastric digestion. *Food & function*, 7(1), 30-45.

Schmidt SB, Eisenhut M, Schneider A. Chloroplast Transition Metal Regulation for Efficient Photosynthesis. *Trends Plant Sci.* 2020 Aug;25(8):817-828. doi: 10.1016/j.tplants.2020.03.003. Epub 2020 Apr 3. PMID: 32673582.

Solti, Á., Kovács, K., Basa, B., Vértés, A., Sárvári, É. & Fodor, F. (2012) Uptake and incorporation of iron in sugar beet chloroplasts. *Plant Physiology and Biochemistry*, 52, 91-97.

Stoltzfus, R. J. (2001) Defining iron-deficiency anemia in public health terms: a time for reflection. *The Journal of nutrition*, 131(2), 565S-567S.

Tang, J., Wang, P., Xie, Z., Wang, Z. & Hu, B. (2021) Effect of iron plaque on antibiotic uptake and metabolism in water spinach (*Ipomoea aquatic* Forsk.) grown in hydroponic culture. *Journal of Hazardous Materials*, 417, 125981.

Tenenbaum, M. & Pollard, H. (1985) *Ordinary differential equations: an elementary textbook for students of mathematics, engineering, and the sciences* Courier Corporation.

Thomine, S. & Lanquar, V. (2011) Iron transport and signaling in plants. *Transporters and pumps in plant signaling*, 99-131.

Tijsskens, L. M. M., Schijvens, E. P. H. M., & Biekman, E. S. A. (2001). Modelling the change in colour of broccoli and green beans during blanching. *Innovative Food Science & Emerging Technologies*, 2(4), 303-313.

Trumbo, P., Yates, A. A., Schlicker, S. & Poos, M. (2001) Dietary reference intakes. *Journal of the American Dietetic Association*, 101(3), 294-294.

Tudoreanu, L. & Phillips, C. J. C. (2004) Empirical models of cadmium accumulation in maize, rye grass and soya bean plants. *Journal of the Science of Food and Agriculture*, 84(8), 845-852.

Uusiku, N. P., Oelofse, A., Duodu, K. G., Bester, M. J. & Faber, M. (2010) Nutritional value of leafy vegetables of sub-Saharan Africa and their potential contribution to human health: A review. *Journal of food composition and analysis*, 23(6), 499-509.

Verma, P., George, K. V., Singh, H. V. & Singh, R. N. (2007) Modeling cadmium accumulation in radish, carrot, spinach and cabbage. *Applied Mathematical Modelling*, 31(8), 1652-1661.

Wang, Y., Kang, Y., Zhong, M., Zhang, L., Chai, X., Jiang, X. & Yang, X. (2022) Effects of iron deficiency stress on plant growth and quality in flowering chinese cabbage and its adaptive response. *Agronomy*, 12(4), 875.

Waters, B. M. & Sankaran, R. P. (2011) Moving micronutrients from the soil to the seeds: genes and physiological processes from a biofortification perspective. *Plant Science*, 180(4), 562-574.

Student ID: 20194859

White, P. J. & Broadley, M. R. (2009a) Biofortification of crops with seven mineral elements often lacking in human diets – iron, zinc, copper, calcium, magnesium, selenium and iodine. *New Phytologist*, 182(1), 49-84.

White, P. J. & Broadley, M. R. (2009b) Biofortification of crops with seven mineral elements often lacking in human diets—iron, zinc, copper, calcium, magnesium, selenium and iodine. *New Phytologist*, 182(1), 49-84.

Zielińska-Dawidziak, M. (2015) Plant ferritin—a source of iron to prevent its deficiency. *Nutrients*, 7(2), 1184-1201.

Öztekin, G. B., Uludağ, T. & Tüzel, Y. (2018) Growing spinach (*Spinacia oleracea* L.) in a floating system with different concentrations of nutrient solution. *Applied Ecology & Environmental Research*, 16(3).

Şimşek, O. & Çelik, H. (2021) Effects of iron fortification on growth and nutrient amounts of spinach (*Spinacia oleracea* L.). *Journal of Plant Nutrition*, 44(18), 2770-2782.

Zhang, Y., Liu, C., & Yang, C. (2012). Analysis of heat-induced disassembly process of three different monomeric forms of the major light-harvesting chlorophyll a/b complex of photosystem II. *Photosynthesis research*, 111, 103-111.

9.0 Appendices

Appendix 1: Original nutrient salts for Hoagland stock solution, including MES hydrate buffer powder



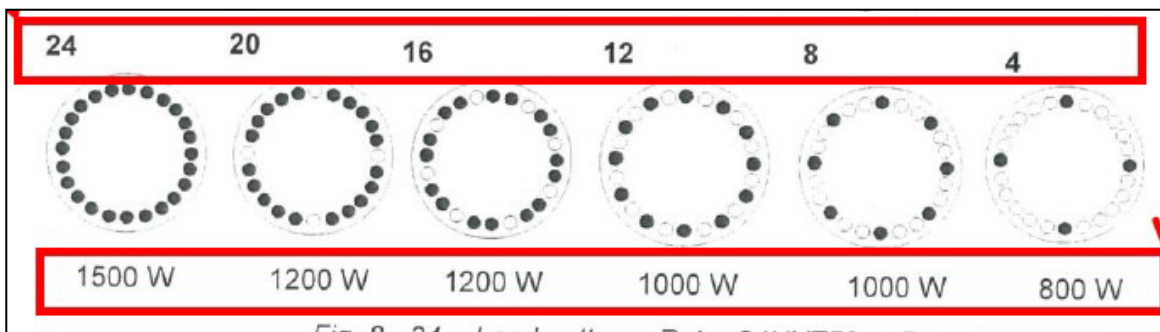
Appendix 2: Dissolving coarser material with a magnetic stirrer (Radleys Tech)



Appendix 3: Using the Mettler Toledo (FE20/EL20 benchtop) pH probe



Appendix 4: Varying setups of Teflon vessels in microwave rotor based on the number of samples



Appendix 5: Specimen graph of temperature and power fluctuations during microwave digestion run











Appendix 6: Dry weight (DW) values of spinach root and stem + leaf material on the final 10 days of growth (13/09 – 04/10/2021) of Harvest 9 (23/08 – 04/10/2021)







Dry weight (g)

Appendix 7: Total fresh weight (FW) and dry weight (DW) values of plant material on the final 10 days of growth (13/09 – 04/10/2021) of Harvest 9 (23/08 – 04/10/2021)

Total weight (g)

Extracurricular activities, training courses and conferences

TRAINING LOG			
Procedure/equipment	Signature of trainee	Trainer name (s)	Date of first training
Centrifugation		<ul style="list-style-type: none"> • Randa Darwish • Mohamed A. Gedi 	17/05/19
Acid digestion & ICP-MS		<ul style="list-style-type: none"> • Randa Darwish • Saul-Vasquez Reina 	14/08/19
Spectrophotometry		<ul style="list-style-type: none"> • Randa Darwish • Mohamed A. Gedi 	16/08/19
Operating the fume hood		<ul style="list-style-type: none"> • Khatija Nawaz-Hussain • Marlies Fischer 	21/07/19
Using electrical conductivity (EC) probe			21/10/19
Dry ashing protocol		<ul style="list-style-type: none"> • Randa Darwish • Mohamed A. Gedi 	11/11/19
Light microscopy		<ul style="list-style-type: none"> • Poramat Sutcharit 	02/11/19

Air-drying materials – aspiration		<ul style="list-style-type: none"> • Mohamed A. Gedi 	11/11/19
Lipid extraction & analysis		<ul style="list-style-type: none"> • Mohamed A. Gedi 	27/11/19
New laboratory COVID-19 guidelines (SB Food Sciences)		<ul style="list-style-type: none"> • Khatija Nawaz-Hussain • Richard Argent 	22/09/20
Online Course: Computer Modelling In Science (BIOS2016 UNUK)		<ul style="list-style-type: none"> • Dov J. Stekel • Leah Band • Andrew French 	05/10/20 (17/05/21)
New laboratory COVID-19 guidelines (SB Gateway Building)		<ul style="list-style-type: none"> • John Corrie 	14/06/21
Online Course: Health & Safety - eLearning Instructions for Fire Safety		<ul style="list-style-type: none"> • Paul Wilson 	13/10/22

TRAINING COURSES

Course name	Course location	Start date	Duration	Training points achieved
Literature searching and the literature review	Online (stand-alone course)	01/10/18	1 day	2
Shut up and write	University Park Campus	17/04/19	0.5 days	0

CELE – effective academic presentation	Jubilee Campus	01/05 – 29/05/19	5 days	0
Using posters to communicate research	University Park Campus	13/05/19	0.5 days	1
Nature of the doctorate and supervision process	Sutton Bonington Campus	14/05/19	0.5 days	1
Planning your research	University Park Campus	23/05/19	0.5 days	1
Research ethics for Sutton Bonington doctoral researchers	Sutton Bonington Campus	07/06/19	0.5 days	1
Preparing for the viva	University Park Campus	10/06/19	0.5 days	1
Introduction to Endnote for researchers	Queen's Medical Centre	21/06/19	0.5 days	1
Problems with academic writing	University Park Campus	05/07/19	0.5 days	0.5
How to be an effective doctoral student	University Park Campus	18/07/19	1 day	3